Seismic Response of Reinforced Concrete Structures Affected by Reinforcement Corrosion

Dissertation

submitted to and approved by the

Faculty of Architecture, Civil Engineering and Environmental Sciences
University of Braunschweig – Institute of Technology

and the

Faculty of Engineering
University of Florence

in candidacy for the degree of a
Doktor-Ingenieur (Dr.-Ing.) /
Dottore di Ricerca in Risk Management on the Built Environment *)

by
Paola Simioni
Born 12 October 1980
from Bassano del Grappa (VI), Italy

Submitted on	31 March 2009
Oral examination on	30 May 2009
Professorial advisors	Prof. Anna Saetta Prof. Harald Budelmann

2009

*) Either the German or the Italian form of the title may be used.

ACKNOWLEDGMENTS

We never reach important goals in life without the help of people who surround us, whether with their material or moral support. This is why I owe my thanks to several persons who accompanied me until the accomplishment of my PhD and, in different ways, contributed to each episode of the last three years.

For this my gratitude goes first to my tutor, Prof. Anna Saetta, who introduced me to the subjects of reinforced concrete durability and earthquake engineering, from whose conjunction the topic of my thesis was born. In these years she always supported me with her expertise and constant availability and soon an understanding far beyond the plain student-tutor relationship grew between us.
Another person whom I can never thank enough is Dr. Luisa Berto, who followed me starting from my diploma thesis, with great competence and patience. I always enjoyed the conversations we had, which were both scientifically and privately enriching.
Furthermore, I would like to express my thankfulness to Prof. Budelmann for supervising my thesis from the German side. I appreciated the fruitful discussions with him and I always cherished his politeness and availability, which allowed me feeling comfortable and talking freely and openly.
I am also grateful to Prof. Borri and Prof. Peil for their efforts as coordinators of the Graduate College, because they made possible living this experience. In particular, I always appreciated the internationality of the program, which taught me that differences not always divide people, but can also join them. Seeing the world from different perspectives enriched me as a person and greatly extended my vision of life. I am really happy that I was given this overwhelming opportunity.

Additionally I would like to thank the other members of my research group, which I was considering as my second family in these years: Renato, for stimulating my progress in his unique way; Massimiliano and Roberto, for often raising my mood and for understanding when this was needed; Alessandro, for opening my mind and making me laugh so much; Leopoldo, Giuseppe, Laura, Tommaso and Lorenzo, to whom I wish to make the same overwhelming experience I made.
Also I owe an affectionate thank to Silvio, who hosted me in his office during my stays at the TU Braunschweig and soon became rather a great friend than a colleague.

Certainly my deepest gratitude goes to my family, who never stopped supporting me, even during my sporadic presence at home in the last three years. They have always given me the freedom to make my own choices, putting my benefit above all else and teaching me the respect for people as the first rule in life.

All the persons I mentioned contributed to a great extent. Nevertheless, my greatest motivation was and is definitely Timm, from whom I mostly learnt the "international" lifestyle and the philosophy of doing all my best, without forgetting of being. And if I thank him at the end of these lines, it is not because he embodies the conclusion of my experience in the Doctoral School, but on the contrary the beginning of everything that will come from now on.

ABSTRACT

Durability of RC structures is a well known critical issue, requiring a time-dependent assessment of the structural performance. In fact, the progressive deterioration of the materials properties may significantly affect the response of the whole structural system, compromising the capability of the structure to withstand the loads for which it was designed. Thus, civil engineers are concerned not only with the need for durable design, but also with the importance of maintenance, inspection and, if necessary, reparation/rehabilitation interventions during the structure's service life.
Experience shows that corrosion of reinforcing steel may be cited as the major source of degradation, increasing the structural vulnerability to extreme loads and natural hazards. In particular, the variation of the mechanical properties of steel, concrete and their interfacial layer induced by corrosion may result in the reduction of the load bearing capacity and, in some cases, also the shift of the failure mechanism from the ductile to the fragile type. These aspects become a main issue in safety assessment, with noteworthy implications in seismic prone areas, where the ductility characteristics of the structure are of primary importance for a good seismic behaviour.
In order to support decision makers with a better comprehension of the matter of safety assessment, the concept of risk management has recently become of great concern also in civil engineering, being already popular in other disciplines. The general procedure developed within the International Graduate College IGC 802 allows managing risk in any situation or field in which an undesired or unexpected event could be significant, providing a greater insight of its possible outcomes and thus giving the possibility to control its impacts.
In the submitted dissertation a methodology is presented to investigate the effects induced by increasing levels of environmental degradation on the seismic response of RC structures, focusing on the consequences of reinforcement corrosion on the local and global structural behaviour.
Referring to the risk management procedure, both seismic shaking and reinforcement corrosion were identified as the hazards endangering the system. Within the risk analysis phase, a new module for the specific management of steel corrosion was proposed ("corrosion risk management chain").
The evaluation of the structural vulnerability was carried out at two different levels of investigation. A "micro" level approach allowed describing the influence of corrosion on the bond-slip behaviour between reinforcing bars embedded in concrete and concrete itself. A new bond law was developed, able to describe the degradation of bond strength due to environmental attacks, in pull-out and beam tests.
By means of the "macro" level approach it was possible to describe the variation of the seismic performance of a RC building at the end of its service life respect to the time of construction. It was assumed that, in accordance to the climatic characteristics of the site, the structure suffered of a moderate corrosion attack due to carbonation, resulting in the reduction of load bearing capacity and structural ductility.
In view of the high level of uncertainty involved in the assessment of the time-variant degradation of RC constructions, the research was carried out in a probabilistic framework. First, sensitivity analyses were performed both in the micro and macro models, in order to recognize the most influencing variables affecting the response parameters. Afterwards, in line with the formulation accepted within the Graduate College, the structural risk related to the combined effects of earthquake and corrosion was calculated as probability of occurrence of the two hazards times expected damage. In particular, the probability of corrosion initiation was evaluated by means of a durability model for the assessment of deteriorating RC members, while the probability of occurrence of a seismic event during the structure's service life was chosen first in compliance with the European Standards limit

states and secondly derived from the site-specific hazard map. Non linear static analyses were then performed to estimate the corresponding expected damage in terms of reduction of structural ductility in the capacity curves of the corroded building respect to the undamaged condition.
It is worth observing that, if repeated at different time periods, the proposed methodology can provide an estimate of the risk trend over time for the considered construction, or alternatively it can be applied at a territory level to rank different buildings in priority lists of intervention.

TABLE OF CONTENTS

LIST OF FIGURES

LIST OF TABLES

CHAPTER 1 INTRODUCTION

1.1 Introduction

Civil engineering is concerned with the optimal management of its facilities, which constitute a vital backbone of any society, since they allow undertaking activities, such as the production and transport of energy, they provide space for living or business and they permit the transportation of people and goods.

From the beginning of the twentieth century, reinforced concrete became of common use in the construction of civil engineering structures and infrastructures. Initially it was considered as an intrinsically durable construction material, showing a good performance even under unfavourable environmental conditions, and durability was regarded as a marginal issue. Nevertheless, especially from the second half of the twentieth century, degradation of RC structures turned into a crucial problem. In fact, developments in concrete technologies were mainly aimed at improving the mechanical performance of the material, with general decrease in the quality levels at the construction sites. Moreover, reinforced and prestressed concrete were largely used also in particularly aggressive environments, such as tidal or industrial scenarios, with consequent high costs for rehabilitation.

Nowadays, durability is a well known critical issue and civil engineers are aware not only of the need for durable design of reinforced concrete, but also of the importance of maintenance, inspection and, if necessary, reparation/rehabilitation interventions. In all this, the economic restrictions play also a decisive role, thus maximization of the utility combined with minimization of the costs are the target of the engineering decision-making process.

In order to support decision makers with a better comprehension of the matter of safety assessment and its impacts, the concept of risk management has recently become of great concern also in civil engineering, being already popular in other disciplines. The general procedure developed within the International Graduate College IGC 802 allows managing risk in any situation or field in which an undesired or unexpected event could be significant, providing a greater insight of its possible outcomes and thus giving the possibility to control the impacts.

In this framework, especially regarding existing RC structures, rather than to make observations on an already deteriorated structure, it is more desirable to be able to predict the likelihood and likely extent of future deterioration, as well as the associated structural response. In particular, the evaluation of the probability of occurrence of the harmful event endangering the system under consideration, or its components exposed to the hazard, is a fundamental module of the risk managing procedure. This allows accounting for the large uncertainty which is intrinsic in the estimation and prediction of the structural response of reinforced concrete members, especially when affected by degradation phenomena.

Actually, the progressive deterioration of RC structures over time requires a time-dependent evaluation of the structural performance and safety, which can be realistically assured only in probabilistic terms. The response to external excitations depends on the actual level of structural damage, which generally implies the reduction of the load bearing capacity and, in some cases, also the shift of the failure mechanism from the ductile to the brittle type.

These aspects become a main issue in safety assessment, with noteworthy implications in seismic prone areas, where the ductility characteristics of the structure are of primary importance for a good seismic behaviour.
Experience shows that among the different degradation phenomena which the structure may suffer during its service life, the corrosion of reinforcing steel may be cited as the most detrimental effect endangering the structural performance in terms of load bearing capacity and ductility characteristics. Indeed, reinforcement corrosion is a long-term process that weakens the structural elements, increasing their vulnerability to extreme loads and natural hazards, such as seismic excitations.
Corrosion of the reinforcement is generally associated with concrete carbonation or chlorides penetration, implying significant variations of the mechanical properties of both steel and concrete, as well as of the interfacial layer between the two materials. In particular, the hysteretic behaviour of RC structures is strongly dependent on the interactive action between steel and concrete, that is to say the bond-slip relationship, e.g. [Bertero et al., 1983]. As a matter of fact, it is well known that in reinforced concrete one of the causes of brittle failure is the sudden loss of bond between reinforcing bars and concrete at the anchorage zones, which may cause severe local damage up to collapse of the structure under seismic shaking.

1.2 Motivation and scope of the research

Considering that concrete is one of the most common materials used in infrastructure facilities, it is not surprising that, especially in the last two decades, efficient design and maintenance of such structures have become a great societal concern.
According to a report of the Bayerische Ingenieurkammer Bau (2004), more than half of the budget spent for construction activities in developed countries such as Germany is related to retrofit of structures, [Diamantidis and Bazzurro, 2007]. This confirms the crucial and increasing demand for the assessment and rehabilitation of existing constructions, especially in industrialized areas, revealing the limited current knowledge regarding the most appropriate methodology to be applied and the safety levels to be allowed.
A considerable amount of research work has been carried out in recent years, demonstrating the increasing interest of the scientific community on this topic. Significant efforts have been allocated by the engineering profession to improve the basis for decision-making with regard to modelling, analysis, maintenance planning and rehabilitation techniques of deteriorating structural systems. In spite of the improvements in our basic understanding, analytical capabilities and computational power, the presence of uncertainty in engineering issues, especially in the assessment of RC constructions, cannot be avoided. Thus, a consistent treatment of uncertainties together with a set of probabilistic models for the assessment of the statistical characteristics of the future degradation and performance of the structure is necessary in order to enhance a cost-efficient allocation of activities and resources, [Faber, 2006].
In structural design, the system performance is usually assessed with reference to the initial time of construction. Nevertheless, since structures are inevitably exposed to several sources of damage and aggressive environments, their structural performance should be considered as time-dependent. In fact, the progressive deterioration of the material properties may significantly affect the response of the whole structural system, compromising the capability of the structure to withstand the loading for which it was designed. Therefore, a consistent approach to the design of RC structures should account for the structural performance not only at the initial stage, but also during the whole expected service life.

At present, durable design of reinforced concrete against chemical-physical damage is based on simple criteria, associated with prescribed environmental conditions, which introduce threshold values for concrete cover, water-cement ratio, cement content and quality, etc. However, these indirect evaluations of the effects of structural damage are not sufficient and also the global effects of the local damage phenomena on the overall performance of the system should be taken into account, [Biondini et al., 2008].
With reference to reinforcement corrosion, some models have been proposed for the description of its temporal and spatial evolution, e.g. [Stewart, 2004]. However, a realistic model describing the loss of bond associated with corrosion has not been developed yet, [Faber, 2006].
All the mentioned aspects acquire even greater relevance if the structure is struck by a natural hazard, such as a seismic event. The Izmit earthquake occurred in Turkey in August 1999 caused an impressive devastation in terms of structural damage and loss of human lives, not comparable with the effects of earthquakes of similar intensities occurred in other countries. In spite of the awareness that this region is a highly seismic prone area, 120.000 houses were damaged beyond repair, 50.000 houses were heavily damaged, 2000 other buildings collapsed and 4000 other constructions were heavily damaged. The total collapse as well as minor or heavy damages on RC buildings were attributed to the degradation of concrete caused by lack of proper concrete mix design and use of improper practices in producing concrete: inadequate cement quantity, lack of sieve analysis and proper gradation of aggregate, use of unwashed sea sand containing seashells, lack of vibration after concrete pouring, insufficient curing of concrete and no attention to weather conditions, no quality control of the specimens. Above all, the use of sea sand, and consequently the presence of chlorides inside the concrete mix, led to severe corrosion of the reinforcing bars and in some cases to the complete loss of steel-concrete bond. In the final report about the disaster, it was concluded that steel corrosion may anticipate the time to structural failure up to a period of 10-20 years, even under static loads only.
In view of these observations, the present dissertation aims at investigating the effects induced by environmental degradation phenomena on the response of RC structures to seismic excitations. In particular, the variation of the seismic behaviour in presence of increasing levels of degradation is analysed, focusing on the consequences of reinforcement corrosion on the local and global structural behaviour. To this aim, a methodology has been developed to study the evolution of the structural performance from its initial undamaged state (i.e. at the time of construction), until the end of the service life for which the construction was designed. Such procedure allows calculating the *Structural Risk* associated with the long-term performance of the structure, taking into consideration the possible damage phenomena which could occur during its lifetime. Furthermore, a new micro-level model is proposed to include the effects of corrosion in the bond-slip behaviour, with the result of accounting for the degradation of bond strength and the occurrence of slippage of the reinforcing bars under severe corrosion attacks.

1.3 Overview

Since the research has been carried out in line with the risk management framework, Chapter 2 gives first of all an overview of the procedure developed within the Graduate College for managing risk due to natural and civilization hazards on buildings and infrastructures. The three steps constituting the risk management chain are described in detail, with reference to the specific hazards dealt with in the present thesis, i.e. corrosion and seismic shaking. In Chapter 3, an approach to be regarded as part of the main risk management scheme is proposed to specifically treat corrosion risk. This introduces the following Chapter 4, in which the

phenomenon of reinforcement corrosion in RC structures is extensively described in terms of physical-chemical mechanism and effects on the structural behaviour. In particular, the steel-concrete mutual interaction is considered and the two modelling approaches developed to describe the degradation of bond induced by steel corrosion are presented and validated by means of numerical simulations of experimental tests (pull-out and beam tests) available in the literature.

Afterwards, Chapter 5 focuses on the assessment of structural safety and reliability in the probabilistic framework, first with an introduction about codes provisions and the most recent achievements of the scientific community, followed by the description of the methodology developed during this study to evaluate the probability of occurrence of corrosion phenomena and the calculation of the *Structural Risk*. The whole methodology is then practically applied in Chapter 6 to analyse two case studies, with the aim of demonstrating the applicability of the suggested models for the assessment and prediction of the seismic response of RC constructions suffering from environmental degradation. Moreover, fragility estimates of a corroding RC column with regard to rotation failure are provided, in compliance with the Standards provisions.

Finally, Chapter 7 summarises the achievements of the research, highlighting the most important points and offering an outlook of future investigation still required in this field.

CHAPTER 2 THE RISK MANAGEMENT PROCESS

The concept of risk management has become widely accepted in the last years, being applicable to a huge variety of activities, decisions and operations, involving public as well as private enterprises, groups or single individuals. The present chapter aims at describing the procedure for risk management developed within the IGC 802, which has been adopted in the present dissertation as the backbone of the methodology proposed for managing risk on RC constructions due to seismic excitations along with reinforcement corrosion.

2.1 Introduction

The Australian and New Zealand Standard - AS/NZS 4360: 2004 "Risk Management" - sets the basis of a generic strategy for managing risk, specifying the elements of the risk management process in an independent format respect to any specific industry or economic sector and including both potential gains and potential losses. In particular, the AS/NZS endows with the following definition:

"Risk management is an iterative process consisting of well-defined steps which, taken in sequence, support better decision-making by contributing a greater insight into risks and their impacts. The risk management process can be applied to any situation where an undesired or unexpected outcome could be significant or where opportunities are identified. Decision makers need to know about possible outcomes and take steps to control their impact".

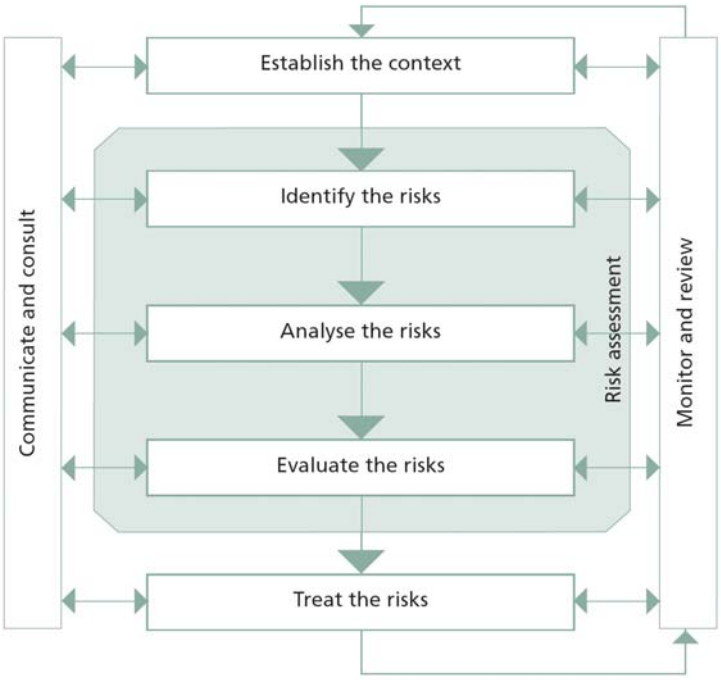

Figure 2.1 Overview of Risk Management by AS/NZS 4360 (2004)

Apart from its generic formulation, the design and implementation phases of the risk management chain are evidently influenced by the specific needs of the individual or organization dealing with it. Figure 2.1 depicts the flow-chart of the system proposed by the Australian and New Zealand code, which has been adopted also by other countries.
The approach granted by the AS/NZS 4360 has been further developed within the International Graduate College IGC 802, e.g. [Pliefke et al., 2007], and has been adjusted according to the main purposes of the Doctoral School, i.e. for managing risk due to natural and civilization disasters.
In her "Components of Risks – A Comparative Glossary", Katharina Thywissen, [Thywissen, 2006], highlights the variety of definitions existing for each single term related to disaster reduction and the resulting lack of a standardized terminology accepted at an international level. This leads to a general confusion and misunderstanding, a shared language and concepts being fundamental for widening the understanding, communication and effectiveness of all the multiple disciplines involved in disaster reduction. Thus, the procedure for managing risk developed within the IGC 802 has also the important role of providing a common and generally recognised framework in which the researchers may interdisciplinary interact.
The Risk Management Process, called for brevity "RMP" from now on, consists of three main components, as shown in Figure 2.2: *Risk Identification*, *Risk Assessment* and *Risk Treatment*.

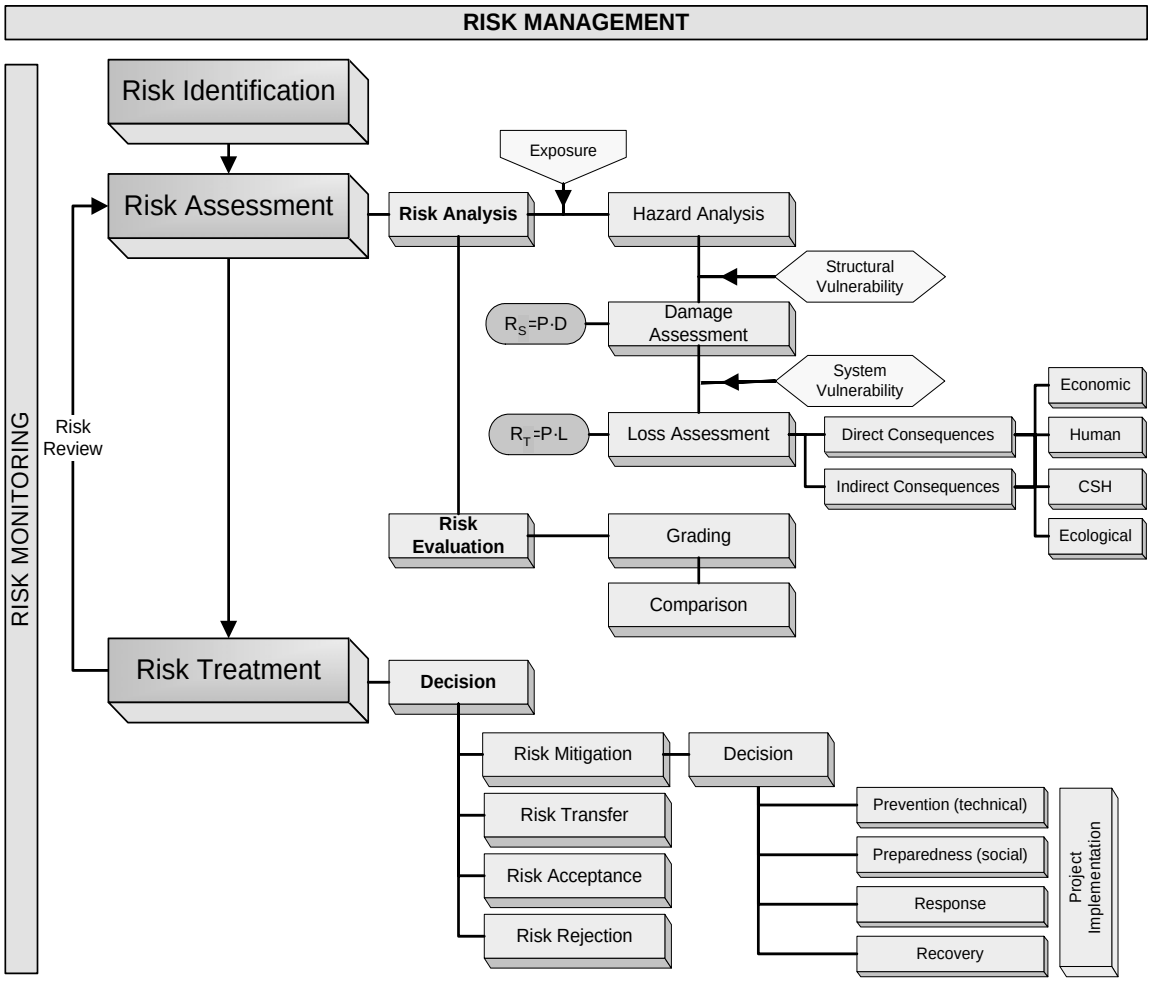

Figure 2.2 The Risk Management Process developed within the IGC 802 [Pliefke et al., 2007]

These phases are performed in sequence throughout the process, accompanied by a *Risk Review* and continuous *Risk Monitoring*. The Risk Review aims at updating the risk process by constantly including new information, acquired knowledge and experience, representing the evolution of risk over time.
It is worth noting that the Risk Review step is performed only for risks that have already run through the whole process at least once. Each iteration of the Risk Review module indicates the effectiveness of the potential implementation within the RMP of risk reduction interventions, while the Risk Monitoring procedure captures the exchange of information among all people actively or passively involved in the RMP. This exchange ensures the interdisciplinary collaboration among researchers and the identification of new hazards rising from the constantly changing environment.
In the specific case of corrosion-affected structures, it is important to emphasize the significance of this multidisciplinary partnership, since a reliable assessment of a RC structure suffering environmental degradation phenomena can be performed only by a multidisciplinary team composed by corrosion specialists and structural engineers, [Rodriguez et al., 2001].
The RMP is described more in detail in the following sections, focusing attention on the steps of the chain that have been explicitly treated in this dissertation.

2.2 Risk Identification

The prerequisite to start the performance of the RMP through the Risk Identification phase is the awareness of a dangerous situation (*Risk Perception*) that can be expressed by the question "what can happen and where?"
Differently from the case of earthquake records, a database of corrosion phenomena does not exist up to now. In particular, corrosion attacks in progress often produce not visible external signs and may be detected only by means of in depth inspections. Thus, knowledge about potentially dangerous scenarios arising from steel corrosion may be attained mainly through in-field observations or reports on past events. For example, in [Çağatay, 2005] some RC constructions damaged during the Adana–Ceyhan and the Izmit earthquakes (Turkey), occurred respectively on the 27th of June 1998 and on the 17th of August 1999, were inspected (see also Section 2.2.1). In a number of buildings, in which sea sand was found inside the concrete mix, significant steel reinforcement corrosion due to the penetration of chlorides was observed. In the final report on the catastrophe it was concluded that the presence of sea sand in concrete may be more dangerous than low compressive strength of concrete, since the time to structural failure may be anticipated up to a period of 10-20 years, even under static loads only.
After the identification of risky situations, the RMP proceeds with the following steps. First, the system to investigate has to be delineated within the model domain, which can be a single building (as in the present work) or infrastructure or structural element, but in general also a city, a region or even a whole country, depending on the type of natural disaster under consideration. It should be noted, [Faber, 2007], that any component in a system can be modelled as a system itself, as shown in Figure 2.3. Secondly, all sources of events that may endanger the functionality of the system have to be identified. These events are named *hazards*.
With reference to the aforementioned case study described in [Çağatay, 2005], both the occurrence of a seismic event and the simultaneous incidence of an ongoing corrosive attack may be recognised as the hazards affecting the system, similarly to the topic of the present research.

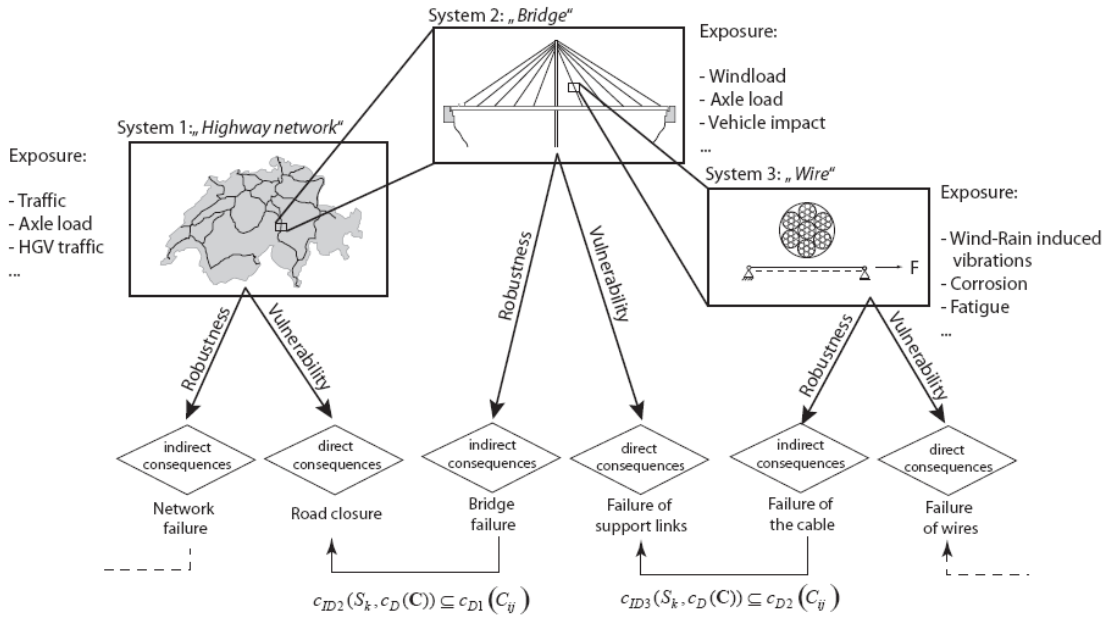

Figure 2.3 Generic system characterization at different scales in terms of exposure, vulnerability and robustness [Faber, 2007]

2.2.1 Natural and technological disasters

Dealing with the management of risk due natural and civilization hazards, it is convenient first to classify the induced disasters, being a clear and common language an essential aspect in exchanging information and promoting the interdisciplinary interaction between researchers and stakeholders.

Recently, the Center for Research on the Epidemiology of Disasters (CRED) has led an initiative to develop a disaster category classification for operational databases, in order to create a standardized hierarchy and terminology for all global and regional databases.

Two main categories are distinguished, natural and technological disasters. The natural disaster category is divided into six sub-groups, which in turn cover 12 disaster types and several sub-types (Figure 2.4).

Table 2.1, Table 2.2 and Table 2.3 grant some data on the effects of natural disasters in Italy in the period 1900-2008, according to the worldwide database EM-DAT (Emergency Events Database). Data are sorted respectively by number of total people killed, number of total people affected and economic damage costs.

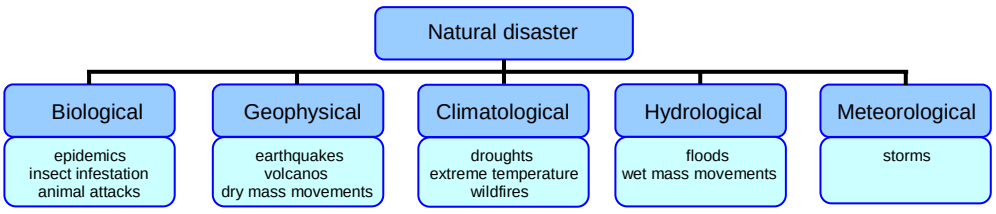

Figure 2.4 Natural disasters classification [EM-DAT, 2007]

The catastrophic events related to technical matters have started to receive wide public attention in particular from the early 1960's. A summary of the worldwide technological disasters in the period 1900-2008 is given in Figure 2.5, in which data are interpolated with smoothed lines. It can be observed as the number of reported disasters increased sharply in the last decades, especially between the 1980's and the 1990's.

Table 2.1 Top 10 natural disasters in Italy for the period 1900-2008 sorted by number of total people killed [EM-DAT, 2008]

Disaster	Date	People killed
Earthquake (seismic activity)	28 Dec 1908	75'000
Earthquake (seismic activity)	13 Jan 1915	29'980
Extreme temperature	16 Jul 2003	20'089
Earthquake (seismic activity)	23 Nov 1980	4'689
Earthquake (seismic activity)	8 Sept 1905	2'500
Mass movement wet	9 Oct 1963	1'917
Earthquake (seismic activity)	23 Jul 1930	1'883
Earthquake (seismic activity)	6 May 1976	922
Volcano	18 Apr 1906	700
Mass movement wet	25 Oct 1954	297

Table 2.2 Top 10 natural disasters in Italy for the period 1900-2008 sorted by number of total affected people [EM-DAT, 2008]

Disaster	Date	People affected
Flood	7 Oct 1970	1'301'650
Flood	3 Nov 1966	1'300'000
Earthquake (seismic activity)	23 Nov 1980	400'000
Earthquake (seismic activity)	6 May 1976	218'222
Flood	14 Nov 1951	170'000
Earthquake (seismic activity)	28 Dec 1908	150'000
Earthquake (seismic activity)	15 Jan 1968	55'563
Flood	14 Oct 2000	43'000
Earthquake (seismic activity)	26 Sep 1997	38'100
Earthquake (seismic activity)	9 Sept 1976	32'000

Table 2.3 Top 10 natural disasters in Italy for the period 1900-2008 sorted by economic damage costs [EM-DAT, 2008]

Disaster	Date	Damage US$ (000's)
Earthquake (seismic activity)	23 Nov 1980	20'000'000
Flood	01 Nov 1994	9'300'000
Flood	14 Oct 2000	8'000'000
Earthquake (seismic activity)	26 Sep 1997	4'524'900
Extreme temperature	16 Jul 2003	4'400'000
Earthquake (seismic activity)	06 May 1976	3'600'000
Flood	03 Nov 1966	2'000'000
Wildfire	Mar 1990	880'000
Drought	Apr 1997	800'000
Earthquake (seismic activity)	31 Oct 2002	796'000

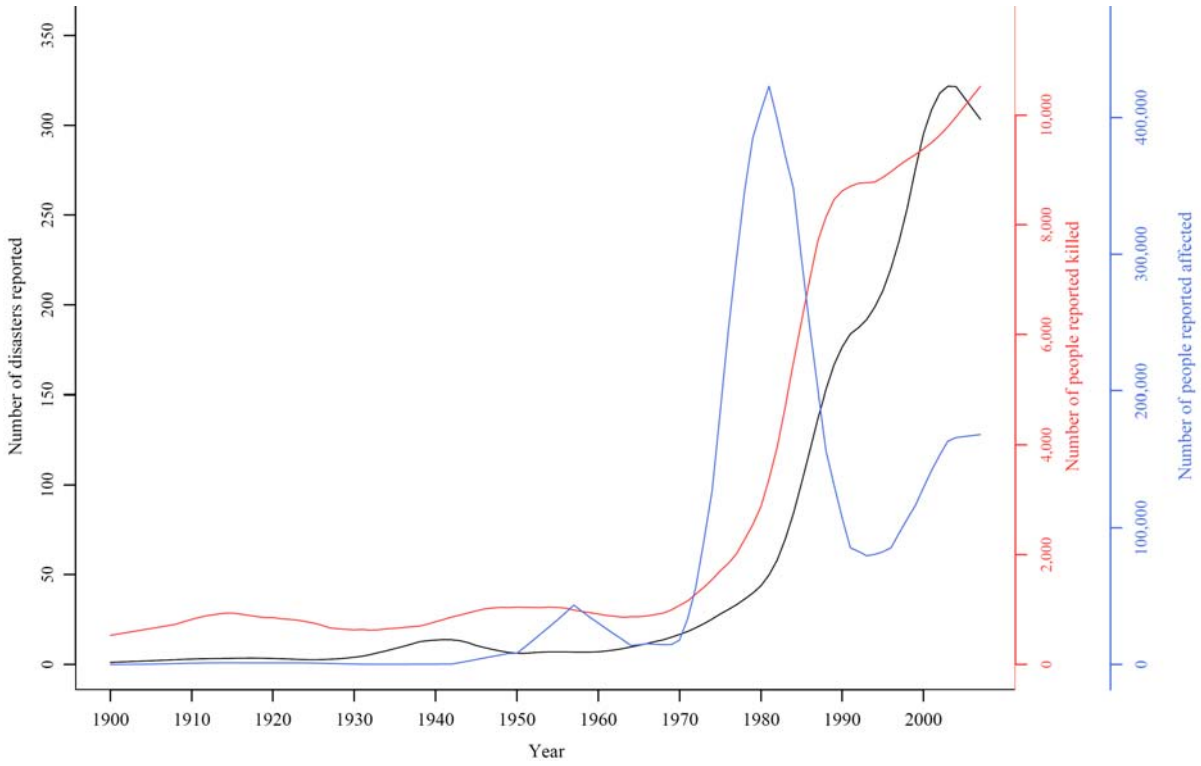

Figure 2.5 World technological disaster summary 1900-2007 [EM-DAT, 2008]

In the EM-DAT a distinction is made between collapse of industrial structures ("industrial accident") and collapse of domestic/non-industrial structures ("miscellaneous accident"). In particular, concerning buildings collapse, Table 2.4 summarizes some events. An interesting consideration may be derived on this subject. It is evident that in industrialized countries the structural design is safer than in developing countries. As a consequence, collapse is usually avoided, and accordingly the number of fatalities. Nevertheless, also the value of the structures is higher in modern countries, as well as the related repairing costs in case of structural damage or failure (see also Table 2.6). Thus, respect to poor nations, the damage in economic terms is larger. For this reason, a desirable structural design aims not only at preventing collapse and loss of human lives, but also at limiting damage and assuring the preservation of the functionality of the most important (strategic) facilities even after the occurrence of severe disasters.

Table 2.4 Collapses of buildings (EM-DAT, 2006)

Year	Structure	Location	Country	Lives lost	Affected people
1978	temple	Jonestown	Guyana	900	0
1995	department store	Seoul	South Korea	458	922
1982	Luzhniki Stadium	Moscow	Russia	340	0
1980	building	Sincelejo	Colombia	165	500
2005	garments factory	Palash Bari	Bangladesh	151	100
1993	Hotel Royal Plaza	Nakhov Ratchasima	Thailand	135	270
1984	bridge	Kerala	India	125	0
1990	school	Port Harcourt	Nigeria	100	0
1989	football stadium	Sheffield	United Kingdom	95	200
2004	building	Konya	Turkey	94	28

2.2.2 Corrosion-induced disasters

An emblematic example of the catastrophic effects of steel corrosion in addition to lack of bond in RC structures subject to a seismic event is represented by the collapse of the Cypress Street Viaduct in Oakland, California (Figure 2.6).
The structure was in use until the Loma Prieta earthquake occurred on the 17th of October 1989, when a consistent portion of the upper level collapsed onto the lower one. The supports on the sides broke and split outward causing the upper-level to fail. The softening behaviour of the system prior to failure of the connection was attributed to the deterioration of the column bars bond within the joint, resulting in significant bars slippage.

Figure 2.6 Collapse of Cypress Street Viaduct in Oakland, California (Loma Prieta earthquake, 1989) [http://en.wikipedia.org]

Another example of a corrosion-induced disaster is represented by the already mentioned case reported by [Çağatay, 2005] (Section 2.2). The author provides an interesting report on earthquake-induced disasters in Turkey. In spite of the awareness that this region is a highly seismic prone area (Figure 2.7), the Izmit earthquake (1999) caused terrible devastation in terms of structural damage and loss of human lives, not comparable with the effects of earthquakes of similar intensities occurred in other countries. According to reports from September 1999, 120.000 houses were damaged beyond repair, 50.000 houses were heavily damaged, 2000 other buildings collapsed and 4000 other constructions were heavily damaged.

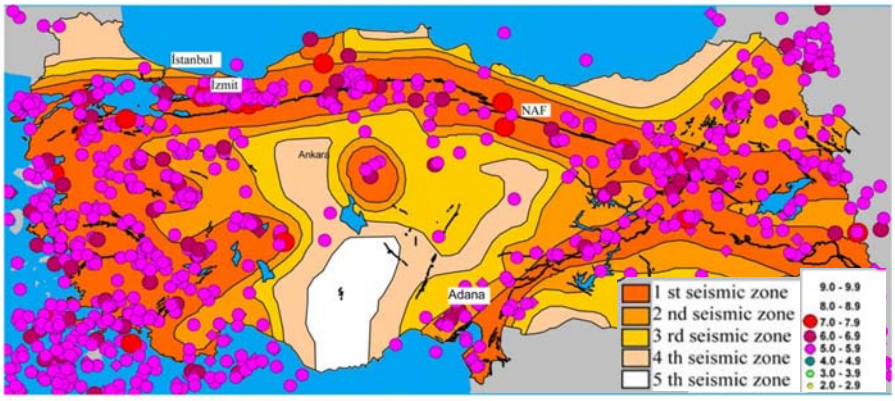

Figure 2.7 Earthquake zone map of Turkey [Çağatay, 2005]

Figure 2.8 Izmit earthquake: collapsed buildings [http://www.geo.uib.no]

Figure 2.9 Izmit earthquake: mosque [http://www.ce.jhu.edu]

Figure 2.8 and Figure 2.9 show an impressive devastation scenario, with highly not uniform distribution of damage among adjacent buildings: some constructions are completely destroyed, while some others are lightly damaged or incredibly not affected by the earthquake. For example, the mosque and a contiguous high building in Figure 2.9 are apparently in an undamaged condition, while all the surrounding constructions are reduced to rubble.

Çağatay attributes such catastrophe to the negligence and ignorance in: allocating high-rise buildings on alluvial deposits having unsuitably low bearing pressures, seismic designing, supplying of adequate lateral reinforcement, and especially concrete quality. In particular, the total collapse as well as minor or heavy damages on RC structures were attributed to the lack of proper concrete mix design and use of improper practices in producing concrete: inadequate cement quantity, lack of sieve analysis and proper gradation of aggregate, use of unwashed sea sand containing seashells (Figure 2.10), lack of vibration after concrete pouring, insufficient

curing of concrete and no attention to weather conditions, no quality control of the specimens being taken for most of the buildings. Above all, the use of sea sand, and consequently the presence of chlorides inside the concrete mix, led to severe reinforcement corrosion (Figure 2.11) and in some cases complete loss of steel-concrete bond (Figure 2.12).

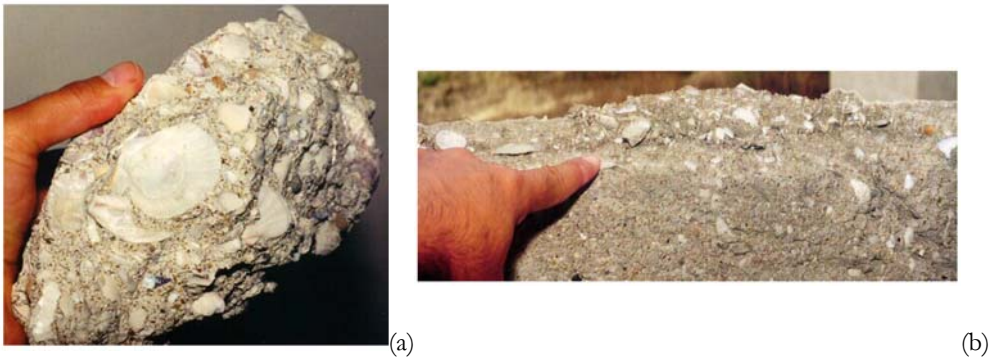

(a) (b)

Figure 2.10 Izmit earthquake: seashells found in (a) a piece of concrete; (b) a beam [Çağatay, 2005]

Figure 2.11 Izmit earthquake: corrosion of reinforcement in columns [Çağatay, 2005]

Figure 2.12 Izmit earthquake: corrosion-induced loss of steel-concrete bond [Çağatay, 2005]

Structural collapse may be also produced by corrosion of steel tendons. An example is offered by the Congress Hall in Berlin (Figure 2.13). On the 21st of May 1980, 23 years after the construction, the roof of the building collapsed. The report on the catastrophe drew the following conclusion: "The collapse of both the southern outer roof and the peripheral tie of the Berlin Congress Hall was due to inadequate structural planning and unsatisfactorily executed construction of the outer roofs and, consequently, to corrosion-induced fractures in the tendons bearing the roof arch".

Figure 2.13 Roof of the Congress Hall (Berlin, 1980) [http://www.hkw.de]

The collapse of Lowe's prestressed concrete bridge in Concord, USA, on the 21st of May 2000 was also attributed to corrosion of prestressing wires (Figure 2.14). The bridge was only six years old at the time of collapse. It was found that the grout applied to the beams contained calcium chloride; small cracks in concrete allowed the combination between moisture and those chlorides, accelerating the detrimental corrosion of the strands.

Figure 2.14 Lowe's Speedway footbridge (USA, 2000) [Faber, 2007 - Wolmuth and Surtees, 2003]

2.3 Risk Assessment

After the Risk Identification, the Risk Assessment module applied to the circumscribed hazardous location initiates. This phase, summarized in Figure 2.15, is the most crucial part of the RMP. It is divided into two sub-procedures: the *Risk Analysis*, representing the most sophisticated part and aiming at the quantification of risk parameters and then risk itself, and the *Risk Evaluation*, whose task is the comparison with other competing risks.

It should be noted that the Risk Assessment is applicable at any scale of the system (components, sub-systems or the system as a whole). In this framework, a hierarchical approach is possible, allowing for utilization of a wide range of *indicators of risk*, which may be considered as any quantifiable characteristics of the system providing information about risk, especially with regard to exposure, vulnerability and robustness, [Faber, 2007]. For example, in the case of a

load bearing structure, risk indicators may be location (e.g. earthquake prone area) and environment (e.g. tidal scenario) for exposure, age of the structure or materials properties as corrosion indicators for vulnerability, structural ductility and joints quality for robustness (Figure 2.16).

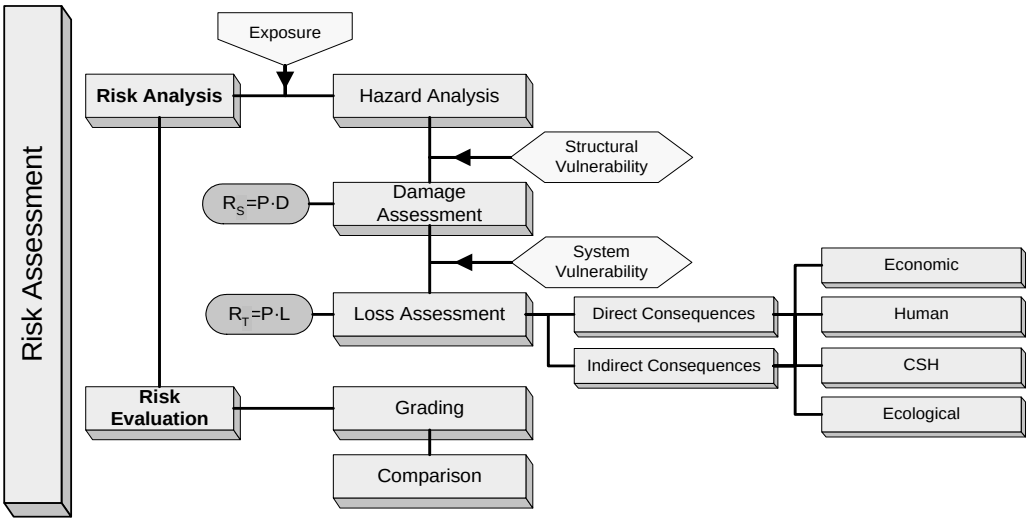

Figure 2.15 Risk Assessment phase of the RMP developed within the IGC 802 [Pliefke et al., 2007]

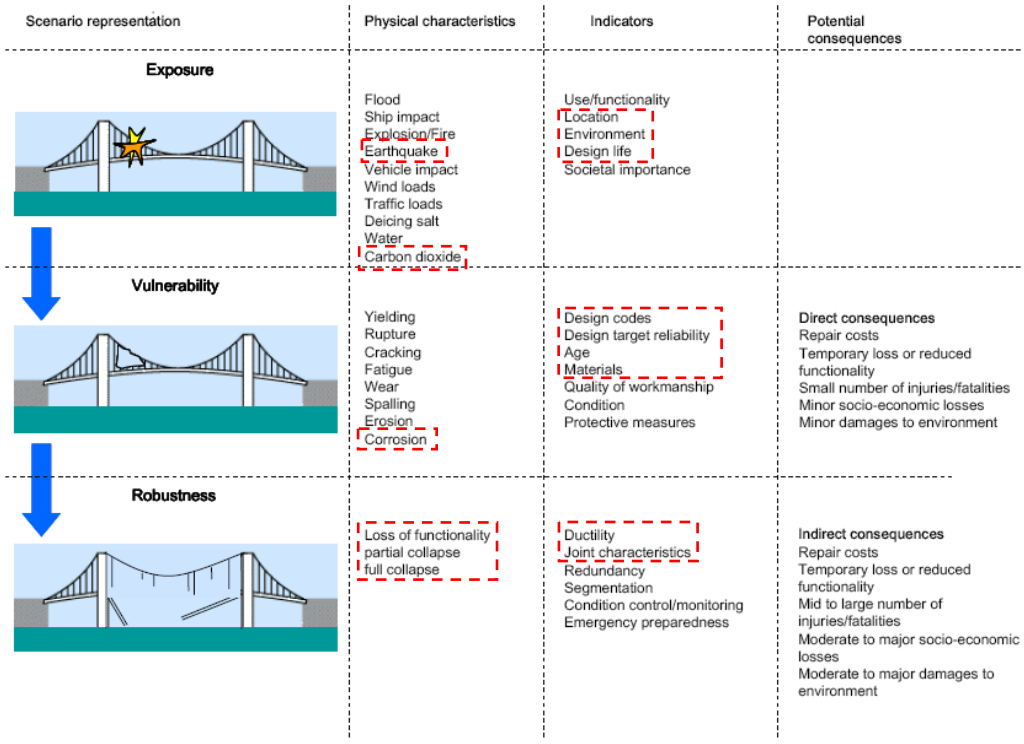

Figure 2.16 Physical characteristics, risk indicators and consequences in the system representation [Faber, 2007] (investigated aspects in evidence)

2.3.1 Risk Analysis

The Risk Analysis procedure starts with the *Hazard Analysis*, consisting in the evaluation of the intensity and frequency parameters of each hazard type identified in the Risk Identification phase with respect to the considered system.

A hazard can be in general a storm or a flood, as well as a certain magnitude earthquake or a certain category hurricane, and can be measured in [Intensity measure/time unit]. Independently from the different definitions belonging to each specific discipline, the hazard is characterized by the notion of probability or likelihood of occurrence. A hazard is not an event itself, but it is a threat which can manifest itself in an actual harmful event. Every specific hazard magnitude is related to a site-specific return period T_R, defined as:

$$T_R = -\frac{T_d}{\ln\left(1-P_f\right)} \tag{2.1}$$

where T_d is the service life of the structure and P_f is the probability of exceedance. For example, the probability of exceedance of 10% in 50 years of an earthquake corresponds to a return period of 475 years. Some indicative values for the design service life are given by [CEB-FIP, 2006] in relation to the structural typology (Table 2.5).

As for the topic of the present thesis, the task of this phase is mainly the quantification of the corrosive attack and the calculation of its probability of occurrence, as it will be described in Section 5.4.

Table 2.5 Indicative values for the design service life [CEB-FIP, 2006]

Design service life [yr]	Structural type
10	Temporary structures
10-25	Replaceable structural parts, e.g. gantry girders, bearings
15-30	Agricultural and similar structures
50	Building structures and common structures
100	Monumental buildings, bridges and other civil engineering structures

Afterwards, depending on the hazard under consideration and on the quantified hazard data, it is necessary to subdivide the components of the system into "elements at non risk" (EaNR) and "elements at risk" (EaR). Therefore, *Exposure* defines the number of EaR that may be affected by the considered harmful event, and it can be measured as a dimensionless factor between 0 and 1. The EaNR, being by definition not exposed to the hazard, can be excluded from the further analysis. On the contrary, the EaR are exposed and consequently may be endangered by the impact of the hazard. An EaR can be a building or an infrastructure and it is characterized by several parameters that have to be determined: precise location within the system, information about the functional use (residential, commercial, industrial), occupancy (inventory of contents, number of people living or working inside) and construction type (building materials, number of storeys, year of construction).

In order to reduce the complexity of the analysis, it is possible to group the elements at risk having similar characteristics into EaR classes and to perform the further analysis only on one typical EaR of the class, assuming that all the other elements of the same class will behave in a similar way. For instance, let us consider a reinforced concrete building. When considering a carbonation-induced corrosive attack, it is obvious that not all the structural elements (beams, columns, foundation system) are equally exposed. The EaR class may be composed by the external beams and columns, especially the ones located at the corners of the building and along

the perimeter, while the other internal members, being not exposed, will form the EaNR class. Different considerations may be done in case of a chloride-induced attack, since the identification of the most exposed elements generally depends on the relative collocation of the source of the attack respect to the system components. The example of the earthquake occurred in Turkey, cited in Section 2.2, represents an extreme case in which the presence of the aggressive agent inside the concrete mix makes all the structural elements potentially at risk, independently from their location respect to the surrounding environment.

After the EaR classes identification, the structural response of each EaR (or EaR class) to the considered hazard has to be predicted and the *Determination of Damage* phase initiates. It is important to emphasize that damage is not measured in monetary units, but only in physical terms, e.g. water height, crack width, storey drift.

The relation between the hazard loading and the resulting damage is called *Structural Vulnerability* (see also Section 2.3.1.1), that is a peculiar characteristic of the EaR (or EaR class) indicating the degree of physical susceptibility towards the impact of the hazard. Vulnerability can be measured as [Damage measure/intensity measure].

In the context of the hazards dealt with in the present dissertation, damage related to corrosion may be defined locally in terms of reduction of concrete area (due to cracking and cover spalling), reduction of steel cross-section and failure of bond between reinforcement and surrounding concrete associated with the occurrence of bar slippage. Form a global point of view, damage due to the combined action of corrosion and seismic shaking may be ascribed to the reduction of resistance and structural ductility of the damaged construction respect to the undamaged condition.

In [Fischer et al., 2002] damage is defined as the "distance" between the current state of the structure and the controlling collapse mechanism. For the damage assessment, the authors adopt the fuzzy logic, i.e. a membership between an element x to a set A measured by a characteristic function $m_A(x)$ whose possible values are contained in the range [0, 1]. The value 1 means that x completely belongs to A. With these assumptions, five fuzzy sets are considered as damage levels: none (N), small (S), medium (M), large (L) and total (T). The identification of the damage levels may be performed quite easily by an expert, otherwise a photographic guide may be useful to recognize the different damage levels in typical structures. On this context, a useful tool could be provided by the EMS-98 classification (see §2.3.1.1 and APPENDIX A)

After the Determination of Damage, the *Loss Assessment* has to be performed. The consequences endured by the EaR (class) at a certain level of damage have to be investigated, taking into account the characteristic parameters of each EaR (class). These consequences may be direct or indirect. Direct consequences occur at the same time of the disaster and are directly connected to the capacity of the system to withstand the natural forces and to provide immediate help. Indirect consequences occur later in time, resulting from the direct consequences, and are related to the resilience, i.e. the capacity to maintain functionality and to assure recover after the disaster. A further subdivision of each consequence class is given into tangible consequences, that are economic consequences directly measurable in monetary units, and intangible consequences, that can not be directly quantified, i.e. human consequences (e.g. injuries and fatalities), CSH consequences (i.e. loss of cultural social and historical values), ecological consequences (e.g. pollution of the environment).

As for RC structures subject to corrosion, inspection and maintenance planning allow the assessment of the present condition and the even more important prediction of the future development of structural degradation. As for the economic consequences, a fundamental topic is the concept of optimization of the costs related to the service life economic risks, i.e. the

minimization of the costs for inspection and testing, the costs for maintenance and strengthening strategies composed of preventive and corrective repair measures, as well as the costs due to future failures. It is shown, [Faber, 2002], that for a structure affected by corrosion, half-cell potential measurements may be utilized to update the probability of excessive repair after for example 50 years.
Figure 2.17 and Table 2.6 show the so called "law of five" by De Sitter, according to which the repairing costs for RC structures increase exponentially with the degradation level at the moment of the intervention. The cost of adequate prevention carried out during the stages of design and execution are minimal compared to the savings they make possible during the service life and even more compared to the cost of rehabilitation. The "law of five" can be stated as follows: one euro spent in getting the structure designed and built correctly is as effective as spending 5 euro when the structure has been constructed but corrosion has yet to start, 25 euro when corrosion has started at some points, 125 euro when corrosion has become widespread.
This evidences the interest in monitoring the health state of the construction in order to detect unfavourable degradation phenomena at their very onset.

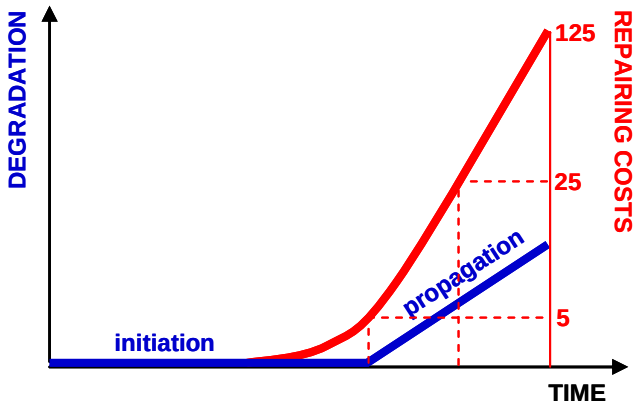

Figure 2.17 The "law of five" by De Sitter in Tuutti's diagram

Table 2.6 The "law of five" by De Sitter

Actual phases within structural life	Relative costs
Conceptional planning, design (expert judgement), construction	1
Production phase and use of the structure	5
Small repair (maintenance)	25
Extensive repair (bearing structure change), possible destruction	125

The direct relation between the Hazard and the consequential Loss is called *System Vulnerability*, indicating the total potential the hazard has on the EaR (class). The System Vulnerability can be measured as [Loss measure/intensity measure].
Afterwards, the quantification of risk has to be performed, according to two possible definitions: *Structural Risk* and *Total Risk*.
The *Structural Risk* can be calculated as the annual probability of occurrence of the *Hazard* multiplied by the correspondent expected *Damage*, measured in [Damage measure/year]:

$$R_S = Probability \times Damage \tag{2.2}$$

The Total Risk can be expressed as the product between the annual probability of occurrence of the Hazard and the expected Loss, measured in [Loss unit/year]:

$$R_T = Probability \times Loss \tag{2.3}$$

On the one hand, the Structural Risk is of major importance for engineers, since it allows the prediction of the structural behaviour and of the response of a structure or structural element under a potential hazard loading. On the other hand, the Total Risk is more exhaustive, since it may comprise the full hazard potential accounting for tangible as well as intangible consequences to the system. As a matter of fact, from the previous definitions it ensues that two identical buildings struck by the same *Hazard*, with the same *Probability* and expected *Damage*, will be characterized by the same *Structural Risk*. But, if we consider, for example, also the use of the structure (e.g. if one of the two buildings contains valuable goods, such as works of art, or is occupied in average by a greater number of people) the *Total Risk* may be significantly different. Nevertheless, the problem of the conversion of non appraisable consequences into monetary units has to be solved. Alternatively, the *Total Risk* can be split into the relative contributions of each consequence class.
In the present thesis, only the *Structural Risk* throughout the structure's service life is investigated, while the *Loss Assessment* and the *Risk Evaluation* phases are not included in the analysis. In particular, given that two hazards endanger simultaneously the building under consideration, i.e. reinforcement corrosion and seismic shaking, *Probability* in Eq.(2.2) is split into two components:

$$Probability = P(corr) \times P(seism) \tag{2.4}$$

where *P(corr)* and *P(seism)* are respectively the likelihood of occurrence of corrosion and earthquake excitation, calculated as described in Section 6.2.4. The two hazards are reasonably assumed to be mutually independent, since the occurrence of one event makes it neither more nor less probable that the other occurs, thus allowing calculating the total probability according to Eq.(2.4), i.e. as for uncorrelated events.
Moreover, *Damage* in Eq.(2.2) is identified with the consequences of the seismic action on the corroding structure, suitably merging the effects of the two perilous events, as explained in the application of the methodology to the case studies (Section 6.2.7).
For the sake of completeness, another expression to define disaster risk from the engineering point of view should be mentioned:

$$Risk = Hazard \times Vulnerability \times Exposure \tag{2.5}$$

According to [Pliefke et al., 2007], this formula, given the additional *Exposure* multiplier, suits better for the analysis of entire systems, composed of both endangered objects (EaR) and non endangered ones (EaNR). Nonetheless, when *Structural Vulnerability* is taken into consideration, definition (2.5) is conceptually equivalent to definition (2.2), as *Structural Vulnerability* links the *Hazard* to the *Damage* state of each exposed element and the *Hazard* impact is implicit in the *Probability* multiplier. As for the present thesis, the risk formula (2.2) best fits with the subject and aim of the research, given that the analysed building is totally exposed to the hazards. If the *System Vulnerability* is used instead, expression (2.5) is analogous to expression (2.3), since *System Vulnerability* connects the *Hazard* module directly to the *Loss* of the system or of the single EaR, by incorporating all direct and indirect consequences that might go in line with the disaster and transforming them to the time the disaster takes place.

2.3.1.1 Structural vulnerability

The European Macroseismic Scale, [EMS-98, 1998], proposes a differentiation of structures (buildings in particular) into six vulnerability classes, as shown in APPENDIX A. Four building typologies are included, i.e. masonry, reinforced concrete, steel and wood structures. For each type, the table indicates with a circle the most likely vulnerability class(es) and with a line the probable range (dashed line where this is uncertain).
A classification of damage for RC buildings is also suggested by [EMS-98, 1998] (APPENDIX A). Five damage grades are identified, approximately representing the increase in the strength of shaking. It should be noted that not all possible combinations of vulnerability class and damage grade are mentioned for each degree of the scale. It is assumed that proportionate numbers of buildings will suffer lower grades of damage. It is also important to distinguish between structural and non-structural damage, and between damage to the primary (i.e. load bearing/structural) system and damage to the secondary (i.e. non-structural) elements (e.g. infills or curtain walls).

Figure 2.18 Example of damage (a) grade 3 and (b) grade 4 on RC buildings [EMS-98, 1998]

Figure 2.19 Examples of damage grade 5 on RC buildings [EMS-98, 1998]

Figure 2.18a shows an example of a RC frame building damaged by an earthquake occurred in Mexico City in 1985. The structure suffered cracks in columns and infill walls with detachment of pieces of plaster. Partial failure of the brick infills also occurred in some zones of the building. Overall, the structural damage (to the columns) is moderate and the non-structural damage (to the infills) is heavy. Consequently, the damage level may be identified with grade 3. A more severe damage was undertaken by the RC frame shown in Figure 2.18b, after Irpinia earthquake, in Sant' Angelo dei Lombardi, Basilicata, Italy (1987). Several exterior infills failed entirely, resulting in a very heavy non-structural damage. In some cases, also beam-column joints were seriously damaged. This is an example of damage grade 4. Finally, two cases of damage grade 5 are shown in Figure 2.19. In particular, the picture on the left portrays a RC framed building after North Pelopponissos earthquake, Aegion, Greece (1995), in which the middle part of the structure entirely collapsed. The figure on the right shows a RC wall building after Great Hanshin earthquake, occurred in Kobe, Japan in 1995, in which the ground floor completely failed.
Finally, in APPENDIX A the short form of the EMS-98 intensity degrees is provided, giving a simplified and generalized view of the EM Scale.

2.3.2 Risk Evaluation

After the Risk Analysis phase is concluded, the Risk Evaluation module starts. In this procedure, by means of adequate risk measures, the risk under consideration is compared to other risks that may affect the system. To this aim, exceedance probability (EP) curves are commonly adopted for the graphical representation of risk. In these curves, the probability that a certain level of loss is exceeded in a specific time period is plotted against different loss levels, which may be expressed in monetary terms, fatalities or other proper measures.
Figure 2.20 illustrates an example of an EP curve for dollar losses to homes in Los Angeles from an earthquake, [Kunreuther, 2004], built by combining the set of events that could produce a given loss and then determining the resulting probabilities of exceeding losses of different magnitudes. In this way, both uncertainties associated with the probability of occurrence of an event and the magnitude of dollar losses are included. This uncertainty is reflected in the 5% and 95% confidence interval curves in the figure.

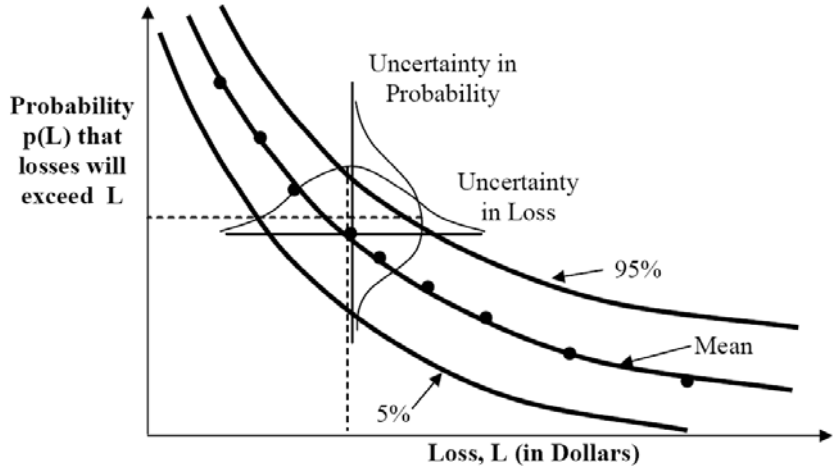

Figure 2.20 Example of exceedance probability curves [Kunreuther, 2004]

2.4 Risk Treatment

The last of the three sub-procedures into which the RMP is subdivided is the Risk Treatment phase (Figure 2.21). On the basis of mathematical and economic theories, this procedure consists in deriving a *Decision* about the way to handle risk in presence of other competing risks, choosing between *Reduction*, *Transfer*, *Acceptance* or *Rejection* of the risk.

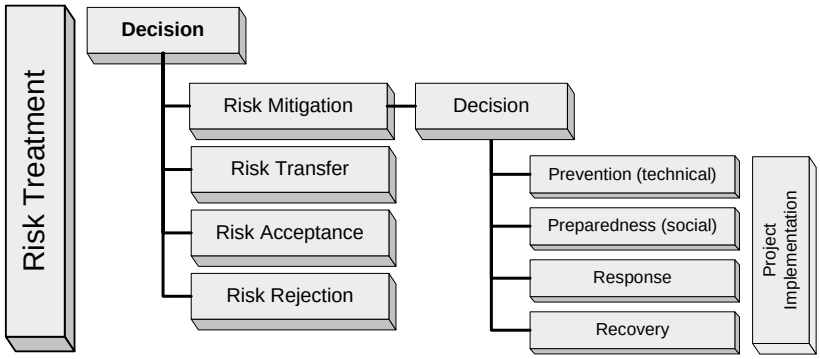

Figure 2.21 Risk Treatment phase of the RMP developed within the IGC 802 [Pliefke et al., 2007]

If the risk reduction project is intended to be performed, several *Risk Mitigation* initiatives may be implemented, in order to reduce the vulnerability of the system.
Pre-disaster and post-disaster interventions can be distinguished. Technical *Prevention* strategies (e.g. structural strengthening and construction detailing improving seismic resistance, dampers against dynamic actions or dykes against floods) and social *Preparedness* (e.g. evacuation plans and emergency training) are pre-disaster interventions. Among the post-disaster strategies, *Response* represents all the activities performed immediately after the disaster, such as the organization of help and shelter for the injured, as well as the coordination of emergency forces, while *Recovery* covers the activities necessary until the pre-disaster status of the system is restored.
With reference to new structures, the compliance with the recent durability codes, e.g. [CEB-FIP, 2006], for example in terms of prescriptions for concrete mix design and minimum concrete cover, as well as inspection and maintenance, should guarantee a satisfactory response of the structure to environmental attacks and assure the fulfilment of the risk reduction. Similar considerations can be drawn for the observance of the seismic design codes. Concerning existing buildings, the matter is obviously more challenging, since prevention initiatives have to be carefully planned in order to preserve the regularity of the structure in terms of strength and stiffness ratios between the structural elements and not to reduce the global ductility by means of local interventions.
Detailed information on the decision analysis in the framework of structural reassessment is available in the Probabilistic Assessment of Existing Structures by [JCSS, 2001].
However, it should be emphasized that guidelines and recommendations proposed by the Codes are still not exhaustive to date, even tough an appreciable effort has been done in the last decade.

The procedure for managing risk presented in this chapter has the advantage of being sufficiently general to be applicable to a number of different fields. The possibility to follow this approach in the specific context of the present work will be illustrated in CHAPTER 6 with the application to real case studies, for which the risk management procedure (RMP) constitutes the backbone of the assessment methodology.

CHAPTER 3 THE CORROSION RISK MANAGEMENT

In the present thesis, reinforcing steel corrosion, in combination with seismic excitation, constitutes the Hazard of the RMP. In view of the complexity of such phenomenon and the importance of its accurate evaluation, a specific procedure for managing corrosion risk has been developed and is presented in this chapter. This approach provides a rigorous and coherent tool to be used when dealing with the safety assessment of corroding RC members.

3.1 Introduction

The Hazard Analysis phase of the Risk Assessment step described in Chapter 2 is herein treated as a *Corrosion Risk Management Chain* within the main Risk Management Process, with the aim to specifically treat risk due to corrosive attacks (Figure 3.1).

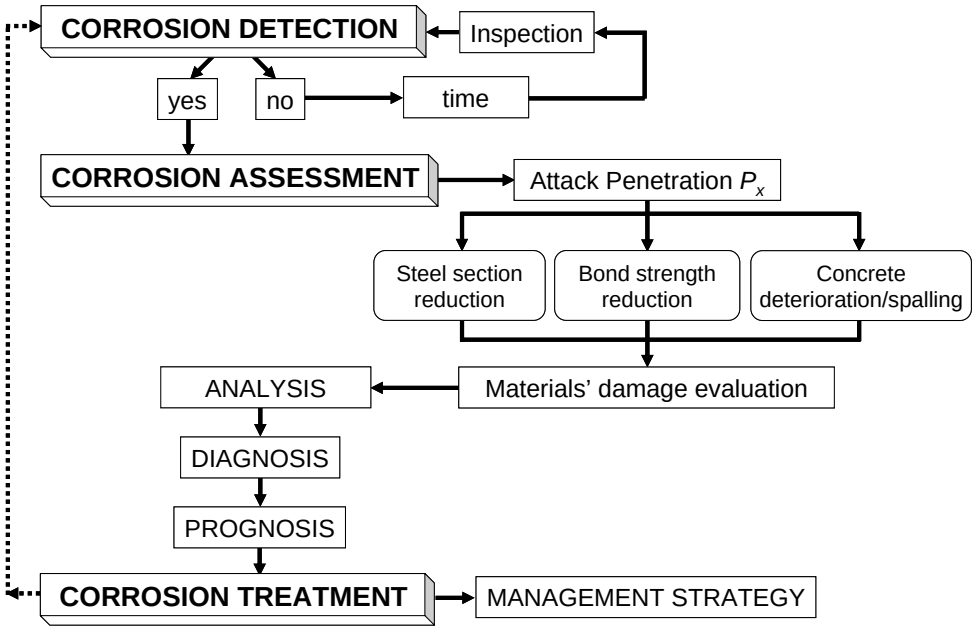

Figure 3.1 The proposed Corrosion Risk Management Process

The same subdivision in three major phases as in the RMP is adopted for the proposed sub-procedure: first the *Corrosion Risk Detection* phase, in which the potential presence of an ongoing corrosion attack in the considered structure is revealed by means of inspection techniques, providing information with different levels of accuracy (from a first rough visual inspection to a more sophisticated investigation, e.g. through corrosion rate sensors). As corrosion has been detected, the *Corrosion Risk Assessment* phase starts, implying the evaluation of the corrosion attack penetration and the correspondent damage on the materials. Thus, the *Analysis* is performed, including the effects of corrosion on steel, concrete and the interfacial layer between them. Afterwards, the *Diagnosis* and *Prognosis* on the structural member health condition are

formulated, providing the basis for the concluding *Corrosion Risk Treatment* phase, in which recommendations are given on the frequency of future inspections and the urgency of intervention.
Of interest, the procedure proposed by [Rodriguez et al., 2001] for evaluating the Index of Structural Damage ISD of corrosion-affected RC structures (Figure 3.2) can be easily associated with the RMP composition: Step 1 corresponds to the Hazard Analysis; Step 2 the Structural Vulnerability assessment, while Step 3 is the Damage Evaluation phase.
The suggested procedure is explained more in detail in the following sections.

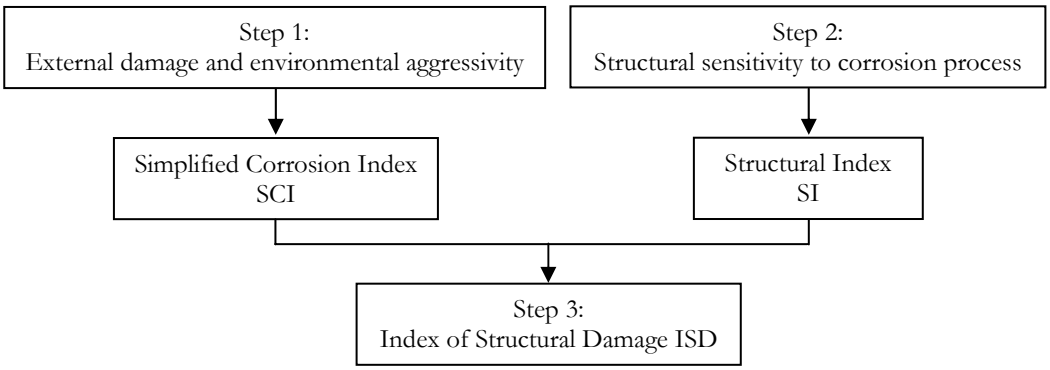

Figure 3.2 Structural damage calculation for corroding RC structures [Rodriguez et al., 2001]

3.2 Corrosion Risk Detection (Inspection phase)

In the first phase, corrosive attacks in progress must be detected by means of inspection. Half-cell potential measurements may be adopted, indicating whether corrosion has initiated or not and thus providing a support in deciding the planning of protective and corrective maintenance measures.
The importance of a prompt detection of an ongoing corrosion attack is evident. Indeed, if the progress of deterioration is recognized at an early stage, minor and relatively inexpensive interventions may be sufficient to reduce the risk of major and expensive future repairs (see Table 2.6). Obviously, all these considerations are strongly related to the importance of the structure under investigation.
Thus, the task of the Inspection Phase is the collection of data necessary as input for the subsequent Corrosion Assessment. Three steps may be distinguished within the Detection Phase: preliminary visual inspection, desk work, in-situ testing.
These steps can be carried on separately or simultaneously, and the first and the last may be merged together if enough information is supplied.

3.2.1 Preliminary visual inspection

Specific provisions on the procedure to be implemented for the inspection of a structure are given in general by the Codes or by the structures' owners and may depend on their experiences and available recourses for the maintenance interventions.
According to [Rodriguez et al., 2001], the following three aspects should be accounted for:

- structural typology: all the components of the structural system must be identified and the most critical elements, i.e. the elements at risk (EaR), must be isolated;

- exposure aggressivity: among the several classifications available in the literature and in the Codes, the exposure classes given by EN 206 are suggested (see APPENDIX B);
- damage level: a preliminary classification may consist of damages due to structural behaviour (e.g. cracks due to shear effects) and damages due to corrosion (e.g. cracking, delamination, spalling).

Concerning corrosion-induced damages, [Rodriguez et al., 2001] identifies three major types:

- rust spots deriving from corrosion products;
- cracking, usually parallel to the reinforcing bars, so that they can be distinguished from cracks of structural nature;
- cover spalling, due to the expansive action of corrosion products forming on the steel bar surface, normally located on compression zones of bending elements or in columns.

Figure 3.3 shows a useful sketch to identify and localise damages in a RC column.

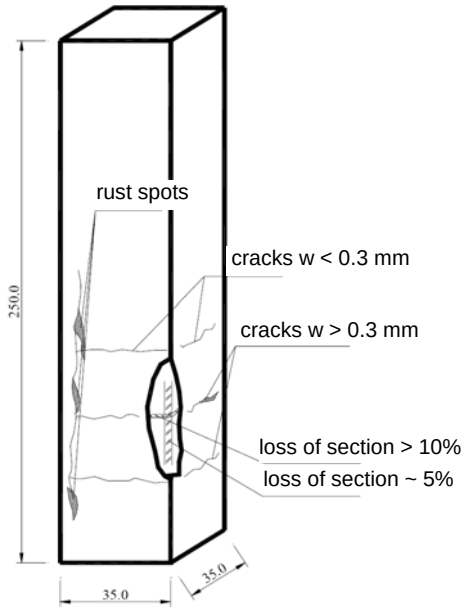

Figure 3.3 Damage identification and localisation [Rodriguez et al., 2001]

3.2.2 Desk work

Desk work consists in collecting data concerning the background of the structure (e.g. age of construction, as built drawings if available, information on previous interventions, etc.), identification of exposure aggressivity (e.g. on the basis of EN 206) and classification of damages as a function of indicative parameters, such as concrete properties, penetration depth, concrete cover, bar diameter reduction, corrosion rate, resistivity.

3.2.3 In-situ testing

The number of in-situ tests to perform should be as smallest as possible, both to preserve the integrity of the structure and to limit the costs. The tests which are considered compulsory according to [Rodriguez et al., 2001] concern: elements geometry, materials strength, reinforcement detailing mechanisms of penetration of aggressive agents and deterioration, corrosion rate.

In the present thesis, special attention is paid to the estimation of the corrosion rate, being one of the most unpredictable parameters influencing the calculation of the corrosion-induced loss of steel section. As a matter of fact, it is well known that the rate of steel corrosion may vary significantly, both within the same structural member and over time.
Structural health monitoring (SHM) techniques can largely improve the quantification of corrosion rate and consequently the evaluation of structural safety. Using a considerable number of corrosion rate sensors placed throughout the component under investigation, the spatial and temporal variations of corrosion rate may be monitored and predicted, allowing the collection of more reliable input data for the following analyses, as described in [Marsh and Frangopol, 2007].
In recent times, SHM programs adopting permanently embedded sensors have become progressively more established, in particular for critical structures, such as RC bridges. This technique allows detecting any anomalous behaviour from its first commencement, providing continual real-time data. In contrast hand-held portable sensors give only discrete-in-time data.
[Grantham et al., 1997] present an interesting example of the practical application of inspection and corrosion rate measurement techniques to a real case. The structure to be assessed was a four-level RC car park, under a multi-storey building. Serious deterioration and severe reinforcement corrosion due to the carriage of de-icing salts on the underside of the cars were detected. An initial survey revealed that the concrete in the slabs was of very low quality and the concrete cover was extremely variable and often inadequate. The assessment comprised first a visual inspection, followed by half-cell potential measurements, chemical analyses to estimate cement and chloride contents and a detailed petrographic appraisal of concrete. The linear polarization technique was adopted for corrosion rate measurement. Different surveys were performed in successive periods. At the time of the first investigation, i.e. at the end of autumn period, it was found that the corrosion rate was reasonably low, with an average value of 0.24 $\mu A/cm^2$. Further monitoring over the first year was recommended to check corrosion rates over the different seasons. The second survey revealed a sensible variation in the measurements and corrosion rates doubled between the end of the autumn and the end of the winter periods, reaching an average value of 0.52 $\mu A/cm^2$. This confirms the necessity not to rely on a single set of data readings when undertaking this type of task, since measurements strongly depend on seasonal variations.
A non destructive method for corrosion initiation detection in concrete members is proposed in [Budelmann and Holst, 2008], based on novel calibration-free mini-sensors consisting of this iron filaments.

3.2.4 Exposure levels

As for *Exposure* and the identification of the EaR, it is convenient to distinguish, in relation to the topic of the present dissertation, and especially with regard to corrosion, between three different levels:

- territory exposure: which buildings in a certain region/area are exposed to the *Hazard*?
- construction exposure: which structural elements of the building are exposed?
- member exposure: which parts of the structural element are exposed?

The identification of the buildings at risk at a territory level, for example, may be extremely useful to identify the targets of the most urgent interventions to be funded by a public administration within a certain municipality or district. This is meant as a preliminary rough selection and recognition of the constructions for which subsequent more detailed numerical and in-situ investigations will be carried on, as described in Section 6.2.9.

In the present dissertation two hazards are considered to simultaneously endanger the system under consideration, i.e. earthquake and corrosion. A possible approach for the identification of the "seismic-corrosion-EaR" is the superposition of the map of the region to investigate with the hazard maps of the two harmful events. Concerning earthquakes, hazard maps and seismic microzoning studies are often available, e.g. the seismic maps provided by [OPCM 3519, 2006] as a result of the new seismic classification of the Italian territory (see as an example Figure 6.14). This holds not true for corrosion, since such databases do not exist to date. Nevertheless, a "carbonation hazard map" could be created using the carbon dioxide maps plotted by software for the analysis of environmental pollution. As an example, the program DISPER 4.0 (the demo version is available on line) calculates the pollutant concentration in each point of the air considering all pollutant sources and conditions of the atmosphere, plotting the results in terms of isolines. Thus, the pollutant map can be superimposed with the map of the region to investigate, as shown in Figure 3.4. Afterwards, in order to create a "seismic-corrosion hazard map" a further superposition should be done between the "carbonation hazard map" and the "seismic hazard map", allowing the identification of the buildings most exposed to the combined effects of a seismic shaking and a corrosion attack of certain intensities.

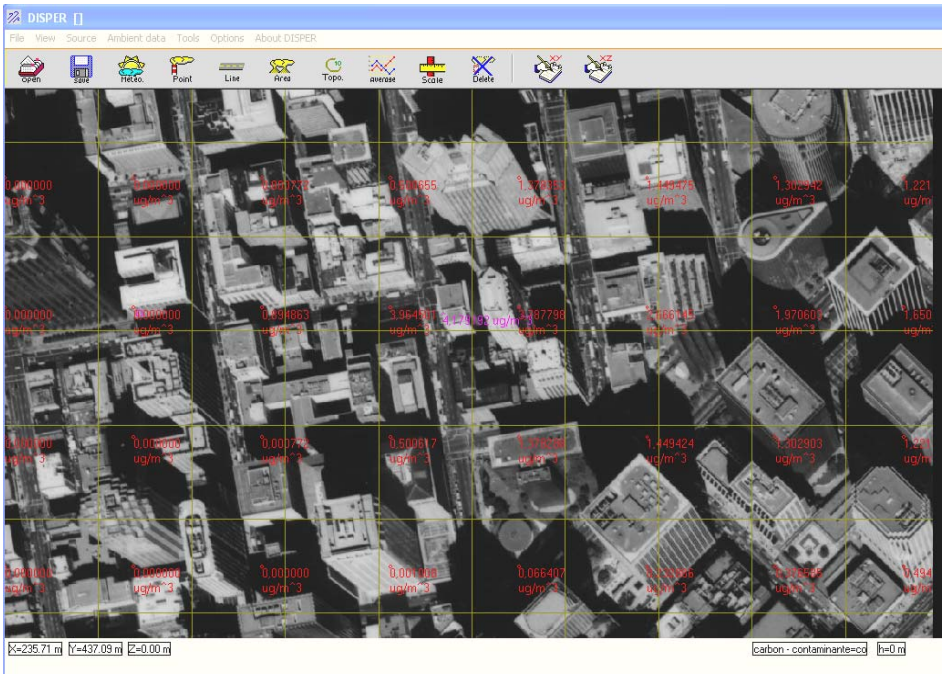

Figure 3.4 Example of "carbonation hazard map": CO_2 concentration values (in red) for given environmental conditions (max value in pink) plotted on the map of an area to investigate

3.3 Corrosion Risk Assessment

As in the main RMP, the Corrosion Assessment Phase is the most relevant module. At this step, the extent of the corrosion attack is evaluated, in relation to both the present performance of the structure (*Diagnosis*) and its future evolution (*Prognosis*). The formulation of the diagnosis makes use of all data collected in the inspection phase, with the purpose of establishing whether corrosion has started or not. If the answer is affirmative, the corrosion penetration attack is calculated, as well as the correspondent damage on the materials' properties.

The Prognosis may be formulated for example according to [Rodriguez et al., 2001] in terms of urgency of intervention, which is ranked in four different levels depending on the severity of the corrosion-induced damage. Further details are endowed with in the cited work, while a schematic representation of the procedure suggested by Rodriguez is given in Figure 3.5.
With regard to durability prognosis of RC structures, an adaptive model to be used as a component of a predictive life cycle management system is proposed in [Rigo et al., 2005]. The model uses information deriving from inspection or monitoring to improve the prognosis by updating. An application to expanding chemical attacks on concrete under real exposure conditions is described in [Budelmann, 2008]

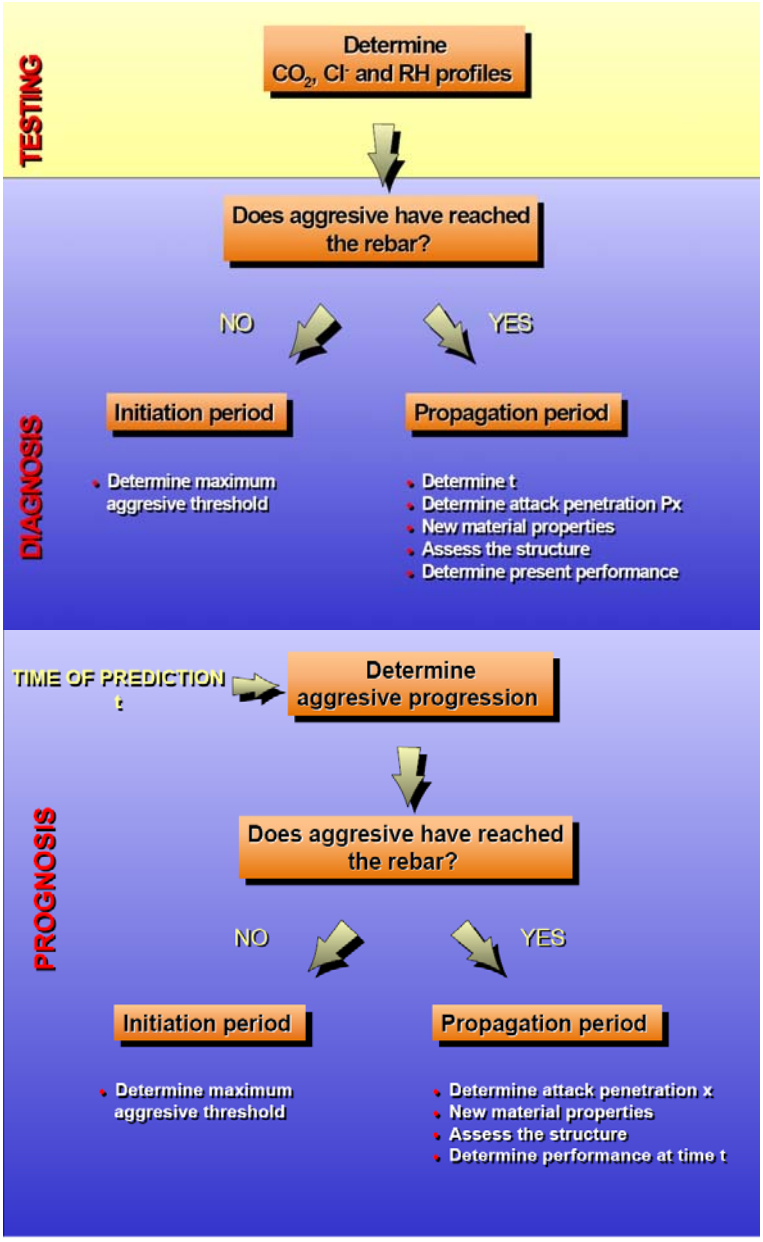

Figure 3.5 Diagnosis and prognosis processes [Rodriguez et al., 2001]

3.4 Corrosion Risk Treatment

In this concluding phase, the management strategy to be pursued for dealing with corrosion risk is presented. The present PhD thesis does not include the Risk Treatment phase. Nevertheless, some considerations are herein proposed. In particular, future research could be addressed to the investigation of prevention initiatives for Risk Mitigation, such as measures for avoiding or at least reducing the penetration of aggressive agents inside the concrete matrix, e.g. by means of protective painting or cathodic protection. Especially for carbonation-induced corrosion, proper compaction (aiming at reducing the w/c ratio) and curing of the concrete cover help to reduce the diffusivity of carbon dioxide, and consequently the rate of carbonation (see e.g. Figure 5.18). Furthermore, the detrimental effect of a lower $Ca(OH)_2$ reserve in concretes containing supplementary cementing materials can also be compensated by reducing their w/c ratio and increasing the curing regime. In this way it is possible to prevent the reinforcement depassivation, which is the well-known cause for the onset of corrosion processes. As a matter of fact, even if carbonation of the outer concrete layers cannot be avoided, the rate of carbonation progress can be maintained sufficiently low, so that the pollutant does not reach the reinforcement surface during the service life of the structure. This should be the aim of modern design, [Saetta et al., 1993a].
As for repair and rehabilitation interventions, a technique commonly used to recover RC members affected by reinforcement corrosion, especially in tidal environments, comprises the following steps: removal of damaged concrete outer layers; application on the reinforcing steel with a corrosion inhibitor solution (e.g. nitrite salts, borate salts, amine salts, oxygenated hydrocarbons) and saturation of the concrete surrounding the rebars; application of a new concrete cover with the same modulus of elasticity as the removed material. The passivating painting is generally sprayed, if necessary in multiple spray applications at opportune time intervals.
Both protection and repair of corroding members may be obtained also with fibre reinforced polymer (FRP) wraps, providing confinement to the expansive forces caused by reinforcing bar corrosion and thus enhancing the structural performance. Experimental tests about the utilization of FRP protection of three different types (glass, carbon or aramid) are proposed in [Neale et al., 2005].

In this chapter, a procedure similar, for its arrangement, to the main RMP has been proposed for evaluating reinforcement corrosion and its impacts on RC members. Moreover, in view of the considerable number of parameters involved in the problem and the high level of uncertainty affecting them, the assessment phase of the procedure is dealt with in a probabilistic framework in CHAPTER 5. Afterwards, the method is applied for predicting the seismic response of a RC structure at the end of its service life, in presence of a corrosive attack of moderate intensity which may be ascribed to spread carbonation (CHAPTER 6).

CHAPTER 4 REINFORCEMENT CORROSION

In CHAPTER 3 a general procedure for managing corrosion-induced risk on RC structures has been presented. CHAPTER 4 aims at investigating more in detail the complex phenomenon of reinforcement corrosion, recognised as one of the major causes of degradation in these types of structures. Attention is focused on the consequences of steel corrosion on the structural response of RC members, emphasizing the major aspects which are then numerically modelled in Section 4.4 with regard to the local effects on the steel-concrete bond behaviour, and in CHAPTER 6 considering the global effects on real RC buildings.

4.1 Introduction

In the modern design of reinforced concrete structures, a reliable estimation of the deterioration level plays a crucial role, especially in seismic prone areas. These considerations may be referred to both new constructions and existing buildings needing retrofit and/or strengthening interventions, since the response to external excitations changes with the increasing degree of structural damage.

The variation of the mechanical characteristics of the materials over time is a consequence of the chemical, physical and environmental attacks that the structure may suffer during its service life. Several RC buildings are affected by visible signs of degradation as well as invisible defects, even if constructed in recent times. Primarily this occurs in particularly aggressive environments (e.g. tidal or industrial scenarios) and when poor quality materials (e.g. low concrete grades) or not controlled techniques (e.g. absence of detailing practices) are adopted.

It is usually very difficult to identify the initial reason why reinforced concrete is no longer able to withstand external or internal attacks, since deterioration and failure generally stem from more than one cause, [Saetta et al., 1995]. Experience shows that reinforcement corrosion is one of the most dangerous sources of degradation, producing detrimental effects on stiffness, ductility and deformation capacity of exposed RC members, whose reliable strength may be significantly compromised. For this reason, steel corrosion is a critical parameter in assessing the residual strength and service life of aged RC constructions.

Among the most frequent environmental attacks leading to corrosion, concrete carbonation (Figure 4.1) and the penetration of chloride ions in tidal environments (Figure 4.2a) or due to the use of deicing salts (Figure 4.2b) should be mentioned, e.g. [CEB-FIP, 2006].

The penetration of chlorides normally induces a localized attack on the steel bar surface (the so called "pitting corrosion"), while concrete carbonation usually produces a uniformly distributed attack.

In general, chlorides penetration is a problem typical of countries like North America or Germany, where this is the primary mechanism of deterioration due to the extensive use of deicing salts during wintertime. On the contrary, carbonation-induced corrosion is often the major problem in old-aged European concrete buildings, [Marie-Victoire et al., 2006]. Nevertheless, according to [CEB-FIP, 2006] (Figure 4.3), the concentration of carbon dioxide in the atmosphere (generally in the range of 0.03 percent by volume) has increased over the last 50 years to such an extent that deterioration due to carbonation has become more likely to occur.

Figure 4.1 Carbonation-induced corrosion after 50 years service life (Istituto Marchiondi, Milan, Italy) [Pedeferri, 2005]

Figure 4.2 Chloride-induced corrosion (a) in tidal environment (Manfredonia harbour, Italy) and (b) produced by deicing salts (bridge in Cisa highway, Italy) [Pedeferri, 2005]

Of interest, highest rates have been found inside buildings, whereas lowest rates have been reported in coastal areas, [Tesfamariam and Martín-Pérez, 2008]. In addition, the increasing use of supplementary cementing materials in the concrete mix (especially high levels of fly ash up to 50% of cement weight) leads to higher penetration depths, especially in poorly cured, low strength concrete. This makes concrete more vulnerable to carbonation than Portland cement concrete, for given w/c ratio and exposure conditions, [Thomas, 2004].

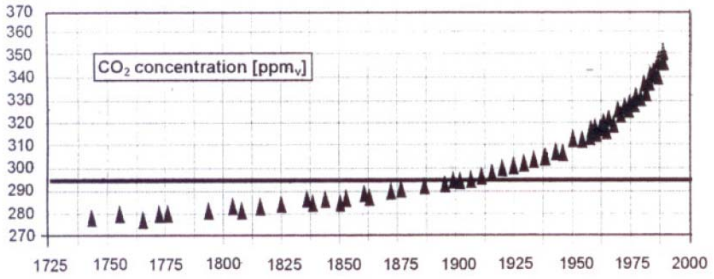

Figure 4.3 Progress of carbon dioxide concentrations in the atmosphere [CEB-FIP, 2006]

In recent years, extensive progress has been made in the early detection of corrosion problems, as well as in understanding the causes and the mechanisms of reinforcement corrosion. To this aim, a number of researchers have worked on both the experimental and numerical investigation of such a complex phenomenon, demonstrating the worldwide growth of interest in this subject. Just to cite a few examples, [Almusallam et al., 1996a], [Mangat et al., 1999], [Castel et al., 2000a-b] and [Rodriguez et al., 1997] should be mentioned for their experimental studies in artificially induced corrosion conditions, and [Perno et al., 1999] for natural corrosion. Conversely, other authors, e.g. [Spacone et al., 2000], [Dekoster et al., 2003], [Coronelli and Gambarova, 2004], [Wang et al., 2006], have contributed to the numerical modelling of the behaviour of corroded RC members.

The modification of the mechanical characteristics of the structural elements due to corrosion may have noteworthy implications on their seismic behaviour, especially when the columns of frame buildings are affected (e.g. Figure 4.4a-b). If a structure is designed for a certain level of ductility and resistance in order to withstand a specific earthquake excitation with an adequate level of security, this capability may be not preserved over time. In fact, under corrosive attacks, a progressive loss of structural ductility may take place and consequently a decreasing capacity to dissipate energy.

In many cases, not only a reduction of the load bearing capacity, but also a significant variation of the failure mechanism, in particular from the ductile to the brittle type, is evidenced with increasing levels of corrosion. For example, the typical ductile collapse mode in which plasticity is concentrated at the beams' ends (Figure 4.5a) may be replaced by brittle mechanisms such as the soft-storey failure modes shown in Figure 4.5b-c.

Figure 4.4 Severe corrosion of RC columns due to (a) carbonation and (b) deicing salts spread by passing vehicles in an overpass [Pedeferri, 2005]

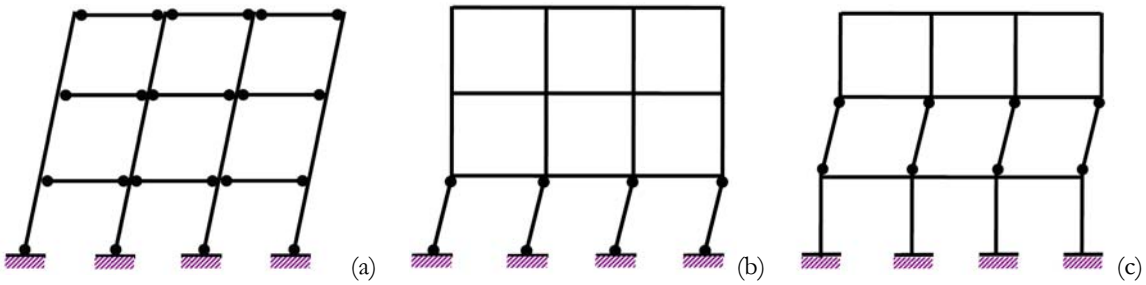

Figure 4.5 Failure mechanisms

In the following sections, the mechanisms of carbonation and chlorides penetration are described more in detail. Afterwards, the structural effects of corrosion are recalled and reviewed, with particular attention to the aspects included in the successive numerical investigations.

4.1.1 Carbonation-induced corrosion

It is important to emphasize that carbonation is in most instances not harmful for concrete itself, but it may be harmful for a RC member as it reduces the pH-value of the pore solution to such an extent that the embedded steel is no longer protected against corrosion, [CEB–FIP, 1992].

In particular, carbonation is caused by the penetration of atmospheric carbon dioxide into the concrete and by the chemical reaction with the calcium hydroxide of hydrated cement to form calcium carbonate. This reaction can be written as:

$$CO_2 + Ca(OH)_2 \overset{H_2O}{\rightarrow} CaCO_3 + H_2O \tag{4.1}$$

and it requires the presence of oxygen and water to be activated. Thus, whereas a dry concrete will promote the diffusion of carbon dioxide, the lack of moisture will stall the reaction given in Eq.(4.1). Hence, the diffusion of carbon dioxide within concrete is facilitated through aerated pores, but it is very slow when pores are filled with water (four to six orders of magnitude slower than in air), according to [Pedeferri and Bertolini, 2000].

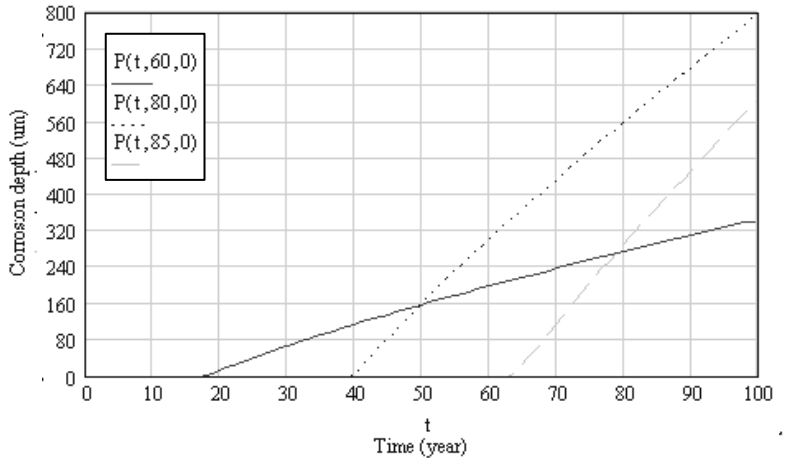

Figure 4.6 Effect of relative humidity on corrosion depth over time [Hallberg, 2005]

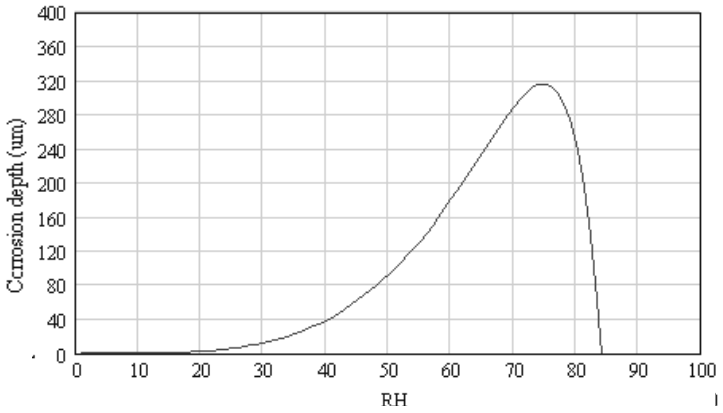

Figure 4.7 Variation of corrosion depth with relative humidity [Hallberg, 2005]

This trend is confirmed by the experimental evidence. For example, Figure 4.6 shows the variation of the carbonation depth over time for three different values of the relative humidity (60, 80, 85%) for a 56-year-old structure with a concrete cover of 15 mm, [Hallberg, 2005].
It can be observed that the higher the relative humidity, the higher the rate of corrosion (slope of the curves) and the later corrosion will begin. Moreover, according to Figure 4.7, the interval of optimum relative humidity for promoting carbonation has been observed to be 60% to 80%, as stated also in [Pedeferri and Bertolini, 2000].
The calcium carbonate produced in the reaction has the beneficial effect of filling the voids upon its precipitation, reducing the average pore size of the concrete. Nonetheless, the consumption of calcium hydroxide in the electrochemical reaction reduces the degree of alkalinity in the concrete pore solution, resulting in the depassivation of the reinforcing steel when the pH > 11.5 (passive status) falls below about 9 and consequently in the onset of the corrosion process.

Figure 4.8 Test with phenolphthalein solution to assess the carbonation depth [Pedeferri, 2005]

The most common method to detect the ongoing of a carbonation attack in concrete is to spray a freshly broken concrete surface with a pH indicator, e.g. a phenolphthalein solution. Uncarbonated concrete (with high pH values) turns pink, whereas carbonated concrete (with low pH values) remains colourless, [Tesfamariam and Martín-Pérez, 2008] (Figure 4.8).
Finally, another aspect should be noticed. For concretes made of Portland cements, the capillary porosity of the paste is significantly reduced by carbonation if the water/cement ratio is less than about 0.70. This may result in a considerable increase of compressive strength and of surface hardness of the concrete, [CEB-FIP, 1992].

4.1.2 Chloride-induced corrosion

Chlorides penetration is a complex phenomenon, involving various factors such as diffusion of chloride ions and movement of chlorides due to permeation of water into concrete. The latter process conveys a greater quantity of ions than the pure diffusion process does. The basic parameters that should be considered when studying the risk of chloride-induced corrosion are essentially the diffusion characteristics of concrete (depending on pore-size distribution) and the chloride-binding capacity of concrete, [Saetta et al., 1993b].

Diffusion takes place in presence of a gradient of the concentration. Under a non-stationary and unidirectional flow, the process follows the second Fick's law:

$$\frac{\partial C}{\partial t} = D\frac{\partial^2 C}{\partial x^2} \tag{4.2}$$

where C is the total chlorides content at time t and at distance x from the concrete surface, and D characterises the diffusion rate.

Chlorides may be present in concrete as contaminants of concrete mix ingredients (the so called "internal chlorides") or as dissolved ions penetrating unprotected concrete in structures exposed to marine environments or to deicing salts (the so called "external chlorides"). Moreover, chlorides may assume a number of states, i.e. free (dissolved in the pore solution); chemically bound, physically bound or in a chemisorbed state. Only the first case is generally recognised as responsible of concrete degradation due to embedded steel corrosion. This corrosive action is continuously opposed by the film-repairing action of hydroxyls (passivation layer).

It was probabilistically proved by [Haussmann, 1967] that corrosion can start only when the ratio of free chloride to hydroxyl concentration (Cl^-/OH^-) exceeds the threshold value 0.63. This limit is reported also by [Pedeferri, 2005] for structures exposed to the atmosphere, while higher values are indicated for submerged concrete.

Figure 4.9 illustrates the influence of the w/c ratio on the chloride penetration rate for the laboratory tests performed by [Collepardi and Biagini, 1989]. The penetration of Cl^- ions into concrete specimen immersed in a 10% $CaCl_2$ aqueous solution is plotted over time. The specimens were cured 28 days in standard conditions and cast with w/c = 0.32, 0.44 and 0.55. It can be observed that the chloride penetration depth increases with the w/c ratio, i.e. with the increase of the diffusion coefficient. Numerical models able to reproduce this trend are available in the literature, such as the diffusive model developed by [Saetta et al., 1993b], fitting very well with the experimental evidence, as shown in Figure 4.9 (continuous lines).

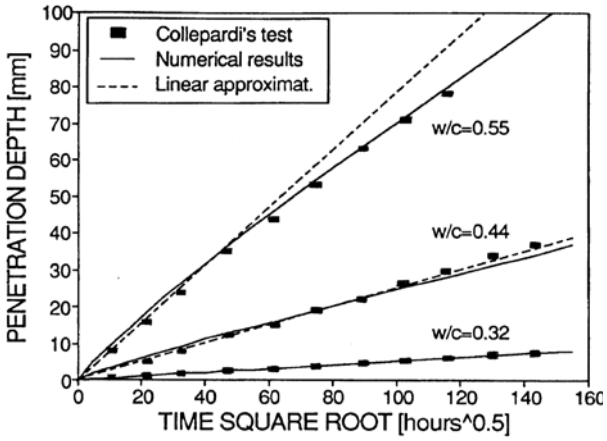

Figure 4.9 Chlorides penetration depth vs. immersion time [Saetta et al., 1993b]

4.2 Effects of corrosion on the structural behaviour

It has been already emphasized that reinforcing bars corrosion produces significant effects on the structural behaviour of RC members. This phenomenon involves not only steel (e.g. in terms of cross-section loss), but also concrete and the mutual interaction between the two materials by reducing bond strength.

The effects of steel corrosion are summarized in Figure 4.10, distinguishing between the "local" effects, i.e. at the RC member level, and the "global" effects, i.e. at the RC structure level.

It is worth noting that, among the global consequences of corrosion on the structural performance, together with the reduction of ductility and load carrying capacity, also the shift of the failure mechanism and detrimental torsional effects may occur (see Section 6.3).

4.2.1 Steel section reduction

As mentioned above, two main typologies of corrosion attack may be distinguished, Figure 4.11. In the case of pitting corrosion, the reduction of steel area is localized in a limited region of the bar surface, as generally produced by chloride ions penetration, Figure 4.12. Conversely, a uniformly distributed attack on the bar surface with a relatively limited reduction of bar cross section is the typical effect of a carbonation attack. In both cases, the main consequence is the reduction of resistance and load bearing capacity of the structural element.

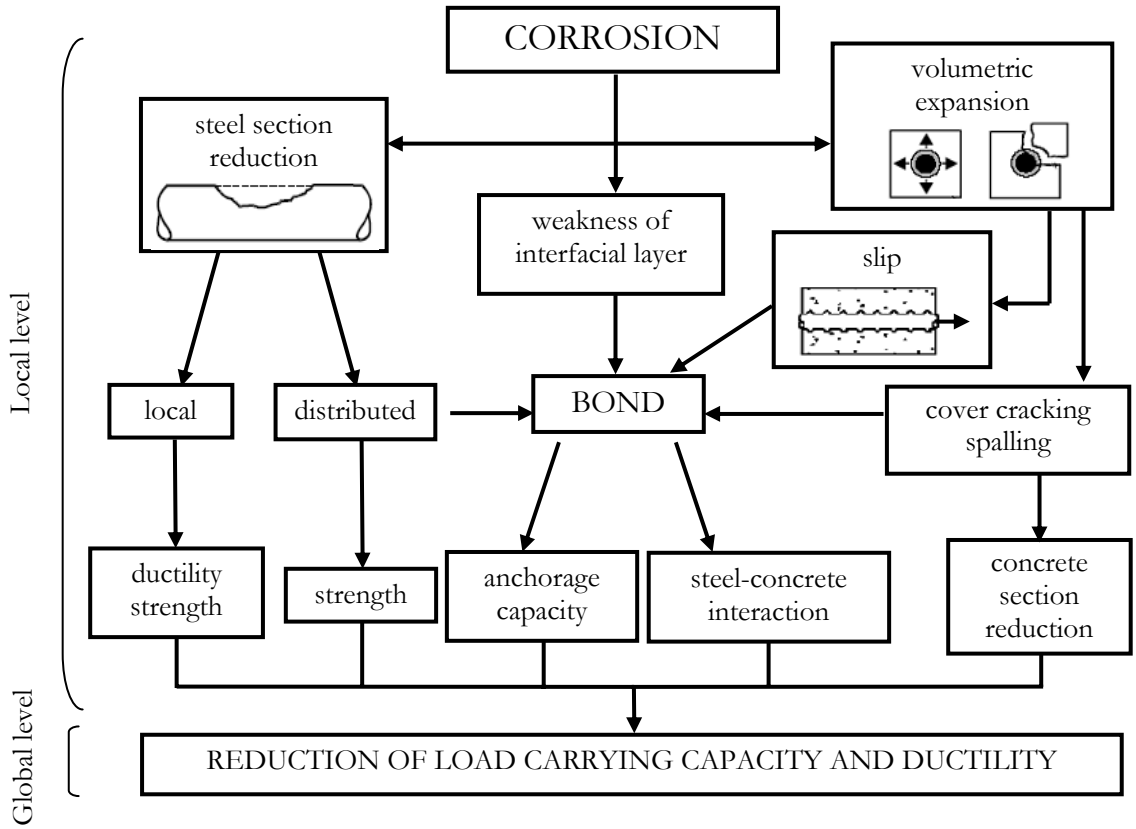

Figure 4.10 Corrosion effects on the structural performance

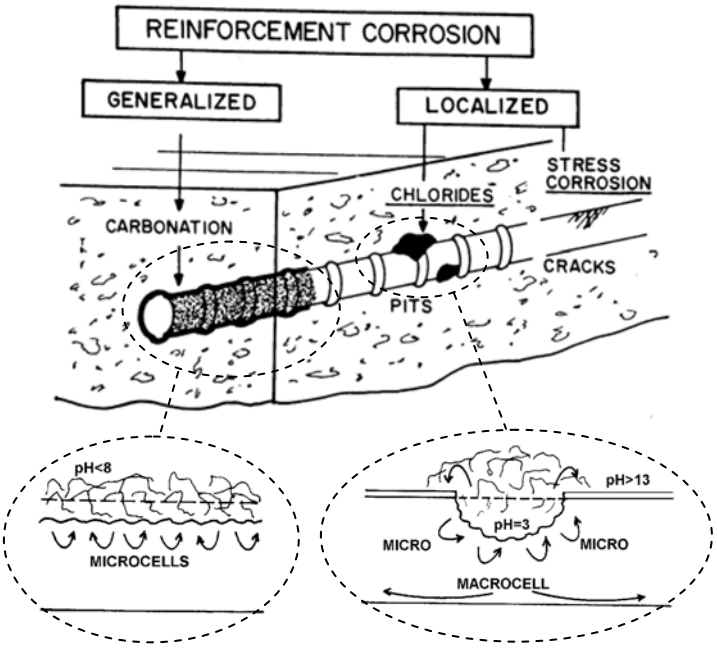

Figure 4.11 Types and morphology of corrosion in concrete [Rodriguez et al., 1994]

Figure 4.12 Localised rebar section reduction due to pitting corrosion [Pedeferri, 2005]

The tests performed by [Cairns et al., 1999] and by [Castel et al., 2000] have shown that there is a sort of balance between the strength loss resulting from the reduced section and the strength increase due to the hardening of the undamaged material in the same section, deriving from the precipitation of the calcium carbonate produced in the carbonation reaction (see Section 4.1.1). However, the notch effects of the pits induce large and highly localized strains in the steel, compromising the bars ductility (see Section 4.2.2).

For small rebar diameters, as in the case of the stirrups, localized corrosion may produce significant effects, with a reduction of the section until 50% in less than 20 years, since the chlorides reach the bar, e.g. [Rodriguez et al., 1994]. In the case of a distributed corrosion type, lower reductions of transversal rebars section are generally observed.

The depth of the corrosive attack penetration may be evaluated by means of the following expression:

$$P_x = 0.0116 \cdot i_{corr}\left(t - t_{in}\right) = 0.0116 \cdot i_{corr} t_p \tag{4.3}$$

where P_x is the average value of the penetration in mm (i.e. decrease of rebar diameter); 0.0116 is a conversion factor from $\mu A/cm^2$ into mm/year; i_{corr} is the average corrosion rate in $\mu A/cm^2$; t_{in} is the so called "initiation time" (in years), that is the time necessary until the aggressive front reaches the bar surface. Finally, t_p is the "propagation time", which depends on the environmental exposure, e.g. submerged, tidal splash or atmospheric environment, [Faber, 2006]. Using Eq.(4.3) the residual transversal section of the corroded bar can be evaluated from the residual diameter Φ_t at time t; given by:

$$\Phi_t = \Phi_0 - \alpha P_x \tag{4.4}$$

where Φ_0 is the nominal diameter in mm; α is a coefficient depending on the type of attack, which can be assumed equal to 2 for distributed corrosion up to 10 for pitting corrosion.
Figure 4.13 shows a schematic description of the time-evolving degradation process of RC structures ascribed to corrosion phenomena. The initiation time t_{in} indicates the depassivation of the outer layer of the reinforcement and depends, among the other factors, on the penetration rate of carbonation and, obviously, on the cover thickness.
In view of its noteworthy implications in assessing the safety condition of a RC structure affected by a corrosive attack, the evaluation of the initiation time will be investigated in the following section and, given the high level of uncertainty governing the parameters involved, a statistical approach will be adopted.
It is interesting to note that, as outlined in [Faber, 2006], a generally acceptable basis has been identified and agreed within the research community with regard to the modelling of the initiation phase of the degradation process in RC structures. However, at present no consensus has been achieved regarding the propagation phase (see also [DuraCrete, 2000] and [CEB-FIP, 2006]).

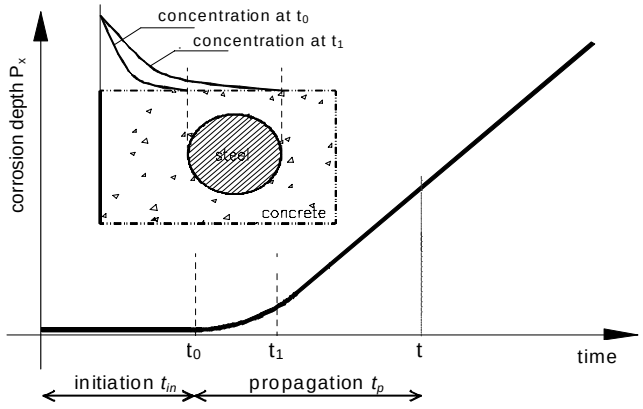

Figure 4.13 Evolution of the corrosion process over time

4.2.1.1 Evaluation of the corrosion initiation time

The corrosion initiation time has been chosen as the most representative parameter controlling the deterioration mechanism of a corroding RC member. Among the different approaches available for its evaluation, two possibilities are here discussed, with reference to a carbonation-induced attack: a simplified method, relating the carbonation depth d to the square root of time t, and a more sophisticated procedure based on the diffusive model developed by [Saetta et al., 1993a-1999].

As for the simplified approach, the classic expression derived by Venuat and Alexandre (1969) from empirical data is used (with $m = 2$):

$$d = k_{CO_2} t^{\frac{1}{m}} = k_{CO_2} \sqrt{t} \tag{4.5}$$

The application of this formula requires assuming that the value of the carbonation depth d thus obtained coincides with the mean value of the distribution of the depth of carbonation function. The term k_{CO_2} in Eq.(4.5) represents the carbonation coefficient, which can be calculated as:

$$k_{CO_2} = \sqrt{2 \frac{D_g}{a} (c_1 - c_2)} \tag{4.6}$$

where D_g [m^2/s] is the diffusion coefficient of the CO_2 penetrating into the concrete, a [mol CO_2/m^3] is the amount of the carbonatable material and (c_1 – c_2) [mol CO_2/m^3] is the concentration difference between the outside environment and the uncarbonated concrete.
The initiation time for corrosion t_{in} is defined as the time necessary until the aggressive agent reaches the reinforcing bar surface, i.e. when the carbonation depth equals the concrete cover c. From this definition and from Eq.(4.5), it follows:

$$t_{in} = \left(\frac{c}{k_{CO_2}} \right)^2 \tag{4.7}$$

It should be also noted that the square root relationship between the carbonation depth and time predicts much higher penetration depths for experimental data obtained from very dense or wet concretes. In these cases, a better fit is obtained when $m > 2$, [Pedeferri and Bertolini, 2000].
Expression (4.5) was reviewed and verified by other authors (e.g. Fattuhi, 1998, Ewertson and Petersson, 1993), both numerically and experimentally, in laboratory as well as real environmental conditions. The relationship seemed to fit only in the case of constant environmental conditions (constant diffusion coefficient in time and location), representing the main limit of this basic approach, as this requirement is rarely met in actual RC structures.
The second more sophisticated method for evaluating t_{in} accounts for the fact that corrosion, and consequently the deterioration process, actually starts when the concentration of CO_2 reaches a certain threshold value in correspondence to a depth equal to the concrete cover. This approach, allowing a more accurate evaluation of t_{in}, is implemented in the diffusive model for the durability analysis of RC structures developed by [Saetta et al., 1993a-1999] and then improved in additional studies, [Saetta et al., 2004], [Saetta, 2005]. In particular, the corrosion initiation time is obtained by solving the following set of differential equations, governing the diffusion and transport process of aggressive species within the porous matrix of concrete:

$$\begin{aligned}
&\textit{moisture flow:} && \frac{\partial h}{\partial t} = div\left(D_h \cdot \nabla h\right) + \frac{\partial h_s}{\partial t} + K \cdot \frac{\partial T}{\partial t} + \frac{\partial h_{\mathcal{R}}}{\partial t} \\
&\textit{heat flow:} && \rho \cdot C_q \cdot \frac{\partial T}{\partial t} = div\left(b \cdot \nabla T\right) + \frac{\partial Q_h}{\partial t} + \frac{\partial Q_{\mathcal{R}}}{\partial t} \\
&\textit{pollutant flow:} && \frac{\partial c_s}{\partial t} = div\left(D_g \cdot \nabla c_s\right) + \frac{c_s}{\alpha} \cdot \frac{\partial w_f}{\partial t} + \frac{\partial c_{\mathcal{R}}}{\partial t} \\
&\textit{rate of chemical reaction:} && \frac{\partial \mathcal{R}}{\partial t} = v = \alpha_4 \times f_1(h) \times f_2(c) \times f_3(\mathcal{R}) \times f_4(T)
\end{aligned} \tag{4.8}$$

Specifically, from the solution of the system of equations, the time-related trends of moisture and aggressive substance spreading through the material can be evaluated. This provides a measure of the carbonation depth, i.e. the penetration of the pollutant inside concrete, as a function of time and consequently the time necessary until the penetration of the aggressive agent equals the concrete cover may be derived.
The main independent variables in Eq.(4.8) are:

- c_s diffusive species concentration (in the present case CO_2);
- h relative humidity content;
- T temperature;
- $\mathcal{R}$ degree of chemical reaction.

The parameters ρ and C_q represent respectively the mass density and the isobaric heat capacity of the concrete, Q_h is the outflow of heat per unit volume of solid, b is the heat conductivity and w_f the free water content. Moreover, f_1, f_2, f_3 and f_4 are functions describing respectively the influence of the presence of water, of the concentration of the aggressive species, of the degree of chemical reaction and of temperature on the evolution of the chemical process. The partial derivatives respect to time $\partial(\cdot)_{\mathcal{R}}/\partial t$ denote the change of the parameter in brackets due to the chemical reaction per time unit:

$$\frac{\partial h_{\mathcal{R}}}{\partial t} = \alpha_1 \frac{\partial \mathcal{R}}{\partial t}; \quad \frac{\partial Q_{\mathcal{R}}}{\partial t} = \alpha_2 \frac{\partial \mathcal{R}}{\partial t}; \quad \frac{\partial c_{\mathcal{R}}}{\partial t} = \alpha_3 \frac{\partial \mathcal{R}}{\partial t} \tag{4.9}$$

where α_1, α_2, α_3, as well as α_4 in Eq.(4.8), are parameters that vary according to the characteristics of concrete and reagents. The detailed meaning of the other variables and parameters may be found in the previously cited works.
In the carbonation process, the degree of chemical reaction $\mathcal{R}$ can be defined as the ratio between the actual concentration and the maximum concentration of the pollutant, $[CaCO_3]/[CaCO_3]_{max}$. Assuming that the diffusivity coefficients of relative humidity D_h and of the aggressive substance D_g within the porous matrix of concrete as well as the other material parameters are known (depending on the concrete mix-design), the system of equations (4.8) can be solved numerically by means of an iterative procedure. In particular, after the classical space discretization using a Galerkin procedure within the finite element approach, a system of coupled ordinary differential equations in time can be obtained, for which the time discretization is carried out by means of a Wilson type one-step algorithm.

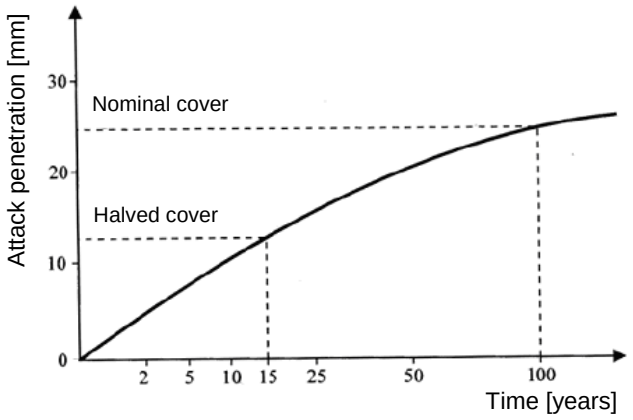

Figure 4.14 Reduction of t_{in} for local reductions of the concrete cover (CEB) [Pedeferri, 2005]

Finally, it is interesting to note how the reduction of the concrete cover may significantly influence the time for corrosion initiation. Given the relationship between penetration depth d and time t of Eq.(4.5), in the case $m = 2$, if the concrete cover is reduced to half of the nominal thickness, the initiation time is reduced to one fourth, and even more for very dense concretes ($m > 2$), as shown in Figure 4.14: corrosion may start after 15 years, in contrast with the initiation time of 100 years predicted for the undamaged condition.

4.2.1.2 Evaluation of the corrosion rate

Another fundamental parameter in Eq.(4.3) is the corrosion rate i_{corr}, varying over time along with humidity and temperature and generally measured as corrosion current density (in $\mu A/cm^2$), which gives the quantity of metal that transforms into oxides by unit of reinforcement surface and time (in mm/year). The measurement of i_{corr} is made by means of a reference electrode, which indicates the electrical potential, and an auxiliary electrode, which gives the current, e.g. [Rodriguez et al., 2001].

In recent years, a number of formulations have been proposed in the literature, mainly based on empirical expressions, to calculate the corrosion rate, varying from deterministic approaches to fully probabilistic contexts, e.g. [Val et al., 1997], [Stewart, 2004], [CEB-FIP, 2006], [Marsh et al., 2008], [Sudret, 2008].

Typical values of i_{corr} obtained in laboratory or measured on real size structures are ranked in Table 4.1, as suggested by different authors.

[Vu et al., 2000] propose an empirically derived expression for the calculation of the corrosion rate at the beginning of chloride-induced corrosion propagation, $i_{corr}(1)$ in $\mu A/cm^2$, as a function of the w/c ratio and of the thickness of the concrete cover (in cm):

$$i_{corr}(1) = \frac{37.8(1 - w/c)^{-1.64}}{cover} \tag{4.10}$$

Moreover, the following expression is proposed, relating i_{corr} with the propagation time:

$$i_{corr}(t_p) = i_{corr}(1) \cdot 0.85 t_p^{-0.29} \tag{4.11}$$

Table 4.1 Classification of i_{corr} [$\mu A/cm^2$]

Corrosion risk	Dhir et al., 1994	Brite/Euram, 1995	Middleton et al., 1998	Rodriguez et al., 2001
negligible	-	< 0.1	-	< 0.1-0.2
low	0.1	0.1÷0.5	0.1÷0.2	0.2÷0.5
moderate	1.0	0.5÷1.0	0.2÷1.0	0.5÷1.0
high	> 10	> 1.0	> 1.0	> 1.0

Actually, most reliability analyses assume a constant corrosion rate during the propagation period, [Vu et al., 2000]. However, the formation of rust on the bar surface, reducing the diffusion of iron ions away from the steel bar, suggests that the corrosion rate will decrease over time. In particular, it will diminish rapidly during the first years after the initiation period, then more slowly approaching a nearly uniform level (Figure 4.15).

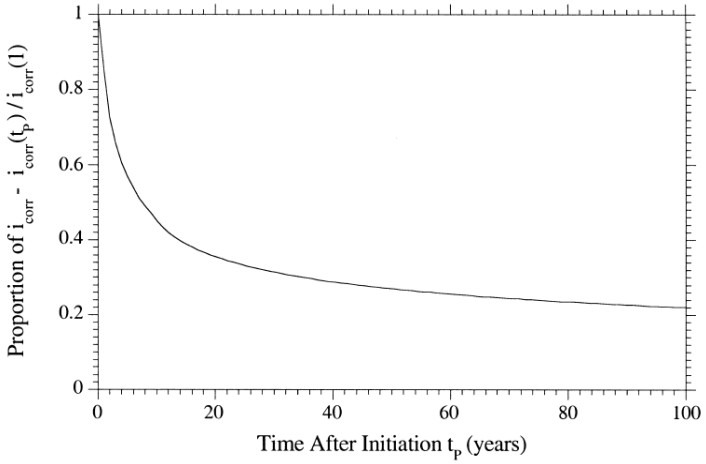

Figure 4.15 Variation of the corrosion rate with time [Vu et al., 2000]

Table 4.2 Suggested ranges of i_{corr} for EN 206 exposure classes [Rodriguez et al., 1994]

Exposure class		i_{corr} [μA/cm²]	
0	No risk of corrosion	~0.01	
Carbonation induced corrosion		Partially carbonated	Totally carbonated
C1	dry	~0.01	~0.01
C2	wet - rarely dry	0.1 – 0.5	0.2 – 0.5
C3	moderate humidity	0.05 – 0.1	0.1 – 0.2
C4	cyclic wet - dry	0.01 – 0.2	0.2 – 0.5
Chlorides induced corrosion			
D1	moderate humidity	0.1 – 0.2	
D2	wet - rarely dry	0.1 – 0.5	
D3	cyclic wet - dry	0.5 – 5	
S1	airborne sea water	0.5 – 5	
S2	submerged	0.1 – 1	
S3	tidal zone	1 - 10	

Of interest, basing on the exposure classes classification proposed by EN 206, [Rodriguez et al., 1994] have associated to each class a range of the representative corrosion rate (obtained by averaging the instantaneous values of i_{corr} recorded), for both carbonation and chloride-induced corrosion (Table 4.2).

Another interesting novel approach to the problem of durability analysis has been proposed by [Biondini et al., 2004], who modelled the diffusion process by using cellular automata with proper material degradation laws to account for the mechanical damage coupled to diffusion.

It should be remarked that also empirical expressions, e.g. [Pedeferri et al., 2000], are available in the literature for the estimation of the initiation time of corrosion due to carbonation, even though merely in standard exposure conditions.

In the considered case studies, the corrosion rate has been evaluated on the basis of the climatic characteristics of the site and the average concrete strength, as explained in Section 6.2.3.

4.2.2 Modification of the mechanical characteristics of the reinforcing bars

Some experimental tests, e.g. [Almusallam, 2001], [Kobayashi, 2006] and [Apostolopoulos and Papadakis, 2008], evidence that steel yield and ultimate stresses may be reduced with increasing corrosion levels. Nevertheless, as shown in Figure 4.16a-b, the effects are generally moderate. It is worth noting that these outcomes should be evaluated with caution because of the complexity of measuring the effective residual section of the rebar after its breaking. Moreover, the experimental results are often not directly comparable: in some cases the tension is referred to the integer section, in other cases to the residual one, [Rodriguez et al., 2001]. In particular, the two terms, effective stress and apparent stress, in the legend of Figure 4.16a-b are explained as follows. The apparent stress is calculated as the quotient of the load capacity, divided by the initial, uncorroded section of the steel bars. According to the standards, this considers the mass, and therefore the cross-sectional area of the specimens, constant over time. On the contrary, the effective stress is the quotient between the load capacity and the actual cross-section of the corroded specimens, which is calculated as a function of the mass and length of each specimen.

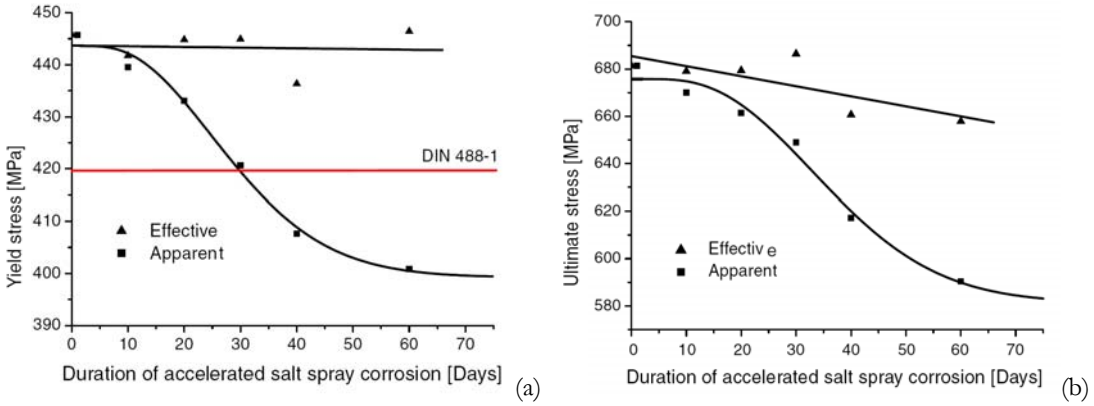

Figure 4.16 Reduction of (a) yield and (b) ultimate stress due to corrosion [Apostolopoulos and Papadakis, 2008]

With more agreement it is recognized by the scientific community the trend to a significant reduction of steel ultimate elongation, and consequently of steel ductility, even for small section reductions. This indicates that corrosion of reinforcing steel increases its brittleness.

Concerning this aspect, [Castel et al., 2000] evidence that under pitting corrosion the notch effects of the pits induce large and highly localized strains in the steel. Since the length of the defect is short, the average strain over a finite length of the bar is smaller than the local strain at the pit. Hence, the bar breaks at an average strain smaller than the ultimate strain of the virgin material and, when pitting reaches 50% of the section, the bar behaviour becomes very brittle, [Palsson et al., 2002].

Similar results derive from the experimental tests performed by [Almusallam, 2001] on reinforcing bars corroded to different levels and by [Apostolopoulos and Papadakis, 2008] (Figure 4.17a-b). As the degree of corrosion or the time of exposure increase, the corresponding elongation of the bar before failure decreases sharply. In particular, Figure 4.17a illustrates that reinforcing steel bars with 12.6% or higher reinforcement corrosion showed a brittle behaviour during the tests, while Figure 4.17b evidences that after 20 days of exposure to salt spray the limit value of 14% for the elongation to failure prescribed by the German Standards is no more satisfied.

[Rodriguez et al., 2001] have also demonstrated a significant reduction of rebars ductility and consequently a reduction of the maximum elongation until 30% and 50% for loss of cross section of 15% and 28% respectively. Although these values are acceptable considering the limits of ductility imposed by [Eurocode 2, 2004], such reductions may decrease the capacity of redistribution of bending moments.

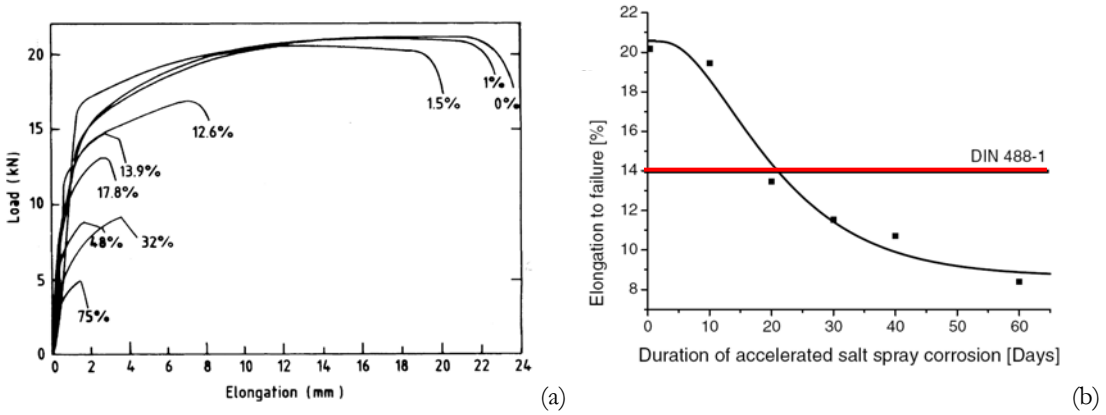

Figure 4.17 Reduction of steel ductility with increasing degree of corrosion: (a) [Almusallam, 2001]; (b) [Apostolopoulos and Papadakis, 2008]

4.2.3 Degradation of the concrete cover

As a consequence of the radial pressure generated by the increasing volume of the corrosion products (i.e. iron oxides) forming along the steel bar surface, the tensile stresses in the concrete surrounding the rebars may exceed the tensile strength. The main effects are cover cracking, possible delamination of the outer layers of concrete and total cover expulsion (Figure 4.18).
Of interest, the degree of the volumetric expansion of corrosion products is different in the case of uniform or local corrosion. In particular, the tendency of the corroded bar to split the concrete cover is less with local than with uniform attacks.
On the basis of experimental studies, e.g. [Rodriguez et al., 1996], the relationship between concrete cracking produced by iron oxides and the degree of corrosion has been derived. In order to take into account the degradation of concrete in the zones surrounding the compressed rebars, some authors have introduced proper variations to the concrete constitutive relationship by reducing the compression strength and assuming a more brittle post-peak behaviour, e.g. [Coronelli and Gambarova, 2004] (Figure D.10a).

Figure 4.18 Concrete cover expulsion

In a simpler way, other authors have proposed to reduce the transversal concrete section by eliminating the concrete cover in the calculation of the ultimate moment, e.g. [Rodriguez et al., 2001], [Pardi et al., 2001]. Following such an approach, Rodriguez has determined some simplified relationships suggesting the possible elimination of the concrete cover in correspondence to the compressed bars and stirrups as a function of the corrosion level.
It is important to note that, when considering complete cover spalling, steel bars slippage effects play a significant role, which cannot be neglected in an effective analysis (see Section 4.2.4).

4.2.4 Degradation of steel-concrete bond strength

The expansive action of corrosion products, resulting in the opening of longitudinal cracks and the modification of the interface layer (in particular, reduction of the ribs height and formation of a soft rust layer around the steel bar), leads to the reduction of the friction component and the failure of the chemical adhesion between steel and concrete. These effects alter the bond interaction along the bar, reducing or even eliminating the beam action mechanism and weakening the flexural stiffness and moment resistance of the member.
Once bond along the shear span is compromised, the arching action for loads transmission to the supports increases. This has several implications for safety, as the development of the yield force of the reinforcement (the tie of the arch) depends greatly on the anchorage details of the bar near the support (usually a cut-off point for flexural reinforcement). The most detrimental consequence is the occurrence of rebar slippage, until total loss of anchorage and the reduction of the confinement level. Such a phenomenon is evident especially when the bar is stressed and undergoes lateral contractions due to Poisson's effect.
In the last two decades, the effects of corrosion on bond strength have been the subject of an intensive literary production, in terms of experimental as well numerical studies, with different levels of accuracy in relation to the field of application, i.e. from the micro-modelling level of the system bar – surrounding concrete up to the structural level. This confirms the growth of interest of the scientific community on this matter, e.g. [Al-Sulaimani et al., 1990], [Rodriguez, 1994-1996], [Castel et al., 2000], [Coronelli, 2002], [Dekoster et al., 2003], [El Maaddawy et al., 2005], [Bhargava et al., 2008], just to cite a few examples (see also Section 4.3 and APPENDIX C). However, the problem needs further investigation because of its own complexity, mainly due to the several parameters involved, e.g. cover to bar diameter ratio, rebars position, confinement level, concrete quality, cover cracking, corrosion degree, etc. Hence, it is difficult to generalize the results obtained from the experimental tests and to develop wide-ranging and simple numerical models, able to simulate the real behaviour of corroded structures.

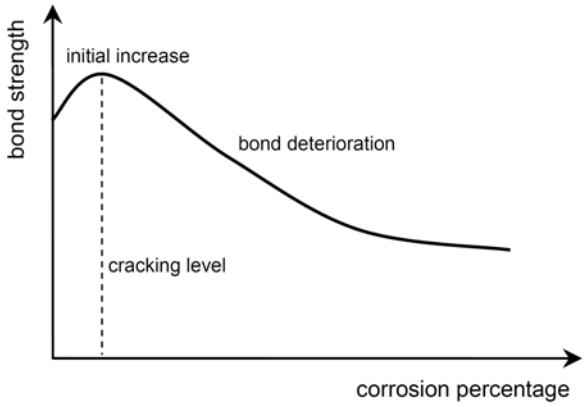

Figure 4.19 Schematic variation of bond strength with corrosion [CEB-FIP, 2000]

The bond degradation phenomenon has been accepted also by the codes. For instance, Figure 4.19 shows the schematic representation of the effects of corrosion on bond strength proposed in [CEB-FIP, 2000]. It can be observed that, for low corrosion levels, a small amount of rust on the bar surface may improve the confining pressure due to drying shrinkage of concrete, producing a slight initial increase of bond resistance. Afterwards, the reduction in rib height lessens the mechanical interlock between the rebar and concrete and a sharp loss of bond is visible. This behaviour is confirmed for example by the experimental tests of [Al-Sulaimani et al., 1990]: bond strength increased with corrosion up to around 1% of corrosion, then decreased rapidly for pullout tests and at a slower rate for beam tests.
It is worth noting that performing the analysis at the section level may be an oversimplification, since the assumption of plane sections and of a perfect bond between steel and concrete may not hold in deteriorated structures, [Coronelli and Gambarova, 2004]. Nevertheless, for moderate levels of corrosion, limited loss of bond has been detected, e.g. [Rodriguez et al., 1994]. Therefore, it is still possible to adopt models based on the hypothesis of the conservation of plane sections, [Bertagnoli et. al., 2006].

4.2.4.1 Bond effects on the moment - curvature relationship

The application of the moment-curvature relations is particularly useful in the non-linear analysis of RC beams, since the gradient of the moment-curvature relation represents the elastic bending stiffness EJ, which includes all the section properties in a typical loading condition.
[Kwak et al., 2002a-b] propose a numerical algorithm including the bond-slip effect into the moment-curvature relation (Figure 4.20). The following basic assumptions are used: (i) conservation of plane sections, so that the longitudinal strain is directly proportional to the distance from the neutral axis; (ii) linear bond stress-slip relation; (iii) minimum length of the elements in which the beam is subdivided equal to three times the concrete cover, that is about the mean crack space at the ultimate loading conditions; (iv) plastic hinge length $L_p = 0.25d + 0.075z$, where d is the section depth and z the distance from the critical section to the point of contraflexure (an element of length L_p is located at the midspan to predict the ultimate strength exactly). The revised curvature ϕ_i' of the i-th element accounting for the bond-slip effect may be calculated as the sum between the curvature ϕ_i corresponding to a moment M under perfect bond and an increment of curvature $\Delta\phi_i$:

$$\phi_i' = \frac{\varepsilon_s - \varepsilon_{cc}}{d} = \phi_i + \Delta\phi_i = \phi_i + \frac{½\left(\varepsilon_{s0}^i + \varepsilon_{sl}^i\right) - ½\left(\varepsilon_{c0}^i + \varepsilon_{cl}^i\right)}{d} \tag{4.12}$$

where ε_{cc} is the concrete strain at the extreme compression fiber, ε_s and ε_c are the steel and concrete strains at the steel interface when considering bond-slip effects.

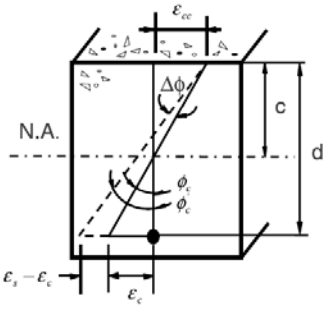

Figure 4.20 Modified curvature of RC section [Kwak et al., 2002b]

4.2.4.2 Modes of bond failure

Bond failure between steel and concrete is generally characterized by two modes, namely pull-out and splitting, e.g. [CEB-FIP, 2000]. If the ratio of concrete cover to bar diameter is large or the concrete is well confined, bond failure occurs in the pull-out mode, due to the shearing off of the concrete keys between the bar ribs. The most important parameters that affect the pull-out bond strength under static and cyclic loading are discussed in detail by [Eligehausen et al., 1983]. Conversely, if the concrete cover is small or the steel bars are closely spaced, tensile splitting cracks tend to develop under the radial component of the rib bearing forces parallel to the steel bars causing premature splitting bond failure.
For most structural applications, bond failures are governed by splitting of the concrete rather than by pull-out. The main parameters that influence the average bond strength of developed or spliced bars when the mode of bond failure is by splitting include the ratio of concrete cover to bar diameter, the development of splice length, the concrete compressive strength, the geometry of the bar ribs and concrete confinement. Nevertheless, the presence of steel corrosion may increase the probability of occurrence of pull-out failure, due to the reduction of steel-concrete interaction.
Furthermore, two sources of slip, and consequently two models, can be recognized according to [CEB-FIP, 2000]: slip due to damage in concrete adjacent to bars exhibited by cracking and crushing, and slip of the interface between steel bar and surrounding concrete. The former model deals with the behaviour of a solid in relatively larger volume of material, while the later model considers a fictitious interface layer and has been investigated in the present research (see Section 4.3).

4.2.4.3 Ultimate bond stress and anchorage length in the Codes

The design value of the ultimate bond stress f_{bd} for ribbed bars given by the Italian Code is:

$$f_{bd} = 2.25 f_{ctd} \tag{4.13}$$

where f_{ctd} is the design value of concrete tensile strength. This relationship is valid when good bond conditions are guaranteed, otherwise the value must be reduced up to 50%.
The European Standard, [Eurocode 2, 2004], suggests the following relationship:

$$f_{bd} = 2.25 \eta_1 \eta_2 f_{ctd} \tag{4.14}$$

where η_1 is a coefficient related to the quality of the bond condition and the position of the bar during concreting, assuming the values $\eta_1 = 1.0$ when "good" conditions are obtained and $\eta_1 = 0.7$ for all other cases and for bars in structural elements built with slip-forms, unless it can be shown that "good" bond conditions exist. The coefficient η_2 is related to the bar diameter as follows: $\eta_2 = 1.0$ for $\Phi \leq 32$ mm and $\eta_2 = (132 - \Phi)/100$ for $\Phi > 32$ mm.
In Figure 4.21 the typical distribution of stresses on a steel bar embedded in concrete is illustrated. Since bond stresses arise from the change in the steel force along the bar length, the effect of bond becomes more pronounced at the end anchorages of the reinforcing bars and in the vicinity of cracks. The transversal concrete stresses are higher in correspondence to the maximum of the bond stresses, i.e. at around the last third of the anchorage length. Thus, in this region, the concrete cover may crack or even spalling may occur. Although bond stresses at the interface layer vary significantly along the anchorage zone, they are commonly assumed constant and the anchorage length is thus evaluated from the equilibrium equation relative to the portion of steel bar embedded in concrete.

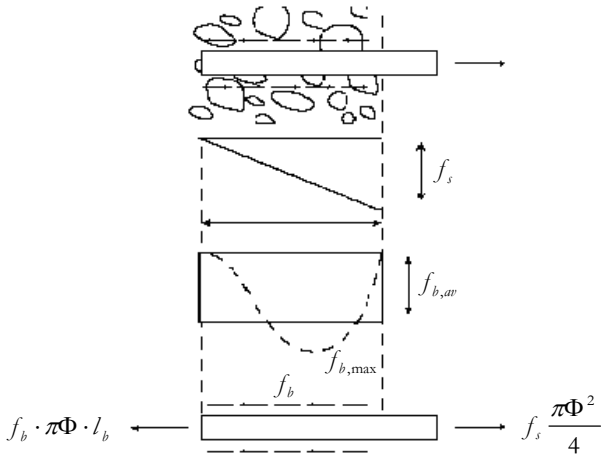

Figure 4.21 Stresses distribution and translational equilibrium in the bar axis direction

Assuming that the steel yield design strength f_{yd} is reached before the ultimate bond strength f_{bd} (correspondent to the bar pull-out), the following equilibrium relationship:

$$f_{yd}\frac{\pi\Phi^2}{4} = f_{bd}\pi\Phi \cdot l_{b,rqd} \tag{4.15}$$

provides the "basic" required anchorage length $l_{b,rqd}$, which must assure that the bond forces are safely transmitted to concrete avoiding longitudinal cracking or spalling, as prescribed by the codes:

$$l_{b,rqd} = \frac{\Phi \cdot f_{yd}}{4 f_{bd}} \tag{4.16}$$

Thus, $l_{b,rqd}$ is proportional to the bar diameter Φ and to the material properties. It should be noted that the ultimate bond strength f_{bd} must be cautiously chosen: only in presence of perfect bond condition the mean value of f_{bd} can be used in the analysis.
In the European Standard a distinction is made between "basic" and "design" anchorage length:

$$l_{bd} = \alpha_1\alpha_2\alpha_3\alpha_4\alpha_5 \cdot l_{b,rqd} \geq l_{b,\min} \tag{4.17}$$

where α_1, α_2, α_3, α_4 and α_5 are coefficients depending respectively on the shape of bars, the concrete cover, the transverse confinement, the type of anchorage and the axial force on the bar (tension or compression) and $l_{b,min}$ is the minimum anchorage length if no other limitation is applied:

- for anchorages in tension: $l_{b,min} > \max\{0.3\ l_{b,rqd}; 10\ \Phi; 100\text{ mm}\}$
- for anchorages in compression: $l_{b,min} > \max\{0.6\ l_{b,rqd}; 10\ \Phi; 100\text{ mm}\}$

The values of the parameters and further details are available in section 8.4.4 of [Eurocode 2, 2004].

4.2.5 Local torsional effects

It was noted by [Capozucca, 1995] that damage produced in concrete by steel corrosion causes also the inclination of the neutral axis, necessary for the internal equilibrium of the section. Therefore, simple bending deriving from a certain load, which also depends on the extent of the

damage, turns into biaxial bending. The shear centre can also be displaced from its original position, resulting in the generation of unexpected torsional effects, which are negligible in massive sections, but may have significant consequences in thin-walled sections, designed only for bending stresses. As a consequence, in the case of torsion for corroded beams, the concrete strut in compression is inclined with respect to the plane of the cross section of the beam, so that the component of compression force causes deformation of the stirrup and longitudinal bar near the corrosion-damaged zone.

4.2.6 Effects of corrosion on structural ductility

It has been experimentally demonstrated, e.g. [Almusallam et al., 1996a], that with increasing levels of reinforcement corrosion RC members exhibit a progressive loss in their ductile behaviour, with undesirable consequences, especially under seismic excitations. Figure 4.22 shows the load – deflection curves for the RC slabs tested by [Almusallam et al., 1996a] at different corrosion degrees: a sudden (brittle) failure without considerable deflection was the typical failure mode for the members corroded more than 1.5%. This behaviour was attributed to the loss of steel section and of bond strength. With 25% of corrosion, the reduction in the ultimate flexural strength of the slabs was 60%, while in case of a 60% corrosion the flexural strength was similar to that of unreinforced slabs.

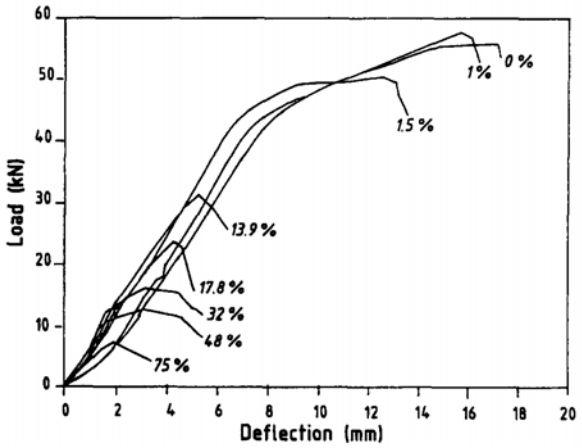

Figure 4.22 Reduction of structural ductility with increasing corrosion [Almusallam et al., 1996a]

4.3 Modelling bond behaviour

4.3.1 Introduction

As already mentioned in Section 4.2.4, due to its significance for practical design, bond behaviour has been investigated by many researchers and technical committees, e.g. [CEB-FIP, 2000]. As a result, numerous empirical formulas and complex code provisions for bar anchoring length and reinforcement detailing have been published, that can also constitute a basis for numerical models. Despite this, bond slip is typically ignored since considerable uncertainty about this complex phenomenon still exists, as a consequence of the several parameters involved. In particular, considering the complication in the numerical modelling given by the necessity to double the nodes for accounting for bars slippage, most finite element studies of RC structures neglect bond-slip effects. Moreover, in the opinion of some researchers this effect is included in the tension stiffening model and consequently specific attention to the problem is

not required. Thus, a perfect connection between concrete and reinforcement bars is commonly assumed in most numerical nonlinear analyses of RC structures in engineering practice. Although this approach is usually appropriate, there are cases in which the effect of bond - slip cannot be disregarded. According to [Kwak et al., 2006], correlation studies with experimental tests demonstrate that considering the bond-slip effect improves the accuracy of the numerical results and is essential in the cyclic and dynamic analysis of RC structures. In contrast, ignoring the bond-slip effect leads to an overestimation of the energy absorption capacity and the stiffness of the structure during cyclic excitation, i.e. the fundamental period and the displacement response of the structure are underestimated.
APPENDIX C offers an overview of the most significant approaches recently proposed in the literature for describing the bond behaviour in RC members, both in undamaged conditions and under the effect of environmental degradation phenomena, such as corrosion. First, an introduction about the primary aspect of the modelling of the reinforcement embedded in concrete is presented. Moreover, a summary of bond-slip relationships is given in chronological order.

4.3.2 Modelling approaches

The first problem to face when modelling the response of a structural member is the definition of an effective tool of analysis. Especially for reinforced concrete, a non linear model able to describe the evolution of the structural degradation and the progressive redistribution of stresses over time is required. To this aim, several methods have been developed, implemented in both research codes and general-purpose software. Apart from their peculiar characteristics, these models differ for their own complexity, the level of accuracy, the computational cost and the applicability fields. On the one hand, highly sophisticated models have been proposed in the last decades within the framework of the finite element method, in order to account for the coupling effect between mechanical and environmental damage, both in the static and the dynamic field, e.g. [Coronelli and Gambarova, 2004], [Wang, 2004], [Saetta et al., 1999]. Within this context, the distributed plasticity approach should be also mentioned, since fiber-section models accounting for corrosion effects and reinforcing bars slippage are available in the literature, e.g. [Spacone et al., 2000]. On the other hand, in view of the computational complexity of detailed formulations, in particular when seismic analyses of real structures are performed, the concentrated plasticity approach is widely adopted. Moreover, these models may take into consideration the effects of material degradation by properly modifying the constitutive relationships assigned to the plastic hinges in relation to the deterioration level.
Two different approaches have been identified and followed in the present research. The first possibility is to operate at a "micro" level by means of an accurate finite element model, in which proper damage laws varying as a function of the corrosion degree are implemented. In this way, it is possible to carry on detailed analyses of the critical zones, such as beam-column and column-foundation joints, where plastic hinges may form. The second possibility consists in attributing, at a "macro" (sectional) level, specific moment-curvature relationships to the plastic hinges as a function of the degradation level.
In a reliable numerical analysis, the changes in the elements geometry caused by damage evolution as well as in the material properties are of crucial importance. Thus, for simulating the corrosion effects on the structural performance of RC members, both the mentioned approaches should be able to capture the following major features:

- steel cross area reduction, in the longitudinal bars and in the stirrups;
- changes in steel ductility;

- reduction of concrete section and the changes in the strength and ductility of concrete, due to micro-cracking, cover cracking and spalling;
- deterioration of bond and its dependence on the corrosion level of the reinforcing bars.

It is worth noting that the development of a general model accounting for all these aspects is still a challenging task, in spite of the recent progress of the scientific research on this topic. Unfortunately, experimental data are often lacking or hardly comparable, generally showing a close coupling between each single effect. In particular, the effects of bond deterioration on the response of RC members cannot be completely distinguished from those due to steel section loss and concrete spalling (see for example [CEB-FIP, 2000]). Some attempts to separate the single effects have been made, among others, by [Castel et al., 2000a-b] with an apposite experimental programme, and by [Dekoster et al., 2003] using numerical analyses. In all cases, a strong dependence on the specific study case can be observed, evidencing the advisability of further investigation on this issue.
In the present dissertation, a practical methodology for modelling the main effects of corrosion on concrete, steel and bond strength is proposed. In particular, the "micro" level approach will be illustrated in the following sections, enclosing the proposal for a new bond law.

4.3.3 Concrete material modelling

Damage induced by mechanical loading interacts with the environmental factors and accelerates the deterioration process, [CEB-FIP, 1992]. For these reasons, a reliable tool for the assessment of the time-variant performance of concrete structures, especially in presence of aggressive environments, should be able to account for both the diffusion process of aggressive agents within the concrete matrix and the corresponding mechanical damage, as well as for the coupling effects between diffusion, damage and structural behaviour.
In general, the damaging processes in RC structures undergoing diffusion are very complex. Moreover, the available information about environmental agents and material characteristics is usually not sufficient for a detailed modelling, [Biondini et al., 2008a].
Herein, the coupled mechanical-environmental damage model developed by [Saetta et al., 1999] is adopted to describe concrete behaviour in presence of environmental degradation. The model, based on the hypothesis of "strain equivalence", couples the two-parameter mechanical damage model derived from [Farja et al., 1998] with an environmental damage parameter, in order to develop a sufficiently general approach to study the evolution of deterioration processes in RC structures.

4.3.3.1 Mechanical damage model

The isotropic damage model adopted for concrete encloses two independent internal damage variables, d^+ for the tensile stresses, d^- for the compressive ones. Thus, the different nonlinear behaviour of the material under tensile or compressive loading is accounted for, as well the crack closure effect upon loading reversal. According to this formulation, the effective stress tensor is split into two components, $\bar{\sigma}^+$ and $\bar{\sigma}^-$, respectively related to its tensile and compressive behaviour. Correspondingly, two equivalent effective stresses, $\bar{\tau}^+$ and $\bar{\tau}^-$, are introduced, which are associated with a damage criterion similar to the Drucker–Prager model in the triaxial compression field with a cap–closure in the tensile field. The constitutive law can be written in the form:

$$\sigma = \left(1 - d^+\right)\bar{\sigma}^+ + \left(1 - d^-\right)\bar{\sigma}^- \tag{4.18}$$

with the damage variables d^+ and d^- depending on the equivalent effective stresses according to:

$$d^+ = 1 - \frac{r_0^+}{\bar{\tau}^+} \cdot exp\left(A^+ \cdot \left(1 - \frac{\bar{\tau}^+}{r_0^+} \right) \right) \tag{4.19a}$$

$$d^- = 1 - \frac{r_0^-}{\bar{\tau}^-} \cdot \left(1 - A^-\right) - A^- \cdot exp\left[B^- \cdot \left(1 - \frac{\bar{\tau}^-}{r_0^-} \right) \right] \tag{4.19b}$$

where r_0^+, r_0^- are the current damage thresholds which control the size of the expanding damage surfaces, and A^+, A^-, B^- are material parameters, for which a more detailed description is given e.g. in [Saetta et al., 1998a].
With these assumptions, Eq.(4.19a-b) reproduces both the softening branch of the brittle material under monodimensional tensile test and the hardening effect of material under compression with the successive softening after the maximum compressive strength is achieved, as shown in Figure 4.23.
The mesh dependency associated with the strain softening behaviour has been overcome for the energy aspect by adopting a simplified regularization approach called "enhanced local method", [Saetta et al., 1999]. This method considers the specific fracture energy as a function of the mesh element size.

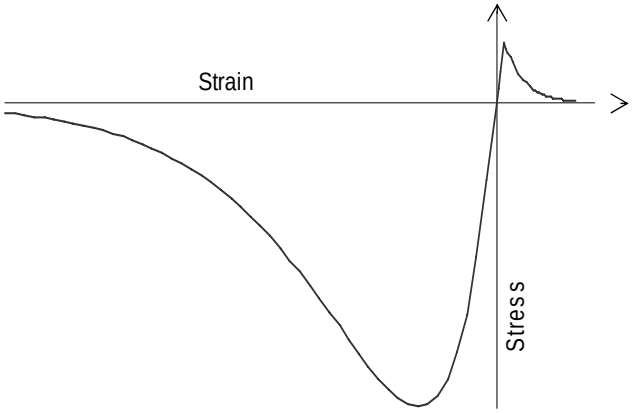

Figure 4.23 Constitutive law for concrete

Following this approach, the parameter A^+ depends on the fracture energy of the material and on a characteristic length related to the size of the finite element used in the mesh.
Finally, the occurrence of plastic deformation has been introduced in the model according to the proposal of [Farja et al., 1998] with the adoption of the following relationship:

$$\dot{\varepsilon}^p = \beta E H\left(\dot{d}^-\right) \frac{\left\langle \bar{\sigma} : \dot{\varepsilon} \right\rangle}{\bar{\sigma} : \bar{\sigma}} D_0^{-1} : \bar{\sigma} \tag{4.20}$$

where $\beta \geq 0$ is a material parameter controlling the rate intensity of inelastic strain, and $H\left(\dot{d}^-\right)$ is the Heaviside step function of the compressive damage rate.
More details about the model are given in the already cited papers.

4.3.3.2 Coupled environmental-mechanical damage model

In order account for the mechanical effect of a physical-chemical attack, a coupled chemical–mechanical damage model has been used (schematically represented in Figure 4.24). An additional internal variable, called "environmental damage" d_{chem}, has been introduced in the stress-strain relationship (see [Creazza et al., 1995], [Oñate et al., 1995], [Saetta et al., 1998a-b, 1999]), similarly to the approach by [Pijaudier-Cabot, 1998] and [Gerard, 1998]. The parameter d_{chem} is defined as:

$$d_{chem} = (1-\varphi)\left(1 - \frac{1}{1+(2\mathcal{R})^4}\right) \tag{4.21}$$

where $\varphi = f_{ck,damaged} / f_{ck,initial}$ represents the relative residual strength of the material, only due to the chemical phenomena, achieved when the chemical reaction $\mathcal{R}$ is completely developed.
Independently from its specific definition, the environmental damage parameter is assumed to be represented by an increasing function with time, which means $d_{chem} \geq 0$. Moreover, since the chemical-physical degradation acts almost in the same way in tension and compression, a unique parameter is introduced for both stresses. With this assumption, in order to include the effect of environmental degradation, Eq.(4.18) becomes:

$$\sigma = (1-d_{chem})\left[(1-d^+)\overline{\sigma}^+ + (1-d^-)\overline{\sigma}^-\right] = (1-d^{*+})\overline{\sigma}^+ + (1-d^{*-})\overline{\sigma}^- \tag{4.22}$$

where d^{*+} and d^{*-} are the coupled damage parameters.

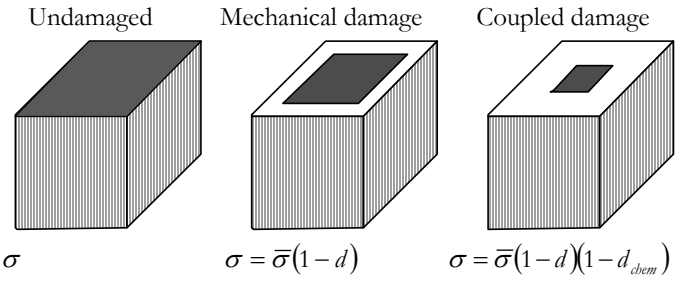

Figure 4.24 Combined action of mechanical and environmental damage

4.3.4 Steel material modelling

Within the framework of the finite element method, in order to model the reinforcement embedded in concrete, two main approaches can be distinguished: the "smeared approach", with steel smeared on concrete elements, and a "detailed approach", in which steel and concrete are modelled as distinct elements. The first method, which is frequently used for analysing the global behaviour of RC structural elements, is not directly applicable when corrosion phenomena are considered. Actually, this approach can not easily simulate the loss of bond between steel and concrete, which is a critical issue in presence of corrosion, unless suitable adjustments are carried out on the approach itself. For this reason, the detailed approach has been preferred in this work. Among the different finite elements which the method allows to use, four-node steel plane elements have been chosen. The connection to concrete is realized by means of apposite interface elements and a typical elasto-plastic constitutive law with isotropic hardening has been adopted (Figure 4.25).

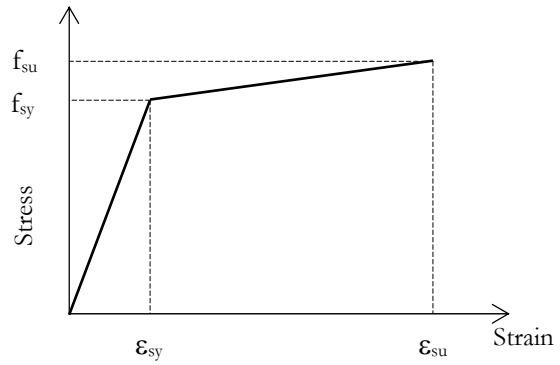

Figure 4.25 Constitutive law for steel

4.3.5 Bond modelling

To date, in spite of many difficulties, several experimental bond stress - slip relations and analytical models have been proposed for the nonlinear analysis of RC structures. These proposals range between very sophisticated and complex local models and simplified global approaches.

Within the framework of finite element modelling, two different possibilities may be distinguished for modelling bond-slip behaviour. On the one hand, a *phenomenological model* is based on the assumption of a well-defined interface between concrete and steel, realized by means of discrete or continuous elements. On the other hand, a *detailed model* provides a fine discretization of the steel bar and the shape of the ribs, e.g. [CEB-FIP, 2000].

The phenomenological model requires specific constitutive laws for the interface elements, which should take into account the most significant physical aspects of bond phenomena and the geometrical characteristics of the bond zone, i.e. bar size, rib size, bar spacing, etc. In agreement with this approach, bond stress may be regarded as shear stress over the surface of the bar, even though implying a significant simplification of the real behaviour, which consists of three main stress transfer mechanisms between concrete and steel: adhesion, friction and mechanical interaction. Conversely, the detailed model allows accurate analyses, considering the influence of any geometrical characteristics involved in bond behaviour, but requiring a very refined discretization to attain satisfactory accuracy in the solution. Therefore, considering that the final aim of the current study is concerned with analyses of real structures, the phenomenological approach has been preferred to the detailed model, which often implies excessive computational effort.

It is worth underlining that in presence of reinforcement corrosion, the problem of bond modelling becomes even more complex, and the theoretical description of the relationship between corrosion level and reduction of bond strength becomes a challenging task. For this reason, simplification hypotheses are necessary.

With the aim of predicting the bond strength at varying levels of corrosion, two different constitutive relationships for bond modelling have been formulated in the present research: a "frictional" type law (Figure 4.26a) and a "damage" type law (Figure 4.26b), both considering the deterioration of the steel-concrete interface.

In the "frictional" law, the effects of corrosion can be taken into account by varying the bond strength τ_{max} and the initial stiffness as a function of the corrosion degree, but with no changes in the shape of the bond stress-slip curve.

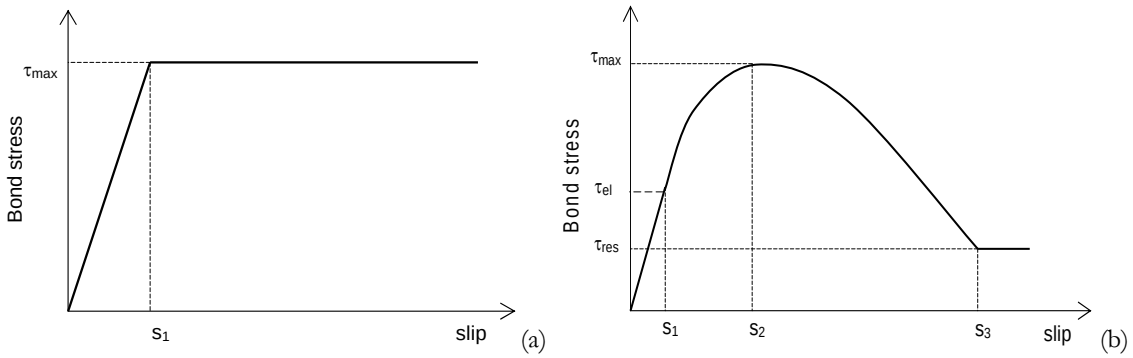

Figure 4.26 Constitutive laws for interface elements: (a) frictional model, (b) damage model

The relationship proposed by [Rodriguez et al., 1994] for evaluating the bond stress τ_{max} as a function of the corrosion percentage has been adopted:

$$\tau_{\max} = 0.6\left(0.5 + \frac{c}{\Phi}\right) f_{ct}\left(1 - \beta x^{\mu}\right) + \frac{k A_{tr} f_y}{s \cdot \Phi} \tag{4.23}$$

where x is the corrosion penetration depth, c/Φ the cover to bar diameter ratio, β μ and k empirical constants, $A_{tr} f_y$ and s the stirrup section, yield strength and spacing respectively.
This expression, which distinguishes the two contributions of concrete (first term of the sum in the right-hand side of Eq.(4.23)) and transverse reinforcement including the confining action (second term of the sum), derives from the fitting of various experimental bond-test data and depends on both the material and geometrical characteristics of the test specimens.
Differently from the "frictional" law, in the "damage" law the bond strength as well as the shape of the bond stress-slip curve are assumed depending on the corrosion level. The relationship has been chosen similarly to the constitutive law for concrete in compression (Figure 4.23). In particular, the opportunity to describe the effects of corrosion on bond introducing in the bond law a unique damage parameter has been investigated. The main advantage is evidently the reduction of the number of input data and the possibility to relate the damage variable directly to the level of corrosion. To this aim, by following the approach described in Section 4.3.3.2 for the chemical-environmental damage in concrete, a corrosion bond damage parameter d_{bond} similar to the variable d_{chem} of Eq.(4.21) has been introduced in the bond law and defined as a monotonically increasing function of the corrosion level. The values of d_{bond} range between 0 and 1, where clearly 0 represents absence of corrosion, while 1 stands for total damage.
Hence, expression (4.22) for concrete stresses may be adjusted for the $\tau - s$ relationship as follows:

$$\tau = \left(1 - d_{bond}\right)\left(1 - d\right)\bar{\tau} \tag{4.24}$$

where $\bar{\tau} = G\gamma$, being G the elastic shear modulus and $\gamma = s/t$ the shear strain; t is the interface thickness; d is the damage variable evolving according to Eq.(4.19b), as described in Section 4.3.3.1.
Alternatively, Eq.(4.24) may be rewritten as a function of the slip s as:

$$\tau = \left(1 - d_{bond}\right)\left(1 - d\right)\overline{G}s \tag{4.25}$$

by defining $\overline{G} = G/t$ which is a property of the interface element related to its height t, representing the initial slope of the $\tau - s$ curve.
As illustrated in Figure 4.27a, the unique parameter d_{bond} allows describing the reduction of both bond stiffness and peak stress with increasing corrosion levels. Nonetheless, it can be observed that the change in shape of the post-peak branch of the curve is nor properly accounted for. Therefore, in order to better represent the increasing brittleness in bond behaviour as the corrosion process evolves, a possibility is to modify the parameter β in Eq.(4.20) according to the corrosion level, as shown in Figure 4.27b.
In this way, the combined action of d_{bond} and β varying along with the corrosion level, assures the capability of the model to effectively simulate the main effects of corrosion on bond behaviour.

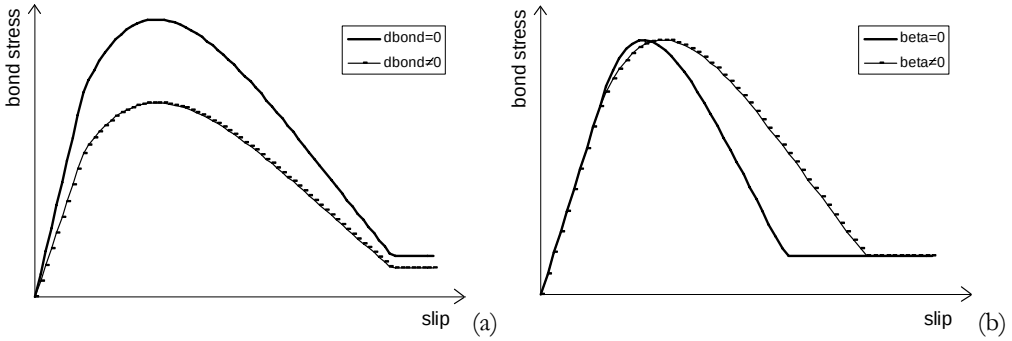

Figure 4.27 Influence of (a) d_{bond} and (b) β on the damage type bond law

In the following section, in order to evaluate the reliability and accuracy of the two proposed bond laws, some experimental tests are numerically simulated. The comparison between laboratory data and numerical results demonstrates the different performance of the two bond laws, even though both approaches show a good agreement with the experimental evidence.

4.4 Validation of the proposed bond laws

Micro-level analyses have been performed using the in-house software *Dante*, developed at the Department of Construction and Transportation of the University of Padova, Italy. The code is interfaced with *Gid* for the analysis of the output results, while the general-purpose software *Straus7* has been used to carry out some initial comparative analyses.
The two-parameter damage law for concrete (including the coupling between mechanical and environmental damage) and the elasto-platic constitutive law for steel implemented in the research code have been already explained in Sections 4.3.3 and 4.3.4.
In the following, some preliminary tests performed to adjust the proposed frictional and damage type laws are briefly presented, while Sections 0 and 4.4.3 describe the application of the models for simulating some experimental tests available in the literature, i.e. a pull-out test and a beam-test performed by [Al-Sulaimani et al., 1990], at increasing levels of corrosion.

4.4.1 Preliminary tests

At the present stage of the research, only bi-dimensional modelling has been carried on. As a consequence, merely tangential stresses have been considered in the analyses, neglecting the radial stresses, which are responsible of the compression of concrete between the reinforcement ribs. Certainly, such a hypothesis implies a simplification of the real three-dimensional

phenomenon. Nevertheless, considering the scope of the research, this is considered an acceptable assumption.

On this topic, it is worth noting that recently a number of researchers have proposed sophisticated bond models based on detailed three-dimensional analyses of the interaction between concrete and bars. The common characteristic of those approaches is the use of 3D models of concrete and reinforcement with 2D interface between them. For example, [Lundgren and Gylltoft, 2000] developed an interface bond model based on the plasticity theory with fully three-dimensional features. In this model, the splitting stresses of the bond action are included, and the bond stress depends not only on slip, but also on the radial deformation between the reinforcing bar and concrete. The advantage of these sophisticated approaches is that the interfacial behaviour can be accurately modelled using conventional material models, such as plasticity. Debonding as well as dilatancy and other bond characteristics can be modelled as well. However, the main drawback is represented by the extremely high computational cost, which limits the applicability of these models in the analysis of real RC structures. In addition, the development of appropriate finite element meshes is not straightforward, as it is generally not supported by existing automatic mesh generation tools, [Jendele and Cervenka, 2006].

Different possibilities have been considered for modelling the connection between steel and concrete elements through interface elements. Finally, the mesh typology shown in Figure 4.28a has been adopted, in which steel and concrete have no nodes in common.

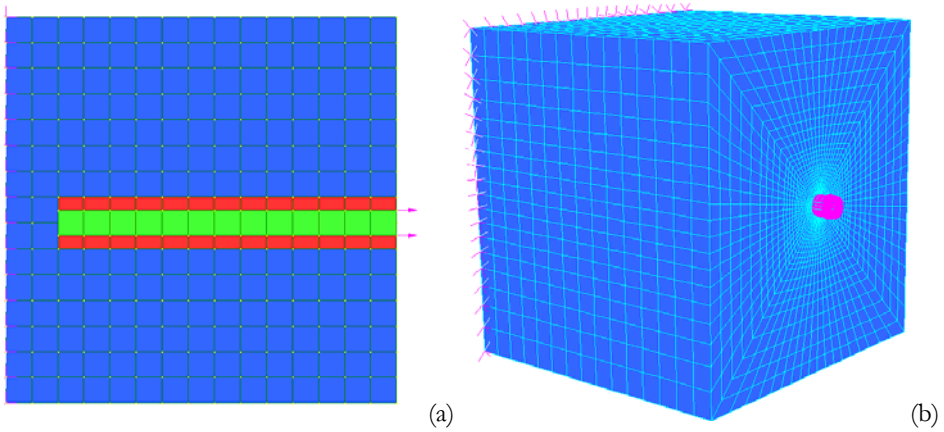

Figure 4.28 FE mesh for pull-out test: (a) 2D model (*Dante*); (b) 3D model (*Straus7*)

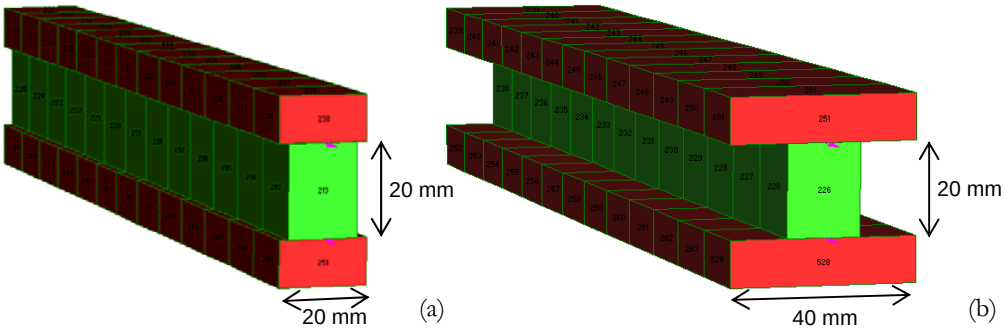

Figure 4.29 Solid view of steel (green elements) and interface (red elements) in the 2D model, with interface depth of (a) 20 mm; (b) 40 mm

Table 4.3 Comparison of the total reaction at fixed concrete nodes

		Total reaction [kN]
Straus7	2D model – interface width 20mm	1417.7
	2D model – interface width 40mm	1831.7
	3D model – mesh 13419 elements	1425.0
	3D model – mesh 28008 elements	1359.1
Dante	2D model - interface width 20mm	1422.4

A first validation test has been performed considering a 300 mm cubic specimen fixed at one face, with a centrally embedded 20 mm bar to which an increasing axial displacement is applied. The results obtained with *Dante* of the 2D model have been compared with the outcomes of the corresponding 3D model realized with *Straus7* (Figure 4.28b). The aim of the comparison is assessing the reliability of a 2D modelling of a 3D physical phenomenon. In particular, the assumption of the most appropriate width of the interface elements, ranging between 20 mm (i.e. equal to bar diameter) and 40 mm, is investigated (Figure 4.29a-b).
Two different meshes of the 3D model in Straus7 have been considered: one with around 13400 brick elements and the other refined up to more than 28000 elements, in order to assess the mesh-size effects. The total reactions at the fixed concrete nodes for the different models are summarized in Table 4.3. As it can be appreciated from the comparison of the results obtained with Straus7, the more realistic 3D model is well approximated by the 2D model with 20 mm interface width. Very close results are obtained with the correspondent 2D model in Dante, thus, in the following analyses, the width of the interface has been assumed equal to the bar diameter.

4.4.2 Simulation of an experimental pull-out test

[Al-Sulaimani et al., 1990] have investigated the influence of reinforcement corrosion and cracking on bond behaviour and bond strength of RC members, considering four different stages of corrosion: non-corrosion, precracking, cracking and postcracking. Such levels have been experimentally obtained by impressing direct current for increasing periods to the reinforcing bar embedded in the specimen submerged in water. In particular, pull-out tests have been performed for simulating severe local degradation, causing significant changes in the rebars surface condition and in the height of the ribs. A schematic drawing of the corrosion setup for pull-out specimen is shown in Figure 4.30. A constant current density of 2 mA/cm^2 was adopted to provide the desired corrosion levels in a reasonable time.

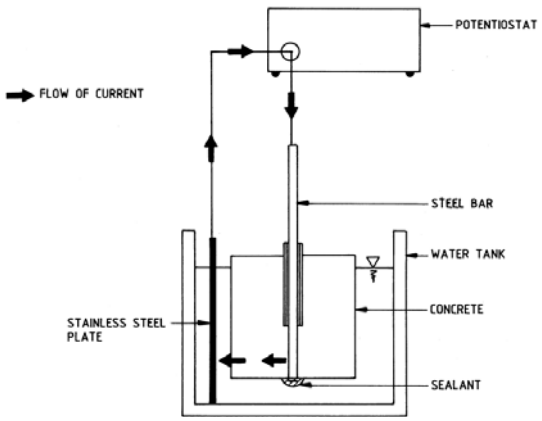

Figure 4.30 Corrosion setup for pull-out specimen [Al-Sulaimani et al., 1990]

In the present thesis, the Test Series no.1 has been simulated, consisting in a 150 mm cubic specimen with a centrally embedded 10-mm-bar subject to pull-out, with a cover-to-bar diameter ratio equal to 7.5 and an embedment length-to-bar diameter ratio of 4.0. The steel had average yield strength of 450 MPa and the concrete had a w/c ratio of 0.55 and an average compressive strength of 30 MPa. Table 4.4 shows the corrosion levels experimentally obtained and the corresponding corrosion percentage, measured as loss of metal relative to the original bar weight.

Table 4.4 Corrosion levels of in experimental pull-out test by [Al-Sulaimani et al., 1990]

Corrosion stage	Corrosion percentage
precracking	0.87 - 1.50%
no corrosion	0%
cracking	4.27%
postcracking	6.7 - 7.8%

The experimental evidence shows an approximately linear trend in the bond stress - slip relationship until, in correspondence to the bond breakdown (around 60-75% of the ultimate bond resistance), the curve's slope changes sharply becoming almost horizontal. From this point, slip further increases with no significant loss of bond resistance.
In the numerical simulation performed with *Dante*, [Berto et al., 2007a], the bar is subject to controlled displacement at its free end. A mesh of 262 four-node plane elements has been used (Figure 4.31a-b) and an interface height $t = \Phi/2$ has been assumed according to the model formulation. The input data assumed for the numerical analyses are given in Table 4.5 and Table 4.6, for concrete/steel and interface respectively. As for β, d_{bond}, τ_{max} and $\overline{G}$ in Table 4.6, the values are given for the four corrosion levels of the non-corrosion, precracking, cracking and postcracking stages.
The bond stress has been calculated as the external load on the bar divided by total surface area of the embedded portion of the bar, thereby representing an average value of stress along the bonded length. For the steel rebar an ultimate strain $\varepsilon_{su} = 8\%$ has been adopted regardless of the corrosion degree, since in the present case of limited corrosion percentages (<10%) no appreciable influence of this parameter is found.

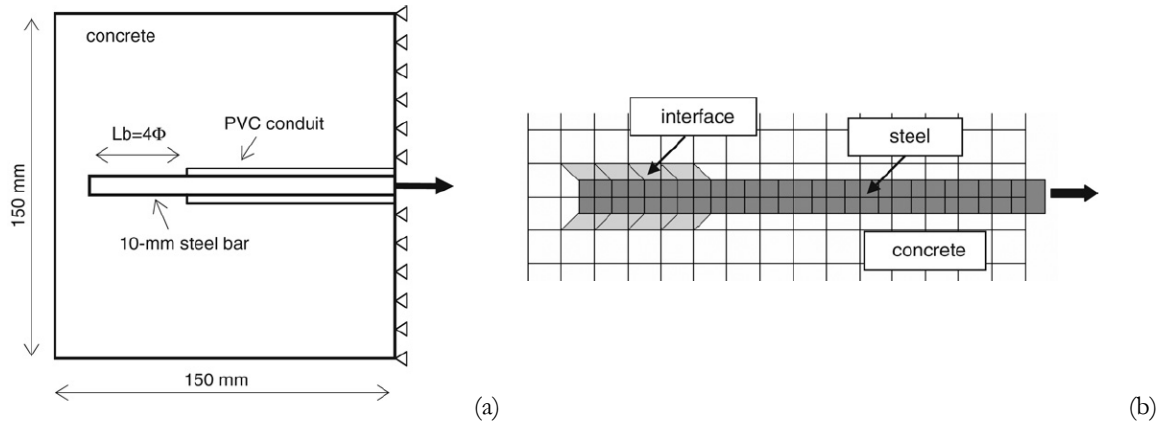

Figure 4.31 (a) Schematic drawing of the pull-out specimen; (b) detail of the FE mesh

Table 4.5 Concrete and steel properties (pull-out test)

Concrete		Steel	
Young's modulus [MPa]	26000	Young's modulus [MPa]	206000
Poisson's ratio	0.2	Poisson's ratio	0.3
f_c [MPa]	30	f_{sy} [MPa]	450
f_t [MPa]	3	hardening parameter	2640
fracture energy [Nmm/mm²]	0.05	ε_{su}	0.08
damage parameter A	0.95		
damage parameter B	1		
$f_{c,2D}/f_{c,1D}$	1.2		
$f_{c,1D\ elastic}$ [MPa]	20		

Table 4.6 Interface properties: damage and frictional type laws (pull-out test)

Damage type law		Frictional type law	
Young's modulus [MPa]	8000		
Poisson's ratio	0.2		
τ_{max} [MPa]	21	$\overline{G}$ [N/mm³]	670 (0%) 420 (4.27%) 190 (6.7%) 80 (7.8%)
damage parameter A	0.8		
damage parameter B	0.5		
$\tau_{elastic}$ [MPa]	16		
β	0.97 (0%) 0.96 (4.27%) 0.87 (6.7%) 0.82 (7.8%)	τ_{max} [MPa]	16 (0%) 14 (4.27%) 8 (6.7%) 4 (7.8%)
d_{bond}	0 (0%) 0.1 (4.27%) 0.48 (6.7%) 0.74 (7.8%)		

For example, even assuming $\alpha_{\max}^{pit} = 0.5$ in Eq.(D.16), the corresponding reduction of the steel ductility, i.e. $\varepsilon_{su} = 6.4\%$, does not modify the sample response. In addition, the environmental damage parameter d_{chem} (see Section 4.3.3.2) has not been accounted for in the example, since no significant concrete degradation was evidenced in the test conditions.

Firstly, a FE analysis has been performed using the frictional bond law for the interface. As shown in Section 4.3.5, this model requires the evaluation of two parameters, τ_{max} and G. Regarding the peak stress τ_{max}, Eq.(4.23) has been adopted and, assuming the values $\beta = 0.17$ and $\mu = 0.8$ for the empirical constants, a good interpolation of the experimental data relative to the pull-out test by [Al-Sulaimani et al., 1990] is obtained (Figure 4.32).

Concerning the evaluation of the initial slope G of the $\tau - s$ relationship, a trial and error process has been followed. Experimental data relative to four corrosion levels were available: 0%, 4.27% 6.7% and 7.8%. To fit these data, the value of G has been calibrated for three levels (0%, 4.27% and 7.8%) and the corresponding curves are shown in Figure 4.33a. Thus, the relationship between shear modulus G and corrosion degree has been derived by means of a linear regression (Figure 4.34). In this way, it was possible to predict the value of G to use in the simulation the

bond stress – slip curve referring to the corrosion degree 6.7%. The results shown in Figure 4.33b confirm a quite good agreement with the experimental data. Nevertheless, as already emphasised, the frictional model is not able to reproduce the descending branch of the curve.
The same pull-out tests have been performed using the damage type model. Similarly to the previous case, the values of d_{bond} and β have been calibrated for the corrosion percentages 0%, 4.27% and 7.8% (Figure 4.35a). The values of the two parameters corresponding to the 6.7% corrosion level have been predicted by the interpolation curves shown in Figure 4.36a-b obtained from the values relative to the other three corrosion degrees.
The comparison between numerical and experimental results (Figure 4.35b) demonstrates the reliability of the proposed approach to predict the main features of the corrosion phenomenon.
Both the suggested bond models are able to effectively simulate the effects of corrosion on bond behaviour in pull-out tests. Nonetheless, in view of the better performance of the damage law especially in reproducing the post peak behaviour, only this second approach will be followed in the following analyses regarding the simulation of a beam-test.

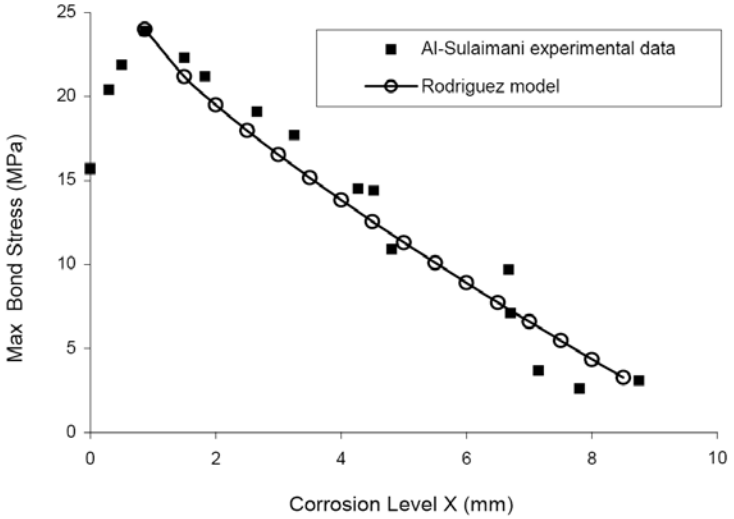

Figure 4.32 Bond stress vs. corrosion level for pull-out specimen: model by [Rodriguez et al., 1994] applied to [Al-Sulaimani et al., 1990] pull-out test results

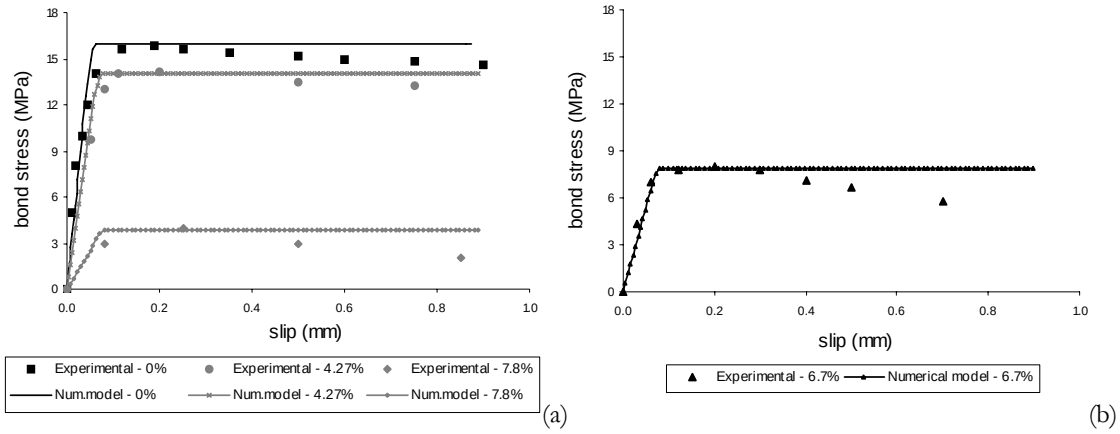

Figure 4.33 Bond stress vs. free-end slip for different degrees of corrosion (frictional law): (a) calibration; (b) prediction for 6.7% of corrosion

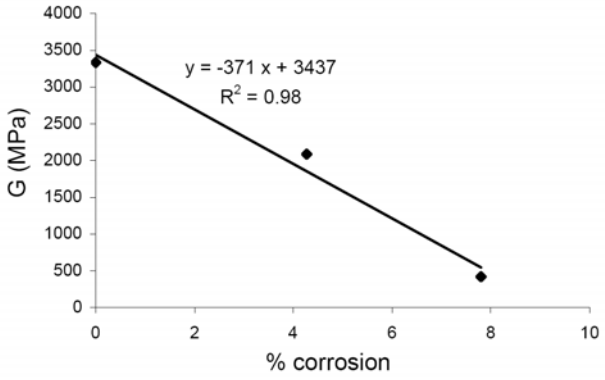

Figure 4.34 Corrosion percentage vs. bond stiffness

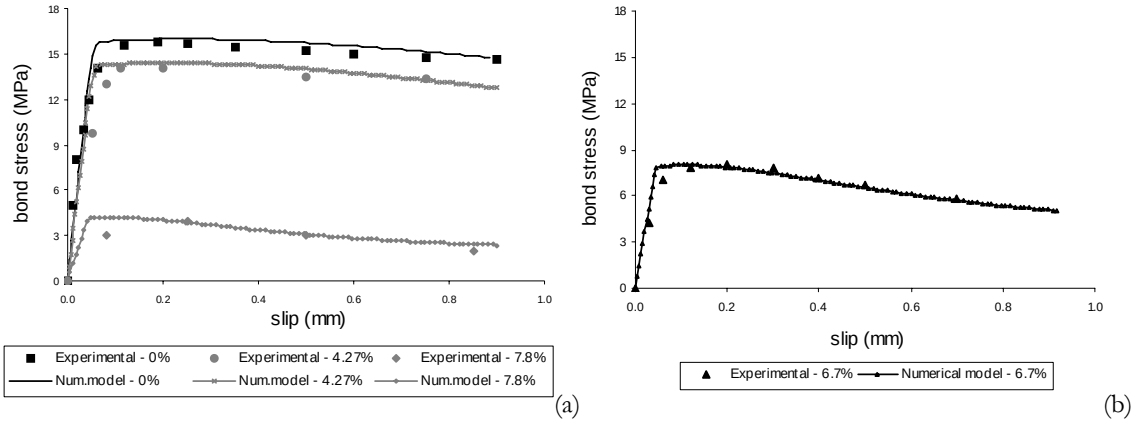

Figure 4.35 Bond stress vs. free-end slip for different degrees of corrosion (damage type law): (a) calibration; (b) prediction for 6.7% of corrosion

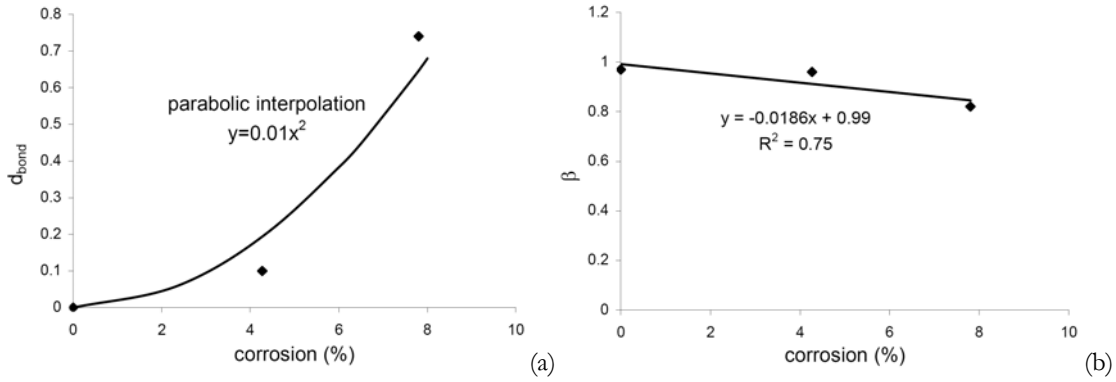

Figure 4.36 Corrosion percentage vs. bond damage parameters: (a) d_{bond}; (b) β

4.4.3 Simulation of an experimental beam test

In the present section, some preliminary results concerning the numerical simulation of the experimental beam tests performed by [Al-Sulaimani et al., 1990] are presented, [Berto et a., 2007a]. Two series of tests have been considered: Series IV, failing in flexure, and Series III, failing in bond, i.e. before the reinforcing steel reached the yield point characterizing failure in flexure. The different failure mechanism was experimentally obtained by reducing the embedment length of the reinforcement from 300 mm in Series IV to 144 mm in Series III beams. In this way, the precedence of bond failure over flexural and shear failures was insured. Each specimen was 150 × 150 mm in cross-section and 1000 mm in length, reinforced with one 12 mm bottom bar, two 10 mm top bars and 6 mm closed stirrups at 50 mm spacing. The concrete had average compressive strength of 40 MPa and the steel had average yield strength of 450 MPa. The specimens were tested as simply supported beams under a two-point loading with a total span of 900 mm and a shear span of 300 mm.

The experimental results demonstrated that, in the case of Series IV beams, where the reinforcement was detailed with an adequate embedment length, the bond stress corresponding to the ultimate flexural load was less then in the case of Series III beams, designed to fail in bond. In these specimens, the ultimate flexural load was unaffected by corrosion up to 1.5% and reduced by 12% for 4.5% corrosion, probably due to reduction in the bar cross-section, as stated by the authors.

For the FE mesh, consisting of 392 four-node plane elements, the same modelling technique used for the pull-out test has been adopted (Figure 4.31b).

As already pointed out in Section 0, the frictional type model is slightly lacking in reproducing the real bond behaviour. For this reason, only the damage type model is adopted.

The value of the main parameters assumed in the model are summarized in Table 4.7. As in the pull-out test, the environmental damage parameter d_{chem} has not been accounted for, since no considerable concrete damage was evidenced in the experimental tests.

It is worth noting that the low value attributed to the Young's modulus of concrete (Table 4.7) stems from the fact that the specimens were probably extensively cracked before loading. Unfortunately, no information on this aspect is provided in the paper.

Figure 4.37a-b shows the load vs. midspan deflection curves, respectively for Series IV and Series III beams, in the pre- and post-cracking stages of corrosion (0.17-4.1% corrosion for Series IV, 0.11-4.5% corrosion for Series III).

Table 4.7 Interface properties: damage type law (beam test)

Young's modulus [MPa]	6000
Poisson's ratio	0.2
τ_{max} [MPa]	25
damage parameter A	0.77
damage parameter B	2.5
$\tau_{elastic}$ [MPa]	15
β	0.98 (0.11% - Series III)
	0.95 (4.5% - Series III)
	0.98 (0.17% - Series IV)
	0.95 (4.1% - Series IV)
d_{bond}	0 (0.11% - Series III)
	0.10 (4.5% - Series III)
	0 (0.17% - Series IV)
	0.10 (4.1% - Series IV)

The effects of steel section loss and bond deterioration in the FE modelling have been also investigated separately. On the one hand, for Series IV beams, the introduction of the bond deterioration effect has no significant influence. In fact, if this effect is not considered, the load-midspan deflection curve is essentially identical to that shown in Figure 4.37a, in which both effects are included. This may be ascribed to the flexural-type failure mode of these beams, for which the capacity is most likely reduced due to bar cross-section loss, according to [Al-Sulaimani et al., 1990]. On the other hand, for Series III beams, the steel section loss has minor influence in the load-midspan deflection curves, since in this case bond behaviour is the governing effect, being the beams designed for bond failure. Thus, the curves of Figure 4.37b do not change significantly if the steel section loss is not accounted for in the numerical simulation.
Finally, the load versus rebar free-end slip curves have been simulated for the Series III beams failing in bond, at the pre-cracking (0.11% corrosion) and post-cracking (4.5% corrosion) levels. The reinforcing bar slip for the i-th element has been calculated accounting for both the contributions of concrete cracking and loss of steel-concrete bond as follows:

$$slip^i = slip^i_{crack} + slip^i_{bond} = L^i(\varepsilon^i_c - \varepsilon^i_s) + (disp^i_{bond,c} - disp^i_{bond,s}) \tag{4.26}$$

where both the components due to cracking and bond loss are given by the difference of the displacements of concrete and steel nodes, averaged to obtain a mean value for the element.

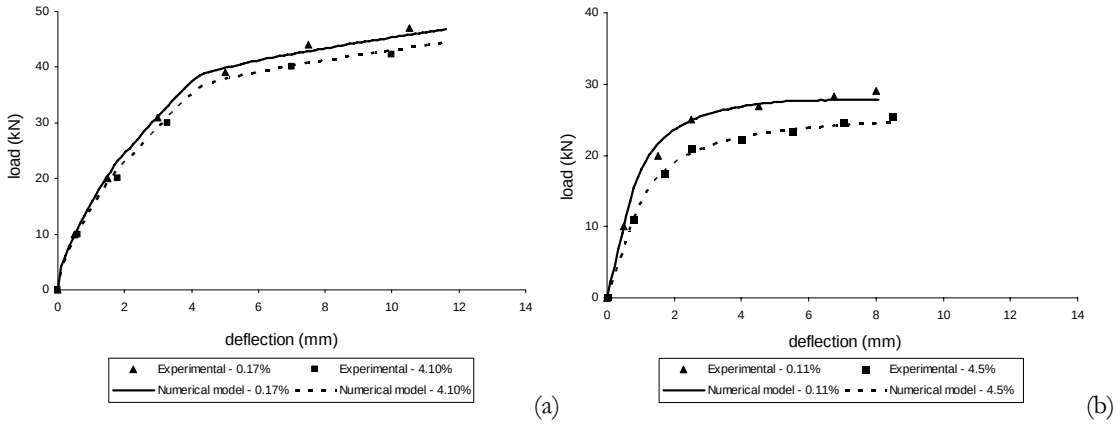

Figure 4.37 Load vs. midspan deflection for (a) Series IV; (b) Series III beams

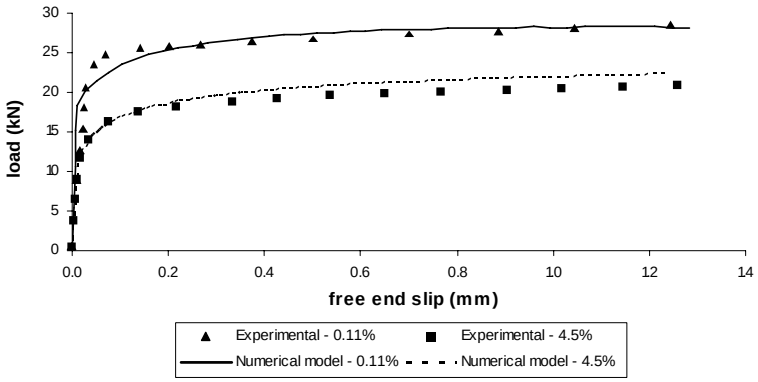

Figure 4.38 Load vs. rebar free-end slip for Series III beams

The good agreement between numerical results and experimental evidence is illustrated in Figure 4.38, indicating the sudden bond breakdown at a load of around 25 kN and 20 kN for the pre-cracking and post-cracking stages respectively.

4.4.4 Sensitivity analysis

A sensitivity analysis has been performed using the probabilistic software Optislang, with the aim of investigating the influence of the input parameters of the bond model, listed in Table 4.8, on the variability of the output parameters, i.e. the bond strength τ and the slip s.

Table 4.8 Input parameters of the sensitivity analysis

Symbol	Description	Mean value	COV	Distribution
	Concrete properties			
E_c	Young's modulus	26000 MPa	0.12	Normal
f_c	Compressive strength	30 MPa	0.16	Log-normal
f_t	Tensile strength	3 MPa	0.20	Normal
G_{f_c}	Fracture energy	0.05 Nmm/mm^2	0.10	Normal
γ_{c_c}	Shear retention factor	1E-7	0.10	Normal
A_c	Damage parameter (see Eq.(4.19))	0.95	0.10	Normal
B_c	Damage parameter (see Eq.(4.19)	1.00	0.10	Normal
β_c	Damage parameter (see Eq.(4.20))	0.80	0.10	Normal
	Steel properties			
E_s	Young's modulus	206000 MPa	0.08	Normal
A_s	Steel section	7.85 mm^2	0.10	Log-normal
f_y	Yield strength	450 MPa	0.12	Log-normal
	Interface properties			
E_{int}	Young's modulus	8000 MPa	0.12	Normal
f_{c_int}	Compressive strength	33 MPa	0.16	Log-normal
f_{t_int}	Tensile strength	3 MPa	0.20	Normal
G_{f_int}	Fracture energy	0.05 Nmm/mm^2	0.10	Normal
γ_{c_int}	Shear retention factor	1E-7	0.10	Normal
A_{int}	Damage parameter (see Eq.(4.19))	0.80	0.10	Normal
B_{int}	Damage parameter (see Eq.(4.19))	0.50	0.10	Normal
β_{int}	Damage parameter (see Eq.(4.20))	0.95	0.10	Normal
d_{bond}	Bond damage parameter	0.1; 0.48; 0.74	0.10	Normal

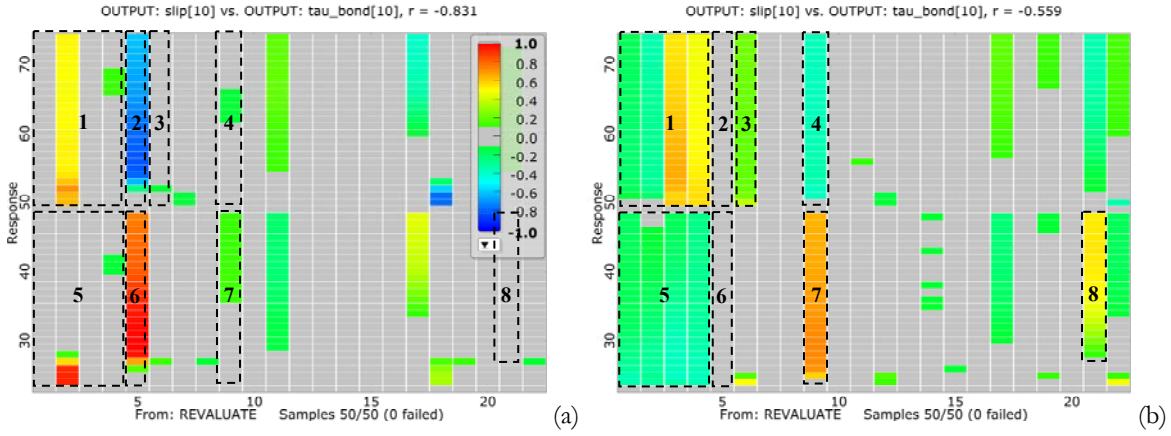

Figure 4.39 Sensitivity analysis: correlation matrix for corrosion levels (a) 4.27% and (b) 7.8%

Table 4.9 Input vs. output parameters in the correlation matrixes sectors

Sector	Input parameter vs. slip	Sector	Input parameter vs. bond strength
1	d_{bond}	5	d_{bond}
2	A_s	6	A_s
3	E_c	7	$f_{c,int}$
4	$f_{c,int}$	8	β_{int}

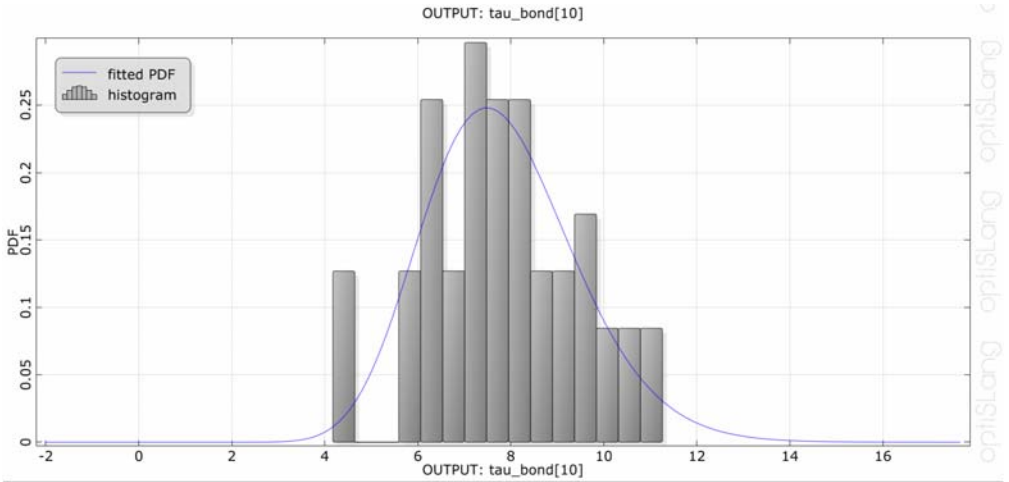

Statistic data			
Min:	4.173	Max:	11.26
Mean:	7.827	Sigma:	1.64
CV:	0.2095		
Skewness:	-0.05639	Kurtosis:	2.622
Fitted PDF: Gamma			
Mean:	7.827	Sigma:	1.64

(a)

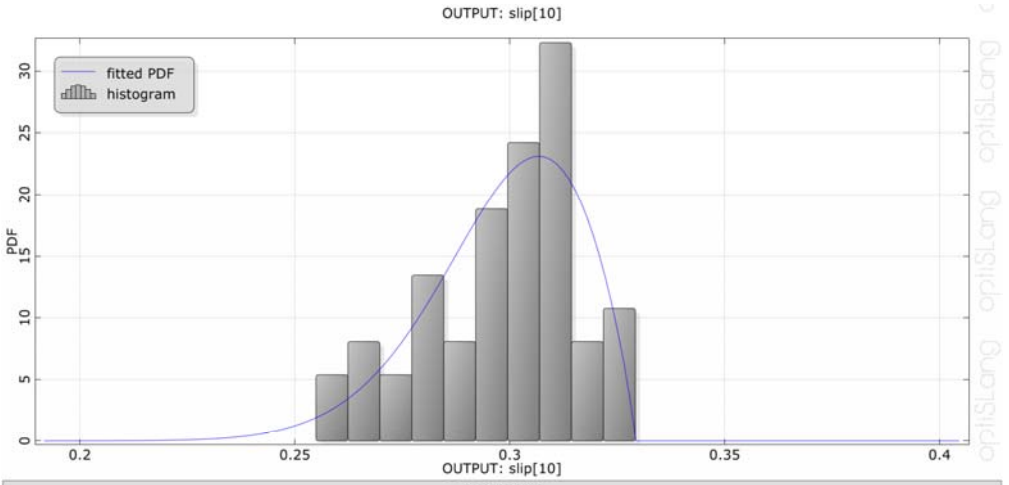

Statistic data			
Min:	0.2549	Max:	0.3292
Mean:	0.2982	Sigma:	0.01774
CV:	0.0595		
Skewness:	-0.544	Kurtosis:	2.68
Fitted PDF: Extreme Typ III (Min) Weibull			
Mean:	0.2982	Sigma:	0.01774
Upper cut:	0.3292		

(b)

Figure 4.40 Probability density function of (a) τ_{max} and (b) $s(\tau_{max})$ for corrosion level 6.7%

The most appropriate variation coefficient and distribution type have been chosen referring to the literature (see Table 5.10) or simply assumed, if not available due to lack of data, e.g. [Val and Trapper, 2008].
The importance of performing this type of investigation, in view of the inevitable uncertainties affecting the material, geometrical and damage variables of the model, is underlined in Section 5.3.1.
In order to keep the necessary number of samples, i.e. solver runs, as low as possible, the Latin Hypercube Sampling method has been chosen. Therefore, according to Eq.(5.8), a number of samples $N = 50 > 2(n_i + n_o) = 2 \cdot 24 = 48$ (22 inputs and 2 outputs) is sufficient.
The results of the investigation for the 4.27% and the 7.8% corrosion degrees are shown in Figure 4.39 in terms of correlation matrix. It can be observed that the influence of the input parameters changes as the level of corrosion increases. In particular, eight sectors are highlighted in the graphs and the corresponding input vs. output parameters are listed in Table 4.9. Of interest, it can be observed that, with increasing levels of corrosion, the influence of the steel section (sectors 2 and 6) decreases, while $f_{c,int}$ and β_{int} become more influential, with respect to both output parameters.
Finally, for the 6.7% corrosion level, Figure 4.40a-b shows the histogram and fitted probability density function for the maximum bond strength τ_{max} and the corresponding slip $s(\tau_{max})$.

In this chapter, steel corrosion has been investigated, highlighting the physical aspects of the phenomenon which have been considered in the numerical simulations. In particular, the results presented in Section 4.4 show the potentiality of the proposed damage bond model in capturing the local behaviour of corroded RC members, for which the steel-concrete interaction may be significantly compromised. A probabilistic framework is considered in the following chapter, in which the matter of reinforcement corrosion is included in the crucial issue of safety assessment.

CHAPTER 5 SAFETY ASSESSMENT

The matter of safety assessment is a challenging task, especially with regard to RC structures, whose structural performance may significantly vary over time due to a number of causes, among which the degradation of the materials should be mentioned. For this reason, a probabilistic approach is strongly required. A procedure for calculating the probability of occurrence of a corrosive attack is proposed in this chapter, accounting for the random nature of the parameters involved by means of sensitivity and robustness analyses. The so attained likelihood of steel corrosion constitutes, together with the likelihood of a seismic event, the probability of occurrence of the hazards, which allows calculating the structural risk as described in CHAPTER 6 in compliance with the risk management procedure presented in CHAPTER 2 and CHAPTER 3.

5.1 Introduction

The safety of buildings is perceived by society as an essential attribute of daily life, [JCSS, 2001b]. Concerning new structures, the task of assuring adequate safety levels has been extensively investigated, even though not yet exhaustively. Nevertheless, the crucial and increasing demand for the assessment and rehabilitation of existing structures, especially in the industrialized areas, has revealed the limited current knowledge regarding the most appropriate methodology to be applied and the safety levels to be allowed.

As a matter of fact, the assessment of an existing structure may strongly differ from the design of a new one. First, the knowledge on the loads and resistance parameters is obviously completely different. In addition, special attention must be paid to the parts of the existing construction in which an actual danger in relation to the observed behaviour of the structure has been identified.

Therefore, specific procedures and tools are necessary in order to assess the safety of existing constructions. According to [JCSS, 2001b], the following fundamental goals should be pursued:

- to standardize methods and terminology (the lack of a unified and internationally accepted vocabulary has been already pointed out in Section 2.3.1 regarding risk management);
- to be operational for consulting engineers;
- to be generally applicable for different materials and structural types;
- to be useful as guidelines of pre-codification state, i.e. to build the basis of future codes, standards or recommendations.

From a general point of view, a structure is safe when the effects of the applied actions are not larger than the corresponding resistance. However, when dealing with concrete structures, the structural performance must be considered as time dependent, as a consequence of the progressive deterioration of the mechanical properties of the materials and the resulting reduction of the load bearing capacity of the structural system (Figure 5.1).

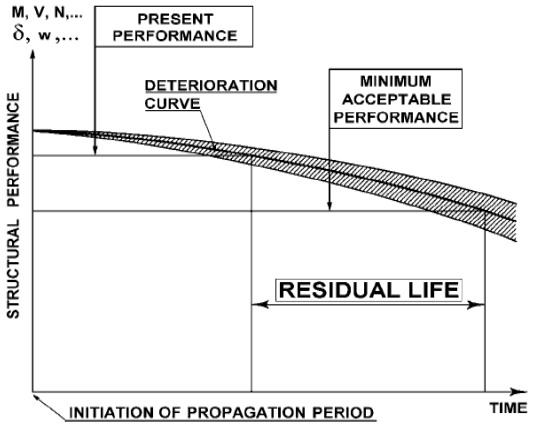

Figure 5.1 Structural deterioration with time [Rodriguez et al., 2001]

Therefore, in order to assure an adequate level of structural performance during the whole service life of the structure, the structural model must account for structural deterioration, [Biondini et al., 2008a]. Both the demand and the resistance may vary during time and a durability analysis aimed at a reliable evaluation of the actual structural lifetime should be able to account for such variability.

5.2 Probabilistic assessment of structural durability

5.2.1 Introduction

The assessment of structural durability can be dealt with in two ways. One possibility is to analyze the evolution in the structure's performance, following the so called *performance principle*, or in alternative the evaluation of its service life, according to the so called *service life principle*, [Sarja and Vesikari, 1992].

In the former case, a suitable model is used to calculate a function that measures the performance, usually indicated as *R*, and this must always be bigger than the expected loads *S*. In the latter case, the service life T_c is calculated using a prediction model and the resulting value must be greater than the expected service life T_e.

The two methods lead to the same results and can be compared in three different ways:

1. using a *deterministic* approach, i.e. by directly comparing the calculated and expected values:

$$R(T_e) > S(T_e) \qquad T_c > T_e \tag{5.1}$$

2. using a *stochastic* approach, making sure that the probability P_f of $R < S$ (or $T_c < T_e$) is lower than the maximum allowable probability of failure P_{max}:

$$P_f = P\{R - S < 0\} < P_{\max} \qquad P_f = P\{T_c < T_e\} < P_{\max} \tag{5.2}$$

3. using a method based on the definition of a safety factor γ_t applied to the service life to convert the value for the expected life into a design value: $T_d = \gamma_t T_e$ and subsequently using the deterministic criterion: $R(T_d) > S(T_d)$ (or $T_c > T_d$).

With reference to the phenomenon of reinforcement corrosion, it has been shown in Figure 4.13 how the service life of the structure can be expressed as the sum of the corrosion initiation time

t_{in} and the corrosion propagation time t_p. In the case of concrete carbonation, as already described in Section 4.2.1.1, failure due to corrosion initiation can be regarded as the probability that the carbonation front reaches a depth d equal to the thickness of the concrete cover, starting the depassivation of the steel bar and thus the corrosion process:

$$P_f = P\{cover \leq d\} < P_{\max} \tag{5.3}$$

It is worth noting that this approach disregards the contribution of the corrosion propagation time in the assessment of the design life of the structure. Nevertheless, in the present work, such probability of corrosion initiation is not regarded as a real failure probability, but represents the component due to corrosion of the probability of occurrence of the hazards (corrosion and earthquake) in the calculation of the *Structural Risk*. The contribution of the propagation time is then included in the evaluation of the effects of corrosion (in particular, in the steel section reduction) and consequently in the corresponding expected damage undermining the structure.
In the case of a deterioration process such as carbonation and/or chlorides ingress, the limit state function may be quite complex, being a combination of physical and chemical processes along with a variable mechanical load (Figure 5.2).

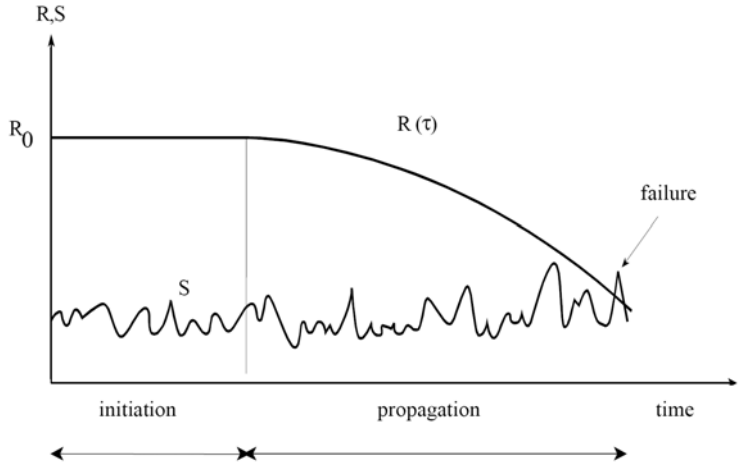

Figure 5.2 Failure due to a combination of physical, chemical and mechanical processes [JCSS, 2001a]

It should be kept in mind that also in the case of a non-deteriorating time independent resistance and a stationary loading condition, the failure probability is also time dependent due to the random fluctuations of the load. This, however, is usually not considered as a durability problem, [JCSS, 2001a].

5.2.2 Codification framework

Codes have changed significantly over time due to technology development and experience gained with the performance of structures when struck by past hazardous events. In general, the codes reflect the increasing awareness of the engineering society for the importance of risk-based decision making in design and maintenance, [Vrouwenvelder, 2008].
To cite some examples, the ISO TC 98, the SIA 462 (Switzerland), the Danish Technical Research Council, the ACI 437R, the JCSS (Joint Committee of Structural Safety), the Dutch Recommendations should be mentioned.
Regarding existing structures, the [JCSS, 2001a] distinguishes between the following code types:

- pre-normative research, including for example code committee work, documents of international associations or organizations;
- guidelines and recommendations in use: a large number of countries (the USA, Canada, Switzerland, the UK) have presented documents for particular categories of structures, such as bridges, towers or normal buildings and also recommendations associated with particular aspects like seismic parameters modelling;
- applicable code type documents, available and actually utilizable only in a few countries.

Nowadays it is commonly accepted that the safety of structures should be expressed in terms of reliability, defined as the ability (usually expressed in probabilistic terms) of a structure or a structural member to fulfil the specified requirements, including the design working life, for which it has been designed (see Section 5.5).

In line with this approach, the first clause in EN 1990, Section 2 - Requirements, states: "*A structure shall be designed, and executed in such a way that it will, during its intended life, with appropriate degrees of reliability and in an economical way sustain all actions and influences likely to occur during execution and use, and remain fit for the use for which it is required*".

Accordingly, different levels of reliability may be adopted for structural resistance and for serviceability, i.e. different measures for the socio-economic optimisation of the resources to be used, taking into account the costs, the use and the type of structure, the situation considered in the design and all expected consequences of failures in terms of: (a) risk to life or injury; (b) potential economic losses; (c) degree of social inconvenience; (d) amount of expense and effort required to reduce the risk of failure, [JCSS, 2001a].

Similar consequences may be identified within the Risk Management Process described in CHAPTER 2: points (a), (b) and (c) respectively with the *Human Consequences*, the *Economic Consequences* and the *CSH Consequences* in the Loss Assessment phase, and point (d) with the *Loss Mitigation* phase. It is worth noting that the RMP, for the sake of its completeness, includes also the *Ecological Consequences*, which may be not negligible in the Risk Management of civil engineering facilities.

The different levels of reliability can be achieved by suitable combinations of:

- preventative and protective measures, e.g. implementation of safety barriers, active and passive protective measures against fire, protection against risk of corrosion such as painting or cathodic protection, etc.;
- measures related to design calculations, i.e. representative values of actions and the choice of partial factors;
- measures related to quality management;
- measures aimed to reduce errors in the design and execution phases, and gross human errors;
- measures related to other design matters, such as the basic requirements, the degree of robustness (structural integrity), durability (including the choice of the design working life), the extent and quality of preliminary investigations of the soil and possible environmental influences, the accuracy of the adopted mechanical models, the detailing;
- efficient execution;
- adequate inspection and maintenance according to procedures specified in the project.

For the purpose of reliability differentiation, consequences classes "CC" have been identified in [Eurocode 0, 2002] by considering the consequences of failure or malfunction of the structure, as given in Table 5.1. It is worth noting that, depending on the structural form and decisions

made during design, particular members of the structure may be designed according to the same, lower or higher consequences class than for the entire structure.
Three reliability classes RC1, RC2 and RC3 may be associated with the three consequences classes CC1, CC2 and CC3 described in Table 5.1.
In the context of codifications for the design of new durable concrete structures and the assessment of existing ones, the recent Model Code for Service Life Design, [CEB-FIP, 2006], gives a fundamental contribution. The applicability of the code is related to other documents, in particular the [Eurocode 0, 2002], the Probabilistic Model Code [JCSS, 2001a], the ENV 13670-1 *Execution of concrete structures* (2000) and the ISO 2394 *General principles on reliability of structures* (1998).

Table 5.1 Definition of consequences classes [Eurocode 0, 2002]

Consequences Class	Description	Examples of buildings and civil engineering works
CC3	High consequence for loss of human life, or economic, social or environmental consequences very great	Grandstands, public buildings where consequences of failure are high (e.g. a concert hall)
CC2	Medium consequence for loss of human life, economic, social or environmental consequences considerable	Residential and office buildings, public buildings where consequences of failure are medium (e.g. an office building)
CC1	Low consequence for loss of human life, and economic, social or environmental consequences small or negligible	Agricultural buildings where people do not normally enter (e.g. storage buildings), greenhouses

Table 5.2 Limit states due to environmental attacks suggested by [CEB-FIP, 2006]

Limit state	Type of limit state	Suggested β-values
Depassivation of reinforcement	SLS	1.0 ÷1.5
Cracking due to reinforcement corrosion	Designer decision	-
Spalling of concrete cover due to corrosion	Designer decision	-
Collapse due to loss of steel cross section	ULS	-

The basic idea proposed by the Fib Bulletin is to establish a design approach avoiding deterioration of concrete and embedded steel caused by environmental actions and to prepare the path for the standardization of performance based design approaches. To this aim, four steps should be carried out. The first one requires quantifying the deterioration mechanism with realistic models able to describe the process physically and/or chemically with sufficient accuracy, which means the model should be validated by realistic laboratory experiments and by practical observations. The second step is the definition of the limit states the structure should be designed for, such as depassivation of reinforcement, cracking and spalling of the concrete cover due to reinforcement corrosion, collapse due to loss of steel cross section. The third step is the calculation of the probability that these limit states occur (probability of occurrence). Finally, the fourth step is the definition of the type of the limit states previously defined, i.e. service limit state SLS or ultimate limit state ULS. As for this aspect, some suggestions are given in Table 5.2. For example, depassivation could be classified as SLS, since there is no immediate consequence on structural safety if the reinforcement is depassivated. This means values of the reliability index β in the range 1.0 to 1.5, even tough higher values may be required to ensure the

aesthetic quality of the structure. Cracking and spalling limit states depend on the designer decision: when they occur in anchorage zones without sufficient transversal reinforcement they may lead to collapse (i.e. ULS), otherwise they may be defined as SLS when they have no influence on the bearing capacity of the structural element. According to [Faber, 2006], spalling due to reinforcement corrosion may be considered as ULS, since for most infrastructure facilities it implies the risk of pieces of concrete falling and potentially hitting by-passers or vehicles. The index β is related to the required level of reliability. The relationship between β and the probability of failure P_f is the following:

$$P_f = \Psi(-\beta) \tag{5.4}$$

where Ψ is the cumulative distribution function of the standardised normal distribution.
Approximately, for β-values between 1 and 4, the following relation might be used:

$$P_f \approx 10^{-\beta} \tag{5.5}$$

The standard procedure is to calibrate the reliability level β to current design levels. As long as the current design practice is not obviously unsatisfactory, either from the safety or from the economical point of view, the average reliability is not changed, [Vrouwenvelder, 2008].
The Model Code for Service Life Design may be applied for the design of new structures, for the update of the service life design of existing structures, if real material properties and/or the interaction of environment and structure can be measured (e.g. real concrete covers, carbonation depths, etc.), and finally for the calculation of the residual service life.
Table 5.3 and Table 5.4 give minimum β-values for each reliability class, as recommended by [Eurocode 0, 2002] and [CEB-FIP, 2006], intended for the ULS and the design life time correspondingly. Interestingly, [CEB-FIP, 2006] assigns these values of β for the Exposure Classes XC, XD and XS of Eurocode 2 (see APPENDIX B), related respectively to carbonation-induced corrosion, chlorides-induced corrosion (deicing salts) and corrosion produced by seawater chlorides.

Table 5.3 Recommended minimum β-values, intended for the ULS [Eurocode 0, 2002]

Reliability class	Minimum values for β	
	1 year reference period	50 yr reference period
RC3	5.2	4.3
RC2	4.7	3.8
RC1	4.2	3.3

Table 5.4 Recommended minimum β-values, intended for the design life time [CEB-FIP, 2006]

Reliability class	Minimum values for β	
	Depassivation	Collapse
RC3	1.3 ($P_f \approx 10^{-1}$)	4.4 ($P_f \approx 10^{-6}$)
RC2	1.3 ($P_f \approx 10^{-1}$)	4.2 ($P_f \approx 10^{-5}$)
RC1	1.3 ($P_f \approx 10^{-1}$)	3.7 ($P_f \approx 10^{-4}$)

Corrosion of reinforcement and/or deterioration of concrete (bond failure, lack of sufficient compressive cross section) will clearly decrease the reliability. In order to achieve the structural ULS reliability, corrosion should be excluded. If this is not possible and inspection, maintenance, repair interventions cannot be executed, this will lead to the need of extra reinforcement

(sacrificial cross section) and/or special detailing in order to avoid bond failure within the bonding zone. The dimension of this extra cross section highly depends on the reliability. That means, the higher the reliability with regard to depassivation, the lower the need for extra reinforcement.

As well known, structural failure caused by reinforcement corrosion may be due to loss of steel cross section or to spalling of concrete cover and loss of anchorage. Consequently, critical values need to be defined for ULS. Unfortunately, reliable findings for limit values of corrosion intensities causing spalling do not exist. Limit values will depend on several factors, like bar diameter, bar spacing and environmental conditions (related to the volume of rust products).

Critical values for the loss of rebars section are suggested by [CEB-FIP, 2006]. They represent rough estimates needing confirmation from further research and can be taken as mean values (the cross section is assumed to contain more than three single bars). To differentiate failure modes, robustness classes "ROC" may be defined, as shown in Table 5.5.

Along with the selected reliability class or the importance of the structure and in accordance to national requirements, three design supervision levels "DSL" may be also distinguished (Table 5.6), consisting in various organisational quality control measures, like checking of calculations, drawings and specifications. Moreover, still in accordance with the reliability classes, three execution classes "EXC" can be identified (Table 5.7).

Table 5.5 Robustness classes [CEB-FIP, 2006]

Robustness class	Characteristics	Mean loss of cross section ΔA_s [%]
ROC 3	Bending reinforcement outside of anchorage and laps	25
ROC 2	Shear reinforcement, anchorage zones with confinement	15
ROC 1	anchorage zones without confinement	5

Table 5.6 Design supervision levels [CEB-FIP, 2006]

Design supervision level	Characteristics	Minimum recommended measures
DSL 3	Extended supervision	Checking by an organization different from that which has performed the design (Third Party Checking)
DSL 2	Normal supervision	Checking by different people than those originally responsible and in accordance with the organisation procedure
DSL 1	Normal supervision	Checking by people who performed the design (Self Checking)

Table 5.7 Execution classes [CEB-FIP, 2006]

Execution class	Characteristics	Requirements
EXC 3	Extended inspection	Third Party inspection
EXC 2	Normal inspection	Inspection in line with the procedure of the organisation
EXC 1	Normal inspection	Self inspection

Table 5.8 Operative collapse probabilities per year (GriSiBau, 1981) [Urban, 2006]

Class	Description	Operative collapse probability per year
1	No danger for persons and low economical consequences	$1.34 \cdot 10^{-5}$
2	Danger for persons and/or considerable economical consequences	$1.30 \cdot 10^{-6}$
3	High importance of the structure for the public	$1.00 \cdot 10^{-7}$

As for the probability of collapse, the German GruSiBau (1981) identifies three safety classes (Table 5.8), but no information is given about the possible loss of life and its related probability of occurrence. The simplest measure to describe the risk of human death is the mortality rate, i.e. the probability of dying as the consequence of a certain event. This tool may be used to define acceptable risks for the individuals, as shown in Table 5.9 from different source data.

Table 5.9 Acceptable risk bases [Urban, 2006]

Acceptable risk of one person dying within one year	Relative mortality rate per year	Source
Acceptable risk in British heavy industry (old value)	$4 \cdot 10^{-3}$	[Paté-Cornell, 1994]
Acceptable risk in British heavy industry (new value)	$2 \cdot 10^{-3}$	[Paté-Cornell, 1994]
Acceptable risk on British oil platforms	10^{-3}	[Paté-Cornell, 1994]
Acceptable risk for old buildings	10^{-4}	[Paté-Cornell, 1994]
Maximum tolerable risk for public	10^{-4}	[Hse, 2001]
Acceptable risk	$1.1 \cdot 10^{-5}$	[Comar, 1979]
Acceptable risk Netherlands	10^{-5} - 10^{-6}	[Schneider, 1996]
Acceptable risk of developing cancer	10^{-6}	[Kelly, 1991]
Collapse of building	10^{-7}	[Rackwitz, 1998]
De minimis risk for the public	10^{-8}	[Paté-Cornell, 1994]

5.2.3 Literature review

[Val, 2007] considers the reliability of RC beams associated with the effect of reinforcing steel corrosion on both the flexural and shear strength, with particular attention to the influence of localized corrosion of stirrups on the shear performance. The mechanics of pitting corrosion is modelled by means of a Gumbel distribution, using an empirical approach based on a statistical characterization of the maximum pit depths. The spatial variability of pitting corrosion and the possibility of failure at different beam cross sections (not only at the most loaded one) are also taken into account. The results show that localized corrosion of stirrups has a significant influence on the reliability of RC beams.

A more general approach to the probabilistic prediction of the lifetime of RC plane frames with respect to structural collapse is proposed by [Biondini et al., 2008b]. The effects of the exposition to an aggressive environment are described by the corresponding evolution in time of the axial force-bending moment resistance domains. Through Monte Carlo simulations, the time-variant probability of failure as well as the expected structural lifetime associated with a prescribed reliability level are evaluated. Similarly to the model used for concrete in the present thesis (see Section 4.3.3), a degradation law is introduced to model the structural damage of both

concrete and steel at time *t* by means of two dimensionless time-dependent damage indices $\delta_c(t)$ and $\delta_s(t)$, giving a direct measure of the damage level within the range [0-1]:

$$dA_c(t) = [1 - \delta_c(t)] \cdot dA_{c0} \qquad dA_s(t) = [1 - \delta_s(t)] \cdot dA_{s0} \tag{5.6}$$

where dA_{c0} and dA_{s0} indicate the undamaged areas at time t_0.
Given the scalar load multiplier $\lambda \geq 0$, the structure is assumed to be safe from the deterministic point of view when $\lambda \leq \lambda_c$, being λ_c the "collapse multiplier" associated with failure. In particular, $\lambda_c = \lambda_c(t)$ is a function of time and a random variable, considering the uncertainties involved in the problem. Thus, the probability of failure P_f at a certain time instant t_k can be evaluated by the integration of the density function $f_{\lambda_c}(\lambda_k)$ within the failure domain $D_k = D(t_k) = \{\lambda_k \mid \lambda_k \leq \lambda\}$:

$$P_f(t_k) = P[\lambda \geq \lambda_{ck}] = \int_D f_{\lambda_c}(\lambda_k) d\lambda \tag{5.7}$$

In [Marsh and Frangopol, 2008] the distribution for the corrosion initiation time in a RC deck slab affected by chlorides penetration is calculated using Monte Carlo simulations, providing a mean value 3.33 years, given a 30.2 mm cove (Figure 5.3).

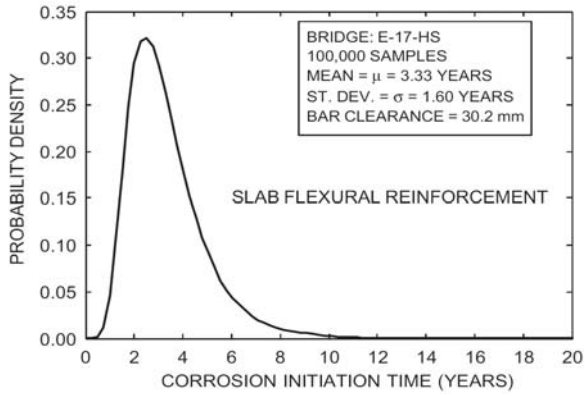

Figure 5.3 Probability density function of corrosion initiation time for RC deck slab flexural reinforcement [Marsh and Frangopol, 2008]

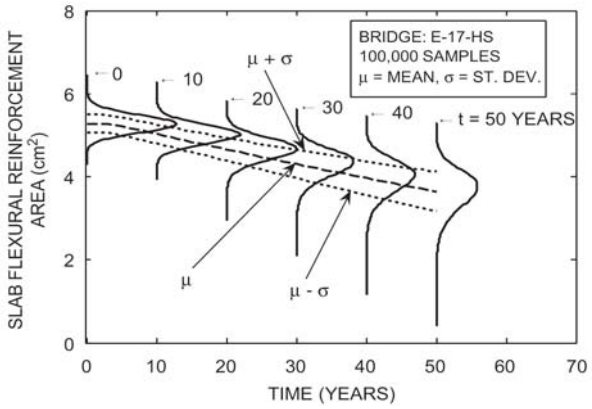

Figure 5.4 Time variation of flexural reinforcement area of RC deck slab [Marsh and Frangopol, 2008]

Afterwards, the distributions for the steel residual sections over the 50-year life time are calculated. As shown in Figure 5.4, the predicted steel area decreases from an initial value of 5.28 cm^2 to a final value of 4.15 cm^2 after 50 years. Moreover, it can be observed how the standard deviation of the distribution increases over time due to increasing uncertainty. The authors assumed a corrosion rate of 0.0582 mm/year (around 5 $\mu A/cm^2$), that is within the range of high corrosion rate values according to Table 4.1.

The model finally incorporates both spatial and temporal variations of the corrosion rate, allowing assumed corrosion rate data from hypothetical sensors at critical locations to be interpolated spatially between sensor locations, and temporally between annual sensor readings.

In [Li et al., 2008] stochastic models are used to estimate the likely time to elapse for the phases of the corrosion process: initiation, corrosion-induced concrete cracking and structural strength reduction. Concerning the first phase, the authors have estimated the probability of corrosion initiation as a function of time, for different threshold values of the chloride content, in both cracked and uncracked concrete (Figure 5.5). As expected, the threshold value determines the final probability of corrosion initiation. Finally, the structural strength reduction is treated in terms of steel section reduction, comparing the residual strength $R_s(t)$ with an acceptable strength $R_a(t) = 0.7\ R_0$, where R_0 is the strength of the original undamaged structure, according to [Amey et al., 1998].

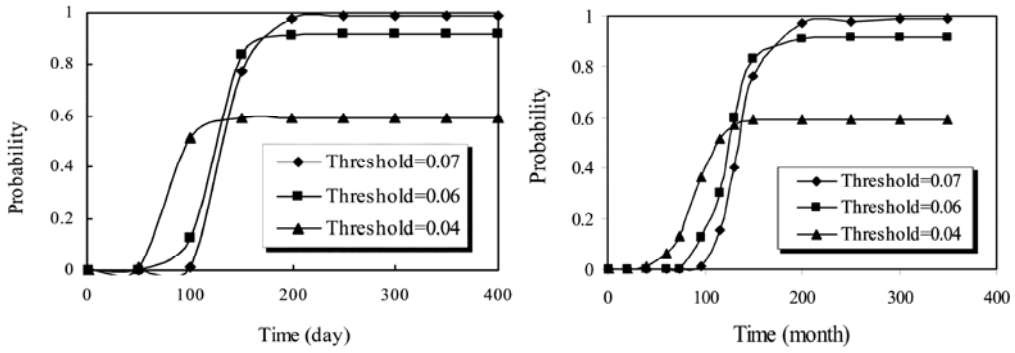

Figure 5.5 Probability of corrosion initiation: (a) cracked; (b) uncracked concrete [Li et al., 2008]

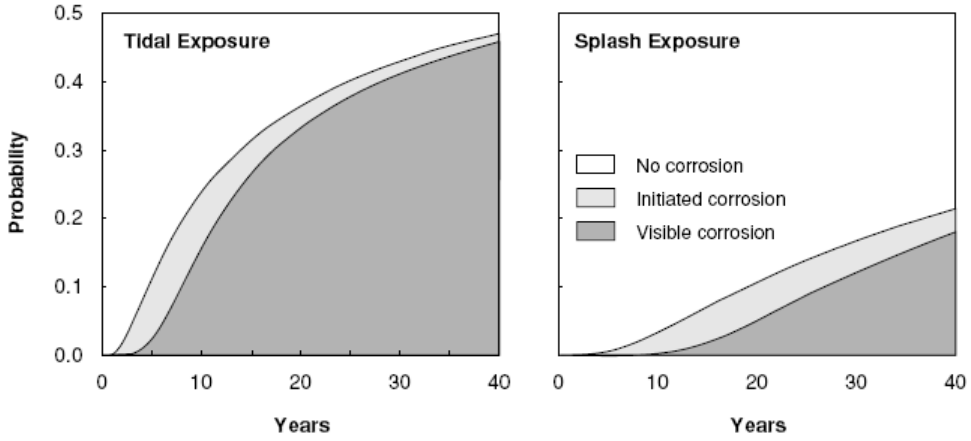

Figure 5.6 Probability of occurrence of the three condition states: no corrosion, initiated corrosion and visible corrosion, for the same element and two different exposure classes [Faber, 2006]

Basing on a probabilistic model for chloride-induced corrosion, [Faber, 2006] calculates the probability that a structural element with given distribution parameters for geometry and environmental exposure conditions falls into one of the three corrosion states: no corrosion, initiated corrosion, visible corrosion. Figure 5.6 shows the significant influence for the same structural element of the condition indicator exposure, assuming first an environmental exposure class corresponding to a tidal environment (left graph), and then a splash zone class (right graph), with all the other parameters kept fixed.
[Val and Trapper, 2008] performed a probabilistic analysis to estimate the time to corrosion initiation in a RC wall and a RC column in a marine environment. The cumulative probability of corrosion initiation plotted against the time of exposure (Figure 5.7), demonstrates that the use of 1-D models of chloride ingress into concrete leads to the overestimation of the time to corrosion initiation and equivalently the underestimation of the probability of corrosion initiation.
A comparison between different software tools for the probabilistic lifetime prognosis is proposed in [Budelmann et al., 2008].

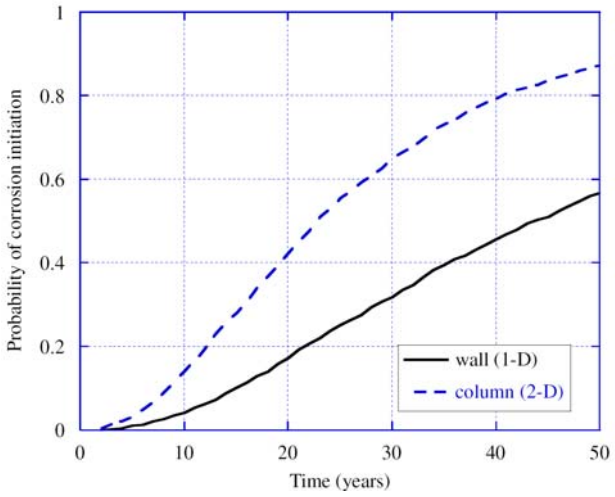

Figure 5.7 Probability of corrosion initiation [Val and Trapper, 2008]

5.3 Analysis of parameters sensitivity

5.3.1 Remarks on uncertainties

Large uncertainty is intrinsic in the estimation and prediction of the structural response of reinforced concrete members, especially when affected by degradation phenomena. In general, when dealing with the assessment of a model or the prediction of certain events, two main types of uncertainty may be distinguished: aleatory and epistemic uncertainties, [Gardoni et al., 2002].
Aleatory uncertainties are inherent to nature and irreducible, since they can not be influenced by the observer or the manner of the observation. Epistemic uncertainties derive from our lack of knowledge, the level of simplification we bring in the matters, the error in measurements, the number of observation samples. All these sources of uncertainties may be reduced, for example by improving the model or by increasing the accuracy of the measurements and the number of samples. It is worth noting that the sensitivity analysis has also the important task to concentrate the generally costly and demanding tests on the really influencing parameters characterizing the

structural response. In this way, the in-situ and/or laboratory tests (especially destructive tests) will be performed only to investigate a restricted number of parameters and only if actually contributing to a better understanding of the structural behaviour.
In the present research, no in-field measurements were available and all information and input data used in the analyses have been acquired from the literature or previous studies. Uncertainties are included by assigning a probabilistic distribution to the most influencing parameters, identified by means of a preliminary sensitivity analysis. Nevertheless, it is difficult at this stage of the research to distinguish between the two types of uncertainties and to assess their distinct influence on the results.

5.3.2 Random nature of material properties

It is well-known, [Biondini et al., 2008a], that due to the uncertainties in material and geometrical properties, in the magnitude and distribution of the loads, in the physical parameters defining the deterioration processes, the deterministic results of a limit analysis cannot be used for reliable quantitative predictions and the time-variant structural safety can be realistically assured only in probabilistic terms. Among the others, the understanding of the influence of material parameters on the numerical results and their probable influence on the risk analysis procedure are aspects of primary importance.
It should be noted that considerable uncertainties are present also in the pristine state, due to model error arising from potential inaccuracies in the model, potentially missing variables, measurement errors and statistical uncertainty, [Choe et al., 2008].
It is common practise among risk analysts to provide information on aleatory variability and epistemic uncertainty, thus always presenting the type of uncertainty as part of the analysis results. Naturally, the parameters differ in all important statistical terms, be it mean value, standard deviation, minimum and maximum values.
Although the scatter of material parameters can be very high, a sight at the literature reveals that even for historic masonry some generalizations concerning the parameters distribution may be done, [Proske, 2002]. The normal and lognormal distributions are the most used. The normal distribution is applied for parameters whose influence depends on a sum of random effects, where none of them has a dominating influence. It is useful especially for the assessment of errors in measurements and it is often adopted as a convenient approximation for distributions that cannot be well determined. Nevertheless, in some cases, the validity of the normal distribution might be not sufficient. This happens for example if the distribution demonstrates a significant tail into one direction. Thus, the lognormal distribution is preferable, often used for the strength of plastic materials and yield stresses, to name only few examples. Interestingly, for practical purposes the difference between normal and lognormal distribution is negligible for coefficients of variation below 0.1.
For instance, the concrete cover should be assumed as a stochastic variable for both existing and new structures, since the actual cover, chosen during the design phase, does vary significantly due to construction practices. According to [CEB-FIP, 2006], the standard deviation may be assumed in the range 8 - 10 mm without particular execution requirements, and equal to 6 mm with additional requirements. Appropriate probability distributions are also suggested.
Finally, Table 5.10 presents a summery of information available in the literature regarding the statistical properties of material and geometrical parameters of interest for the present research. For each parameter, in addition to the mean value and the source, the variation coefficient, the standard deviation and the distribution type assumed by the corresponding authors are given, when available.

Table 5.10 Summery of statistical properties of random variables available in the literature

Parameter	Mean value	Variation coeff.	Standard deviation	Distribution	Reference
Concrete Young's modulus [MPa]	$4600\sqrt{f_c}$	0.12	-	Normal	Vu, 2000/Stewart, 2007
	18820	0.12	-	-	Li, 2004/Sobhani, 2007
Concrete compressive strength [MPa]	26.2	0.18	-	Log-normal	Val, 2007
	49.2	0.06	-	-	Yang, 2007
	35	-	5	Log-normal	Duprat, 2006
	Nominal value	-	5	Log-normal	Biondini et al., 2008b
	28	-	2.8	Normal	Bastidas, 2008
	19.03	-	3.43	-	Marsh, 2008
	57	0.14	-	-	Li, 2008
Concrete tension strength [MPa]	$0.69\sqrt{f_c}$	0.2	-	Normal	Vu, 2000/ Stewart, 2001
	3	0.2	-	-	Li, 2007
	$0.53\sqrt{f_c}$	0.13	-	Normal	Stewart, 2007
Concrete cover [mm]	31	0.2	-	-	Li, 2004
	55	-	11	Log-normal	Faber, 2002
	20	-	4	Log-normal	Duprat, 2006
	59	-	17.7	-	Choe, 2008
	75	-	10	Log-normal	DuraCrete, 2000
	Nominal value + 6	0.25	-	Normal	Val, 2008
Diffusion coefficient	129.0 [mm²/year]	0.10	-	-	Enright, 1998b
	Nominal value D_{nom}	-	0.10 D_{nom}	Normal	Biondini et al., 2008b
	$1.62 \cdot 10^{-8}$ [cm²/s]	-	$0.5 \cdot 10^{-8}$ [cm²/s]	Log-normal	Bastidas, 2008
	158 [mm²/year]	-	15.8 [mm²/year]	Normal	DuraCrete, 2000
	$5 \cdot 10^{-8}$ [m²/s]	0.3	-	Log-normal	Sudret, 2008
w/c = 0.40	220.9 [mm²/year]	-	$25.4 \cdot 10^{-12}$ [m²/s]	Normal	Faber, 2006/Choe, 2008
w/c = 0.45	315.6 [mm²/year]	-	$32.5 \cdot 10^{-12}$ [m²/s]	Normal	
w/c = 0.50	473.0 [mm²/year]	-	$43.2 \cdot 10^{-12}$ [m²/s]	Normal	
Width of beam section [mm]	120	0.1	-	-	Li, 2008
Maximum crack width [mm]	1	0.4	-	Normal	Stewart, 1998b
Critical crack width [mm]	0.45	0.19	-	Uniform	Stewart, 1998b

Parameter	Mean value	Variation coeff.	Standard deviation	Distribution	Reference
Dead load	Nominal value g_{nom}	-	0.10 g_{nom}	Normal	Biondini et al., 2008b
Live load	Nominal value p_{nom}	-	0.40 p_{nom}	Normal	
Concrete/steel damage rate	Nominal value $q_{c,nom}$	-	0.3·$q_{c,nom}$	Normal	Biondini et al., 2006a
Steel content [mm²]	226	0.1	-	-	Li, 2008
Steel Young's modulus [GPa]	210	-	12.6	Normal	Kala and Kala, 2005
Steel-concrete interface depth [μm]	12.5	-	-	-	Li, 2004
Steel yield strength [MPa]	490	0.10	-	Log-normal	Val, 2007
	543	0.15	-	-	Li, 2007
	310.5	0.12	-	Log-normal	Enright, 1998b
	Nominal value f_{sy}	-	30	Log-normal	Biondini et al., 2008b
	420	-	42	Normal	Bastidas, 2008
	308.9	-	3.43	-	Marsh, 2008
	312	0.116	-	Beta	Stewart, 1998a/b
	400	0.1	-	-	Li, 2008
Bar diameter [mm]	12	0.15	-	-	Li, 2004
	35.8	0.02	-	Log-normal	Enright, 1998b
	10	0.1	-	Log-normal	Sudret, 2008
	Nominal value ϕ_{nom}	-	0.10 ϕ_{nom}	Normal	Biondini et al., 2008b
Corrosion rate [μA/cm²]	3	0.2	-	-	Val, 1997
	0.0652 t +1.0105 (**)	0.2	-	-	Li, 2007
	0.3686 ln(t) + 1.13 (**)	0.2	-	-	Li, 2008
	1.5	0.3	-	-	Enright, 1998b
	1	0.2	-	Normal	Stewart, 1998b
	1	0.25	-	Log-normal	Sudret, 2008
Corrosion initiation time [years]	10	0.6	-	-	Enright, 1998b
Corrosion propagation time [years]					
Environment (*): submerged	not expected	-	-	-	
tidal	3.5	-	1.5	Log-normal	Faber, 2006
splash	7.5	-	1.88	Log-normal	
atmospheric	12	-	2	Log-normal	

(*) Exposure classes differentiated for chloride-induced corrosion in marine environments according to [DuraCrete, 2000]
(**) The two expressions, e.g. for t = 30 years, provide current densities of 4.27 and 2.57 μA/cm² respectively

5.3.3 Robustness analysis

In order to obtain meaningful correlations between the input and output variables involved in the numerical analyses, the stochastic sampling methodology called Latin Hypercube Sampling (LHS) is recommended. Indeed, it is well known that the widely used Plain Monte Carlo (PMC) method may distort the prescribed correlation structure and the statistical uncertainty is fairly large when the sample size N is small. As shown in Figure 5.8, given two independent variables X_1 X_2, LHS covers the space of random variables in a significantly superior way. In particular, PMC introduces unwanted correlations into the samples, which become very pronounced if the number of samples is small.

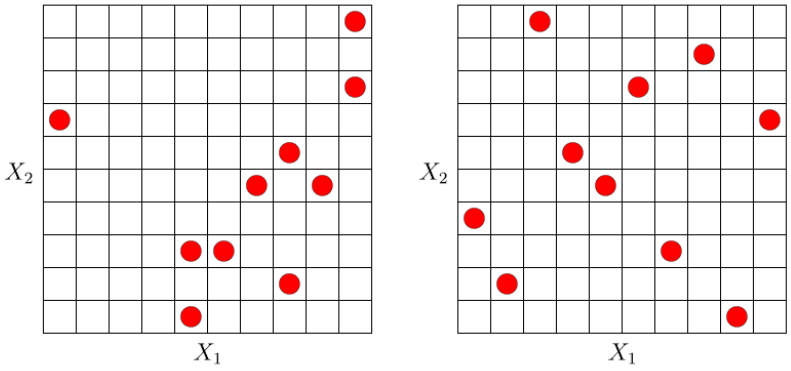

Figure 5.8 10 samples of two uniformly distributed independent variables: (a) Monte Carlo sampling; (b) Latin Hypercube sampling [OptiSlang Manual, 2008]

In the LHS method the domain of each random variable is decomposed into intervals with equal probability. The number of intervals corresponds to the number of samples. One value from each interval is randomly selected with respect to the probability density in the interval. Combining the intervals of a random variable, the so called hypercubes are formed. This is illustrated in Figure 5.9 and in a similar way the representative point within one hypercube. The N representative values obtained for X_1 are paired in a random manner (equally likely combinations) with the n values of X_2 and so on until X_n. These N random combinations are called "latin hypercube samples". If the samples are arbitrarily combined, artificial correlations are introduced, which can be avoided by regrouping the samples.

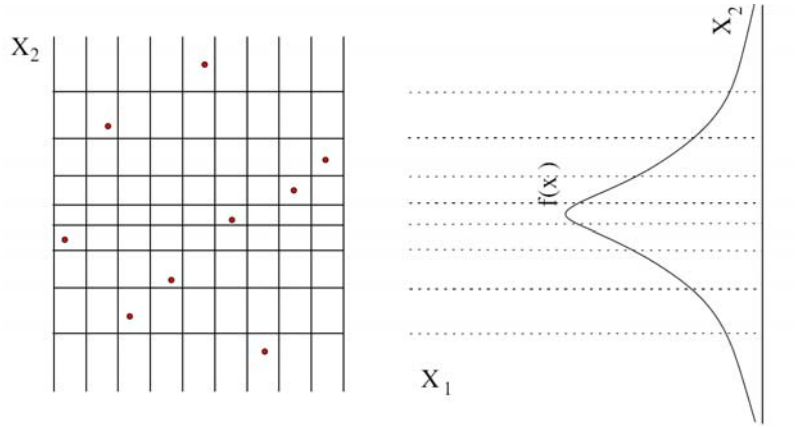

Figure 5.9 Latin Hypercube sampling [OptiSlang Manual, 2008]

Table 5.11 PMC vs. LHS for 95% confidence interval of correlation coefficient [OptiSlang Manual, 2008]

N/ρ	0	0.3	0.5	0.7	0.9
Plain Monte Carlo Sampling					
10	1.261	1.231	1.054	0.757	0.299
30	0.712	0.682	0.557	0.381	0.149
100	0.409	0.374	0.306	0.199	0.079
300	0.23	0.209	0.17	0.116	0.045
1000	0.124	0.115	0.093	0.062	0.023
Latin Hypercube Sampling					
10	0.42	0.382	0.26	0.158	0.035
30	0.197	0.194	0.139	0.073	0.018
100	0.111	0.101	0.071	0.042	0.009
300	0.065	0.057	0.042	0.024	0.006
1000	0.038	0.033	0.025	0.014	0.003

Comparing the estimation errors (standard deviations) of the correlation coefficients resulting from a PMC and a LHS, it turns out that an effective reduction of the sample size by a factor of more than 10 is obtained with the LHS method (see Table 5.11), which is consequently recommended as stochastic sampling method.
To obtain stable statistics, the recommended number of samples N given n design variables is n^2 for PMC, while in the case of LHS sampling, N may be calculated as follows:

$$N \geq 2\left(n_i + n_o\right) \tag{5.8}$$

where n_i is the number of input parameters and n_o is the number of output parameters.
In the following section, with the aim of calculating the probability of occurrence of a corrosive attack, a robustness analysis is performed using the LHS method to evaluate the sensitivity of the response parameter, i.e. the carbonation coefficient at the cover depth, to the design parameters and to identify linear and nonlinear correlations. Thus, the likelihood that corrosion initiates is calculated, combining the research code for the durability assessment of RC structures developed by [Saetta et al., 1993a-1999] with the probabilistic software *Optislang*.
Different graphical representations are available to plot the results of the analyses, e.g. linear and quadratic correlation matrix, histograms, coefficient of determination, Anthill plot, cloud plot, etc. For further details, see APPENDIX D.

5.4 Probability of occurrence of corrosion phenomena

5.4.1 Introduction

The evaluation of risk is based on the probability of impact and the level of impact of a certain hazard. The key to a good risk analysis is to build first a reliable model of the system, then to work out how it would behave in a variety of circumstances. Assigning probabilities to the exposures may be straightforward when dealing with ordinary design loads, but more challenging for other atypical scenarios. Nevertheless, occurrence probabilities must be defined in order to efficiently allocate resources for risk reduction, [Baker et al., 2007].
An example of classification of the probability of occurrence of a certain event is provided in the Australian and New Zealand code 4360 (Table 5.12), given the following meaning of the terms: E extreme risk, immediate action required; H high risk, senior management attention needed; M moderate risk, management responsibility must be specified; L low risk, manage by routine

procedures. A similar classification is proposed by [Mitre] (Table 5.13) and a schematic representation of the risk levels related to four degrees of severity is shown in Figure 5.10. In particular, the five levels of occurrence probability may be explained as:

- frequent: it occurs often. Everyone is exposed. Continuously experienced.
- likely: it occurs several times e. All members are exposed. Occurs frequently.
- occasional: it occurs sometime. All members exposed. Occurs sporadically, or several times in inventory/service life.
- seldom: it is possible to occur. All members exposed. Remote chance of occurrence; expected to occur sometime in inventory service life.
- unlikely: it can be assumed it will not occur. All members exposed. Possible, but improbable; occurs only very rarely.

Table 5.12 Qualitative Risk Analysis Matrix (AS/NZS 4360)

	Consequences				
Likelihood	Insignificant	Minor	Moderate	Major	Catastrophic
A (almost certain)	H	H	E	E	E
B (likely)	M	H	H	E	E
C (moderate)	L	M	H	E	E
D (unlikely)	L	L	M	H	E
E (rare)	L	L	M	H	H

Table 5.13 Probabilities of occurrence by [Mitre]

0 - 10%	Very unlikely to occur
11 - 40%	Unlikely to occur
41 - 60%	May occur about half of the time
61 - 90%	Likely to occur
91 - 100%	Very likely to occur

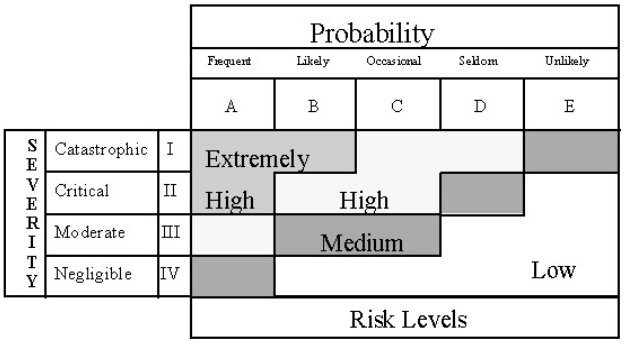

Figure 5.10 Operational Risk Management probability definitions [Mitre]

Merging the risk probability classification suggested by [Mitre] and the classification of corrosion levels proposed by [Rodriguez, 2001], a corrosion risk probability ranking has been developed (shown in three different representations in Figure 5.11), representing the ranges of probability of occurrence of four different corrosion levels, expressed in terms of corrosion rate.

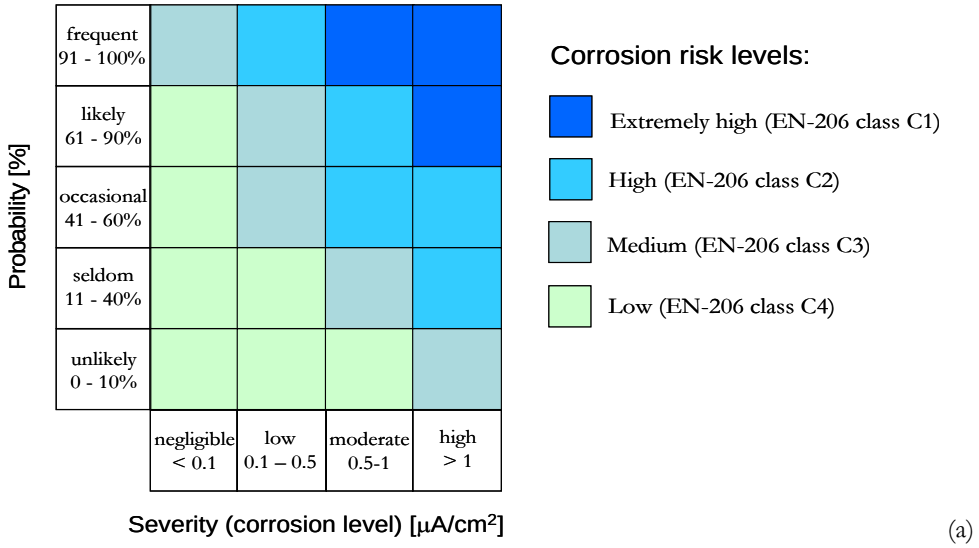

(a)

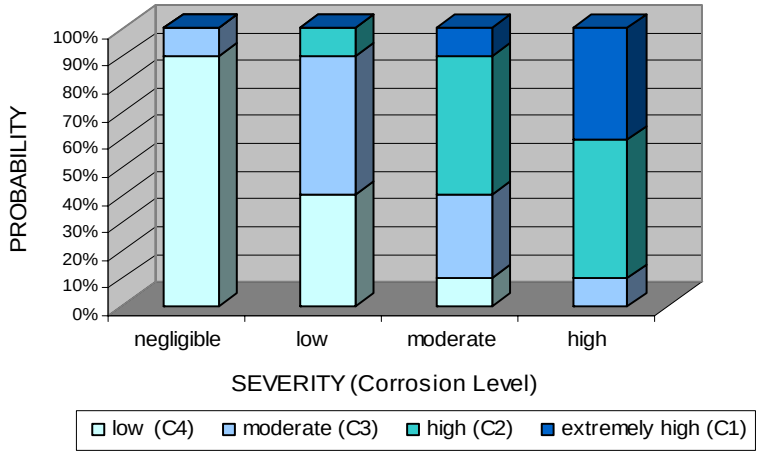

(b)

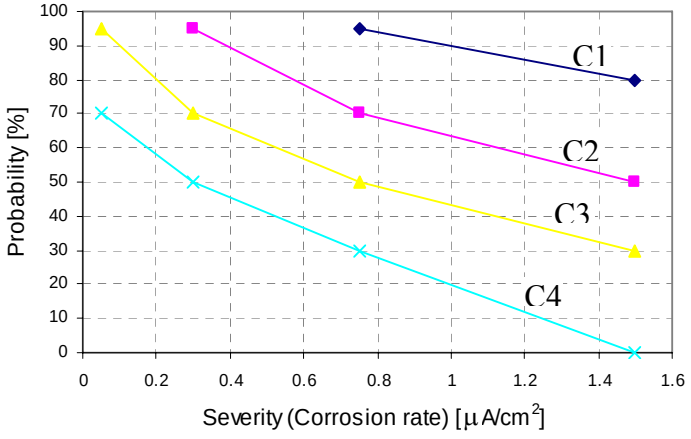

(c)

Figure 5.11 Corrosion risk probability, in three equivalent representations (a), (b), (c)

The four risk levels (extremely high, high, medium and low) have been associated with the four exposure classes proposed by EN 206, respectively XC1, XC2, XC3 e XC4 (see Table 4.2). In such a way, once the location of the structures is known (and consequently the correspondent exposure class), as a function of the measured/calculated corrosion rate in the structure, it is possible to extrapolate the range of probability of occurrence of the specific corrosion risk level. Alternatively, for a certain severity class, one may say which exposure class has the highest as well as the lowest probability of occurrence of the corrosion phenomenon.
It is evident that the drawback of this approach is that not continuous values of the probability of occurrence are given, but only discrete likely ranges. Depending of the problem one is dealing with, a more accurate tool may be necessary.

5.4.2 Probabilistic evaluation of corrosion initiation

As well know, the available information about environmental factors and material characteristics is often very limited and the unavoidable uncertainties involved in a detailed and complex modelling may lead to fictitious results. In particular, both the corrosion current density i_{corr} and the initiation time t_{in} in Eq.(4.3) are highly uncertain variables. Thus, in a fully probabilistic context, all the variables involved in the problem should be considered within the framework of a stochastic durability approach, since they vary locally in a significant way and may cause increased scattering in the results of the analyses. Consequently, not only average values, but also statistical distributions of the parameters should be included. Nevertheless, not all parameters equally influence the output of the analysis and in order to optimize the procedure an investigation on the effective variability of the input data of the numerical model is desirable.
To this aim, the initiation time for carbonation-induced corrosion (Section 4.2.1.1) has been evaluated in a probabilistic framework and used subsequently (Section 6.2.9) in the calculation of *Structural Risk*.
It is assumed that the corrosion process starts when the carbonation coefficient at the bar surface exceeds the threshold value 0.1, [Bono, 1996].

Table 5.14 Input parameters of the sensitivity analysis

Symbol	Description	Mean value	COV	Distribution
	Material properties			
lambda	Concrete thermal conductivity	10^{-4} W/mK	0.05	Log-normal
rho	Concrete density	2200 kg/m^3	0.05	Log-normal
Cq	Concrete specific heat	880 J/kgK	0.05	Log-normal
Dh	Water diffusivity at time t_e	(see Table 5.15)	0.1	Normal
D28_Dinf	Concrete moisturizing coefficient	(see Table 5.15)	0.05	Log-normal
Dg	CO_2 diffusivity at time t_e	(see Table 5.15)	0.1	Normal
alfa1	Water-carbonation interaction coefficient	2.0E-3	0.1	Normal
alfa2	CO_2-carbonation interaction coefficient	0.4	0.1	Normal
alfa3	Carbonation speed reduction coefficient	2.8E-7 s^{-1}	0.1	Normal
	Environment properties			
T0	Initial temperature	23°C	0.1	Normal
Tf	Final temperature	23°C	0.1	Normal
betaT	Temperature surface transmission coefficient	0.01 W/m^{2}K	0.02	Log-normal
RH0	Initial humidity	0.5; 0.7; 0.9	0.05	Log-normal
RHf	Final humidity	0.5; 0.7; 0.9	0.05	Log-normal
betah	Humidity surface transmission coefficient	0.001 m/s	0.02	Log-normal
CO2	CO_2 concentration	3.5E-4	0.05	Log-normal
betag	CO_2 surface transmission coefficient	0.01 m/s	0.02	Log-normal

Table 5.15 Diffusivities coefficients and water/cement ratios

	w/c = 0.4	w/c = 0.5	w/c = 0.6
$D_{h,0}$	4.04 E-12 m²/s	2.02 E-11 m²/s	8.49 E-11 m²/s
$D_{g,0}$	8.90 E-09 m²/s	2.85 E-08 m²/s	8.50 E-08 m²/s
D_{28}/D_{∞}	0.8	0.5	0.2

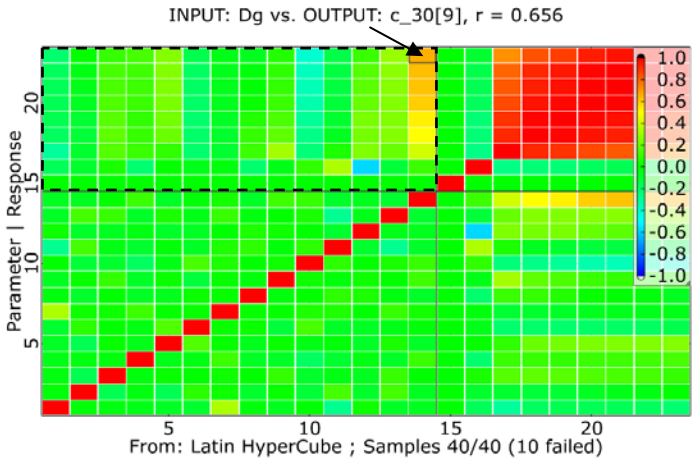

Figure 5.12 Sensitivity analysis: correlation matrix

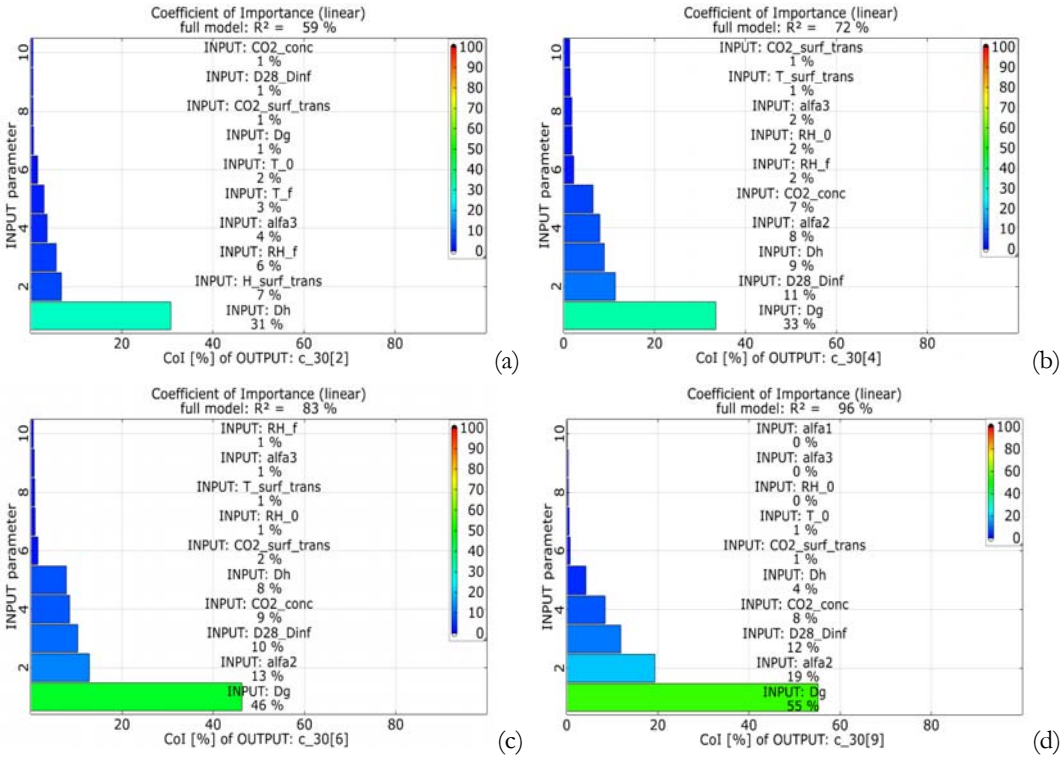

Figure 5.13 Sensitivity analysis: influence of the input parameters on the carbonation coefficient after (a) 10 years; (b) 40 years; (c) 50 years; (d) 60 years

First, using the software *Optislang*, a sensitivity analysis has been performed, aiming at investigating the relative importance of each input parameter on the variability of the output variable, as already stated in Section 5.3.1. The input parameters considered in the analysis are listed in Table 5.14. The variation coefficient and the distribution type have been chosen referring to the literature (see Table 5.10) or simply assumed, when not available due to lack of data, e.g. [Val and Trapper, 2008].
In order to keep the necessary number of samples, i.e. solver runs, as low as possible, the Latin Hypercube sampling method has been chosen. Therefore, according to Eq.(5.8), a number of samples $N = 50 > 2(n_i + n_o) = 2 \cdot 18 = 36$ (17 input parameters and 1 output parameter) is sufficient.

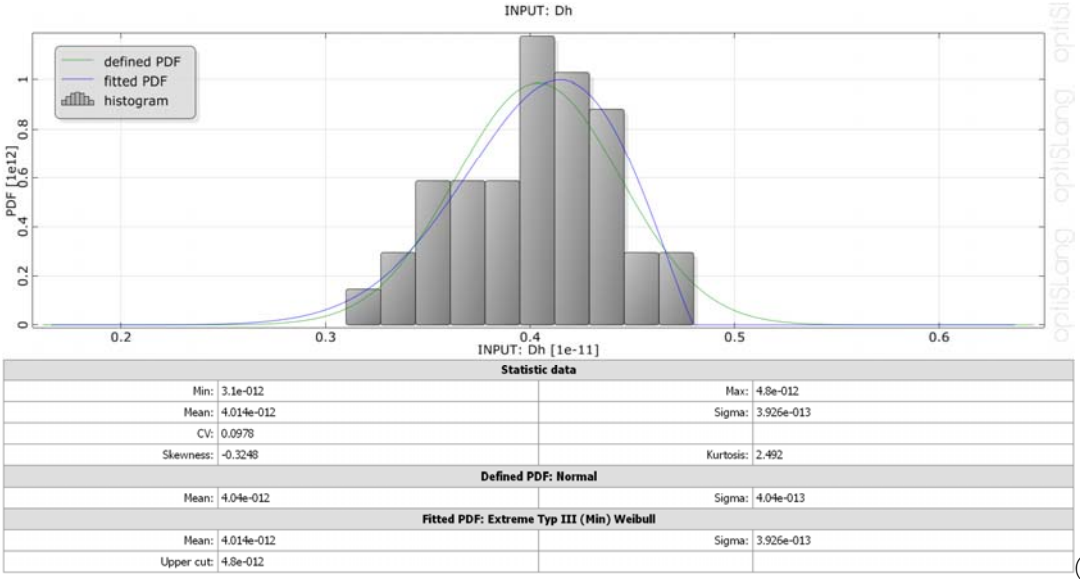

Statistic data			
Min:	3.1e-012	Max:	4.8e-012
Mean:	4.014e-012	Sigma:	3.926e-013
CV:	0.0978		
Skewness:	-0.3248	Kurtosis:	2.492
Defined PDF: Normal			
Mean:	4.04e-012	Sigma:	4.04e-013
Fitted PDF: Extreme Typ III (Min) Weibull			
Mean:	4.014e-012	Sigma:	3.926e-013
Upper cut:	4.8e-012		

(a)

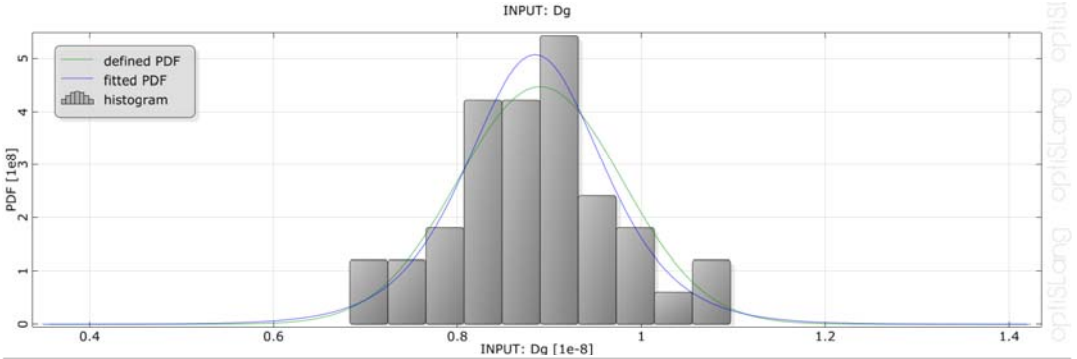

Statistic data			
Min:	6.83e-009	Max:	1.097e-008
Mean:	8.844e-009	Sigma:	8.93e-010
CV:	0.101		
Skewness:	0.1174	Kurtosis:	3.031
Defined PDF: Normal			
Mean:	8.9e-009	Sigma:	8.9e-010
Fitted PDF: Logistic			
Mean:	8.844e-009	Sigma:	8.93e-010

(b)

Figure 5.14 Probability density function of (a) D_h and (b) D_g for w/c = 0.4 and RH = 50%

The results reveal that the diffusion coefficients of humidity D_h and pollutant D_g are the parameters most influencing the carbonation depth at the 30-mm-cover depth, since they represent the most significant numerical characterization of the cement type, the w/c ratio (Table 5.15) and the other factors that distinguish one concrete from another. In particular, Figure 5.12 shows the correlation matrix, with the box of input vs. output variables in evidence.
In Figure 5.13 the influence of the input variables on the carbonation coefficient is represented in terms of "coefficient of importance" graphs. Of interest, it can be observed as the sensibility varies significantly over time: in the first stage, up to 10 years, the diffusivity of humidity D_h has the major weight, then replaced by the pollutant diffusivity D_g and the coefficient α_2 after 50 years. Thus, the same input parameter has a different influence on the same output parameter as time passes. One parameter can lose its significance or vice versa it can acquire importance after some time from the beginning of the process.
In order to define the probabilistic distribution of the diffusivities, experimental data should be collected and analysed from a probabilistic standpoint. As an alternative, it is possible to numerically generate a random series of virtual samples with specified diffusivity characteristics, [Berto et al., 2008b]. This second approach has been followed herein. It is assumed that the diffusivities have a normal distribution and vary around the mean value of the population within a coefficient of variation of 10%. Figure 5.14 shows the histograms (10 classes) of the diffusivities for w/c = 0.4 and RH = 50%. The assigned distribution density function is plotted in green, while the blue line depicts the PDF fitted to the data set. Additional information about estimated statistical values (mean, minimum and maximum value, standard deviation, coefficient of variation, skewness and kurtosis) is given in the text field of the plots. The histogram of the response parameter after 50 years is shown in Figure 5.15, giving information about the type and un-symmetry of the distribution and about skewness and kurtosis as well.

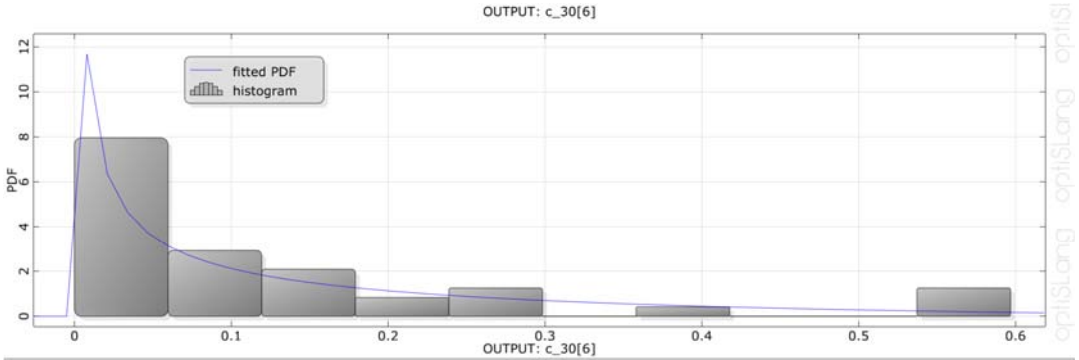

Figure 5.15 PDF of the carbonation coefficient at the cover depth for w/c = 0.4 and RH = 50%

Table 5.16 Diffusivities and carbonation depth after 2 years for different w/c ratios

w/c	D_h	D_g	Carbonation depth (mm)
0.4	4.0221E-12	8.8665E-09	5.5
0.5	1.9744E-11	2.781E-08	8.3
0.6	8.421E-11	8.417E-08	11.6

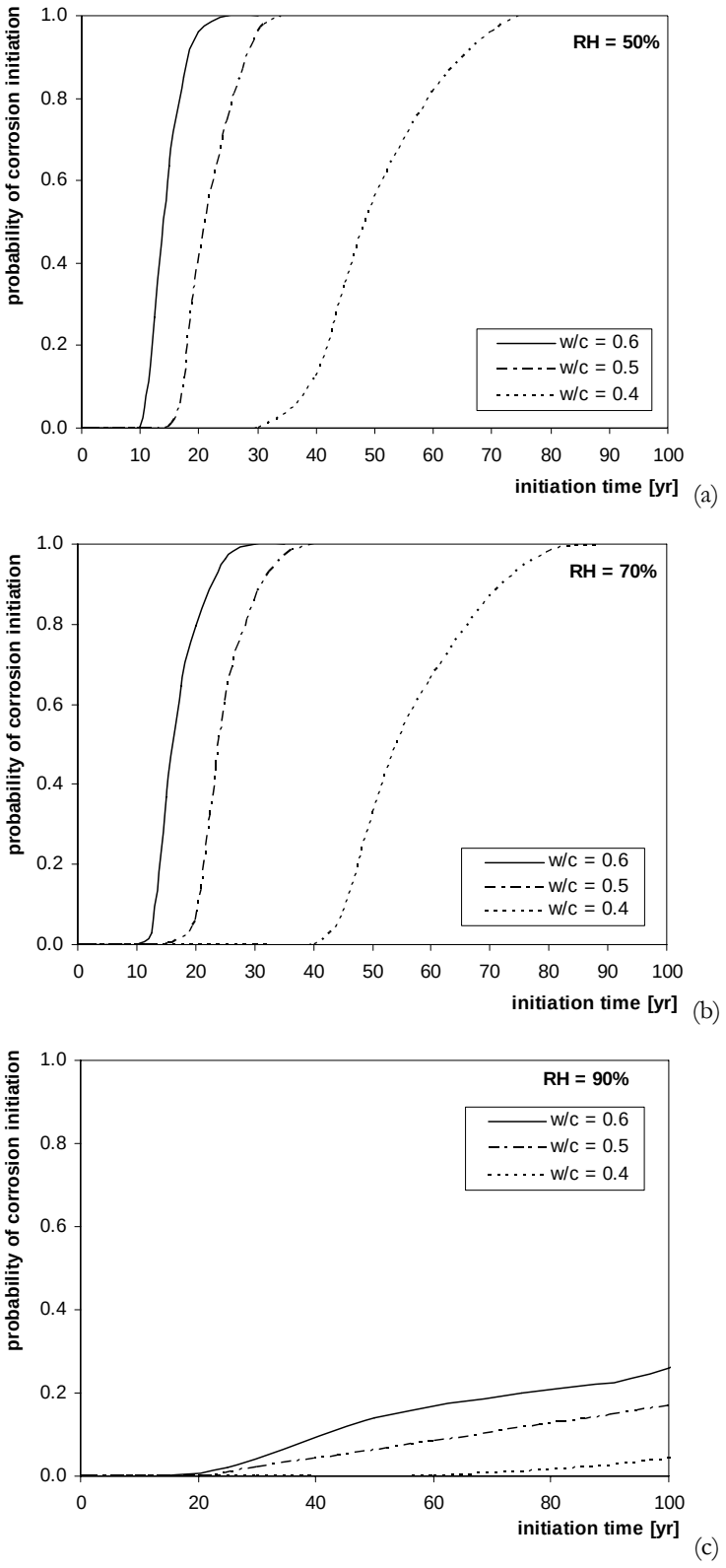

Figure 5.16 CDF of corrosion initiation time for different w/c ratio: (a) RH = 50%; (b) RH = 70%; (c) RH = 90%

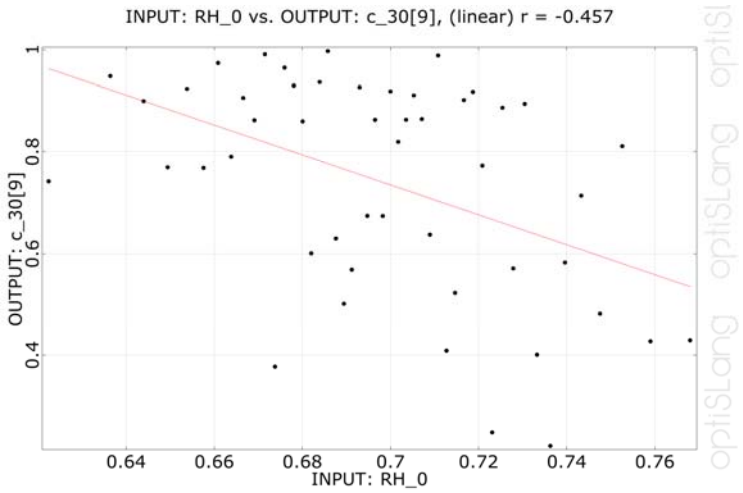

Figure 5.17 Anthill plot of RH vs. carbonation coefficient for RH = 70% w/c = 0.5 (after 40 years)

Table 5.16 shows the values obtained for diffusivity coefficients and carbonation depth after 2 years for three concrete types characterised by w/c = 0.4, w/c = 0.5 and w/c = 0.6. It can be observed that the lower the w/c, the lower its porosity and consequently the lower the CO_2 diffusivity.

From the system of equations (4.8) the statistical distribution of the corrosion initiation time is evaluated and shown in terms of cumulative density functions in Figure 5.16a-c for a relative humidity of 50, 70 and 90%. The graphs illustrate that, for a given concrete type (i.e. for a given w/c ratio), the higher the relative humidity, the higher the time for corrosion initiation. This is in accordance with the fact that the diffusion of CO_2 within concrete is very slow when pores are filled with water, as already explained in Section 4.1.1.

This trend is confirmed also by the Anthill plot of the negative correlation between the relative humidity and the carbonation coefficient, Figure 5.17. The numerical results are in agreement with the experimental evidence, e.g. [Hallberg, 2005]. In fact, as already shown in Figure 4.6, the higher the relative humidity, the higher the rate of corrosion and the later corrosion will begin.

The isopercentile curves of the initiation times are plotted in Figure 5.18 as a function of the w/c ratio, [Berto et al., 2008b]. The two dotted lines identify the range of initiation time values within which 99% of the concrete samples with the specified w/c ratio will fall, while the curves traced with continuous lines show the range of variation of the initiation time with a 50% probability; finally, the dashed and dotted line shows the mean initiation times for each w/c value.

Figure 5.18 presents also a comparison with in-situ measurements of carbonation depths carried out on a number of existing RC structures, characterized by different concrete compressive strengths, [Codacci-Pisanelli et al., 1987], [Al-Khaiat et al., 1997], [Castro et al., 2000].

First of all, it is worth noting that the initiation time, and consequently the durability of concrete with respect to carbonation, rapidly decreases as the w/c ratio increases because a higher w/c ratio facilitates the diffusion of the aggressive substances through the porous medium of concrete. Moreover, the higher the w/c ratio, the narrower the range of initiation time values for a given probability, because any variation in diffusivity becomes less influential. The values of the initiation time obtained for the different w/c ratios are given in Table 5.17 for the 50% and 99% percentiles.

The variation of the time to corrosion initiation with the water to cement ratio is also evidenced in Figure 5.19 for a 25 mm concrete cover, [Vu et al., 2000]. In their paper, the authors emphasize that this effect is usually ignored in corrosion models, leading to an overestimation of corrosion effects for typical w/c values, smaller or equal to 0.5.

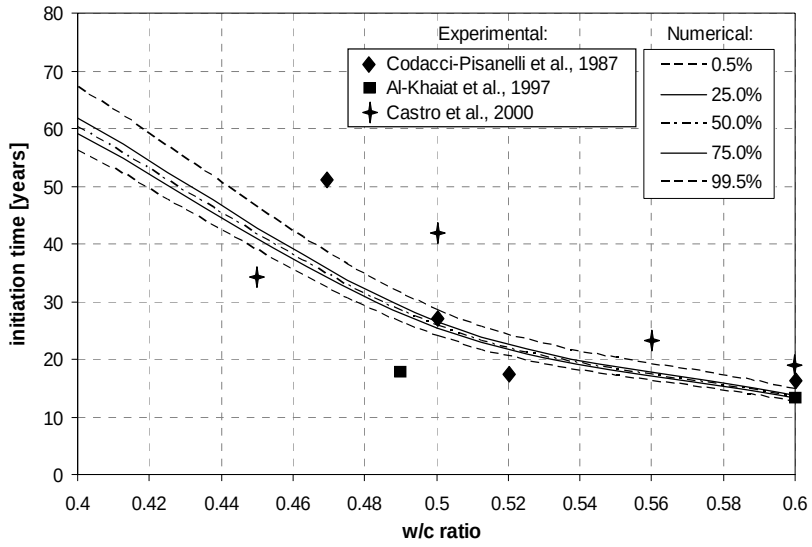

Figure 5.18 Probable corrosion initiation vs. w/c ratio: comparison with experimental data

Table 5.17 Initiation time probabilities (years) for RH = 70%

w/c	99%	50%
0.4	61.7 ± 9.0%	60.4 ± 2.1%
0.5	26.3 ± 8.5%	26.0 ± 2.2%
0.6	13.7 ± 8.0%	13.5 ± 1.9%

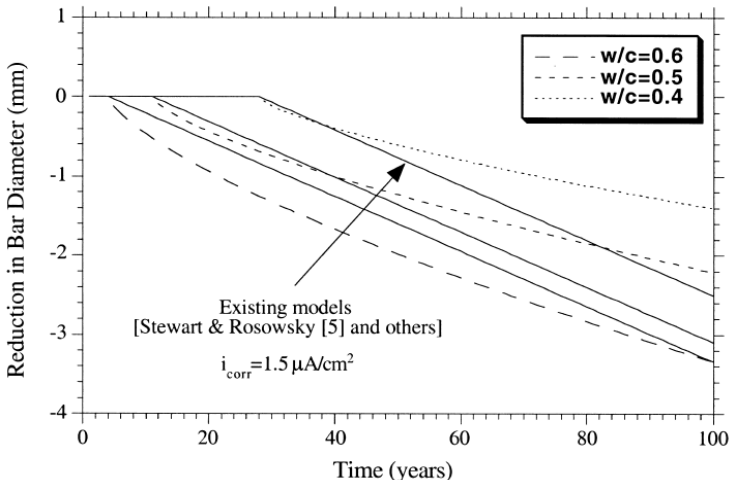

Figure 5.19 Steel section reduction over time for different w/c ratios [Vu et al., 2000]

5.5 Structural reliability

5.5.1 Introduction

Originally, the classical reliability theory was developed for systems consisting of a number of similar components subject to the same loading and behaving in a statistically independent way. The probability of failure of these components was considered in terms of relative failure frequencies observed from experience. Furthermore, due to the fact that failure develops as a direct consequence of an accumulating deterioration process, the main goal was the formulation of probabilistic models for the estimation of the statistical characteristics of the time until failure.
In structural reliability analysis, the problem is essentially different and reliability is quantified as the probability of safe structural behaviour over time, [JCSS, 2001b]. Structural failures are generally rare and result from extreme events, for example a load exceeding the carrying capacity, which may be reduced by deterioration processes, such as corrosion phenomena. In addition, no useful information can be gathered about relative failure frequencies, since almost all structural systems are unique, either due to differences in the materials and geometry or due to differences in loading and exposure conditions, [Faber, 2007].
Thus, when assessing the failure probability for structural components, it is necessary to model both resistances and loads from the probabilistic point of view, including all available statistical information concerning the material properties and the load characteristics (see Section 5.5.2.2).
It is important to distinguish between the reliability of new and existing structures. At the design phase, the reliability assessment is conditional on the analysis and design methods and on the expectation that the realization of the structure will pursue some standard practice formally defined by structural codes and regulations.
For an existing structure, the assessment of reliability aims at demonstrating that the structure will work safely over a specific residual service life. The need for the reliability assessment may arise from a number of causes: deviations from the original project, a change of the use of the structure, the discovery of design and/or construction errors, unfavourable results of periodical investigations of the structure's safety state, signs of damage or unusual incidents during use (e.g. impact of vehicles, fire in the building, earthquake and other natural hazards).
Thus, the reliability assessment is mainly based on the results of predicting hazards and load effects in the future and of assessing material properties and geometry taking into account the present state of the structure. As a consequence, a number of decisions must be taken, regarding:

- the type of inspections to perform (routine inspections are common only for particular structures such as bridges, offshore structures and nuclear power plants);
- the type of analyses to carry on (structural, reliability, cost-benefit analysis, etc.);
- the risks involved in further using the structure and target safety goals to be accomplished;
- the measures to take, in terms of maintenance, repair, strengthening or replacement of the structure, accounting for the economic aspects.

Moreover, the concept of safety for an existing structure generally reflects the state of knowledge of an expert and his particular opinion, which often differs from that of other specialists. Thus, every statement about safety of a construction is highly subjective, even though experience shows that the different points of view of the experts tend to converge to full agreement in the final decision.
It is evident that assessing the *structural reliability* of an existing structure is a challenging task. Additionally, the information about the actual condition, such as in presence of steel corrosion, is often lacking or extremely uncertain. Thereby, a close inspection of the health state and a detailed analysis of the structural behaviour are required and the updating of the information will

influence the initial opinion concerning the structural safety. S*erviceability* is normally easier to assess, since the structure itself shows to be adequate or not for its use, evidencing deflections, cracks, vibrations, etc.

5.5.2 Basic concepts and definitions

5.5.2.1 Limit state

Whether the response of a structure to loading is acceptable or not depends on the requirements that must be satisfied, including safety against collapse and/or limitations on damage. Each of these requirements may be termed as a *limit state* and its violation represents the attainment of an undesirable condition for the structure. Some typical limit states are given in Table 5.18.

Table 5.18 Typical limit states for structures [Melchers, 1999]

Limit state type	Description	Examples
Ultimate (safety)	Collapse of all or part of the structure	Tipping or sliding, rupture, progressive collapse, plastic mechanism, instability, deterioration, corrosion, fatigue, fire
Damage (often included in above)		Excessive or premature cracking, deformation or permanent inelastic deformation
Serviceability	Interruption of normal use	Excessive deflections, vibrations, local damage

Similarly, the Probabilistic Model Code [JCSS, 2001a] defines the following requirements to be fulfilled by the structure:

- Serviceability Limit State Requirement: structures shall remain fit for the use for which they are required;
- Ultimate Limit State Requirement: structures shall withstand extreme and/or frequently repeated actions occurring during their construction and anticipated use;
- Robustness Requirement: structures shall not be damaged by accidental events like fire, explosions, impact or consequences of human errors, to an extend disproportionate to the triggering event.

The three performance requirements prescribed by [Eurocode 8, 2005] are characterised as follows:

- Limit State of Near Collapse (NC): the structure is heavily damaged, with low residual lateral strength and stiffness, although vertical elements are still capable of sustaining vertical loads. Most non-structural components have collapsed. Large permanent drifts are present. The structure is near collapse and would probably not survive another earthquake, even of moderate intensity. The return period T_R of the design action indicated as appropriate for this LS and for buildings of ordinary importance is 2475 years (corresponding to an exceedance probability of 2% in 50 years).
- Limit State of Significant Damage (SD): the structure is significantly damaged, with some residual lateral strength and stiffness, and vertical elements are capable of sustaining vertical loads. Non-structural components are damaged, although partitions and infills have not failed out-of-plane. Moderate permanent drifts are present. The structure can sustain after-shocks of moderate intensity. The structure is likely to be uneconomic to repair. The indicated return period T_R of the design action is 475 years (corresponding to an exceedance probability of 10% in 50 years).

- Limit State of Damage Limitation (DL): the structure is only lightly damaged, with structural elements prevented from significant yielding and retaining their strength and stiffness properties. Non-structural components, such as partitions and infills, may show distributed cracking, but the damage could be economically repaired. Permanent drifts are negligible. The structure does not need any repair measures. The indicated return period T_R of the design action is 225 years (corresponding to an exceedance probability of 20% in 50 years).

5.5.2.2 Probabilistic violation of a limit state

In general, the study of structural reliability is concerned with the calculation and prediction of the probability of a limit state violation at any stage of the structural system life. The probability of occurrence of a limit state violation is a numerical measure of the chance of its occurrence.
Being expressed in probabilistic terms, reliability covers safety, serviceability and durability of a structure, [Eurocode 0, 2002].
In probabilistic assessments, any uncertainty about the variables and scattering of the response, expressed in terms of probability density function, are taken into account explicitly, while traditional safety measures, such as the "factor of safety" or "load factor", are deterministic methods.
The probability density function $f_Q(q)$ is defined as the probability that the load Q assumes a value between q and $q+\Delta q$ as $\Delta q \to 0$. The load Q can be converted to a load effect S by conventional structural analysis procedures and using the same transformations the probability density function $f_S(\cdot)$ can also be obtained.
Resistance, geometry and many other variables may be described in probabilistic terms, as already shown in Section 5.4.2. Figure 5.20 gives another example, illustrating a typical resistance histogram and the fitted probability distribution for the yield strength of steel, [Melchers, 1999]. Steel yield strength can be converted to member resistance R by multiplying by the cross-section area. Thus, it is possible to define a probability density function $f_R(\cdot)$.
Applied loads are generally time dependent and of uncertain value at any point in time. Loads tend to increase with time and resistance to decrease. It is usual also for uncertainties, both for loads effects S and resistances R, to increase with time. Consequently, the probability density functions $f_S(\cdot)$ and $f_R(\cdot)$ become wider and flatter with time and the mean values change as time progresses.

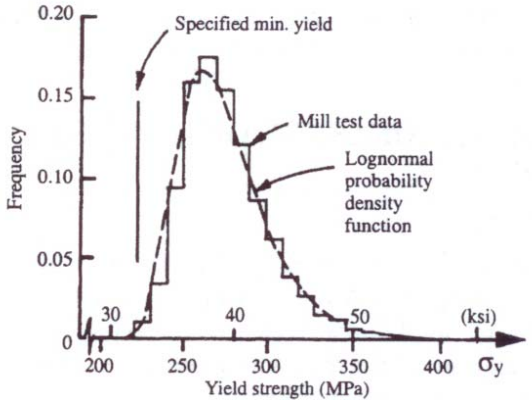

Figure 5.20 Histogram and fitted distribution for steel yield strength [Melchers, 1999]

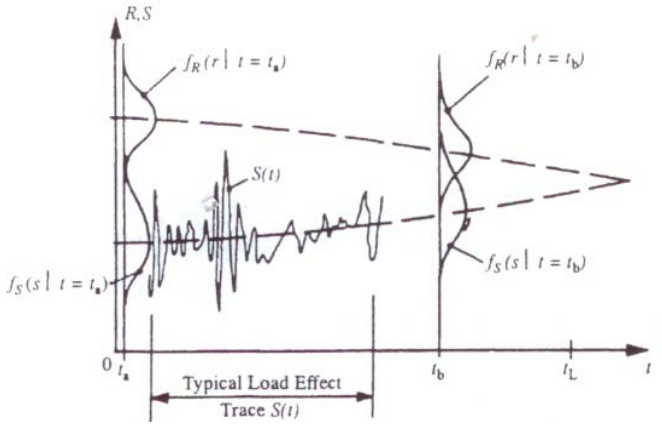

Figure 5.21 Schematic time-dependent reliability problem [Melchers, 1999]

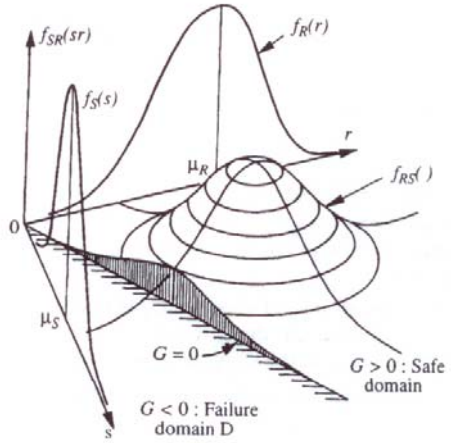

Figure 5.22 Joint density function $f_{RS}(r,s)$, marginal density functions f_R and f_S and failure domain *D* [Melchers, 1999]

Therefore, the general reliability problem can be represented as in Figure 5.21, [Melchers, 1999]: the safety limit state will be violated when, at any time *t*, the resistance *R* is lower than the corresponding load effects *S* (see Section 5.2.1). The probability that this limit state is violated, i.e. the probability of an undesired or unsafe state of the response, is the *probability of failure* P_f, which can be expressed in any of the following forms (omitting *t*):

$$\begin{aligned} P_f &= P(R - S \le 0) \\ &= P\left(\frac{R}{S} \le 1\right) \\ &= P(\ln R - \ln S \le 0) \end{aligned} \tag{5.9}$$

In general, P_f can be written as the probability that the *limit state function* $g(\cdot)$, frequently called *safety margin*, attains non-positive values:

$$P_f = P[g(\cdot) \le 0] \tag{5.10}$$

Some general density functions f_R and f_S and the joint density function $f_{RS}(r,s)$ are shown in Figure 5.22, [Melchers, 1999]. The latter represents the probability that R takes on a value between r and $r+\Delta r$ and S a value between $s+\Delta s$, as Δr and Δs approach zero. Given the failure domain D, the failure probability becomes:

$$P_f = P(R \le S) = \iint_D f_{RS}(r,s) \cdot dr \cdot ds \tag{5.11}$$

For any random variable X, the cumulative distribution function is given by:

$$F_X(x) = P(X) \le x = \int_{-\infty}^{x} f_X(y)dy \tag{5.12}$$

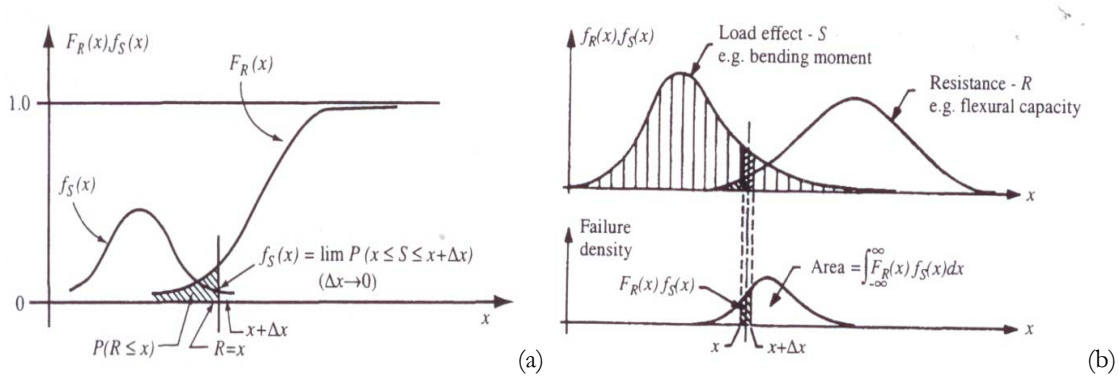

Figure 5.23 Basic *R–S* problem: representation of (a) $F_R(\cdot)\ f_s(\cdot)$; (b) $f_R(\cdot)f_s(\cdot)$ [Melchers, 1999]

When R and S are independent, the probability of failure becomes:

$$P_f = P(R - S \le 0) = \int_{-\infty}^{\infty} F_R(x)f_s(x)dx = \int_{-\infty}^{\infty}[1 - F_S(x)]f_R(x)dx \tag{5.13}$$

known as "convolution integral", Figure 5.23a. $F_R(x)$ is the probability that $R \le x$ or the probability that the actual resistance R of the member is less than some value x, representing failure. The total failure probability is obtained by taking the integral over all x values. This can be also seen in Figure 5.23b, where the density functions $F_R(\cdot)$ and $f_s(\cdot)$ are drawn along the same axis. As when considering the probabilistic modelling of load and resistance variables, prior information may be used when selecting the distribution type for the modelling of the random time to failure for an element of the structural system. The proper choice of the distribution function then depends on the physical characteristics of the deterioration process causing the failure of the component.

With regard to the seismic performance, capacity design criteria and detailing for ductility are used in the design of new structures in order to ensure that, in case of the occurrence of a seismic event with intensity I higher than the design value, the probability of collapse $P_f(I)$ does not increase disproportionately, as shown by the continuous curve in Figure 5.24, [Pinto, 2005]: $P_f(I)$ remains a smoothly increasing function of the intensity I beyond its design value corresponding to the SD limit state. Instead, in case of an existing structure, even if the building has the same $P_f(I)$ as the new one for the SD intensity level (dashed curve in Figure 5.24), the

absence of ductility provisions or the presence of deterioration may cause a brittle collapse, i.e. a sudden increase of $P_f(I)$, for slightly larger values of I.
Of interest, [Sarveswaran and Roberts, 1999] differentiate between "actual" probability of failure, deriving from historical database and statistics related to levels of risk accepted by society (e.g. the Fatal Accident Rate, FAR), and "notional" probability of failure obtained from probabilistic analysis. The first is possible for earthquakes, given the huge amount of registrations made over time, but not for corrosion, due to the lack of available data. Finally, it should be noted that, at present, it is not possible to include in the calculation of the "notional" failure probability human factors affecting structural failures (e.g. errors in design and construction).

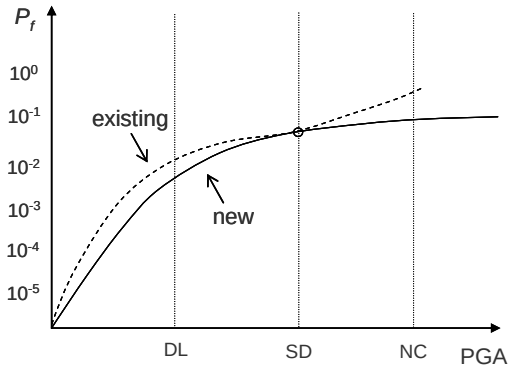

Figure 5.24 Probability of failure as a function of PGA for a new and an existing building [Pinto, 2005]

5.5.3 Fragility estimates

The fragility of a structural component is defined as the conditional probability of failure, i.e. the conditional probability of attaining or exceeding prescribed limit states, for a given set of boundary variables, [Choe et al., 2008; Gardoni et al., 2002].
The Latin Hypercube sampling is recommended as probability-based method to estimate the failure probability as:

$$\overline{P}_f = \frac{1}{N}\sum_{k=1}^{N} I_g\left(x^{(k)}\right) \tag{5.14}$$

where N is the required number of simulations, while $I_g\left(x^{(k)}\right)=1$ if the limit state function $g\left(x^{(k)}\right)\le 0$ and $I_g\left(x^{(k)}\right)=0$ else. In other words, $\overline{P}_f$ gives the number of designs falling in the unsafe domain respect to the total number of designs. N is independent of the dimension n of the problem.
Given P_f the expected probability of failure, the number of required samples should be:

$$N \ge \frac{10}{P_f} \tag{5.15}$$

The expected probability of failure, and consequently the number of samples from Eq.(5.15), may be chosen according to the "Sigma level" approach. Design for "Six Sigma" (i.e. six standard deviations) is a synonymous for "robust design" or "reliability-based optimization", so that quality and reliability are explicit optimization goals. Figure 5.25 shows the normal

distribution of a random response variable X with lower and upper specification limits on 2σ and 6σ level. The chosen limit state function $g(X) \leq 0$ defines the robust design range RD ($\pm 2\sigma$) and the safety design range SD ($\pm 6\ \sigma$) around the mean value $\overline{X}$. The possible sigma levels start at 1σ (robust design optimization) and go up to 6σ (reliability-based design optimization), as shown in Table 5.19, in which the σ levels are ranked depending on the variation of the normal distribution, the defects per million and the associated P_f. The statistical error is given by:

$$\varepsilon = \sigma_{\overline{P}_f} / E[\overline{P}_f] \tag{5.16}$$

For example, a probability of 3.4 out of 1 million is achieved when the performance target is 4.5σ away from the mean value (short term). The additional 1.5σ (long term) leading to a total of 6 standard deviations is used as a safety margin to allow for the fluctuations that the mean value may experience over its lifetime.

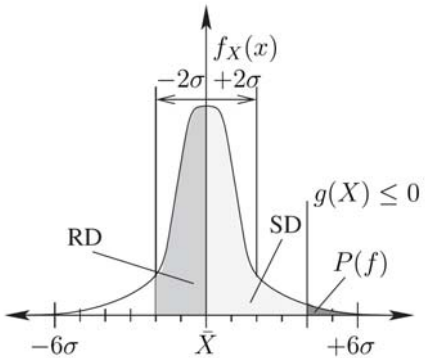

Figure 5.25 Robust design RD ($\geq \pm 2\sigma$) and safety design (SD) ($\geq \pm 6\ \sigma$) depending on specified limit state function $g(X) \leq 0$, [Hueste and Bai, 2007]

Table 5.19 Sigma levels and associated probabilities of failure [Optislang Manual, 2008]

Sigma level	% variation	Probability of failure	Defects per million (short term)
$\pm 1\sigma$	68.26	3.17E−1	317400
$\pm 2\sigma$	95.46	4.54E−2	45400
$\pm 3\sigma$	99.73	2.7E−3	2700
$\pm 4\sigma$	99.9937	6.3E−5	63
$\pm 4.5\sigma$	*99.99932*	*6.8E−6*	*6.8*
$\pm 5\sigma$	99.999943	5.7E−7	0.57
$\pm 6\sigma$	99.9999998	2.0E−9	0.002

In the case of a seismic action, fragility relationships relate the probability of exceeding a performance level (e.g. a drift limit) to the earthquake intensity. An example of seismic fragility relationships for a RC frame structure representative of the 1980s constructions in the Central United States is shown in Figure 5.26, [Hueste and Bai, 2007]. The fragility curves are calculated in terms of probability of exceeding the maximum interstorey drift limits associated with the three limit states Immediate Occupancy (IO), Life Safety (LS) and Collapse Prevention (CP), in line with the global-level performance criteria suggested by FEMA 356 for concrete frame structures, i.e. 1%, 2% and 4% of the global-level drift limits for the three limit states respectively.

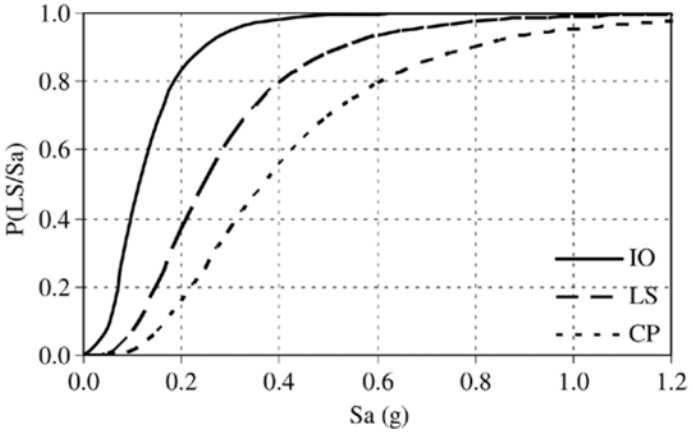

Figure 5.26 Seismic fragility curves for three limit states [Hueste and Bai, 2007]

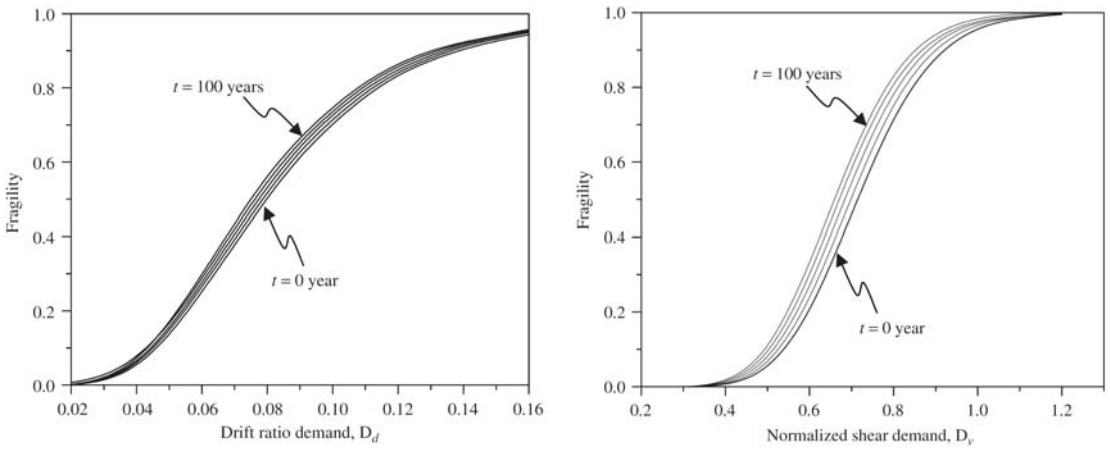

Figure 5.27 Predictive fragility estimates of a RC column for (a) drift demand; (b) shear demand, at intervals of 25 years [Choe et al., 2008]

The probabilistic model by [Choe et al., 2008] allows assessing and predicting the fragility of deteriorating structural components, affected by chloride-induced corrosion. Figure 5.27 plots the predictive fragilities for a corroding RC column subject to shear force and drift demands at time intervals of 25 years, over a 100-year lifetime. The slope and the relative distance between the curves demonstrate that the degradation with corrosion of the shear force capacity is faster than the degradation of the drift capacity.

In this chapter a fundamental component for the calculation of structural risk as described in CHAPTER 2 has been evaluated, i.e. the probability of occurrence of a steel corrosion event. The application of the whole methodology to a real case study is the topic of the following chapter. Moreover, the bases for carrying out fragility estimates of corroding RC members have been set in Section 5.5. A preliminary application of this procedure is proposed in Section 6.2.10, in which the probability of rotation failure of a RC column affected by carbonation-induced corrosion is calculated in compliance with the Italian and European codes provisions.

CHAPTER 6 CASE STUDIES

6.1 Introduction

In this chapter, a practical application of the methodology presented in the previous sections for the estimation/prediction of the seismic response of corroded structures is proposed. Two case studies are considered in order to compare their structural behaviour at the beginning and at the end of an assumed service life of 50 years. In particular, with reference to the risk assessment module of the RMP (Figure 2.15), the methodology consists of the following phases:

Hazard Analysis: 1. Evaluation of the probability of occurrence of corrosion;
2. Environmental analysis;
3. Corrosion rate estimation;
Structural Vulnerability: 4. Corrosion effects evaluation;
5. Pushover analysis of the structure at $t = 0$ and $t = 50$ years;
6. Evaluation of the probability of occurrence of the seismic event;
Damage Assessment: 7. Damage coefficients evaluation;
Risk Calculation: 8. Calculation of *Structural Risk*

Data and information available in the literature as well as results of previous analyses have been used in combination with the new models and approaches developed within the present thesis.
It is worth noting that shear type failures are often neglected in the limit analysis approaches for the lifetime assessment and prediction of concrete structures proposed in the literature, e.g. [Biondini et al., 2008a]. Nevertheless, experience shows that in most cases brittle mechanisms (shear as well as beam-column joint failures) are the first causes of structural collapse in existing buildings, or in general of the dissatisfaction of the limit state considered for the structure, while for new structures such type of failure can be avoided by a proper capacity design.
[Val, 2007] points out the scarcity of studies accounting for the influence of corrosion on shear strength, especially under pitting corrosion, in spite of the shear type failure occurred in a large part of the tests on RC corroded beams available in the literature, e.g. in [Rodriguez et al., 1997].
On this topic, an important remark should be made. It is well known that proper strengthening strategies carried out on existing buildings should preserve, as far as possible, the stiffness and strength ratios between all structural elements, in the attempt to guarantee a ductile behaviour of the construction. According to [Rai, 2005], a few components of an existing building may not have adequate strength and/or deformation capacity (especially shear resistance of the connections), although the building as a whole could adequately withstand the loading. For such components, local retrofitting interventions may be carried out to improve their individual strength and/or ductility, while retaining the basic configuration of the building's lateral force resisting system, so that the overall structural scheme is unmodified. In this way, only brittle failure mechanisms, such as shear and beam-column joints failure, are prevented.
This hypothesis has been assumed herein, so allowing the extension of the analyses up to the formation of the plastic hinge mechanisms. Therefore, it is supposed that specific interventions addressed at increasing locally the strength of elements failing prematurely in shear, as suggested

by [Eurocode 8, 2006], are performed without notably modifying the global strength of the structure.
Besides this, it is worth noting that the present research deals only with uniform steel corrosion affecting RC columns, being the most influencing structural components from the seismic point of view, especially in existing buildings. Recently, models able to describe also the spatial variability of the corrosive attack have been proposed in the literature, e.g. [Stewart, 2004]. A possible approach consists in subdividing the structure into elements with statistically independent degradation properties, whose size depends on by the spatial variability of the most significant factors of the degradation phenomenon. In this way, the spatial characteristics of initial phase of degradation, such as carbonation initiation may be modelled. As an example, considering parameters like concrete permeability, cover depth and diffusivity, [Faber, 2006] suggests to discretize the structure with 0.5 m x 0.5 m individual concrete elements, with the possible need for a smaller size at the edges of the considered surface.
These approaches inevitably require a considerable computational effort, which is not always recompensed by an increased accuracy of the overall results.

6.2 First case study

6.2.1 Presentation of the case study

The first case study is a two-storey, two-span RC structure. The regularity in plan and in elevation of the system allows the analysis of two planar models, i.e. one representative frame for each main direction. The typical frame in the X direction is shown in Figure 6.1a, while Figure 6.1b illustrates the typical sections of beams and columns with the reinforcement details.

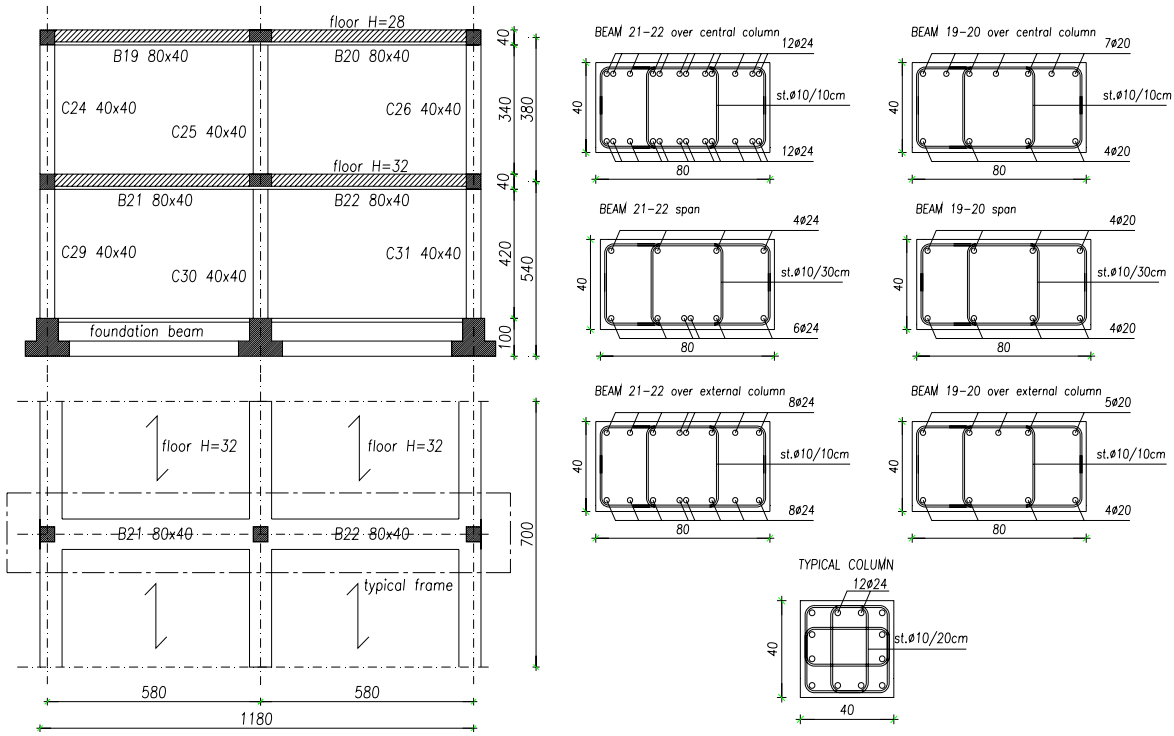

Figure 6.1 (a) Front and plan view; (b) typical sections and reinforcement details (units in cm)

Table 6.1 Floor loads

Load case	1st floor	2nd floor
dead load	8.8 kN/m²	7.3 kN/m²
live load	4.0 kN/m²	0.9 kN/m²

The materials have the following characteristics: a mean value of cylinder compressive strength f_{cm} = 30.5 MPa for concrete and a mean value of yield strength f_{ym} = 430 MPa for steel.
The floor loads are summarized in Table 6.1 and a tributary length equal to the frame spacing (7 m) is considered for the loads on the beams. In the numerical analyses, the column bases have been assumed fixed to the ground, neglecting the soil-structure interaction.
To account for the well-known uncertainties regarding the value of the concrete compressive strength, in line with [Biondini and Frangopol, 2008b] (see Table 5.10), a log-normal probability distribution with a standard deviation of 5 MPa with respect to the nominal value may be assumed. In order to assess the effect of such variability on the capacity curve of the structure, pushover analyses have been performed also with f_c = 25.5 MPa and f_c = 35.5 MPa. The results show that a variation of ±5 MPa around the mean value of the concrete compressive strength does not significantly affect the global response of the structure. In particular, the maximum variation in terms of structural ductility (that is a fundamental parameter from the seismic point of view) is less than 6%. Thus, the concrete compressive strength has been dealt with as a deterministic variable in the performed analyses.

6.2.2 Phase 1: Probability of occurrence of corrosion

As already pointed out in the previous chapter, in view of the inevitable presence of uncertainties, a reliable prediction of the onset and progression of corrosion can be performed only in a probabilistic context. In fact, corrosion processes are highly influenced by material and environmental factors.
In the present thesis, the diffusive model developed by [Saetta, 1992; Saetta et al., 1993a] (explained in detail in Section 4.2.1.1) is adopted to assess the durability of the structure at the end of its service life, i.e. after 50 years from the time of construction. The durability assessment is considered in probabilistic terms, bearing in mind that the parameters in the model (permeability, diffusivity, porosity, mechanical strength, etc.) are aleatory variables.
As described in Section 5.4.2, the probable initiation time for the case study is evaluated by using the model for durability prediction in combination with the software *Optislang* for the probabilistic treatment of the problem.

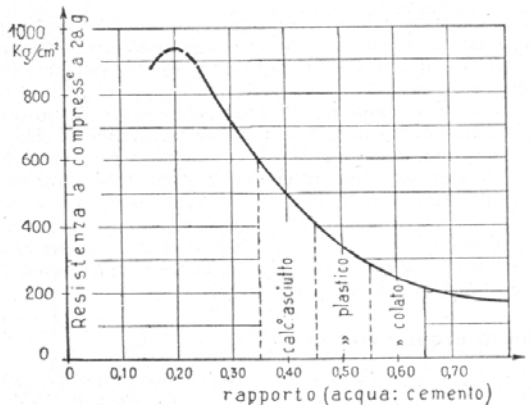

Figure 6.2 Schematic representation of concrete compressive strength vs. w/c ratio [Santarella, 1973]

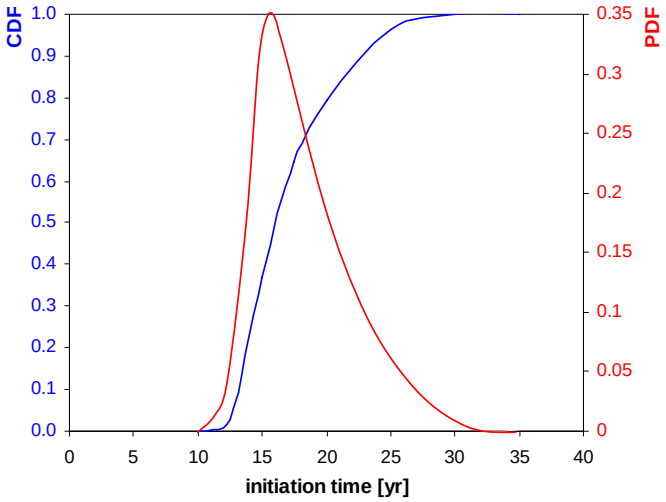

Figure 6.3 Cumulative and probability density functions of corrosion initiation time (w/c = 0.6, R.H. 70%)

Given the medium-low quality of concrete, from the graph in Figure 6.2 relating the w/c ratio to the compressive strength f_c, a cautious value of 0.6 is reasonably assumed for the w/c ratio and from Table 5.15 the corresponding concrete moisturizing coefficient D_{28}/D_{∞} to be set in the model is derived.

In order to account for its considerable seasonal variability, different values of the relative humidity should be assumed in the analyses. For the sake of brevity and with the aim to present an exemplificative application of the methodology, only the case R.H. = 70% is considered herein. Thus, from the cumulative probability of Figure 5.16b, the probability density function is derived (Figure 6.3), providing the value 0.35 for the probability *P(corr)* of occurrence of the corrosion hazard to be used in the calculation of structural risk. It is interesting to note that the value obtained for *P(corr)* is in line with the discrete ranking of corrosion risk levels shown in the matrix representation of Figure 5.11a. In fact, as a function of the "moderate" severity level (corrosion rate) in the range 0.5 to 1 $\mu A/cm^2$ and reasonably assuming for the structure an exposure class XC3 according to the EN-206 classification, a "seldom" probability in the range 11-40% is obtained from the risk matrix.

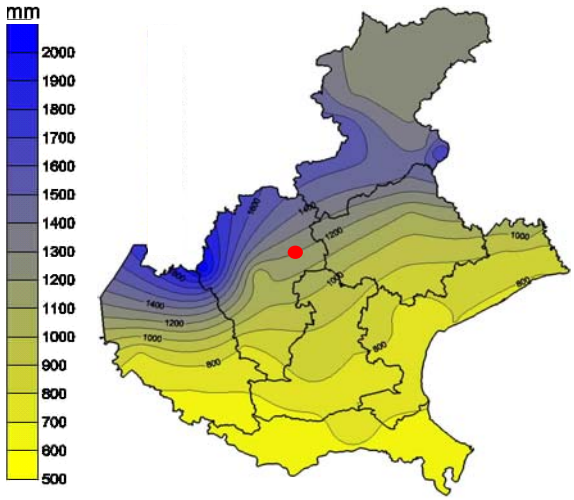

Figure 6.4 Average annual precipitation in the region Veneto, Italy (1993-2002) [http://www.iscattaneo.it]

6.2.3 Phase 2: Environmental analysis

It is now necessary to identify the climatic characteristics of the site where the structure is located, in order to define the main parameters controlling the corrosion phenomenon. In particular, data concerning the average annual precipitations (in hours/year, days/year or mm of rain) are required to proceed with the following phase. In general, this type of information may be easily gathered on line, as shown for example in Figure 6.4, referring to the region Veneto, in the North-East of Italy.
It is assumed that the structure under investigation is located in Bassano del Grappa (red spot on the map), where an average precipitation of 1180 mm per year is recorded.

6.2.4 Phase 3: Corrosion rate

As a function of the climatic characteristics of the site and the range of concrete strength f_c, the yearly averaged resistivity ρ_{av} may be evaluated from Table 6.2, [Andrade and Alonso, 2001]. Afterwards, the maximum expected corrosion rate i_{corr} may be derived from Figure 6.5, [Andrade and Alonso, 2001], in which an exemplificative use of the graph is shown in three steps: (A) measurement points; (B) extrapolation to minimum ρ; (C) maximum expected i_{corr}.
From the annual rainfalls information gathered in Phase 1, the case study belongs to the third climatic zone of Table 6.2, for which, given f_c equal to around 30 MPa, the average resistivity for non-sheltered concrete is estimated equal to 15 kΩcm through linear interpolation. This value falls in the range 10 - 50 kΩcm suggested in [Rodriguez et al., 2001] for the moderate to high corrosion risk.
The graph in Figure 6.5 provides a maximum expected value of the corrosion rate of 0.8 $\mu A/cm^2$. Therefore, according to the corrosion risk classification proposed by [Rodriguez et al., 2001] (Table 4.1), the structure under investigation may be associated with a moderate corrosion class. In this way, the corrosion rate has been directly related to the site (climatic characteristics and presence of protection, i.e. sheltered structure or not) and to a single significant material property, i.e. the concrete compressive strength. This simplified approach has evident advantages for the practical application of the methodology in the professional field.
Obviously, this procedure is advisable for estimating the corrosion rate when, as in the present case, no in-situ measurements are available. It is clearly preferable to have at disposal in-field data collected from readings of corrosion rate sensors placed throughout the structure. Nevertheless, it is important to emphasize, as already mentioned in Section 3.2.3, that different sets of readings over time are necessary to obtain consistent data, as a consequence of the strong dependence of the measurements on seasonal variations of temperature and relative humidity.

Table 6.2 Yearly averaged resistivity for different climatic characteristics [Andrade and Alonso, 2001]

Climatic characteristics			Time of Wetness	Yearly averaged resistivity ρ_{av} [kΩcm]			
h/year	mm rain	rainy days/year		Sheltered concrete		Non-sheltered concrete	
				f_c>30 MPa	f_c<30 MPa	f_c>30 MPa	f_c<30 MPa
<2000	<250	<50	0.25	100	50	50	30
2000-4000	250-750	50-100	0.5	50	30	30	20
4000-6000	750-1000	100-150	0.75	30	20	20	10
>6000	>1500	>150	1	10	5	5	3

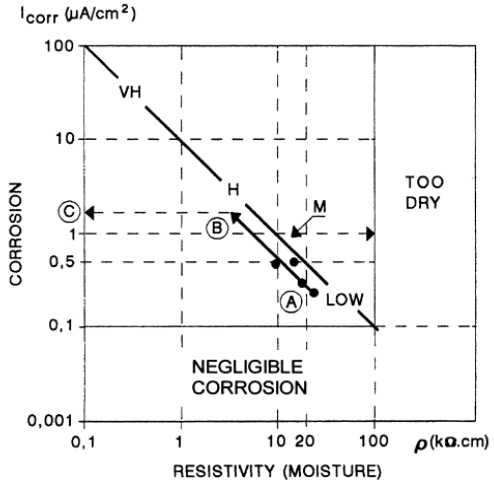

Figure 6.5 Corrosion rate i_{corr} vs. resistivity ρ [Andrade and Alonso, 2001]

6.2.5 Phase 4: Corrosion effects

Among the several effects of corrosion described in detail in Section 4.2, the following major aspects have been included in the analyses:

1. reduction of longitudinal rebars section and reduction of transversal rebars section with the consequent reduction of the lateral confinement pressure in concrete;
2. reduction of rebars ultimate deformation;
3. degradation of the concrete cover.

Possible variations of the ultimate and yield strength of the rebars have not been accounted for in the present work, as a consequence of their negligible values and the objective difficulty to identify a uniform trend in the published experimental results (see Section 4.2.2).
Moreover, since in presence of moderate corrosive levels limited loss of bond has been detected, e.g. [Bertagnoli et al., 2006], the effects of reinforcement corrosion on bond interaction have been disregarded and the hypothesis of the conservation of plane sections has been assumed.

6.2.5.1 Evaluation of the residual steel section

For evaluating the residual steel section, expressions (4.3)-(4.4) have been solved within the probabilistic software *Optislang*, thus including in the analysis the uncertainty related to the values of the initial rebars diameter and especially of the corrosion rate. Referring to the statistical properties summarised in Table 5.10, a log-normal distribution has been assigned to the initial diameter Φ_0 with coefficient of variation 0.05, and a normal distribution to the corrosion rate with coefficient of variation 0.2. For this last CoV a quite high value has been chosen in order to account for measurement errors and strong seasonal variations, as described in Section 4.2.1.1.
As for the initiation time, the results of the previous analysis, summarized in Table 5.17, have been adopted, i.e. a mean value t^*_{in} = 13.5 years, correspondent to the 50% percentile, with percentage variation 1.9%.
An exemplary PDF of the residual steel section $A_{s,t}$ after t = 50 years for the initial section $A_{s,0}$ = 314 mm^2 (diameter Φ_0 = 20 mm) is shown in Figure 6.6. The resulting mean value $A_{s,t}$ = 293.9 mm^2 corresponds to an average penetration depth P_x = 0.34 mm, i.e. a percentage reduction of 6.7% respect to the virgin section (3.5% reduction in terms of bar diameter). The values relative to the other rebar diameters present in the model are summarised in Table 6.3.

These results are in line with data indicated by [Rodriguez et al., 2001], reporting a section reduction of 5% and diameter reduction of 0.5 mm for a 20 mm-bar, with t_p = 25 years and i_{corr}= 1 μA/cm^2 (thus slightly higher than the value assumed here).
The general trend of steel section reduction over time for the 20 mm-bar is shown in Figure 6.7, displaying the mean value μ and the its range of variation. It should be noticed that the degree of uncertainty increases significantly as time passes.

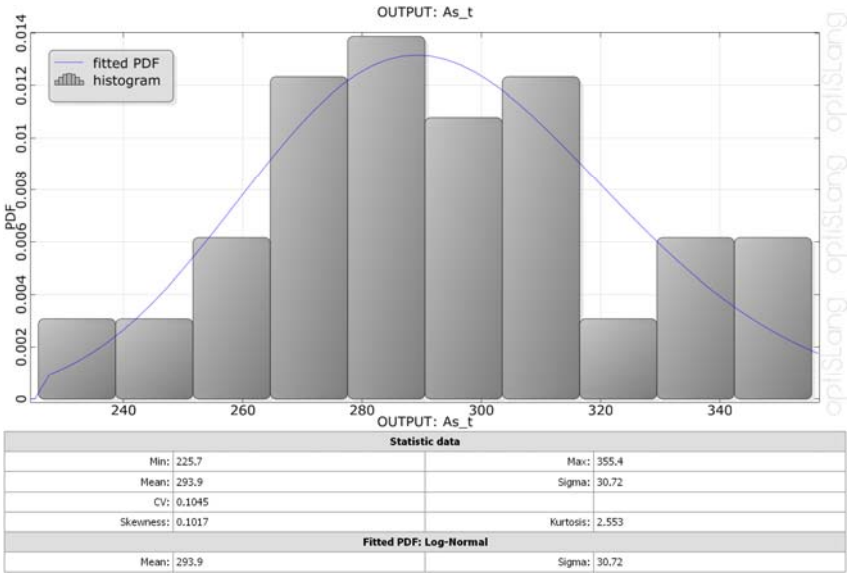

Figure 6.6 Probability density function of the residual steel section (A_{s0} = 314 mm^2)

Table 6.3 Diameters and sections reductions of the corroded rebars

$A_{s,0}$ [mm^2]	$A_{s,t}$ [mm^2]	ΔA_s [%]	Φ_0 [mm]	Φ_t [mm]	$\Delta\Phi$ [%]
452.2	426.2	5.7	24	23.3	2.9
314.0	293.9	6.7	20	19.3	3.5
78.5	67.9	13.5	10	9.3	7.0

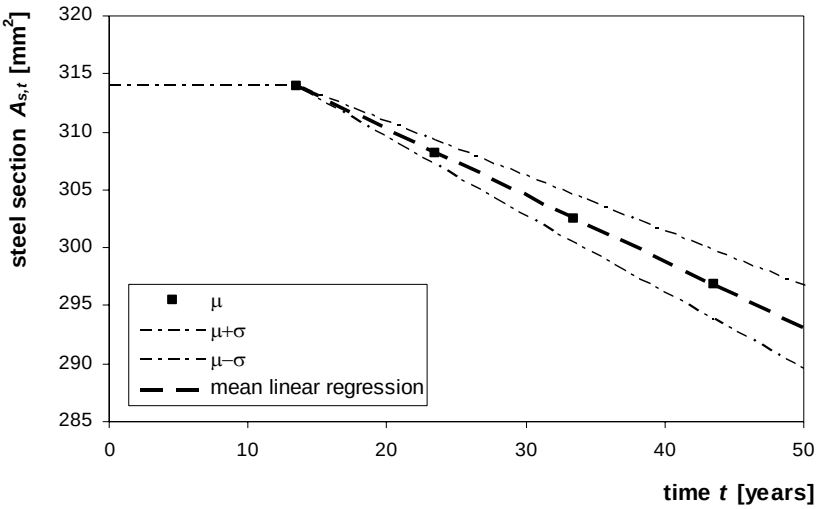

Figure 6.7 Steel section reduction over time ($A_{s,0}$ = 314 mm^2)

In order to judge on the safety of the structure, it is necessary to decide an *acceptable limit* for the corrosion effects evaluated above, with the evident difficulties related to the lack of practical experience in this field and the fact that safety is not just a technical issue. Nevertheless, some hints can be found in the literature. For example, [Gonzalez et al., 1996] observed that any acceptable limit depends on the type of structure and its use. However, the authors refer to a damage level of 25% in terms of steel cross-section reduction, being a prominent value in corrosion-affected concrete structures. This remark is based on data by [CEB-FIP, 2006], which classifies structural deterioration according to external signs, such as rust spots, concrete cracks, cover delamination, as well as cross section reduction of the rebars. In line with this approach, the reductions listed in Table 6.3 indicate a robustness class ROC 2, according to the classification by [CEB-FIP, 2006] given in Table 5.5.
The criterion proposed by [Amey et al., 1998], also adopted by [Li et al., 2008], consists in using as failure criterion a more simplistic 30% of steel area reduction, i.e. an acceptable limit $R_a = 0.7\ R_0$, where R_0 is the original value for the undamaged structure.
Finally, it is worth underlying that the PDF represented in Figure 6.6 may be regarded as the PDF of an expected *local* Damage for the considered EaR in the calculation of structural risk within the Risk Management Process. The combination between seismic and corrosion hazard provides a *global* Damage on the whole structure, as described in Section 6.2.7.

6.2.5.2 Reduction of steel ductility

With reference to the considerations of Section 4.2.2, the percentage reduction of the steel ultimate deformation ε_{su} has been calculated through linear interpolation of the experimental results by [Rodriguez et al., 2001]. A reduction of 21% has been estimated, assuming an average loss of cross section of 9% for the longitudinal bars.

6.2.5.3 Concrete cover degradation

Given the moderate intensity of the corrosive attack, complete spalling of the concrete cover, and consequently reduction of the concrete section, is not considered. Therefore, the degradation of the concrete cover is accounted for by reducing the concrete compressive strength, in line with the approach proposed by [Coronelli and Gambarova, 2004] (see Section 4.2.3). Even for a moderate corrosion level, as considered in this study, the concrete cover strength may fall to very low values (less than 10 MPa), while the concrete core strength is characterized by a minor reduction.
Different approaches could be used to obtain an equivalent value of concrete strength for the damaged members. Herein we refer to the work of [Capozucca and Cerri, 2003] in which the ratio between the peak compressive strengths of the undamaged and damaged concrete (f_{cu} and f_{cd} respectively) has been evaluated for a number of corroded elements. This ratio ranges between 1.5 and 2.5, depending on the corrosion scenario. In particular, the setting assumed in the present case study is similar to the lower corrosion level proposed by the authors. Thus, it is assumed $f_{cu}/f_{cd} = 1.5$, resulting in $f_{cd} = 20$ MPa, which has been assigned to the concrete sections of the damaged columns.
Due to the objective complexity of the phenomenon, the effect of concrete degradation has been handled separately, and two different sets of analyses are distinguished: first considering an undamaged concrete section, secondly using the calculated reduced concrete strength. The results in terms of capacity curves are shown in the following section.

6.2.6 Phase 5: Pushover analysis

6.2.6.1 Introduction

Pushover analyses have been performed using the general-purpose code MIDAS Gen, considering gravitational and seismic loads. A concentrated plasticity approach is followed, with lumped hinges assigned at the ends of the beams and the columns. The results are presented in terms of capacity curves, plotting the base shear force against the control displacement assumed at the centre of mass of the roof level. The fundamentals about the method are given in APPENDIX E.

As recommended by the code guidelines, e.g. [Eurocode 8, 2005], two vertical distributions of the lateral loads, applied at the location of the masses in the model, have been considered, as schematically represented in Figure 6.8: a "uniform" pattern, based on lateral forces proportional to the mass regardless of the elevation (uniform response acceleration); a "modal" pattern, proportional to lateral forces consistent with the lateral force distribution determined in an elastic analysis.

For the sake of brevity, only the results obtained with the uniform loading distribution are described in the following. The storey masses are summarized in Table 6.4.

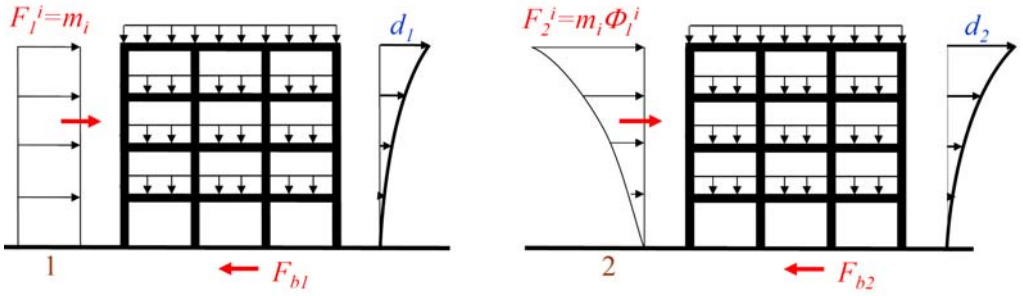

Figure 6.8 Horizontal forces distribution: (a) "uniform pattern"; (b) "modal" pattern [Riva]

Table 6.4 Storey masses

Storey	Level [m]	Mass [kN/g]
1st	4.4	88.8
2nd	8.2	62.6

Different corrosion scenarios have been considered. First, a uniform corrosive attack affecting all the structural elements has been used as reference case to be compared with other more likely patterns, [Berto et al., 2007b]. Afterwards, two scenarios more representative of real exposure conditions have been analyzed: the first one in which the corrosive attack affects all the columns of the ground floor, the second one in which only the columns of one side of the structure are corroded. The first case frequently occurs when the ground floor is used as garage or storage, in line with exposure classes XC3-XC4 according to [Eurocode 2, 2004]. The second case is likely to occur when the construction has a harmful location with respect to its surrounding environment, which may lead to an attack concentrated at one side of the structure.

These two degradation scenarios, being the most significant, will be herein discussed and compared with the case of undamaged structure, i.e. at the beginning of its service life.

It is worth noting that for the columns, characterized by prevalence of axial loads before the seismic excitation, the assumption of an approximately uniform steel loss, due to a carbonation

attack, can be considered as an appropriate and practical assumption. On the contrary, in presence of pitting corrosion, e.g. due to chloride ions penetration, the modelling of not uniformly distributed attacks is usually required (see also Section 6.1).

6.2.6.2 Hinge properties definition

The definition of the hinge properties requires moment–curvature analysis of each element. In this study, Mander's law, [Mander et al., 1988], accounting for the confinement level, and an elasto-plastic law have been adopted for concrete and steel respectively. In particular, moment–curvature analyses have been carried out for each column considering the actual section properties and constant axial forces due to dead loads acting on the elements. On the beams, axial forces are assumed to be zero.
The effects of corrosion described in Section 6.2.5 have been included in the calculation of the moment-curvature relationships of the corroded sections and the corresponding percentage variations of the maximum resistant moment and of the ultimate curvature respect to the pristine sections are listed in Table 6.5.

Table 6.5 Effects of corrosion on resistant moments and ultimate curvatures

Section	Reduction ΔM [%]	Reduction $\Delta\phi_u$ [%]
B21–22 (outer sections)	7	19
B21–22 (inner sections)	7	21
B19–20 (outer sections)	10	21
B19–20 (inner sections)	9	20
C24–C26	6	20
C25–C29–C3	5	20
C30	6	19

From the moment-curvature analyses, the moment-rotation laws of the plastic hinges have been derived according to the classical expressions, e.g. [Park and Paulay, 1975], [Panagiotakos and Fardis, 2001b]:

$$\theta_u = \theta_y + \left(\phi_u - \phi_y\right) L_{pl} \cdot \frac{(L_v - L_{pl}/2)}{L_v} \tag{6.1}$$

where ϕ_u and ϕ_y are respectively the ultimate and yield curvatures, L_v is the distance from the critical section of the plastic hinge to the point of contraflexure, L_{pl} is the plastic hinge length.
Several expressions for L_{pl} are available in the literature and, as well known, these different formulations may significantly affect the evaluation of the element ultimate deformation capacity.
It is worth noting that the aim of the proposed investigation is comparative only. For this reason, and in order to simplify the analysis, only one expression of plastic hinge length is considered. In particular, the following formula suggested by the European Seismic Code for existing buildings (Annex A), [Eurocode 8, 2006], in case of using an appropriate confinement model, has been adopted:

$$L_{pl} = \frac{L_v}{30} + 0.2h + 0.11\frac{d_{bL} \cdot f_y[MPa]}{\sqrt{f_c[MPa]}} \tag{6.2}$$

where h is the depth of the member and d_{bL} is the mean diameter of the tension reinforcement.
Figure 6.9 shows schematically the moment - rotation law assumed for the plastic hinges with the indication of the acceptance criteria corresponding to the three Limit States defined in accordance to [Eurocode 8, 2006].

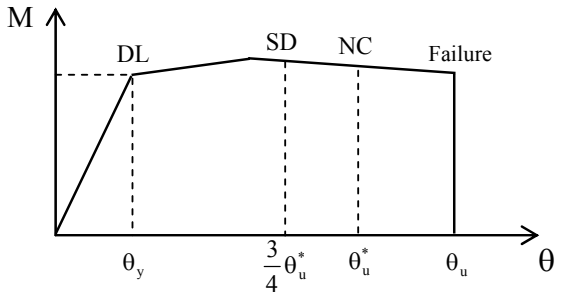

Figure 6.9 Moment - rotation law assigned to the plastic hinges

In particular, in order to account for the reduction of the ultimate rotation θ_u for primary seismic elements, the Near Collapse (NC) status is assumed in correspondence to $\theta_u^* = \theta_u / \gamma_{el}$, with γ_{el} = 1.7 (Annex A(9), [Eurocode 8, 2006]); the Significant Damage (SD) status to a rotation of ¾ θ_u^* and the Damage Limitation (DL) status to the yield rotation θ_y.

6.2.6.3 Capacity curves and collapse mechanisms

The results of the pushover analyses are here presented in terms of capacity curves, first neglecting the effect of concrete cover degradation. Figure 6.10 shows the comparison between the capacity curves obtained for the structure in undamaged condition (at the beginning of the service life) and after 50 years, for two different corrosive scenarios: corrosion of all the ground floor columns and corrosion of the right-side columns. In both cases, a reduction of the load bearing capacity and especially a significant reduction of structural ductility occur with respect to the undamaged condition. The failure mode evidences the formation of a soft storey plastic mechanism, requiring a too high level of local ductility demand in the columns of the soft storey. This behaviour is exhibited by the structure in all the three scenarios illustrated in Figure 6.10, but for lower values of the top floor displacement in presence of corrosion. As a matter of fact, the case study is an existing construction, mainly designed for vertical loads. The considerable distance between the frames of the structure produces rather high loading acting on the principal beams. Therefore the structure can be classified as a typical example of "strong beam – weak column" system and a ductile behaviour is unlikely to occur.
Figure 6.11 illustrates the evolution of the plastic hinge pattern at three different steps of the analysis in the case of ground floor columns corrosion. In particular, Figure 6.11a shows the hinge pattern at yielding, corresponding to the formation of the first hinges (DL status), which occurs for a top displacement of 0.038 m. Figure 6.11b shows the incipient soft storey mechanism with the formation of the first NC hinge at a top displacement of 0.100 m, while Figure 6.11c shows the achievement, at a top displacement of 0.150 m, of the failure limit θ_u for the first hinge and the correspondent soft-storey failure mechanism.

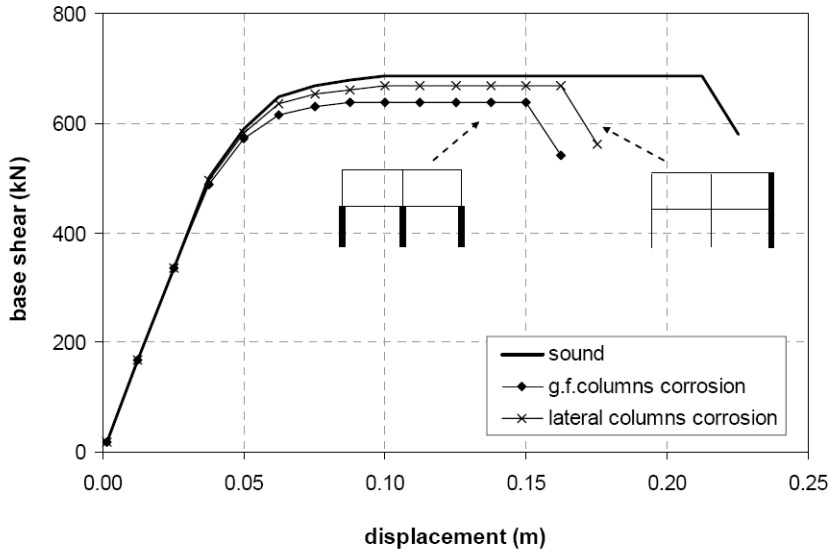

Figure 6.10 Capacity curves of the new and 50-year-old structure for two different corrosion scenarios

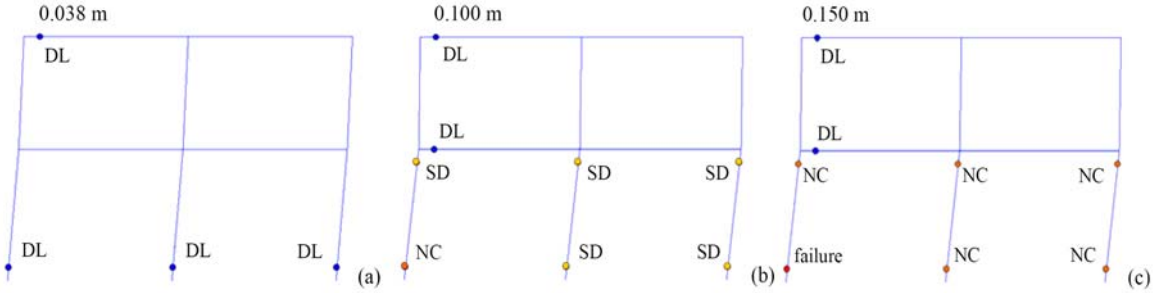

Figure 6.11 Corrosion of the ground floor columns: (a) first DL hinges formation; (b) first NC hinge formation; (c) first hinge failure formation

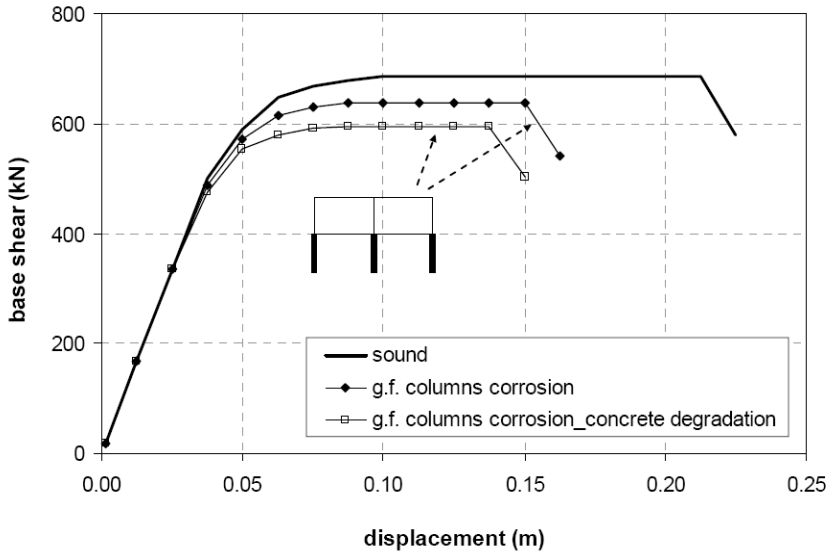

Figure 6.12 Influence of concrete degradation in the case of ground floor columns corrosion

The plastic hinge distribution evidences the bad seismic behaviour of the building. In fact, approaching collapse, the plastic hinges of all the columns of the ground floor range between the NC and failure status, while almost all the beams still behave elastically. In particular, only two plastic hinges at the beams' ends are activated and have reached the DL status.
A similar plastic hinge evolution takes place also in the cases of new structure and of lateral columns corrosion. The achievement of the *failure* status for the first hinge occurs, respectively, for a top displacement of 0.22 m and 0.17 m.
The additional effect of concrete degradation is shown in Figure 6.12. The results indicate a further reduction in terms of resistance and ductility with respect to the undamaged condition, when also the concrete degradation effects are taken into consideration.

6.2.6.4 Seismic response according to European Standards

In accordance with the European Standard, [Eurocode 8, 2005], and the Italian Seismic Code, [OPCM 3431, 2005], the maximum ratios $\rho_i = D_i/C_i$ between the demand D_i obtained from the analysis under the seismic load combination and the corresponding capacity C_i of the i-th element of the structure have been evaluated. In particular, the codes define the ratios ρ_i in terms of ultimate rotation, for ductile failure mechanisms, and in terms of elements and beam-column joints shear, for brittle failure mechanisms. For each verification, failure occurs when the coefficient ρ_i reaches the value 1, which means that the demand becomes equal to the member capacity and the corresponding limit state is achieved.
Regarding the calculation of the rotation capacity, the expression suggested in Annex A of [Eurocode 8, 2005] giving the ultimate chord rotation has been considered:

$$\theta_{um} = \frac{1}{\gamma_{el}} 0.016 \cdot 0.3^{\nu} \left[\frac{\max(0.01;\omega')}{\max(0.01;\omega)} f_c \right]^{0.225} \left(\frac{L_V}{h} \right)^{0.35} 25^{\left(\alpha \rho_{sx} \frac{f_{ywe}}{f_c} \right)} \cdot 1.25^{100\rho_d} \qquad (6.3)$$

where γ_{el} is a reduction coefficient equal to 1.5 for primary seismic elements and 1.0 for secondary seismic elements, meant to convert mean values μ_i to $\mu_i - \sigma_i$ ones (note (9) of Annex A); $\nu = N/b\,h\,f_c$, N is the axial force (positive for compression), b and h are the width and height of the compression zone; ω and ω' are the mechanical reinforcement ratios respectively of the tension (including the web reinforcement) and compression longitudinal reinforcement; f_c and f_{ywe} are the mean values of concrete compressive strength (MPa) and of the stirrup yield strength (MPa), appropriately divided by the confidence factors; L_v is the shear span, assumed equal to $L/2$, where L is the element length; $\rho_{sx} = A_{sx}/b_w s_h$ is the ratio of transverse steel parallel to the direction x of loading; s_h is the stirrup spacing; ρ_d is the steel ratio of diagonal reinforcement (if any), in each diagonal direction; α is the confinement effectiveness factor, depending on the dimensions of the confined concrete core to the centreline of the hoop and the centerline spacing of longitudinal bars laterally restrained by a stirrup corner or a cross-tie along the cross-section perimeter.
In members without detailing for earthquake resistence, Eq.(6.3) is multiplied by a coefficient 0.825.
Table 4.3 of [Eurocode 8, 2005] (APPENDIX F) summarises the values of the material properties to be adopted in evaluating both the demand and capacities of the elements for all types of analysis. Moreover, the criteria that shall be followed for the safety verification of both ductile and brittle elements for all types of analysis are provided.

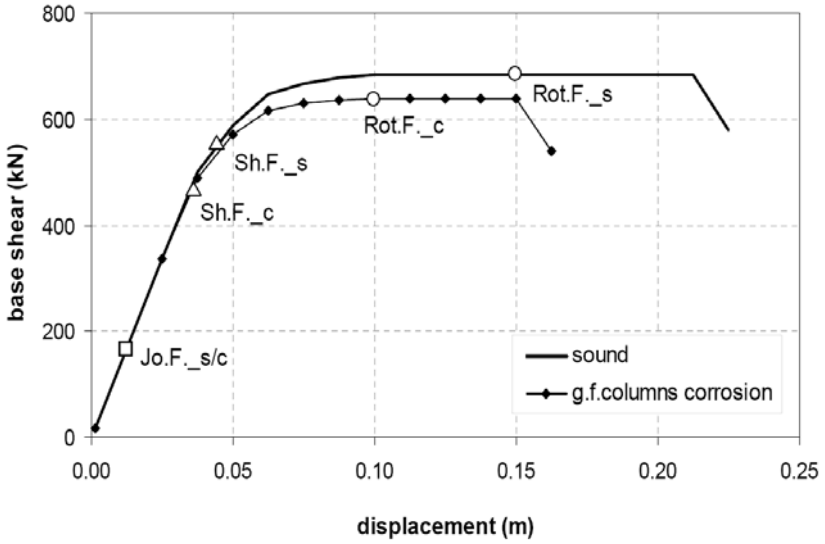

Figure 6.13 Capacity curves for sound and corroded pattern with indication of the failure points

As it commonly occurs in existing RC buildings without detailing for earthquake resistance, the brittle failure mode is the governing mechanism. In fact, as evidenced in Figure 6.13, the failure of beam-column joints is the first to occur in both sound and corroded conditions, corresponding to the "Jo.F._s/c" square mark in the graph. Immediately afterwards, the shear failure takes place, as the "Sh_s" and "Sh_c" triangular marks in the graph confirm, respectively for sound and corroded conditions.

Assuming that all brittle failure mechanisms can be avoided by means of careful strengthening interventions (see Section 6.1), the analyses are continued until the occurrence of plastic collapse. As for the ductile mechanism verification, in line with the European Standard, the rotation capacity of each hinge is assumed equal to the corresponding θ_u^*, i.e. the NC limit state defined in Figure 6.9. The related points in the capacity curves are indicated in Figure 6.13 with the circular marks "Rot.F._s" at a top displacement of 0.150 m and "Rot.F._c" at a top displacement of 0.100 m, respectively for sound and corroded scenarios, [Berto et al., 2008b].

In order to better appreciate the different seismic response of the structure subject to degradation, it may be meaningful to evaluate the maximum peak ground acceleration (PGA) tolerable by the structure before reaching the NC Limit State. Afterwards, the seismic zone where the building can be considered in safe conditions may be identified.

According to Annex B of [Eurocode 8, 2005] (see APPENDIX E), performing a pushover analysis, the target displacement shall be defined as the seismic demand derived from the elastic response spectrum in terms of the displacement of an equivalent single-degree-of-freedom system. In particular, with reference to the capacity curve, the ductile mechanisms are checked in terms of generalized deformation, and the values of the capacities for the NC limit state are obtained from the appropriate expressions given by [Eurocode 8, 2006].

Once the seismic capacity of the structure has been determined, the next step is the computation of the seismic demand related to seismic actions with a certain PGA level. The usual pushover procedure requires the choice of a specific seismic zone, characterized by a given PGA, and the evaluation of the target displacement (which is an estimate of the displacement that the design earthquake will produce on the building) from the ordinate of the elastic displacement response spectrum at the effective period of the building. This period is evaluated using the stiffness of

the bi-linearised capacity curve and the modal mass. In particular, to calculate the target displacement in the short period range the equal displacement principle is applied (elastic and inelastic SDOFs have the same maximum displacement), while in the medium- and long-term, the equal energy principle is applied.

Figure 6.14a illustrates the seismic hazard map of the region Veneto (North-East of Italy) according to the seismic classification of the Italian territory, [OPCM 3519, 2006]. In Figure 6.14b a zoom of the map shows the site where the considered case study is located, which is characterized by a design PGA in the range 0.175 – 0.200 g.

The graphical representation of the target displacements for the three limit states DL, SD and NC corresponding to a value of PGA equal to 0.20 g is displayed in Figure 6.15a-b, for the new and corroded structure respectively. The MDOF and SDOF systems coincide in this case, since the pushover curves refer to the uniform distribution of the lateral forces, implying that the transformation factor $\Gamma = 1$, [Fajfar, 2002]. In both undamaged and damaged conditions, the structure results able to withstand the seismic action without reaching the rotation failure.

To predict the seismic performance of the structure at the end of its service life, another approach may be followed. Besides verifying the compliance with the safety requirements on the basis of the specific seismic input of the site (i.e. a specific PGA), the seismic demand corresponding to the capacity of the structure may be evaluated. This means that, given the ground type of the site, the target displacement d_r is set equal to the capacity displacement and the corresponding PGA is evaluated. This value of PGA represents the maximum design earthquake which the structure can withstand.

This approach has been followed for both the new and corroded frame, demonstrating that the reduction of capacity displacement caused by the corrosive attack results in a significant reduction of the capability to withstand seismic loading.

According to the procedure for the evaluation of the target displacement suggested in [Eurocode 8, 2006] and assuming a ground type B, the values of the target displacements d_r relative to the three limit states (graphically evidenced in Figure 6.13 by the circular marks for the NC status) have been evaluated and listed in Table 6.6.

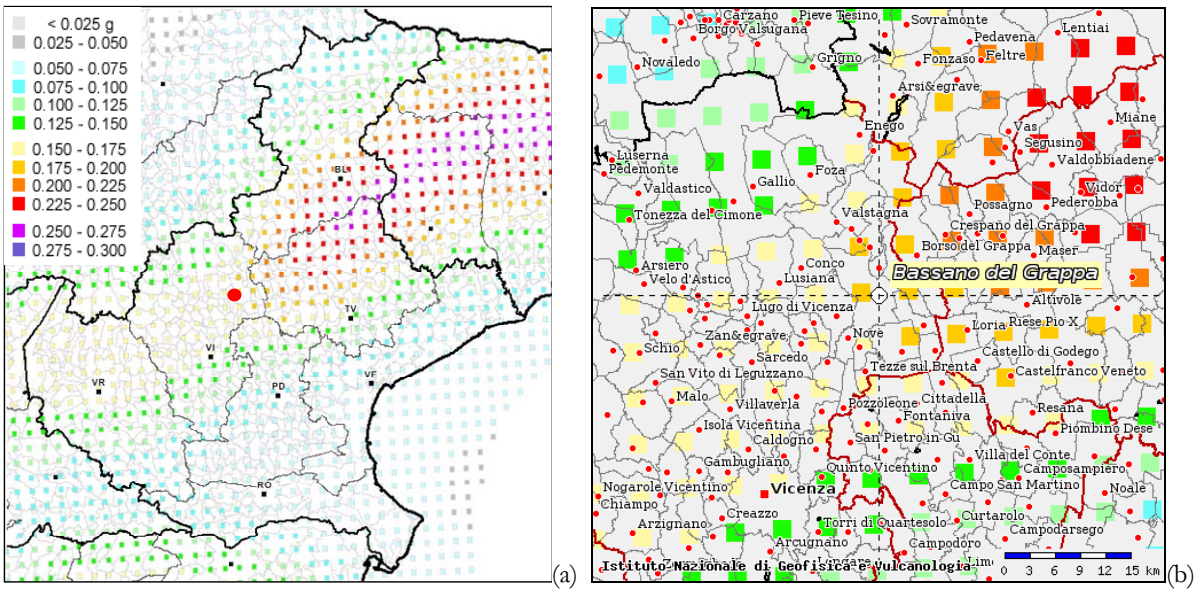

(a) (b)

Figure 6.14 (a) Seismic map of the region Veneto; (b) zoom on the case study site

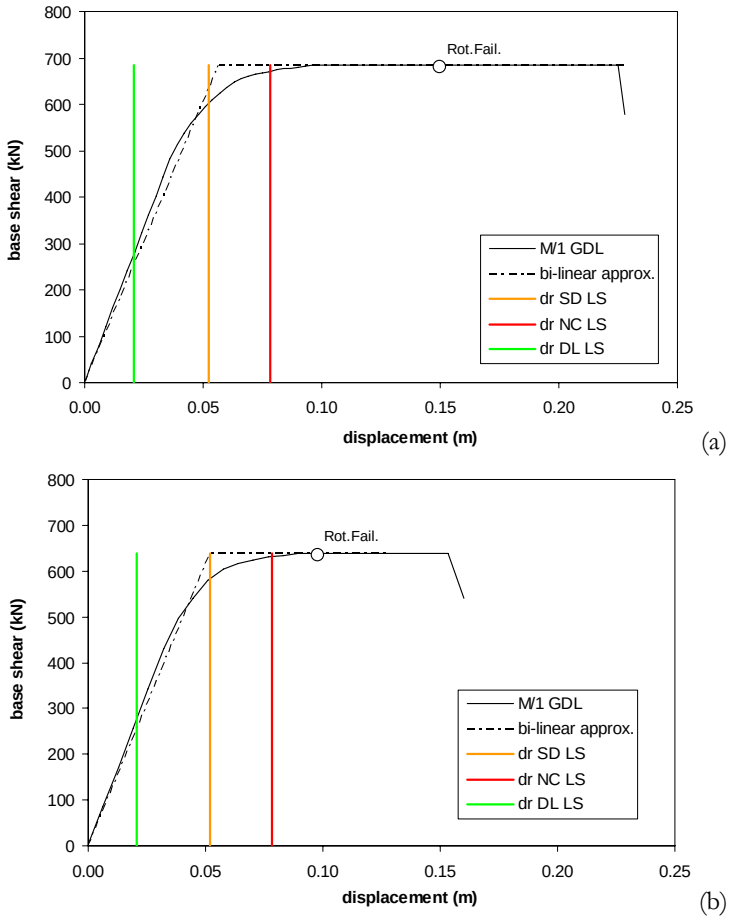

Figure 6.15 Target displacements for PGA = 0.20 g: (a) new structure; (b) corroded structure

In the same table, the values of the corresponding acceleration a_g^A for ground type A, which is generally assumed as reference soil, and a_g^B for ground type B (obtained multiplying by the soil factor 1.2) are also listed. Actually, for most applications, the [Eurocode 8, 2005] describes the hazard in terms of a single parameter, i.e. the value of PGA on ground type A, corresponding to the reference return period T_r = 475 years of the seismic action for the SD requirement, here termed a_{gR_SD}.

In the Italian code [OPCM 3431, 2005], four different seismic zones are defined, respectively characterized by the values of a_{gR_SD} summarized in Table 6.7, together with the values of a_{gR_NC} corresponding to the NC requirement (seismic action with T_r = 2475 years).

The comparison between the values of a_g^A (last two columns of Table 6.6) and the reference values of a_{gR} (Table 6.7) demonstrates that the building is able to withstand the design seismic action typical of a seismic zone I in undamaged condition, i.e. at the time of construction. In fact, the PGA of 0.51 g corresponding to the NC limit state (i.e. capacity value) is in the range characterising Italian seismic zone I. On the contrary, at the end of the service life in presence of a moderate corrosive attack, the a_{gR_NC} becomes equal to 0.35 g, which is in the range of PGA values characterising Italian seismic zone II.

The shift to a lower seismic zone tolerable for the building due to the degradation process affecting the system after 50 years (corroded condition) is schematically illustrated in Figure 6.16.

Table 6.6 Maximum PGA for the three limit states

	Target displacement d_r [m]		a_g^B [g] (ground type B)		a_g^A [g] (ground type A)	
Limit state	Undamaged	Corroded	Undamaged	Corroded	Undamaged	Corroded
NC	0.15	0.10	0.61	0.43	0.51	0.35
SD	0.12	0.08	0.50	0.34	0.42	0.28
DL	0.05	0.04	0.21	0.17	0.17	0.15

Table 6.7 Reference PGA values on ground type A for the SD and NC limit state [OPCM 3431, 2005]

Seismic Zone	SD Limit State a_{gR_SD}/g	NC Limit State a_{gR_NC}/g
Zone I	0.25-0.35	0.375-0.525
Zone II	0.15-0.25	0.225-0.375
Zone III	0.05-0.15	0.075-0.225
Zone IV	≤0.05	≤0.075

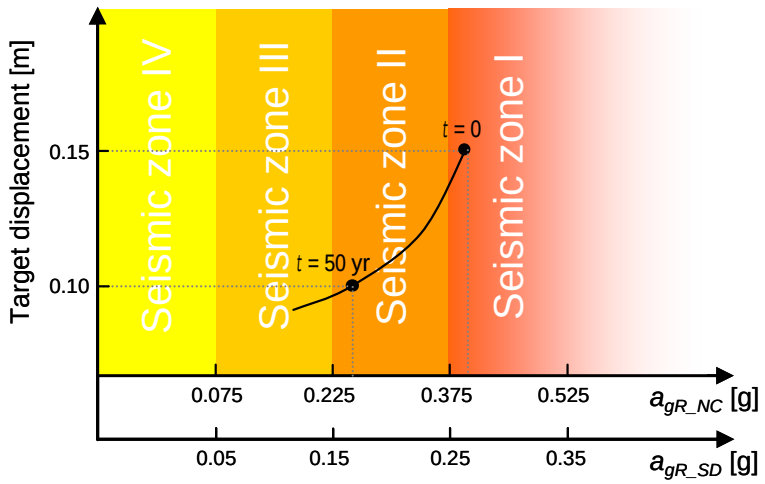

Figure 6.16 Shift of seismic zone tolerable for the building from t = 0 (new structure) to t = 50 years (corroded condition)

6.2.7 Phase 6: Probability of occurrence of the seismic event

Regarding the evaluation of the probability *P(seism)* of occurrence of an earthquake throughout the structure's design life, two approaches have been identified. The first possibility is to refer to the exceedance probabilities in a service life of 50 years prescribed by [Eurocode 8, 2005], i.e. 10% for the Near Collapse (NC) limit state, 2% for the Significant Damage (SD) limit state, 20% for the Damage Limitation (DL) limit state. The second possibility consists in using the characteristics of the seismic event specific of the site under consideration, adopting the hazard maps or seismic microzoning studies available for the location where the building is situated. For example, in the case of the Italian territory, the seismic maps provided by the National Institute for Geophysics and Volcanology (INGV) as a result of the new seismic classification recently proposed by [OPCM 3519, 2006] represent a perfect tool to this aim.

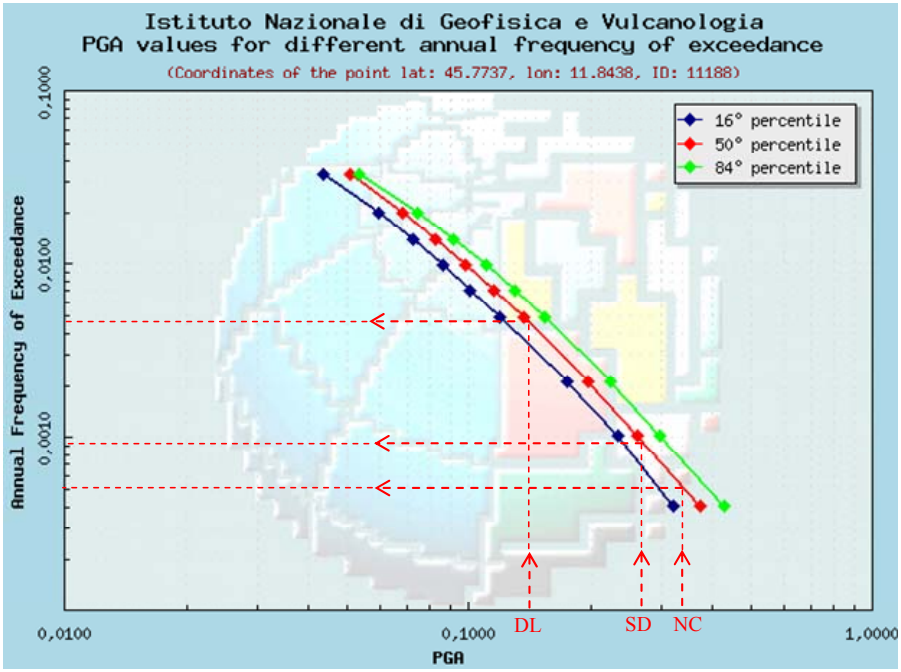

Figure 6.17 Hazard curves at the coordinates of the site of interest (http://esse1-gis.mi.ingv.it)

Table 6.8 Exceedance probabilities for the three Limit State (corroded structure)

Limit state	a_g^A [g]	$AFoE^I$	$T_r{}^I$ [yr]	$P(seism)^I$ (site)
NC	0.35	0.05%	1895	2.6%
SD	0.28	0.09%	1113	4.4%
DL	0.15	0.4%	230	19.5%

In particular, in order to determine the exceedance probability of an earthquake with the maximum values of PGA a_g^A sustainable by the 50-year-old building summarised in Table 6.6, the hazard curve of the site under consideration shown in Figure 6.17 for the 16th, 50th and 84th percentile has been adopted. The graph provides by interpolation the annual frequency of exceedance AFoE for each limit state. Since the AFoE is equal to the inverse of the return period, the value of T_r is derived and from this, using Eq.(2.1), the exceedance probability $P(seism)^I$ referred to the service life T_d = 50 years is calculated. The results are listed in Table 6.8 for the 50th percentile. For example, for the NC status, this means that in the considered site, on average, every 1895 years an earthquake with PGA ≥ 0.35 g will occur.

6.2.8 Damage coefficients evaluation

The evaluation of the expected damage may be carried out in two ways. The first possibility is to calculate the *local* damage, e.g. in terms of steel section reduction, produced by corrosion (see Section 6.2.5.1). But this approach disregards the simultaneous effect of the seismic action. Thus, in a more appropriate way, *global* damage coefficients are herein calculated accounting for both hazards, distinguishing between reduction of bearing capacity $D_{str}(t)$ and reduction of structural ductility $D_{duc}(t)$ at time t.

These damage parameters are estimated from the capacity curves in Figure 6.10 respect to the new building condition (at time t_0) as follows:

$$D_{str}(t) = 1 - \frac{F_{b,\max}(t)}{F_{b,\max}(t_0)} \tag{6.4}$$

$$D_{duc}(t) = 1 - \frac{displ_{\max}(t)}{displ_{\max}(t_0)} \tag{6.5}$$

where $F_{b,max}(\cdot)$ and $displ_{max}(\cdot)$ are respectively the maximum base shear and the maximum displacement in the capacity curves. Evidently, the damage coefficients range between 0 and 1, where 0 represents undamaged condition, i.e. $F_{b,max}(t) = F_{b,max}(t_0)$ and $displ_{max}(t) = displ_{max}(t_0)$, while 1 represents total damage.

The coefficients $D_{duc}(50)$ and $D_{str}(50)$ for the 50-year-old structure are summarized in Table 6.9. In particular, $displ_{failure}$, $displ_{NC}$, $displ_{SD}$, $displ_{DL}$, represent the displacement in the capacity curve at which the first plastic hinge reaches respectively the status *failure*, NC, SD, DL as given in Figure 6.9 (the displacements $displ_{NC}$ correspond to the circular marks "Rot.F." in Figure 6.13).

Due to the fundamental importance of ductility in seismic behaviour, merely the coefficients $D_{duc}(t)$ are considered in the following, also in view of their major value in comparison to the resistance reduction.

As for the evaluation of the seismic performance at time t_0 and t, in relation to the target displacement defined according to Annex B of [Eurocode 8, 2005] (see Section 6.2.6.4), the flow-chart in Figure 6.18 summarizes the procedure to follow with respect to the NC limit state. If the displacement capacity is greater than the displacement demand in the undamaged structure, i.e. at time t_0, the performance of the corroded building is assessed. In case of not fulfilment of the requirement at time t, the total damage state can be assumed, i.e. $D_{duc}(t) = 1$. Otherwise, the damage coefficient can be calculated as indicated in the graph.

Obviously, the described procedure is general and can be applied also for the other limit states.

Table 6.9 Summary of damage coefficients in terms of ductility and strength reduction

	Undamaged building	Corrosion of g.f. columns	Damage coefficient
$displ_{failure}$ [m]	0.213	0.150	$D_{duc,fail}(50) = 0.30$
$displ_{NC}$ [m]	0.150	0.100	$D_{duc,NC}(50) = 0.33$
$displ_{SD}$ [m]	0.122	0.083	$D_{duc,SD}(50) = 0.32$
$displ_{DL}$ [m]	0.045	0.038	$D_{duc,DL}(50) = 0.16$
$F_{b,max}$ [kN]	684.8	638.0	$D_{str}(50) = 0.07$

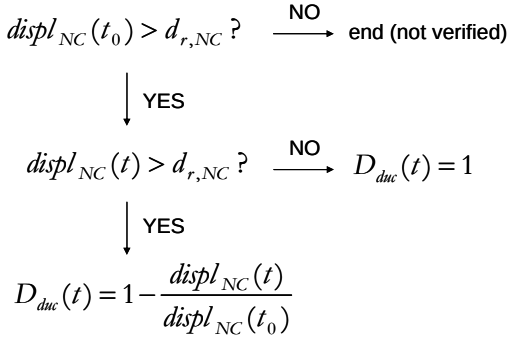

Figure 6.18 Flow-chart for calculating the ductility damage coefficient respect to the NC limit state

6.2.9 Phase 8: Calculation of *Structural Risk*

According to Eq.(2.2), it is now possible to calculate the *Structural Risk* as the *Probability* of occurrence of the hazards in the structure's service life, calculated by means of Eq.(2.4), multiplied by the correspondent expected *Damage*, evaluated as described in the previous section for each intensity level *I*, i.e. for each limit state. The expression to calculate the *Structural Risk* $R_S(t)$ at time t derives from the total probability theorem, e.g. (Kottegoda and Rosso 2008), and, in the case of discrete probabilities, is given by the sum of the products between the probability of damage P^I and damage D^I:

$$R_S(t) = \sum_I P^I \cdot D^I \quad \text{with } I = \text{intensities at the DL, SD, NC Limit State} \tag{6.6}$$

The contributions of $R_S(t)$ are listed in Table 6.10 and Table 6.11 and plotted in Figure 6.19 for the corroded structure, distinguishing between the use of the probabilities of the seismic event granted by the European Standards and those derived from the specific hazard curves of the site.

Table 6.10 Risk contributions for Eurocode's *P(seism)^I* (corroded structure)

Limit state	*P(corr)*	*P(seism)^I* (Eurocode)	*Probability P^I*	*Damage D^I*	*P^I* x *D^I*
DL	35%	20%	7%	0.16	0.0112
SD	35%	10%	3.5%	0.32	0.0112
NC	35%	2%	0.7%	0.33	0.0023
					$R_S(t)$ = 0.0247

Table 6.11 Risk contributions for the specific site *P(seism)^I* (corroded structure)

Limit state	*P(corr)*	*P(seism)^I* (specific site)	*Probability P^I*	*Damage D^I*	*P^I* x *D^I*
DL	35%	19.5%	6.8%	0.16	0.0109
SD	35%	4.4%	1.5%	0.32	0.0049
NC	35%	2.6%	0.9%	0.33	0.0030
					$R_S(t)$ = 0.0189

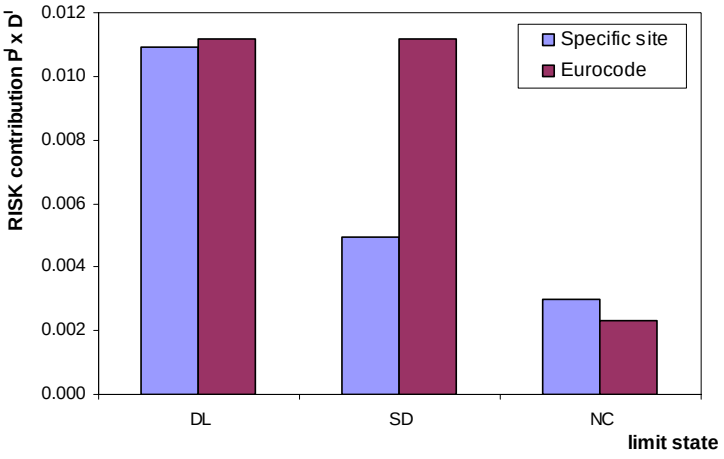

Figure 6.19 Structural risk contributions for the Eurocode's and the specific site's *P(seism)^I*

Whereas the results for the DL and NC limit states are very similar in the two cases, a considerable difference can be noted for the SD status. In particular, a weaker earthquake (i.e. with higher $P(seism)^I$ and correspondingly lower PGA) leads to the achievement of the SD limit state when the Eurocode's probabilities are used. In this sense, considering the results relative to the Standards $P(seism)^I$ values as a "risk demand", the "riak capacity" provided by the structure does not satisfy the requirements. In other words, while conservative values of the structural risk are obtained for the NC status, non conservative ones results for the SD limit state.

6.2.10 Rotation failure of a RC column

In this section, the failure probability with respect to the rotation capacity of a RC member is calculated using the demand over capacity ratio ρ_{rot} as suggested by the European Standards and the Italian Seismic Code for ductile elements (see Section 6.2.6.4). The computation is performed with respect to the element of the structure which first reaches the ultimate rotation at one end. In particular, with reference to Section 5.5.3, the limit state function is $g(\theta) = 1 - \rho_{rot}$, since the ductile failure (ultimate rotation) of the member is reached when the coefficient ρ_{rot} exceeds the value 1, i.e. when the rotation demand exceeds the element capacity. Thus, the failure probability for the i-th element may be expressed as $P_f \mid \rho_{rot}^i \geq 1$.

Table 6.12 Input parameters of the sensitivity analysis

Symbol	Description	Mean value	COV	Distribution
b	Height of the concrete cross-section	400 mm	0.1	Log-normal
h	Width of the concrete cross-section	400 mm	0.1	Log-normal
L	Length of the member	4400 mm	0.1	Log-normal
cover	Concrete cover	40 mm	0.2	Log-normal
f_c	Concrete compressive strength	30.4 MPa	0.16	Log-normal
f_y	Steel yield strength	430 MPa	0.12	Log-normal
As_long	Longitudinal steel section	5428.7 mm² (12Φ24)	0.1	Log-normal
As_st	Transversal steel section	157.1 mm² (Φ10/2b)	0.1	Log-normal
sh	Stirrups spacing	200 mm	0.2	Log-normal
N	Axial load (dead/live combination)	347.9 kN	0.1	Normal

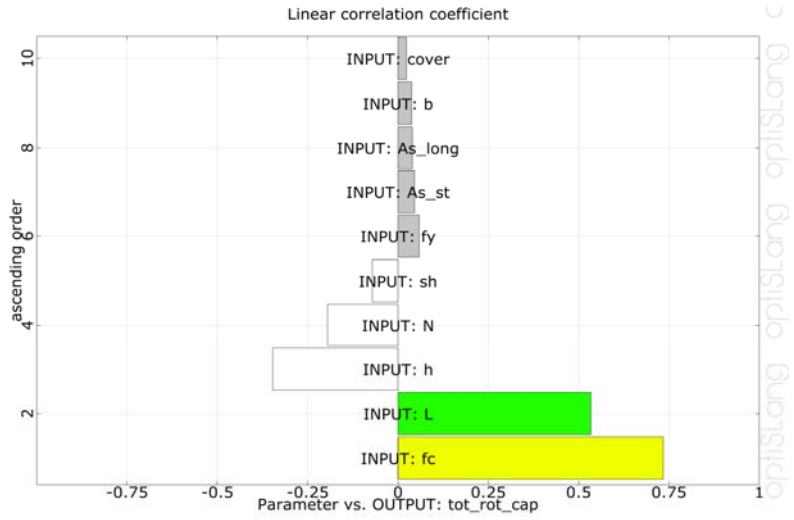

Figure 6.20 Linear correlation coefficient of input parameters vs. rotation capacity

In the considered case study, the first member reaching the rotation failure is the left-hand side column, in the undamaged and corroded condition as well. This happens when the hinge at the basis of the column reaches the ultimate rotation θ_u (Figure 6.9), in correspondence to the reduction of strength in the capacity curves.

A robustness analysis has been performed with *Optislang*, choosing the Latin Hypercube sampling as probability-based method. The input parameters considered in the analysis are listed in Table 6.12. The variation coefficient and the distribution type have been chosen referring to the literature (see Table 5.10). As output parameters, both the rotation capacity given by Eq.(6.3) and the coefficient ρ_{rot} have been considered. According to Eq.(5.8), a number of samples $N = 50 > 2(n_i + n_0) = 2 \cdot 12 = 24$ (10 input parameters and 2 output parameter) is sufficient.

Figure 6.20 illustrates, for the undamaged condition, the linear correlation coefficients (see APPENDIX D) of the input parameters respect to rotation capacity, giving a measure of the strength and the direction of the linear relationship between the variables. It can be observed that concrete strength and length of the RC column have a strong positive correlation with the output parameter, while section height and axial load acting on the member have a significant negative correlation.

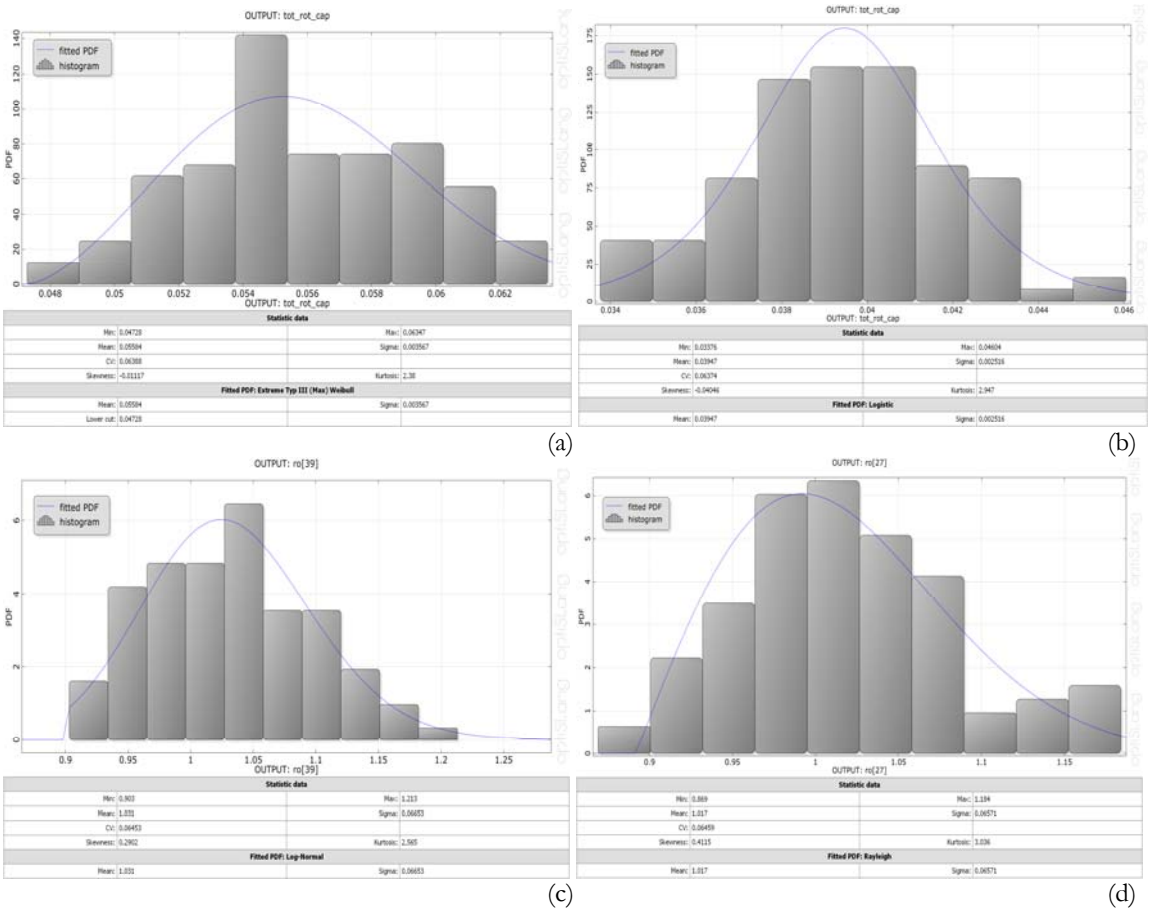

Figure 6.21 Histograms and fitted PDF of (a) rotation capacity and (c) ρ_{rot} (undamaged scenario); (b) rotation capacity and (d) ρ_{rot} (corroded scenario)

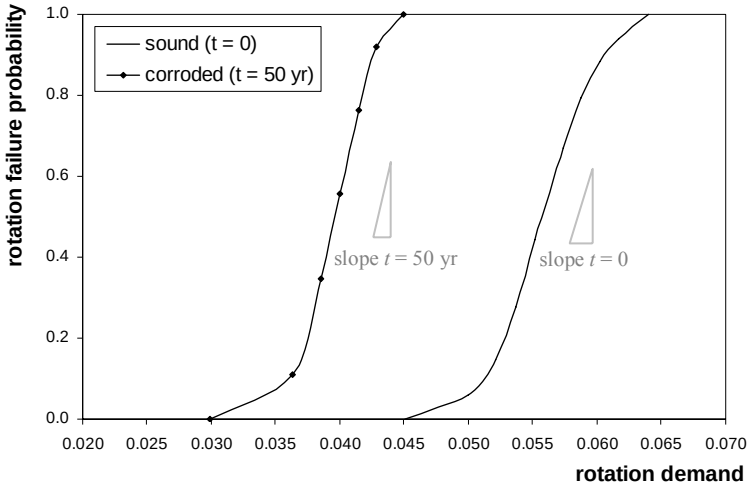

Figure 6.22 Rotation failure probability of the left-side column in undamaged and corroded scenario

Figure 6.21 shows fitted PDF of the rotation capacity and the coefficient ρ_{rot} for both the undamaged and corroded scenario. The fragility estimates are given in Figure 6.22. A considerable reduction of the rotation demand corresponding to the achievement of the limit state ρ_{rot} = 1 can be observed at the end of the service life, respect to the pristine state. Moreover, the comparison of the slope of the two curves evidences that in the 50-year-old structure the rotation failure is reached not only for lower rotations than in the new building, but also slightly faster.

6.3 Second case study

6.3.1 Presentation of the case study

The second case study is a 3D four-storey RC frame building designed according to older building codes, which has been investigated in the framework of the national project ReLUIS (Italian Network of University Labs) launched by the Italian Department of Civil Protection (DPC), with the aim of validating and improving the new Italian Seismic Code, proposing alternate procedures when deemed necessary, and providing practical examples to practicing engineers.

The plan view (Figure 6.23a) evidences a double symmetry, stated that the stair is not considered in the model (Figure 6.23b). The interstorey height is equal to 3.2 m. The dimension of the sections of all the elements, both beams and columns, is 300x600 mm^2. The typical reinforcement details for beams and columns are listed in Table 6.13 and Table 6.14. The materials have the following characteristics: a mean value of cylinder compressive strength f_{cm} = 33.5 MPa for concrete and a mean value of yield strength f_{ym} = 500 MPa for steel. The applied floor loads are 6.0 kN/m^2 as dead load and 2.0 kN/m^2 as live load. The storey masses are 325.3 kN/g for the first storey and 400.5 kN/g for the other three storeys.

The same hypothesis regarding the type and intensity of the corrosive attack as in the first case study are here assumed (Phases from 1 to 4 of the methodology).

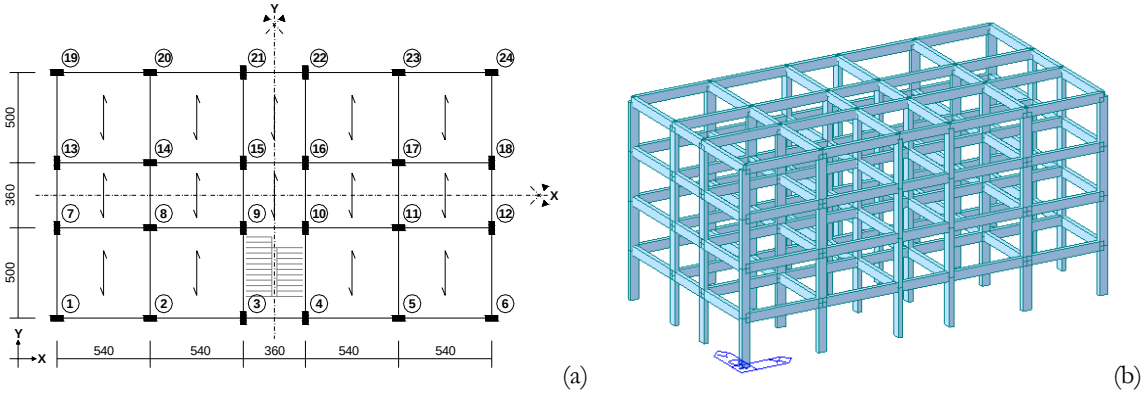

Figure 6.23 (a) Geometry of the building (units in cm); (b) 3D finite element model

Table 6.13 Typical reinforcement details for beams

	Beam 1-2		Beam 2-3		Beam 3-4		Beam 1-7		Beam 7-13	
	1	2	2	3	3	4	1	7	7	13
top	8ϕ16	8ϕ16	8ϕ16	5ϕ16	5ϕ16	5ϕ16	6ϕ16	9ϕ16	9ϕ16	9ϕ16
bottom	6ϕ16	5ϕ16	5ϕ16	3ϕ16	3ϕ16	3ϕ16	5ϕ16	9ϕ16	9ϕ16	9ϕ16
stirrups	ϕ8/10cm									

Table 6.14 Typical reinforcement details for columns

	Column n. 1, 2, 5, 6, 19, 20, 23, 24	Column n. 3, 4, 7-18, 21, 22
along the 60 cm side	8+8ϕ16	9+9ϕ16
along the 30 cm side	6+6ϕ16	8+8ϕ16
stirrups	ϕ8/20cm	

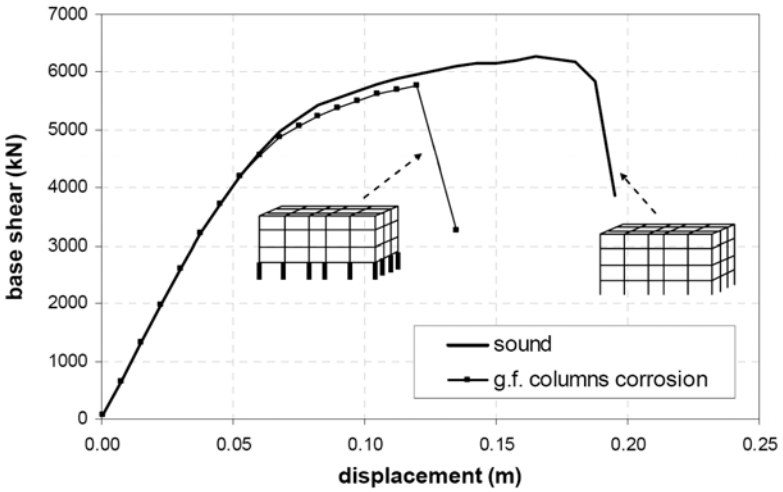

Figure 6.24 Capacity curves in X direction: new and 50-year-old structure

6.3.2 Capacity curves and collapse mechanisms

The seismic response in terms of capacity curves of the undamaged structure and in presence of corrosion of the ground floor columns, for the uniform loading distribution of lateral forces in X direction is shown in Figure 6.24. Similarly to the first case study, it is assumed that all brittle mechanisms are prevented by means of suitable strengthening interventions, and the analyses are carried on until the formation of the plastic hinges mechanisms.

Figure 6.25 illustrates some significant plastic hinge patterns, comparing the structural performance at the beginning and at the end of the service life, in the case of corrosion of the ground floor columns.

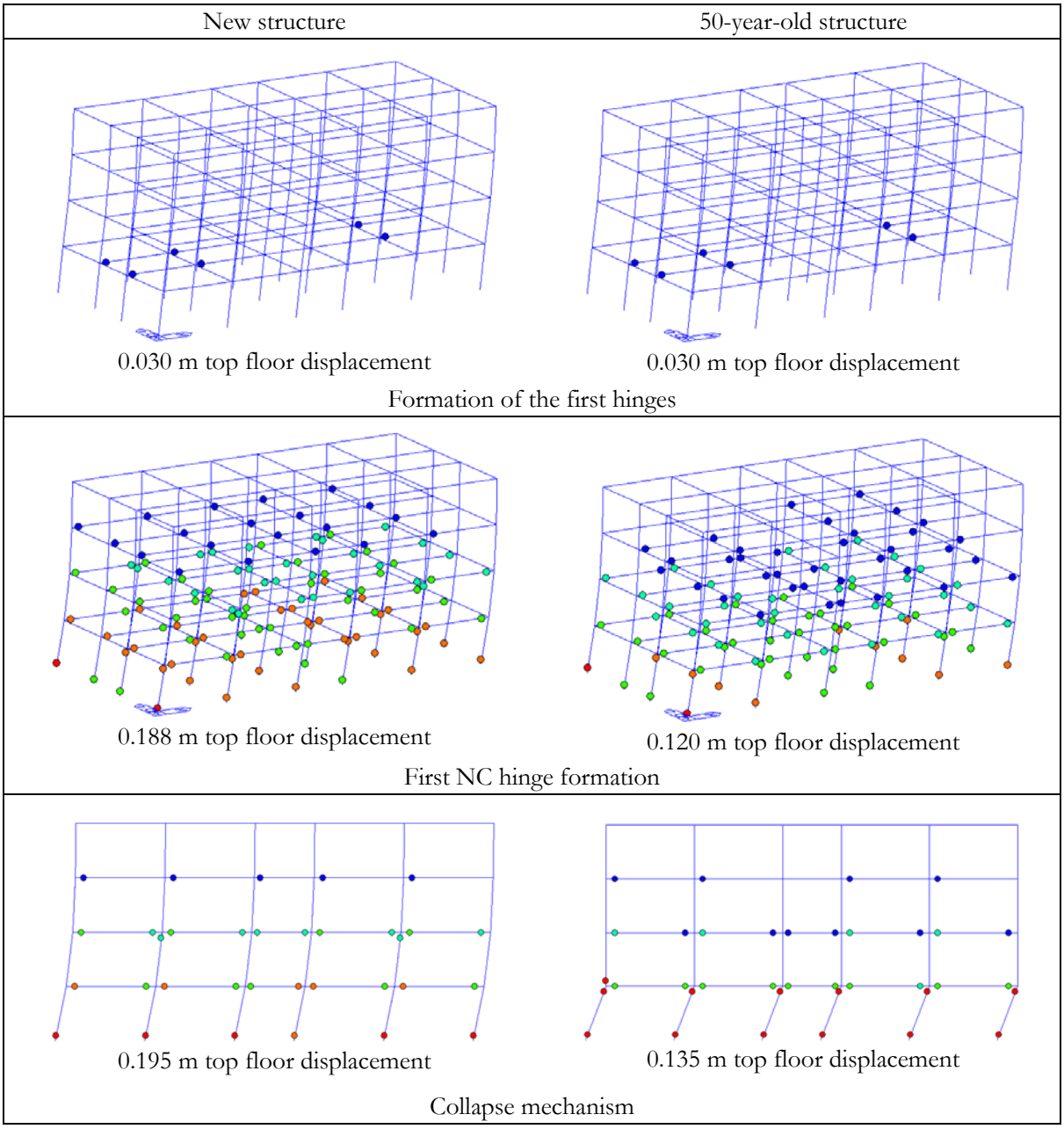

Figure 6.25 Hinge status (X direction): new and 50-year-old structure

Respect to the previous case study, the collapse mechanism in pristine conditions, starting at a top displacement of around 0.18 m (peak of the capacity curve), is closer to a global one, ensuring an overall ductile behaviour. The ductility demand is adequately distributed throughout the structure, with plastic hinges opening in both columns and beams of all storeys. On the contrary, in the structure affected by the carbonation attack, a soft-storey failure mechanism is evidenced in correspondence to a top displacement of 0.12 m. It can be observed that the formation of the plastic hinges and their evolution is anticipated in the corroded scenario, in which the structure evidences a reduction of the load bearing capacity and a significant reduction of ductility with respect to the undamaged state. Nevertheless, the most significant difference between the two conditions is represented by the shift of the collapse mechanism from a global ductile one in the pristine structure to a brittle one (soft-storey mechanism) in the 50-year-old building.
Concerning the influence of concrete cover degradation, estimated as described in Section 6.2.5.3, Figure 6.26 shows the capacity curves in case of ground floor columns corrosion, both with and without the effect of damaged concrete. The trend is similar to that observed in the first case study, evidencing a further reduction of resistance and ductility, [Berto et al., 2008a].

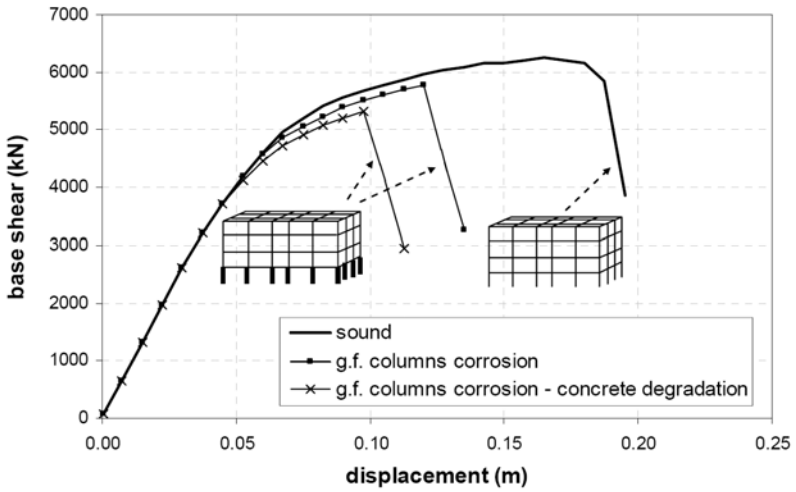

Figure 6.26 Influence of the concrete degradation in the case of ground floor columns corrosion

6.3.3 Global torsional effects

In Section 4.2.5 it has been pointed out that corrosion may induce local torsional effects on the structural element suffering the degradation attack. Such effects may be produced also at a global scale when the corrosive attack in not symmetrically distributed throughout the building and a seismic excitation occurs.
This behaviour has been confirmed by analysing the case of corrosion affecting three columns of a corner of the building, at the ground and first floor. The capacity curves deriving from the pushover analyses along X and Y directions are compared in Figure 6.27a-b.
Given that the major differences between the behaviour of new and corroded structure arise along Y direction, in which a significant reduction of ductility can be identified, further considerations will regard only this second case (Figure 6.27b). In particular, with reference to the corroded scenario, Figure 6.28 shows the plan view of the deformed configuration corresponding to a top displacement of 0.16 m, i.e. at the peak of the capacity curve, before the sudden loss of resistance.

It can be observed that the occurrence of a non symmetrical corrosive attack may result in detrimental torsional effects, unlike the case of symmetric corrosion distribution, as confirmed also by the 3D views of Figure 6.29. Therefore, the performance of the structural system may be strongly affected and the quantitative estimation of the torsional effects is required. Actually, pushover analyses may significantly underestimate the deformations at the stiff/strong side of a torsionally flexible structure, [Eurocode 8, 2005], requiring further verifications and eventually the use of more accurate and challenging tools of investigation, such as time history analyses.

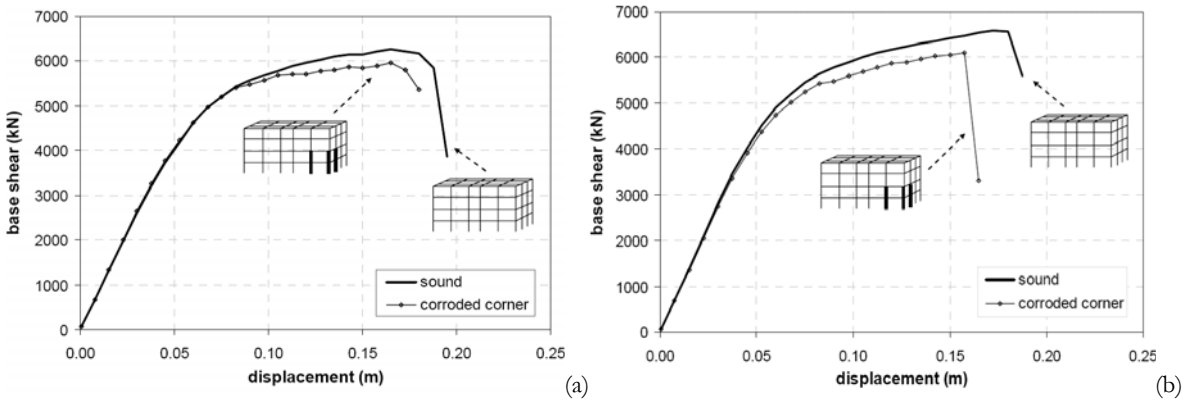

Figure 6.27 Capacity curves of the new and 50-year-old structure with corrosion of one corner of the building: (a) X direction; (b) Y direction

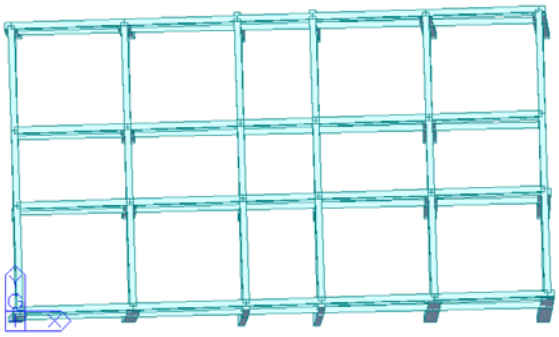

Figure 6.28 Torsional effects in the case of non symmetric corrosive attack (plan view)

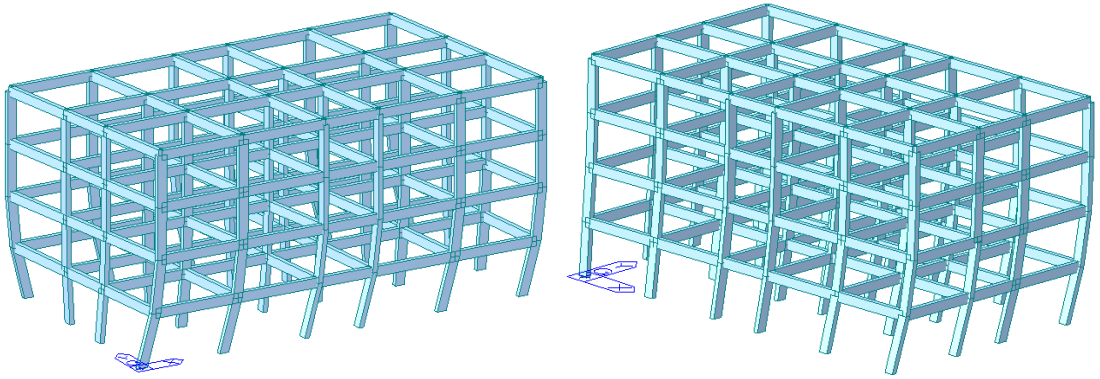

Figure 6.29 Torsional effects in the case of non symmetric corrosive attack (3D views): (a) displacement in X direction; (b) displacement in Y direction

In CHAPTER 6 all the results achieved in the previous chapters have been merged within a unique methodology, which has been applied for the seismic assessment of two case studies affected by a carbonation attack of moderate intensity. The procedure goes along with the general risk management process described in CHAPTER 2 (and more specifically for the corrosion issue in CHAPTER 3) and accordingly has been subdivided in eight phases. As explained in CHAPTER 5, a probabilistic approach has been followed to account for the random nature of the parameters involved in the problem. Thus, it has been possible to calculate the structural risk associated with the simultaneous effects of a seismic and a degradation event endangering a RC structure. In particular, it has been shown how the methodology can be practically applied, combining information gathered from the literature or available on line with the analyses performed with general-purpose software.
Some indications about further potential applications of the proposed methodology may be finally provided. One the one hand, the calculation of structural risk described in Section 6.2.9 at the time t corresponding to the end of the building's service life may be repeated for other time periods, with the aim of deriving the trend of risk over time for the considered building. A qualitative example is shown in Figure 6.30a, at the exposure level of the single building. In the same graph it is possible to appreciate the effect of the potential implementation of risk mitigation interventions, in order to judge on their actual effectiveness. On the other hand, for a given value of time, the procedure may be applied at a territory exposure level to the buildings in a certain area of interest, in order to identify the constructions at higher risk, to which prior intervention strategies should be addressed, as schematically illustrated in Figure 6.30b. This second possibility may be regarded as a more advanced and accurate procedure respect to that mentioned in Section 3.2.4 for the creation of a "seismic-corrosion hazard map", and could be useful to the competent authorities in the safeguarding of the cultural and historical heritage in reinforced concrete.

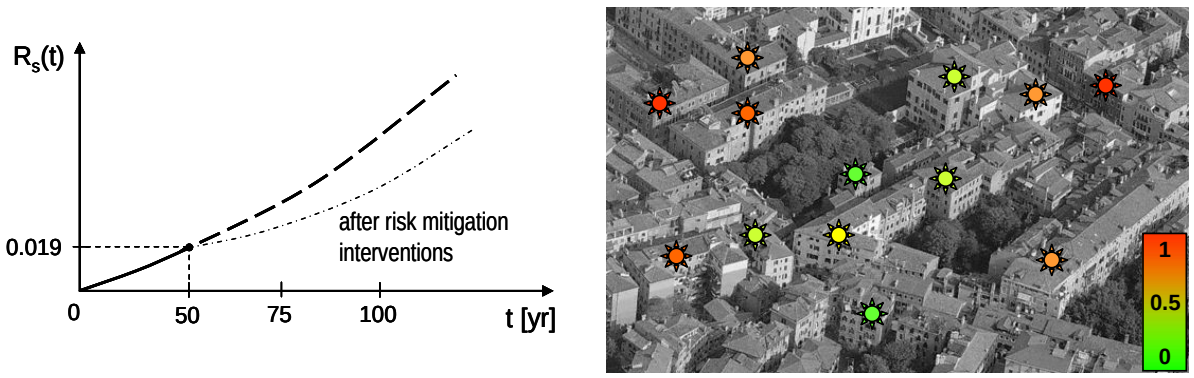

Figure 6.30 Qualitative examples: (a) Structural risk over time (single building exposure); (b) Structural risk at territory exposure

CHAPTER 7 SYNOPSIS

7.1 Summary

The risk management concept has recently become of great interest also in civil engineering, being already common in different disciplines. Its general formulation assures the applicability of this innovative method in a huge variety of activities, providing a greater insight of harmful events and their impacts and thus supporting the decision-making process and the ranking in risk priority classes.

Although most of the codes include rough definitions, a detailed calculation of risk is missing. Moreover, several definitions of the same terms describing the risk management procedure are available, resulting in a general ambiguity and confusion between analysts and decision makers.

In the present dissertation, the approach for managing risk due to natural and civilization hazards on structures and infrastructures developed within the International Graduate College IGC 802 was followed. A practical methodology was proposed for the assessment of the seismic performance of RC structures affected by degradation phenomena up to the end of their design life.

First, the necessary tools of analysis were adjusted, starting from the steps of the risk management chain investigated in the present dissertation. Both seismic shaking and reinforcement corrosion were identified as the hazards endangering the system (risk identification phase). The risk analysis module was accomplished by defining the exposure conditions (identification of the elements at risk) and by analysing the identified hazards with the introduction of a new module for the specific and rigorous management of steel corrosion ("corrosion risk management chain").

Afterwards, two levels of investigation were recognised and followed for evaluating the structural vulnerability: on the one hand, a "micro" level analysis performed by means of an accurate finite element model, in which a damage law varying as a function of the corrosion degree was implemented; on the other hand, a "macro" (sectional) level analysis based on the assignment of specific moment-curvature relationships to the plastic hinges as a function of the degradation level.

The first approach allowed describing the influence of corrosion on the bond-slip behaviour between the reinforcing bars embedded in concrete and the surrounding concrete itself. In particular, a new bond law was developed, introducing a damage parameter called d_{bond} able to describe the degradation of bond strength due to environmental attacks. The model was formulated according to two different approaches, a frictional type and a damage type law, and validated by the numerical simulation of experimental pull-out and beam tests available in the literature.

By means of the macro-level approach it was possible to describe the variation of the seismic performance of a RC building at the end of its service life (50 years) respect to the initial stage, i.e. at the time of construction. It was assumed that, in accordance to the climatic and environmental characteristics of the site, the structure suffered of a corrosion attack of moderate intensity due to spread carbonation of the concrete cover, resulting in several detrimental effects

such as the loss of steel section and steel ultimate elongation, and the overall reduction of load bearing capacity and structural ductility. The effect of concrete cover degradation was also considered and separately treated in the analyses.
In view of the high level of uncertainty affecting in general any structural analysis, and especially the evaluation of the time-variant degradation of RC constructions, the research was carried out in a probabilistic framework. In particular, sensitivity analyses were performed both in the micro and macro models, in order to recognize the most influencing variables affecting the response parameters. At the macro-level, by means of a durability model for the assessment of deteriorating RC structures, it was possible to evaluate the probability of occurrence of corrosion over time. Non linear static analyses were performed to assess the corresponding expected damage in terms of reduction of strength and structural ductility in the capacity curves of the 50-year old building (at the end of the design life) respect to the undamaged condition. In relation to the service life of the structure, the probability of occurrence of a seismic event was chosen first in compliance with the three limit states proposed by the European Standards and secondly derived from the hazard map specific for the site under consideration.
Afterwards, the evaluation of the total probability of occurrence of the two hazards and the calculation of the expected damage allowed calculating the structural risk, in line with the formulation accepted within the Graduate College.
Finally, fragility estimates of corroding RC members with reference to rotation failure were evaluated by means of the demand over capacity ratios suggested by the Italian and European seismic codes for the seismic verification of ductile structural elements.

7.2 Conclusions and outlook for further research

The research carried out in these years pointed out some crucial aspects of the structural performance of RC members and structures under seismic shaking and in presence of environmental degradation phenomena, such as the carbonation-induced corrosion of the reinforcing steel embedded in concrete.
The two levels at which the investigation was performed allowed highlighting both microscopic characteristics of the bond behaviour and the macroscopic features of the behaviour of RC structures endangered by the considered hazards.
In particular, at the micro-level a new bond law was proposed according to two different approaches: a frictional type and a damage type law. Both the models are able to effectively simulate the effects of corrosion on bond behaviour, especially the second one, which can reproduce not only the reduction of bond strength as the corrosion level increases, but also the post peak behaviour.
Further refinement of the formulation of the damage parameter d_{bond}, introduced in the bond law to account for the degradation of bond strength, could be included in the model. In particular, the dependence on the stress state of the surrounding concrete should be comprised. In this way the bond law would be able to consider also the presence of different confinement stresses and their variation with the degradation level. As a matter of fact, some experimental tests performed by [Fang et al., 2004] and [Wang and Liu, 2004] have shown that the pullout resistance is not significantly affected by corrosion in presence of adequate confinement steel, confirming the importance of this aspect.
As regards the macro-level, it is worth noting that a moderate level of corrosion was considered in the two case studies. In presence of a more aggressive attack, a complete cover delamination may occur. In such conditions, further investigation is necessary, aiming at the formulation of

accurate methodologies for the description of the cover expulsion as well as of the rebars slippage, which is a typical effect in presence of high levels of corrosion and thus should be included also in the macro-level procedure. Actually, also the most recent models proposed in the literature, e.g. [Choe et al., 2008] and [Marsh and Frangopol, 2008], still neglect the bond loss effect, considering merely the steel section reduction in the assessment of the reduced load carrying capacity of deteriorating RC structures.
Finally, it should be noted that the calculation of structural risk proposed in this study is still at a preliminary stage, being performed in discrete terms by means of discrete probabilities of damage. A desirable improvement consists in the extension to a continuous procedure.

LIST OF LITERATURE

[1] Al Hashemi M., De Sanctis M., Salvatore W., Valentini R., 2007. Effects of corrosion induced damages on tensile and fatigue properties of concrete reinforcing bars. XII Convegno Anidis – L'Ingegneria Sismica in Italia, Pisa, Italy.

[2] Al-Khaiat H., Haque M.N., 1997. Carbonation of some coastal concrete structures in Kuwait. ACI Materials J., 94(6), 1-6.

[3] Almusallam A.A., Al-Gahtani A.S., Aziz A.R., Dakhil F.H., Rasheeduzzafar, 1996a. Effect of reinforcement corrosion on flexural behaviour of concrete slabs. J. of Materials in Civil Engineering, 8, 123-127.

[4] Almusallam A.A., Al-Gahtani A.S., Aziz A.R., Rasheeduzzafar, 1996b. Effect of reinforcement corrosion on bond strength. Construction and Building Materials, ASCE, 10(2), 123-129.

[5] Almusallam A.A., Al-Gahtani A.S., Maslehuddin M., Khan M.M., Aziz A.R., 1997. Evaluation of repair materials for functional improvement of slabs and beams with corroded reinforcement. Proc. Inst. Civil Engineering Structures and Buildings, 122, 27-34.

[6] Almusallam A.A., 2001. Effect of degree of corrosion on the properties of reinforcing steel bars. Construction and Building Materials, 15, 361-368.

[7] Alonso C., Andrade C., Rodriguez J., Diez J.M., 1998. Factors controlling cracking of concrete affected by reinforcement corrosion. Materials and Structures, 31, 435-441.

[8] Al-Sulaimani G.J., Kaleemullah M., Basunbul I.A., Rasheeduzzafar, 1990. Influence of corrosion and cracking on bond behaviour and strength of reinforced concrete members. ACI Str. J., 87(2).

[9] Amleh L. and Mirza M.S., 1999. Corrosion influence on bond between steel and concrete. ACI Structural J., 96(3), 415–423.

[10] Amleh L. and Mirza M.S., 2008. Framework for durability-based design for concrete-steel bond against corrosion. J. of Materials in Civil Engineering, 20(10), 678–681.

[11] Amey S.L., Johnson D.A., Miltenberger M.A., Farzam H., 1998. Predicting the service life of concrete marine structures: an environmental methodology. ACI Materials J., 95(2), 205-214.

[12] Andrade C., Alonso C., Garcia D., Rodriguez J., 1991. Remaining lifetime of reinforced concrete structures: effect of corrosion on the mechanical properties of the steel. Int. Conf. on Life Prediction of Corrodible Structures, NACE, Cambrige, UK, 12/1-12/11.

[13] Andrade C. and Alonso C., 2001. On-site measurements of corrosion rate of reinforcements. Construction and Building Materials, 15, 141-145.

[14] Ang A.H-S. and Tang W.H., 2007. Probability Concepts in Engineering – Emphasis on Applications in Civil & Environmental Engineering. Second Edition, Wiley, England.

[15] Apostolopoulos C.A., Papadakis V.G., 2008. Consequences of steel corrosion on the ductility properties of reinforcement bar. Construction and Building Materials, 22(12), 2316-2324.

[16] Arafa M., Mehlhorn G., 1998. A modified discrete model in the non linear finite element analysis of prestressed and reinforced concrete structures. 2nd Int. PhD Symposium in Civil Engineering, Budapest.

[17] Auyeung Y., Balaguru P., Chung L., 2000. Bond behaviour of corroded reinforcing bars. ACI Material J., 97(2).

[18] Baker J.W., Schubert M., Faber M.H., 2008. On the assessment of robustness. Structural Safety, 30(3), 253-267.

[19] Berra M., Castellani A., Coronelli D., Zanni S., Zhang G., 2003. Steel-concrete bond deterioration due to corrosion: finite element analysis for different corrosion levels. Magazine of Concrete Research, 55(3), 237-247.

[20] Bertagnoli G., Mancini G., Tondolo F., 2006. Bond deterioration due to corrosion and actual bearing capacity. FIB 2nd International Congress. Naples, Italy.

[21] Berto L., Simioni P., Saetta A., 2007a. Numerical modelling of bond behaviour in RC structures affected by reinforcement corrosion. Engineering Structures, 30, 1375–1385.

[22] Berto L., Vitaliani R., Saetta A., Simioni P., 2007b. Meccanismi di collasso di strutture di c.a. degradate soggette all'azione sismica. ANIDIS 2007, XII Convegno Nazionale L'Ingegneria Sismica in Italia, Pisa, Italy. In italian.

[23] Berto L., Saetta A., Simioni P., Vitaliani R., 2008a. Non linear static analyses of RC frame structures: influence of corrosion on seismic response. 8th WCCM8 - 5th ECCOMAS, June 30th - July 5th, Venice, Italy.

[24] Berto L., Vitaliani R., Saetta A., Simioni P., 2008b. Seismic assessment of existing RC structures affected by degradation phenomena. Structural Safety, 31, 284-297.

[25] Berto L., Simioni P., Saetta A., Scotta R., Vitaliani R., 2009. Seismic assessment of existing RC structures: non linear analyses of different building typologies. COMPDYN 2009, ECCOMAS Thematic Conference on Computational Methods in Structural Dynamics and Earthquake Engineering, 22–24 June 2009, Rhodes, Greece.

[26] Bhargava K., Ghosh A.K., Mori Y., Ramanujama S., 2007. Corrosion-induced bond strength degradation in reinforced concrete - Analytical and empirical models. Nuclear Engineering and Design, 237, 1140–1157.

[27] Bhargava K., Ghosh A. K., Mori Y., Ramanujam S., 2008. Suggested Empirical Models for Corrosion-Induced Bond Degradation in Reinforced Concrete. J. of Structural Engineering, 134(2), 221-230.

[28] Biddah A., Strengthening of opening moments joints in reinforced concrete frames using cfrp. The Seventh Annual U.A.E. University Research Conference, College of Engineering, 170-175.

[29] Bigaj A.J., 1999. Structural dependence of rotation capacity of plastic hinges in rc beams and slabs. PhD dissertation, Faculty of Civil Engineering, Delft University of Technology, Netherlands.

[30] Biondini F., 2000. Probabilistic Limit Analysis of Framed Structures. 8th ASCE Specialty Conference on Probabilistic Mechanics and Structural Reliability.

[31] Biondini F., Bontempi F., Frangopol D.M., Malerba P.G., 2004. Cellular Automata Approach to Durability Analysis of Concrete Structures in Aggressive Environments. J. of Structural Engineering, 130(11), 1724-1736.

[32] Biondini F., Bontempi F., Frangopol D.M., 2006a. Probabilistic Service Life Assessment and Maintenance Planning of Concrete Structures. J. of Structural Engineering, 132(5), 810-825.

[33] Biondini F., Frangopol D.M., Malerba P.G., 2006b. Time-Variant Structural Performance of the Certosa Cable-Stayed Bridge. Structural Engineering International, 3, 235-244.

[34] Biondini F., Bontempi F., Frangopol D.M., Malerba P.G., 2006c. Lifetime Nonlinear Analysis of Concrete Structures under Uncertainty. 3rd Int. Conf. on Bridge Maintenance, Safety, and Management IABMAS'06, Porto.

[35] Biondini F., Frangopol D.M., 2008a. Long-Term Performance of Structural Systems. Editorial - Structure and Infrastructure Engineering, 4(2), 75.

[36] Biondini F., Frangopol D.M., 2008b. Probabilistic Limit Analysis and Lifetime Prediction of Concrete Structures. Structure and Infrastructure Engineering, 4(5), 399-412.

[37] Bono M., 1996. Analisi numerica dell'influenza dei parametri caratterizzanti le equazioni della carbonatazione. Diploma thesis, Department of Construction and Transportation, University of Padova.

[38] BRITE/EURAM, 1995. The residual service life of reinforced concrete structures. Final Technical Report, Report No. BRUE-CT92-0591.

[39] Budelmann H., Hariri K., Schmidt-Döhl F., Rostásy F.S., 2000. Monitoring of reinforced and prestressed concrete structures. 6th International Workshop on Material Properties and Design, Bauhaus University, Weimar, Germany.

[40] Budelmann H., Hariri K., Schmidt-Döhl F., Bruder S., Rigo E., 2005. Adaptive prognosis of chemical concrete degradation and probabilistic system analysis as instrument of structural monitoring. 4th International Workshop on Advances in life-cycle cost analysis and design of civil infrastructure systems, May 8-11, Cocoa Beach, Florida, USA.

[41] Budelmann H., Hariri K., Starck T, 2008. Integration of degradation prognosis of concrete structures into life cycle management. 1st International Symposium on Life Cycle Management, June 11-14, Varenna, Italy, 2008.

[42] Budelmann H., Holst A., 2008. New sensors for rebar corrosion monitoring. 4th European Workshop on Structural health monitoring, July 4-8, Cracow, Poland.

[43] Budelmann H., 2008. Degradation prediction tool for concrete structures under chemical attack. ICCRRR 2008, 2nd International Conference on Concrete Repair, Rehabilitation and Retrofitting, November 24-26, Cape Town, South Africa.

[44] Cabrera J. G., 1996. Deterioration of concrete due to reinforcement steel corrosion. Cement and Concrete Composites, 18(1), 47-59.

[45] Çağatay I.H., 2005. Experimental evaluation of buildings damaged in recent earthquakes in Turkey. Engineering Failure Analysis, 12, 440–452.

[46] Cairns J., Millard, S., 1999. Reinforcement corrosion and its effect on residual strength of concrete structures. Proc. 8th Int. Conf. on Structure Faults and Repair, Section 13.2. Ed. Engineering Technics Press, Edinburgh, UK.

[47] Capozucca R., 1995. Damage to reinforced concrete due to reinforcement corrosion. Construction and Building Materials, 9(5), 295-303.

[48] Capozucca R., Cerri M.N., 2003. Influence of reinforcement corrosion - in the compressive zone - on the behaviour of RC beams. Engineering Structures, 25, 1575–1583.

[49] Castel A., François R., Arliguie G., 2000a. Mechanical behaviour of corroded reinforced concrete beams-Part 1: Experimental study of corroded beams. Materials and Structures, 33, 539-544.

[50] Castel A., François R., Arliguie G., 2000b. Mechanical behaviour of corroded reinforced concrete beams-Part 2: Bond and notch effects. Materials and Structures, 33, 545-551.

[51] Castro P., Sanjuán M.A., Genescá J., 2000. Carbonation of concretes in the Mexican Gulf. Building and Environment, 35, 145-149.

[52] CEB–FIP, 1992. Model Code 90. Telford, London.

[53] CEB-FIP, 1996. Reinforced concrete Frames under Earthquake Loading – State of the Art Report, Fib Bulletin n.231. Telford, London.

[54] CEB-FIP, 1998. Ductility of Reinforced Concrete Structures, Bulletin n.242.

[55] CEB-FIP, 2000. Bond of reinforcement in concrete – State of the Art Report, Fib Bulletin n.10. Switzerland.

[56] CEB-FIP, 2006. Model Code for Service Life Design, Fib Bulletin 34. Switzerland.

[57] Choe D., Gardoni P., Rosowsky D., 2007. Closed-form fragility estimates, parameter sensitivity and Bayesian updating for RC columns. J. of Engineering Mechanics, 133(7), 833–843.

[58] Choe D., Gardoni P., Rosowsky D., Haukaas T., 2008. Probabilistic capacity models and seismic fragility estimates for RC columns subject to corrosion. Reliability Engineering and System Safety, 93, 383–393.

[59] Codacci Pisanelli E., Petrangeli M.P., 1987. Indagine sistematica sulla profondità di carbonatazione nei calcestruzzi dei ponti della A1 nel tratto Fabro-Orte. Convegno A.I.T.E.C. La durabilità delle opere in calcestruzzo, Padova, Italy, 55-64.

[60] Collepardi M. and Biagini S., 1989. Effect of water/cement ratio, pozzolanic addition and curing time of chloride penetration into concrete. ERMCO 89.

[61] Coronelli D., 2002. Corrosion cracking and bond strength modelling for corroded bars in reinforced concrete. ACI Structural J., 99(3), 267-276.

[62] Coronelli D., Gambarova P., 2004. Structural assessment of corroded reinforced concrete beams: modeling guidelines. J. of Structural Engineering, 130(8), 1214-1224.

[63] Coronelli D., Mulas M.G., 2006. Modeling of shear behavior in reinforced concrete beams. ACI Structural J., 103(3), 372-382.

[64] Cosenza E., Manfredi G., Polese M., Verderame G.M., 2005. A multilevel approach to the capacity assessment of existing rc buildings. J. of Earthquake Engineering, 9(1), 1-22.

[65] Creazza G., Saetta A., Scotta R. Vitaliani R., Oñate E., 1995. Mathematical simulation of structural damage in historical buildings. STREMA 95, Structural Studies of Historical Buildings, Crete, Greece, published in Architectural Studies, Materials & Analysis, eds. Brebbia and Leftheris, Comp. Mech. Publ., 1, 111-118.

[66] Decreto Ministeriale 09/01/96. Norme tecniche per il calcolo, l'esecuzione ed il collaudo delle strutture in cemento armato, normale e precompresso e per le strutture metalliche.

[67] Dekoster M., Buyle-Bodin F., Maurel O., Delmas Y., 2003. Modelling of the flexural behaviour of RC beams subjected to localised and uniform corrosion. Eng. Str., 25, 1333-1341.

[68] Dhir R.K., Jones M.R., McCarthy M.J., 1994. PFA concrete: chloride-induced reinforcement corrosion. Magazine of Concrete Research, 46(169), 269–77.

[69] Diamantidis D., Bazzurro P., 2007. Safety acceptance criteria for existing structures. Workshop on Risk Acceptance and Risk Communication, Stanford, USA.

[70] Du Y.G., Clark L.A., Chan H. C., 2005. Residual capacity of corroded reinforcing bars. Magazine of Concrete Research, 57(3), 135–147.

[71] Du Y.G., Clark L.A., Chan H. C., 2005. Effect of corrosion on ductility of reinforcing bars. Magazine of Concrete Research, 57(7), 407–419.

[72] Duprat F., Sellier A., 2006. Probabilistic approach to corrosion risk due to carbonation via an adaptive response surface method. Probabilistic Engineering Mechanics, 21, 207–216.

[73] DuraCrete, 2000. A guideline for durability-based design of concrete structures. Paper by Edvardsen C. and Mohr L (UE-founded project).

[74] Eligenhausen R., Popov E. P., Bertero V.V., 1983. Local bond stress-slip relationships of deformed bars under generalized excitations. Earthquake Engineering Research Council (EERC) Rep. No. 83/23, University of California, Berkeley, California.

[75] El Maaddawy T., Soudki K., Topper T., 2005. Analytical model to predict non linear flexural behaviour of corroded reinforced concrete beams. ACI Structural J., 102(5), 550-559.

[76] El Maaddawy T., Soudki K., Topper T., 2005. Long-term performance of corrosion-damaged reinforced concrete beams. ACI Structural J., 102(5), 649-656.

[77] El Mezaini N., Citipitioglu E, 1991. Finite element analysis of prestressed and reinforced concrete structures. J. of Structural Engineering, 117(10), 2851-2864.

[78] Eligehausen R., Popov E.P., Bertero V.V., 1983. Local bond stress – slip relationships of deformed bars under generalized excitations, Experimental results and analytical model. Report No.UCB/EERC-83/23, College of Engineering, University of California, Berkeley, California.

[79] EM-DAT Emergency Events Database, 2008. Annual disaster review – The numbers and trends 2008. http://www.emdat.be/Database/CountryProfile/countryprofiles.php.

[80] EMS-98 European Macroseismic Scale, 1998. Editor G. Grünthal, European Seismological Commission, Luxembourg. http://www.gfz-potsdam.de.

[81] Enright M.P., Frangopol D.M., 1998a. Failure time prediction of deteriorating fail-safe structures. J. of Structural Engineering, 124(12), 1448-1457.

[82] Enright M.P., Frangopol D.M., 1998b. Probabilistic analysis of resistance degradation of reinforced concrete bridge beams under corrosion. Engineering Structures, 20(11), 960-971.

[83] Eurocode 0, 2002. Basis of structural design.

[84] Eurocode 2, 2004. Design of concrete structures – Part 1-1: General – Common rules for building and civil engineering structures.

[85] Eurocode 8, 2005. Design of structures for earthquake resistance – Part 1: General rules seismic actions and rules for buildings.

[86] Eurocode 8, 2006. Design of structures for earthquake resistance – Part 3: Strengthening and repair of buildings.

[87] Faber M.H., Sorensen J.D., 2002. Indicators for inspection and maintenance planning of concrete structures. Structural Safety, 24, 377–396.

[88] Faber M.H., Straub D., Maes M.A., 2006. A Computational Framework for Risk Assessment of RC Structures Using Indicators. Computer-Aided Civil and Infrastructure Engineering, 21, 216–230.

[89] Faber M.H., 2007. Risk and Safety in Civil, Surveying and Environmental Engineering. Swiss Federal Institute of Technology, ETHZ, Switzerland.

[90] Fajfar P., 2002. Structural analysis in earthquake engineering - A breakthrought of simplified non-linear methods. 12th European Conference on Earthquake Engineering, London, UK.

[91] Fang C., Lundgren K., Chen L., Zhu C., 2004. Corrosion influence on bond in reinforced concrete. Cement and Concrete Research, 34, 2159-2167.

[92] Farja, R., Oliver, J., 1998. A strain-based viscous-plastic-damage model for massive concrete structures. Int. J. Solids and Structures, 35, 1533-1558.

[93] Faust B., 2007. Evaluation of the residual load-bearing capacity of civil structures using fuzzy-logic & decision analysis. PhD thesis, Universität der Bundeswehr, Neubiberg.

[94] Fernández Ruiz M., Muttoni A., Gambarova P.G., 2007. Analytical modeling of the pre- and postyield behavior of bond in reinforced concrete. J. of Structural Engineering, 133(10), 1364-1372.

[95] Fischer T., Alvarez M., De la Llera J.C., Riddell R., 2002. An integrated model for earthquake risk assessment of buildings. Engineering Structures, 24, 979-998.

[96] Gardoni P., Der Kiureghian A., Mosalam K.M., 2002. Probabilistic capacity models and fragility estimates for reinforced concrete columns based on experimental observations. J. of Engineering Mechanics, 128(10), 1024-1038.

[97] Gerard B., Pijaudier-Cabot G., Laborderie C., 1998. Coupled diffusion-damage modeling and the implications on failure due to strain localization. Int. J. of Solids and Structures, 35(31/32), 4107-4120.

[98] Girard C., Bastien J., 2002. Finite-element bond-slip model for concrete columns under cyclic loads. J. of Structural Engineering, 128(12), 1502-1510.

[99] Gonzalez J.A., Feliu S., Rodriguez P., Lopez W., Alonso C., Andrade C., 1996. Some Questions on the Corrosion of Steel in Concrete - Part II: Corrosion Mechanism and Monitoring, Service Life Prediction and Protection Methods. Materials and Structures, 29, 97-104.

[100] MG Grantham, MG Associates, Barnet, Hert, Broomfield J., 1997. The use of linear polarisation corrosion rate measurements in aiding rehabilitation options for the deck slabs of a reinforced concrete underground car park. Construction and Building Materials, 11(4), 215-224.

[101] Harajli M.H., 2007. Numerical bond analysis using experimentally derived local bond laws: a powerful method for evaluating bond strength of steel bars. J. of Structural Engineering, 133(5), 695-705.

[102] Haskett M., Oehlers D.J., Mohamed Ali M.S., 2008. Local and global bond characteristics of steel reinforcing bars. Engineering Structures, 30, 376–383.

[103] Haussmann D.A., 1967. Steel corrosion in concrete. Materials protection, 19-23.

[104] Hueste M.B.D., Bai J-W., 2007. Seismic retrofit of a reinforced concrete flat-slab structure: Part II - Seismic fragility analysis. Engineering Structures, 29, 1178–1188.

[105] Hwan Oh B., Kim S.H., 2007. Realistic models for local bond stress-slip of reinforced concrete under repeated loading. J. of Structural Engineering, 133(2), 216-224.

[106] Jendele L., Cervenka J., 2006. Finite element modelling of reinforcement with bond. Computers & Structures, 84, 1780-1791.

[107] Joint Committee on Structural Safety (JCSS), 2001a. Probabilistic Model Code, www.jcss.ethz.ch.

[108] Joint Committee on Structural Safety (JCSS), 2001b. Probabilistic Assessment of Existing Structures. Edited by D. Diamantidis, RILEM Publications.

[109] Kala Z. and Kala J., 2005. Sensitivity analysis of the effect of initial imperfections on the steel plate girder fatigue limit state. Structural Mechanics, 38(1), 3 – 12.

[110] Kankam C.K., 1997. Relationship of bond stress, steel stress and slip in reinforced concrete. J. of Structural Engineering, 123(1), 79-85.

[111] Keuser M., Mehlhorn G., 1987. Finite element models for bond problems. J. of Structural engineering, 113(10), 2160-2173.

[112] Kobayashi, K., 2006. The seismic behaviour of RC members suffering from chloride-induced corrosion. FIB 2nd Int. Congress. Naples, Italy.

[113] Kottegoda N.T. and Rosso R., 2008. Applied statistics for civil and environmental engineers. 2nd Ed., Blackwell Publishing.

[114] Kunreuther H., 2004. Risk Analysis. Center for Risk Management and Decision Processes, The Wharton School, University of Pennsylvania, Philadelphia.

[115] Kwak H.-G., Kim S.-P., 2001. Bond–slip behaviour under monotonic uniaxial loads. Engineering Structures, 23, 298-309.

[116] Kwak H.-G., Kim S.-P., 2002a. Monotonic moment-curvature relation of an RC beam. Magazine of Concrete Research, 54(6), 423-434.

[117] Kwak H.-G., Kim S.-P., 2002b. Non linear analysis of RC beams based on moment-curvature relation. Computers and Structures, 80, 615–628.

[118] Kwak H.-G., Kim J.-K., 2006. Implementation of bond–slip effect in analyses of RC frames under cyclic loads using layered section method. Engineering Structures, 28, 1715-1727.

[119] Lee H.S., Noguchi T., Tomosawa F., 2002. Evaluation of bond properties between concrete and reinforcement as a function of the degree of reinforcement corrosion. Cement and Concrete Research, 32, 1313-1318.

[120] Li C.Q., 2004. Reliability based service life prediction of corrosion affected concrete structures. J. of Structural Engineering, 130(10), 1570-1577.

[121] Li C.Q., 2007. A Risk-Cost optimized maintenance strategy for corrosion-affected concrete structures. Computer-Aided Civil and Infrastructure Engineering, 22, 335–346.

[122] Li C.Q., Yang Y., Melchers R.E., 2008. Prediction of reinforcement corrosion in concrete and its effects on concrete cracking and strength reduction. ACI Materials J., 105(1), 3-10.

[123] Liel A.B., Haselton C.B., Deierlein G.G., Baker J.W., 2009. Incorporating modeling uncertainties in the assessment of seismic collapse risk of buildings. Structural Safety, 31(2), 197-211.

[124] Lowes L.N., Moehle J.P., Govindjee S., 2004. Concrete-steel bond model for use in finite element modeling of reinforced concrete structures. ACI Structural J., 101(4).

[125] Lowes L.N., Mitra N., Altoontash A., 2004. A beam-column joint model for simulating the earthquake response of reinforced concrete frames. PEER Report 2003/10, Pacific Earthquake Engineering Research Center, College of Engineering, University of California, Berkeley.

[126] Lowes L.N., 1999. Finite element modeling of reinforced concrete beam-column bridge connections. PhD Dissertation, University of California, Berkeley.

[127] Lundgren K., Gylltoft K., 2000. A model for the bond between concrete and reinforcement. Magazine of Concrete Research, 52(1), 53-63.

[128] Luccioni B.M., Lopez D.E., Danesi R.F., 2005. Bond-slip in reinforced concrete elements. J. of Structural engineering, 131(11), 1690-1698.

[129] Maddaloni G., Magliulo G., Martinelli E., Monti G., Petti L., Saetta A., Spacone E., 2008. Non-linear methods for seismic assessment of existing structures: a comparative study on Italian RC buildings. 14th World Conference on Earthquake Engineering, October 12-17, Beijing, China.

[130] Malvar L.J., 1992. Bond of reinforcement under controlled confinement. ACI Materials J., 89(6).

[131] Mander J.B., Priestley M.J.N., Park R., 1988. Theoretical stress–strain model for confined concrete. J. of Structural Engineering, 114(8), 1804–1826.

[132] Mangat P., Elgarf M., 1999. Flexural strength of concrete beams with corroding reinforcement. ACI Structural J., 97(1), 149-159.

[133] Mangat P., Elgarf M., 1999. Bond characteristics of corroding reinforcement in concrete beams. Materials and Structures, 32, 89-97.

[134] Marsh P.S., Frangopol D.M., 2008. Reinforced concrete bridge deck reliability model incorporating temporal and spatial variations of probabilistic corrosion rate sensor data. Reliability Engineering and System Safety, 93, 394–409.

[135] Maslehuddin M., Allam I.A., Al-Sulaimani G.J., Al-Mana A.I., Abduljauwad S.N., 1990. Effect of rusting of reinforcing steel on its mechanical properties and bond with concrete. ACI Materials J., 87(5).

[136] Maurel O., Dekoster M., Buyle-Bodin F., 2005. Relation between total degradation of steel concrete bond and degree of corrosion of RC beams experimental and computational studies. Computers and Concrete, 2(8), 1-18.

[137] Melchers R.E., 1999. Structural Reliability Analysis and Prediction. Second Edition, Wiley, England.

[138] Melchers R.E., 2001. Assessment of existing structures - Approaches and research needs. J. of Structural Engineering, 127(4), 406-411.

[139] Melchers R.E., 2003. Probabilistic model for marine corrosion of steel for structural reliability assessment. J. of Structural Engineering, 129(11), 1484–1493.

[140] Melchers R.E., 2005. Representation of uncertainty in maximum depth of marine corrosion pits. Structural Safety, 27, 322–334.

[141] Melchers R.E., Li C.Q., 2006. Phenomenological modeling of reinforcement corrosion in marine environments. ACI Materials, 103(1), 25-32.

[142] MIDAS Gen. User's Guide, Getting Started & Tutorials.

[143] Middleton C.R., Hogg V., 1998. Review of deterioration models used to predict corrosion in reinforced concrete structures. CUED/D – STRUCT/TR.173, Cambridge University.

[144] Mitre, Risk Management Toolkit, http://www.mitre.org/work/sepo/toolkits/risk/index.html.

[145] Mohamed Ali M.S., Oehlersa D.J., Griffitha M.C., Seracino R., 2008. Interfacial stress transfer of near surface-mounted FRP-to-concrete joints. Engineering Structures, 30(7), 1861-1868.

[146] Mohammed T.U., Otsuki N., Hisada M., Shibata T., 2001. Effect of crack width and bar types on corrosion of steel in concrete. J. of Materials in Civil Engineering, 13(3), 194-201.

[147] Nam C.H., Salmon C.G., 1974. Finite element analysis of concrete beams. J. of the Structural Division, ASCE Proceedings, 100(ST12), 2419-2432.

[148] Neale K.W., Demers M., LabossiereP., 2005. FRP protection and rehabilitation of corrosion-damaged reinforced concrete columns. International J. of Materials and Product Technology, 23(3/4), 348–371.

[149] Ngo D., Scordelis A.C., 1967. Finite element analysis of reinforced concrete beams. ACI J., Title No. 64-14, 152-163.

[150] Oñate E., Hanganu A., Barbat A., Oller S., Vitaliani R., Saetta A., 1995. Structural analysis and durability assessment of historical construction using a finite element damage model. Publication CIMNE, n. 73, Barcelona, Spain.

[151] Ordinanza PCM 3431, 2005. Norme tecniche per il progetto, la valutazione e l'adeguamento sismico degli edifici.

[152] Ordinanza PCM 3519, 2006. Pericolosità sismica di riferimento per il territorio nazionale. All. 1b, 28 aprile 2006.

[153] OptiSlang Manual, 2008. The optimizing Structural Language for Sensitivity Analysis, Multidisciplinary Optimization, Robustness Evaluation and Reliability Analysis, Dynardo, http://www.dynardo.de.

[154] Palsson R., Mirza M.S., 2002. 'Mechanical response of corroded steel reinforcement of abandoned concrete bridge. ACI Structural J., 99(2), 157–162.

[155] Panagiotakos T.B., Fardis M.N., 2001a. A displacement-based seismic design procedure for RC buildings and comparison with EC8. Earthquake Engineering and Structural Dynamics, 30, 1439–1462.

[156] Panagiotakos T.B., Fardis M.N., 2001b. Deformations of Reinforced Concrete Members at Yielding and Ultimate. ACI Structural J., 98(2), 135-148.

[157] Pardi L., Rinaldi, Z. Valente, C., 2001. Strength and ductility changes in bridge decks due to corrosion effects. Proc. Structural Faults & Repair, London.

[158] Park R., Paulay T., 1975. Reinforced concrete structures. John Wiley & Sons.

[159] Pedeferri P., Bertolini L., 2000. La durabilità del calcestruzzo armato. McGraw-Hill.

[160] Pedeferri P., 2005. La corrosione nel calcestruzzo: fenomenologia, prevenzione, diagnosi, rimedi. A.I.C.A.P., Progetto Ulisse.

[161] Perno S., Rinaldi Z., Valente C., Pardi L., 1999. Effetti della corrosione sulla sicurezza di elementi di cemento armato. Giornate AICAP '99, Torino.

[162] Pijaudier-Cabot G., Gerard B., Molez L., 1998. Damage mechanics of concrete structures subjected to mechanical and environmental actions. Euro-C, Computational modeling of concrete structures, De Borst, Bicanic, Mang&Meschke (eds), Balkema Rotterdam.

[163] Pinto P.E., 2005. The Eurocode 8–Part 3: The new European Code for the seismic assessment of existing structures. Asian J. of Civil Engineering (Building and Housing), 6(5), 447-456.

[164] Pliefke T., Sperbeck S.T., Urban M., Peil U., Budelmann H., 2007. A Standardized Methodology for Managing Disaster Risk – An Attempt to Remove Ambiguity. 5th International Probabilistic Workshop, Ghent, Belgium.

[165] Proske D., 2002. Beitrag zur Risikobeurteilung von alten Brücken unter Schiffsanprall. Dissertation, TU Dresden.

[166] Rai D.C., 2005. Review of Documents on Seismic Strengthening of Existing Buildings. IITK-GSDMA Project on Building Codes. Final Report A - Earthquake Codes. www.iitk.ac.in/nicee/IITK-GSDMA/EQ07.pdf.

[167] Repapis C., Vintzileou E., Zeris C., 2006. Evaluation of the seismic performance of existing rc buildings: I. Suggested methodology. J. of Earthquake Engineering, 10(2), 265–287.

[168] Repapis C., Vintzileou E., Zeris C., 2006. Evaluation of the seismic performance of existing rc buildings: II. A case study for regular and irregular buildings. J. of Earthquake Engineering, 10(3), 429-452.

[169] Rilem Report 14, 1996. Durability design of concrete structures. Ed. by Sarja - Vesikari, E & FN Spon, London.

[170] Rigo E., Schmidt-Dfhl F., Kraug M., Budelmann H., 2005. Transreac: a model for the calculation of combined chemical reactions and transport processes and its extension to a probabilistic model. Cement and Concrete Research, 35, 1734–1740.

[171] Riva P. Analisi Statica Non Lineare (Pushover). Presentation, Università degli Studi di Bergamo.

[172] Rodriguez J., Ortega L.M., Casal J., 1994. Corrosion of reinforcing bars and service life of reinforced concrete structures: corrosion and bond deterioration. International Conference 'Concrete across Borders', Odense, Denmark.

[173] Rodriguez J., Ortega L.M., Casal J., Diez J.M., 1996. Corrosion of reinforcement and service life of concrete structures. 7th Int. Conf. On durability of building materials and components, Stockholm.

[174] Rodriguez J., Ortega L.M., Casal J., 1997. Load carrying capacity of concrete structures with corroded reinforcement. Construction and Building Materials, 11(4), 239-248.

[175] Rodriguez J., Andrade C., 2001. CONTECVET - A validated users manual for assessing the residual service life of concrete structures, DG Enterprise, CEC, GEOCISA, Madrid.

[176] Saetta A., 1992. Durabilità delle strutture di calcestruzzo armato e analisi dei fenomeni di diffusione in materiali multifase. PhD Thesis, Universities of Bologna, Padova, Ancona.

[177] Saetta A.V., Schrefler B.A., Vitaliani R.V., 1993a. The carbonation of concrete and the mechanism of moisture, heat and carbon dioxide flow through porous materials. Cement and Concrete Research, 23(4), 761-772.

[178] Saetta A., Scotta R., Vitaliani R., 1993b. Analysis of chloride diffusion into partially saturated concrete. ACI Materials J., 90(5), 441-451.

[179] Saetta A.V., Schrefler B.A., Vitaliani R.V., 1995. 2D Model for carbonation and moisture/heat flow in porous materials. Cement and Concrete Research, 25(8), 1703-1712.

[180] Saetta A., 1996. Analisi di sensibilità dei modelli di previsione del degrado delle strutture di calcestruzzo armato. Giornale del Genio Civile, 10-11-12, 224-240.

[181] Saetta A., Scotta R., Vitaliani R., 1998a. Mechanical Behaviour of Concrete under Physical-Chemical Attacks. J. of Engineering Mechanics, ASCE, 124(10), 1100-1109.

[182] Saetta A., Scotta R., Vitaliani R., 1998b. Reliability of Reinforced Concrete Structures under Chemical-Physical Attack. Invited paper, AJSE 23:2C, Theme Issue Concrete Repair, Rehabilitation & Protection.

[183] Saetta A., Scotta R., Vitaliani R., 1999. Coupled Environmental-Mechanical Damage Model of RC Structures. J. of Engineering Mechanics, ASCE, 125(8), 930-940.

[184] Saetta A., Vitaliani R., 2004. Experimental investigation and numerical modeling of carbonation process in reinforced concrete structures - Part I theoretical formulation. Cement and Concrete Research, (34)4, 571-579.

[185] Saetta A., 2005. Deterioration of Reinforced Concrete Structures due to Chemical-Physical Phenomena: Model-Based Simulation. J. of Materials for Civil Engineering, ASCE, (17)3, 313-319.

[186] Saetta A., Simioni P., Berto L., Vitaliani R., 2008. Seismic response of corroded r.c. structures. International fib Symposium 2008, May 19th - 22nd, Amsterdam, the Netherlands.

[187] Saetta A., Simioni P., 2009. A probabilistic approach for the calculation of seismic risk in RC structures affected by degradation phenomena. ANIDIS 2009, XIII Convegno Nazionale L'Ingegneria Sismica in Italia, Bologna.

[188] Santarella L., 1973. Il cemento armato – La tecnica e la statica. Vol. I, Hoepli Ed., Milano.

[189] Sarja A., Vesikari E., 1992. Durability design of concrete structures. RILEM Report 14, E&FN SPON.

[190] Sarveswaran V., Roberts M.V., 1999. Reliability analysis of deteriorating structures – the experience and needs of practising engineers. Structural Safety, 21, 357-372.

[191] Simioni P. and Saetta A., 2008. Effects of Environmental Degradation on the Response of Reinforced Concrete Structures. Junior Scientist Conference 2008, November 16th - 18th, Vienna.

[192] Sobhani J., Ramezanianpour A.A., 2007. Chloride-induced corrosion of rc structures. Asian J. of Civil Engineering (Building and Housing), 8(5), 531-547.

[193] Spacone E., Limkatanyu S., 2000. Responses of Reinforced Concrete Members Including Bond-Slip Effects. ACI Structural J., 97(6), 831-839.

[194] Stanish K., Hooton R. D., Pantazopoulou S. J., 1999. Corrosion Effects on Bond Strength in Reinforced Concrete. ACI Structural J., 96(6), 915-922.

[195] Stewart M.G., Rosowsky D.V., 1998a. Structural safety and serviceability of concrete bridges subject to corrosion. J. of Infrastructure Systems, 4(4), 146-155.

[196] Stewart M.G., Rosowsky D.V., 1998b. Time-dependent reliability of deteriorating reinforced concrete bridge decks. Structural Safety, 20, 91-109.

[197] Stewart M.G., 2004. Spatial variability of pitting corrosion and its influence on structural fragility and reliability of RC beams in flexure. Structural Safety, 26, 453–470.

[198] Stewart M.G., Al-Harthy A., 2008. Pitting corrosion and structural reliability of corroding RC structures: Experimental data and probabilistic analysis. Reliability Engineering and System Safety, 93, 373–382.

[199] Sudret B., Defaux G., Pendola M., 2008. Probabilistic models for the extent of damage in degrading reinforced concrete structures. Reliability Engineering and System Safety, 93, 410–422.

[200] Tastani S.P. and Pantazopoulou S.J., 2007. Behavior of Corroded Bar Anchorages. ACI Structural J., 104(6), 756-766.

[201] Tesfamariam S. and Martín-Pérez B., 2008. Bayesian belief network to assess carbonation-induced corrosion in reinforced concrete. J. of Materials in Civil Engineering, 20(11), 707-717.

[202] Thomas M.D.A., 2004. The effect of curing and concrete quality on the durability of concrete with high-volumes of supplementary cementing materials. EcoSmart Curing Project, Technical Report, University of New Brunswick, Canada.

[203] Thywissen K., 2006. Components of Risks – A Comparative Glossary, SOURCE, United Nations University, Institute for Environment and Human Security), Bonn, Germany.

[204] EN 206-1, 2006. Concrete - Part 1: Specification, performance, production and conformity.

[205] Urban M., 2006. Earthquake Risk Assessment of Historical Structures. PhD thesis.

[206] USC_RC, Moment Curvature, Force Deflection and Interaction Analysis of Reinforced Concrete Members, http://www.usc.edu/dept/civil_eng/structural_lab/asad.

[207] Val D.V., Melchers R., 1997. Reliability of Deteriorating RC slab bridges. J. of Structural Engineering, ASCE, (128)2, 1638-1644.

[208] Val D.V., 2002. Safety Factors for Assessment of Existing Structures. J. of Structural Engineering, ASCE, (123)12, 258-265.

[209] Val D.V., 2007. Deterioration of Strength of RC Beams due to Corrosion and its Influence on Beam Reliability. J. of Structural Engineering, ASCE, (133)9, 1297-1306.

[210] Val D.V., Trapper P.A., 2008. Probabilistic evaluation of initiation time of chloride-induced corrosion. Reliability Engineering and System Safety, 93, 364–372.

[211] Vrouwenvelder T., 2008. Treatment of risk and reliability in the Eurocodes. Structures & Buildings, 161, 209–214.

[212] Vu K.A.T., Stewart M.G., 2000. Structural reliability of concrete bridges including improved chloride-induced corrosion models. Structural Safety, 22, 313–333.

[213] Vu K.A.T., Stewart M.G., 2005. Predicting the likelihood and extent of reinforced concrete corrosion-induced cracking. J. of Structural Engineering, 131(11), 1681–1689.

[214] Wang X., Liu X., 2004. Modeling bond strength of corroded reinforcement without stirrups. Cement and Concrete Research, 34, 1331-1339.

[215] Wang X., Liu X., 2006. Bond strength modeling for corroded reinforcements. Construction and Building Materials, 20, 177-186.

[216] Wolmuth B. and Surtees J., 2003. Crowd-related failure of bridges. Proceedings of ICE, Civil Engineering, 156, 116–123.

[217] Yang I.H, 2007. Uncertainty and sensitivity analysis of time-dependent effects in concrete structures. Engineering Structures, 29, 1366–1374.

APPENDIX A EMS-98 Tables

Vulnerability Table

	Type of Structure	Vulnerability Class A B C D E F
MASONRY	rubble stone, fieldstone	
	adobe (earth brick)	
	simple stone	
	massive stone	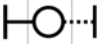
	unreinforced, with manufactured stone units	
	unreinforced, with RC floors	
	reinforced or confined	
REINFORCED CONCRETE (RC)	frame without earthquake-resistant design (ERD)	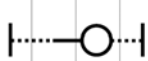
	frame with moderate level of ERD	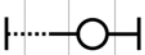
	frame with high level of ERD	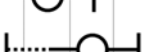
	walls without ERD	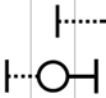
	walls with moderate level of ERD	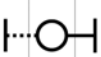
	walls with high level of ERD	
STEEL	steel structures	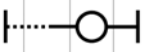
WOOD	timber structures	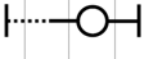

Damage classification for RC buildings

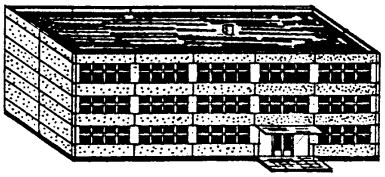

Grade 1: Negligible to slight damage
(no structural damage, slight non-structural damage)
Fine cracks in plaster over frame members or in walls at the base. Fine cracks in partitions and infills.

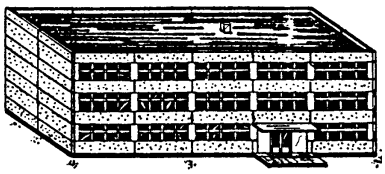

Grade 2: Moderate damage
(slight structural damage, moderate non-structural damage)
Cracks in columns and beams of frames and in structural walls. Cracks in partition and infill walls; fall of brittle cladding and plaster. Falling mortar from the joints of wall panels.

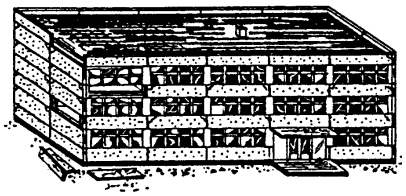

Grade 3: Substantial to heavy damage
(moderate structural damage, heavy non-structural damage)
Cracks in columns and beam column joints of frames at the base and at joints of coupled walls; spalling of concrete cover, buckling of reinforced rods. Large cracks in partition and infill walls, failure of individual infill panels.

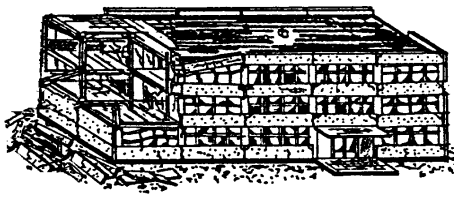

Grade 4: Very heavy damage
(heavy structural damage, very heavy non-structural damage)
Large cracks in structural elements with compression failure of concrete and fracture of rebars; bond failure of beam reinforced bars; tilting of columns. Collapse of a few columns or of a single upper floor.

Grade 5: Destruction
(very heavy structural damage)
Collapse of ground floor or parts (e.g. wings) of buildings.

Intensity Short Form

Intensity	Definition	Description of typical observed effects
I	Not felt	Not felt, even under the most favourable circumstances. No damage to buildings.
II	Scarcely felt	Felt only by very few individual people at rest in houses. No effect. No damage to buildings.
III	Weak	Felt indoors by a few people. People at rest feel a swaying or light trembling.
IV	Largely observed	Felt indoors by many people, outdoors by very few. A few people are awakened. Windows, doors and dishes rattle.
V	Strong	Felt indoors by most, outdoors by few. Many sleeping people awake. A few are frightened. Buildings tremble throughout. Hanging objects swing considerably. Small objects are shifted. Doors and windows swing open or shut.
VI	Slightly damaging	Many people are frightened and run outdoors. Some objects fall. Many houses suffer slight non-structural damage like hair-line cracks and fall of small pieces of plaster.
VII	Damaging	Most people are frightened and run outdoors. Furniture is shifted and objects fall from shelves in large numbers. Many well built ordinary buildings suffer moderate damage: small cracks in walls, fall of plaster, parts of chimneys fall down; older buildings may show large cracks in walls and failure of fill-in walls.
VIII	Heavily damaging	Many people find it difficult to stand. Many houses have large cracks in walls. A few well built ordinary buildings show serious failure of walls, while weak older structures may collapse.
IX	Destructive	General panic. Many weak constructions collapse. Even well built ordinary buildings show very heavy damage: serious failure of walls and partial structural failure.
X	Very destructive	Many ordinary well built buildings collapse.
XI	Devastating	Most ordinary well built buildings collapse, even some with good earthquake resistant design are destroyed.
XII	Completely devastating	Almost all buildings are destroyed.

APPENDIX B Exposure Classes [EN 206-1, 2006]

Class designation	Description of the environment	Informative examples where exposure classes may occur
1 No risk of corrosion or attack		
X0	For concrete without reinforcement or embedded metal: all exposures except where there is freeze/thaw, abrasion or chemical attack For concrete with reinforcement or embedded metal: very dry	Concrete inside buildings with very low air humidity
2 Corrosion induced by carbonation		
XC1	Dry or permanently wet	Concrete inside buildings with low air humidity Concrete permanently submerged in water
XC2	Wet, rarely dry	Concrete surfaces subject to long-term water contact Many foundations
XC3	Moderate humidity	Concrete inside buildings with moderate or high air humidity External concrete sheltered from rain
XC4	Cyclic wet and dry	Concrete surfaces subject to water contact, not within exposure class XC2
3 Corrosion induced by chlorides		
XD1	Moderate humidity	Concrete surfaces exposed to airborne chlorides
XD2	Wet, rarely dry	Swimming pools Concrete components exposed to industrial waters containing chlorides
XD3	Cyclic wet and dry	Parts of bridges exposed to spray containing chlorides Pavements Car park slabs
4 Corrosion induced by chlorides from sea water		
XS1	Exposed to airborne salt but not in direct contact with sea water	Structures near to or on the coast
XS2	Permanently submerged	Parts of marine structures
XS3	Tidal, splash and spray zones	Parts of marine structures
5. Freeze/Thaw Attack		
XF1	Moderate water saturation, without de-icing agent	Vertical concrete surfaces exposed to rain and freezing
XF2	Moderate water saturation, with de-icing agent	Vertical concrete surfaces of road structures exposed to freezing and airborne de-icing agents
XF3	High water saturation, without de-icing agents	Horizontal concrete surfaces exposed to rain and freezing
XF4	High water saturation with de-icing agents or sea water	Road and bridge decks exposed to de-icing agents Concrete surfaces exposed to direct spray containing de-icing agents and freezing Splash zone of marine structures exposed to freezing
6. Chemical attack		
XA1	Slightly aggressive chemical environment according to EN 206-1, Table 2	Natural soils and ground water
XA2	Moderately aggressive chemical environment according to EN 206-1, Table 2	Natural soils and ground water
XA3	Highly aggressive chemical environment according to EN 206-1, Table 2	Natural soils and ground water

APPENDIX C Literature review of bond-slip models

In the description of bond-slip behaviour, attention must be primarily paid to the modelling of the reinforcement. To this aim, three alternative approaches may be adopted: discrete, embedded and smeared model.

The *discrete modelling* of steel reinforcement was the first method used in the finite element analysis of RC structures, originally suggested by [Ngo and Scordelis, 1967]. This approach makes use of a "bond-link element", so that the reinforcing bars are modelled as separate elements, commonly truss or cable elements, connected to concrete through fictitious springs representing bond, as schematically shown in Figure D.1. The location of the steel elements is determined by the layout of the reinforcement. Consequently, the boundaries of the concrete elements have to follow the reinforcing bar. Analyses on beams with web reinforcement and on axially loaded reinforced concrete prisms were performed by the authors.

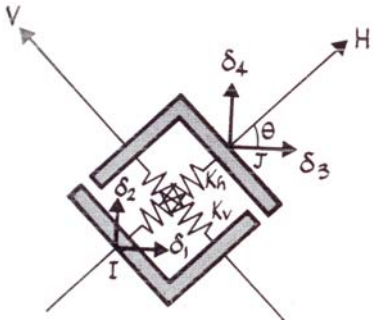

Figure D.1 Linkage element [Ngo and Scordelis, 1967]

[Nam and Salmon, 1974] modelled the concrete members using quadrilateral isoparametric elements with variable stiffness, emphasizing the incorrectness of the constant stiffness approach in the evaluation of the non linear behaviour of reinforced concrete due to cracking. Linear elements were then introduced to represent reinforcing bars under uniaxial stress states and interconnected to the concrete planar elements at nodes only.

The discrete representation of reinforcement is the most direct way of accounting for bond-slip effects and dowel action. It presents the advantage of being simple in concept and able to represent different material properties more precisely than other approaches. Different bond conditions at different nodes can be directly and easily modelled. For example, in the contact element developed by [Keuser et al., 1985], the vertical and horizontal relative displacement between concrete and steel in the local coordinates of steel tendon can be considered. This element is an isoparametric element and has, at the unloaded stage, no physical dimension in the transverse direction. It includes two to four double-nodes and uses linear, quadratic or cubic interpolation functions. In the contact interfacing the two elements connected by a contact element have independent element nodes.

However, in spite of its several advantages, the use of the bond-link element in the finite element analysis imposes also some restrictions. First, the finite element mesh patterns must be arranged in such a way that a reinforcing bar is located along the edge of a concrete element. Secondly, a double node is required to represent the relative slip between the reinforcing steel and concrete. In a complex structure, mainly in three-dimensional models, these requirements lead to a considerable increase in the number of degrees of freedom, not only because of doubling the number of nodes along the reinforcing steel bars, but also because the mesh has to be refined, so that the bars pass along the edges of concrete elements, [Kwak, 2001].

In order to allow independent choice of concrete mesh, [El-Mezaini et al., 1991] used a serendipity isoparametric element with movable side nodes, avoiding a node mapping distortion (Figure D.2). According to this approach, a line as two node truss elements is used to represent the steel, although a quadratic or cubic isoparametric element for concrete is adopted. In this way, reinforcement of arbitrary type and location can be represented and different bond conditions at different nodes can be modelled at the same time. Nevertheless the compatibility between concrete and steel elements cannot be guaranteed. Moreover, cracking, dowel action and other aspects related to the non linear behaviour of RC are not considered.

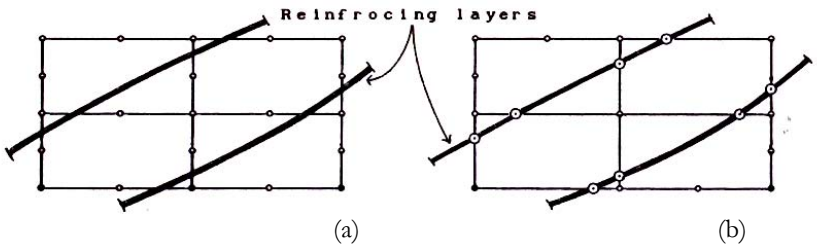

Figure D.2 Reinforcing layers: (a) regular FE mesh; (b) shifted edge nodes [El-Mezaini et al., 1991]

[Arafa et al., 1998] developed a special discrete and smeared representation of main and secondary reinforcement, using a discrete model independent of the concrete finite element mesh. Lagrange and serendipity quadratic and cubic isoparametric elements with movable side and interior nodes were adopted and a contact element with different bond conditions was used to model the bond behaviour between concrete and steel.

With the aim of overcoming the problem of mesh dependency in the discrete models, a number of *embedded formulations* were developed. In general, embedded models are based on the idea of evaluating the stiffness of the reinforcing layer individually in the element in conjunction with isotropic shape functions. The strain compatibility is controlled by an assumed bond-slip relation. Such formulations allow an independent choice of concrete mesh. The same type of elements with the same number of nodes and DOFs are used for both concrete and steel. The disadvantage of this model is that additional DOFs increase the computational effort and a special reinforcement element is required.

Looking at the problem in a more global sense, *smeared approaches* started to be investigated at the end of the 1980s. In this case, the reinforcement is assumed to be uniformly distributed by smearing the reinforcing bar to thin layers of mechanically equivalent thickness within a particular concrete element. However, the smeared model makes sense only for uniformly distributed reinforcing bars. In studies where the detailed local behaviour is of interest, continuous bond elements such as bond-zone elements are most appropriate.

Unlike the classical bond-link element (i.e. spring connecting the rebar to the concrete element) or bond-zone element (i.e. interface described by proper material laws), the model proposed by [Kwak et al., 2001] accounts for the bond-slip effect without employing double nodes. After the determination of the boundary condition at both ends of a reinforcing steel, the deformation of the steel at each node is found through the back-substitution technique from the first to the final steel element using a governing equation based on the equilibrium at each node of steel and the compatibility condition between steel and concrete (Figure D.3). The bond stress-slip model assumed by the authors is the simple trilinear curve shown in Figure D.4, while the model parameters are derived from the material properties of the specimens tested in the experimental studies. According to the authors' opinion, the approximation of the actual behaviour is good in cases which do not exhibit significant slip and associated bond damage. Under monotonic loading, this holds true in all RC members which do not experience anchorage failure. From the experimental tests performed on two simply supported RC beams (with the concentrated loads applied at one-third of the points of the structure in one sample, and at the midspan in the other sample), the authors concluded that the contribution of bond-slip to the load-displacement response of the

specimen increases with the load. Near the ultimate strength of the beam, the magnitude of the bond-slip contribution to the load-displacement response is remarkably increased.
Recently a nonlinear dynamic FE analysis of RC frames subject to both dynamic and cyclic loadings was also performed by [Kwak et al., 2006] using the layered section method. The bond-slip effect was quantified with the force equilibrium and compatibility condition at the post-cracking stage and its contribution was indirectly implemented into the steel stress–strain relation.
Figure D.5 shows the stress-strain relation assumed for concrete: the monotonic envelope curve for the concrete confined by rectangular hoops introduced by Kent and Park, in the compression region; and a linearly elastic behaviour in the tensile region. In particular, the ultimate failure caused by cracking is assumed when the principal tensile strain exceeds the value:

$$\varepsilon_u = \frac{2G_f \ln(3/b)}{f_t(3-b)} \tag{D.1}$$

where b is the element length used in the FE analysis and G_f, considered a material property, is the fracture energy dissipated in the formation of a crack of unit length per unit thickness. The value of ε_u is derived from the fracture mechanics concept by equating the crack energy release with the fracture toughness of concrete G_f. Experimental studies indicate that for normal strength concrete the value of G_f/f_t is in the range 0.005–0.01 mm. If G_f and f_t are known from measurements, then ε_u can be determined.

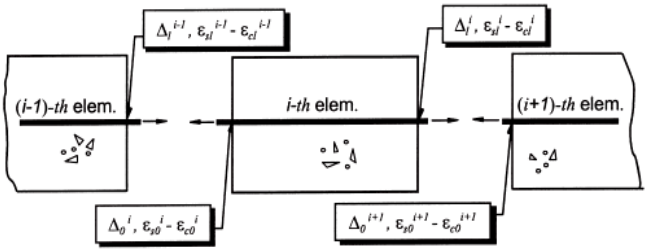

Figure D.3 Subdivided RC axial member [Kwak et al., 2001]

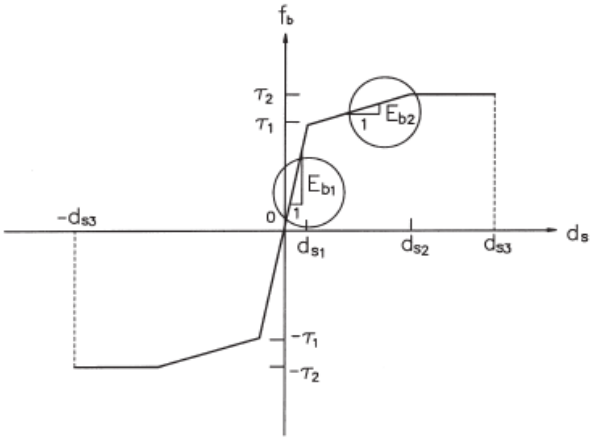

Figure D.4 Bond stress-slip relationship [Kwak et al., 2001]

Concerning the steel stress-strain relation, although it is usually modelled as a linear elastic, linear strain hardening material with a yield stress f_y, in presence of the surrounding concrete the average behaviour changes, as shown in Figure D.6. In particular, a reduction of the yield stress f_y occurs.
Yielding of a RC member takes place when the steel stress at a cracked section reaches the yield strength of the bare bar. However, the average steel stress at a cracked element still maintains an elastic stress that

is less than the yield strength, because the concrete matrix between cracks can still partially resist to tensile forces, owing to the bond with the reinforcement. Consequently, an overestimation of the structural response at the post-yielding range may result.
[Kwak et al., 2006] use the following linear average stress-strain relation, experimentally derived:

$$\begin{aligned} \sigma_s &= E_s \varepsilon_s && \text{for } \varepsilon_s \le \varepsilon_n \\ \sigma_s &= f_n + (0.02 + 0.25B) E_s (\varepsilon_s - \varepsilon_n) && \text{for } \varepsilon_s \le \varepsilon_n \end{aligned} \tag{D.2}$$

where σ_s and ε_s represent the average stress and strain of an embedded bar; f_y and ε_y are the yield stress and the corresponding yield strain of a bare steel bar. The steel stress σ_s is a linear function of the parameter $B = (f'_t/f_y)1.5/\varrho$, limited by the boundary strain $\varepsilon_n = \varepsilon_y(0.93 - 2B)$ for steel yielding, where ϱ is the percentage of the steel ratio and must be greater than 0.5%.
[Luccioni et al., 2005] present a model for fiber reinforced composites, applied to RC elements. When slipping occurs, the stress transfer between the matrix and the steel fibers is affected and a stress reduction results in the fibers. This reduction can be assimilated to a strain reduction related to the interface deformation:

$$\varepsilon^f = \varepsilon^m - \varepsilon_s = \varepsilon - \varepsilon_s \tag{D.3}$$

where subindexes *f* and *m* refer to steel reinforcement fibers and concrete matrix respectively; while ε_s is the strain tensor representing a measure of the interface deformation or slipping.
Assuming an elasto-plastic behaviour for steel, the following stress in the reinforcing bars is obtained from the strain of the composite:

$$\sigma_f = C_f : (\varepsilon - \varepsilon_p - \varepsilon_s) \tag{D.4}$$

and a set of flow rules are defined for the rebars inelastic strains and for the slipping. An elasto-plastic model is assumed for the interface, calibrating most of the constant parameters on the basis of experimental results.
The described model can take into account some effects that cannot be simulated by uniaxial models, like the influence of confinement pressure (independently from other damage or plastic processes that can take place in the concrete matrix), the surface pattern of the reinforcing bars, the dilation of the adhesion zone and the associated cracking. Moreover it has the advantage of not requiring the explicit discretization of the reinforcement and the interface.

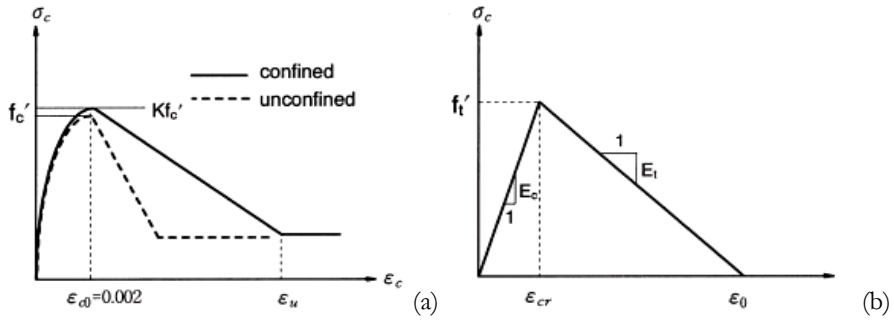

Figure D.5 Concrete stress-strain relation in: (a) compression; (b) tension [Kwak et al., 2006]

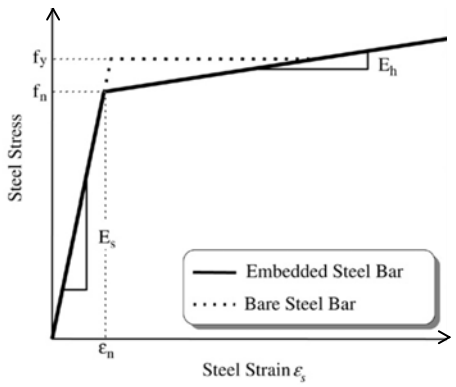

Figure D.6 Stress-strain relation for embedded and bare steel bar [Kwak et al., 2006]

The model proposed by [Jendele and Cervenka, 2006] includes three types of finite elements (Figure D.7): concrete continuum element (2D or 3D), bar truss element (constant strain), bond element (constant slip). A new DOF s is introduced, representing the bond slip in terms of difference between concrete and bar displacements on the element boundary. The bar nodal displacement is calculated as:

$$\tilde{u} = u + s \tag{D.5}$$

and the stress in the bar i with the nodes i, $i+1$ is:

$$\sigma_i = \frac{E}{L_i}\left(\tilde{u}_{i+1} - \tilde{u}_i\right) = \frac{\left(u_{i+1} + s_{i+1} - u_i - s_i\right)}{L_i} E \tag{D.6}$$

The equilibrium condition is given by:

$$\frac{\partial \sigma}{\partial x} \le \tau_{b,\max} \frac{p}{A} \tag{D.7}$$

where p and A stand for the perimeter and cross-sectional area of bar, respectively. If $\tau_b < \tau_{b,max}$, the bond force is transferred to continuum model and the bond behaviour is exhibited by cracks and damage in concrete. If $\tau_b = \tau_{b,max}$, slip on the bar surface can occur. The constitutive function:

$$\tau_{b,\max} = C_b(s) \tag{D.8}$$

defines the maximum bond stress that can be transmitted across the interface for a given slip and it is analogous to a friction law.
A proper choice of the bond stress-slip function $C_b(s)$ is crucial for realistic results.
Due to the assumption of constant strain distribution in the bar, there are two values of stress at each node of a reinforcing bar, which have to be smoothed prior to computation of cohesion stress:

$$\tilde{\sigma}_i = \frac{\left(\sigma_i L_i + \sigma_{i-1} L_{i-1}\right)}{L_i + L_{i-1}} \qquad \tau_i = \frac{\left(\tilde{\sigma}_{i+1} - \tilde{\sigma}_i\right) A}{p L_i} \tag{D.9}$$

The validation of the model by laboratory pull-out tests and by shear failure of beams provided acceptable results at low computational cost. It was found that, if the mesh size in vicinity of the reinforcing bar approached the bar diameter, the bond behaviour was captured by cracking of surrounding concrete. In this case, the bond model might not be necessary since bond modelling becomes important when the bond failure is likely to occur on the bar surface and it is less affected by the cracking of the surrounding concrete, such as in smooth pre-stressing bars.

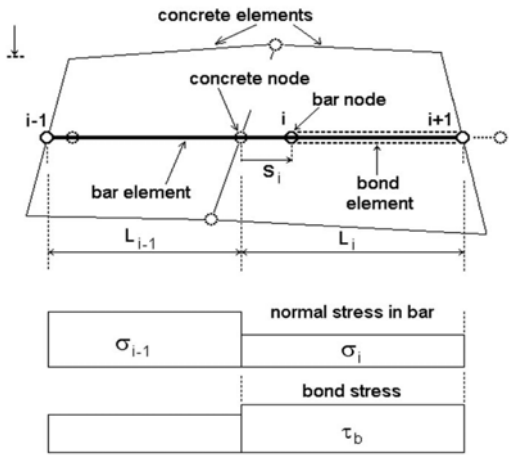

Figure D.7 Model for embedded rebar with bond proposed by [Jendele and Cervenka, 2006]

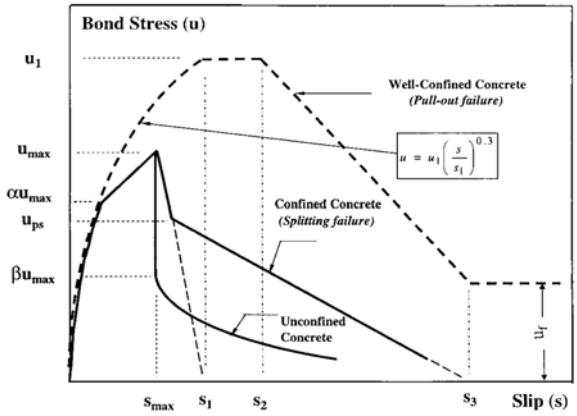

Figure D.8 Local bond stress-slip relationship proposed by [Harajli, 2007]

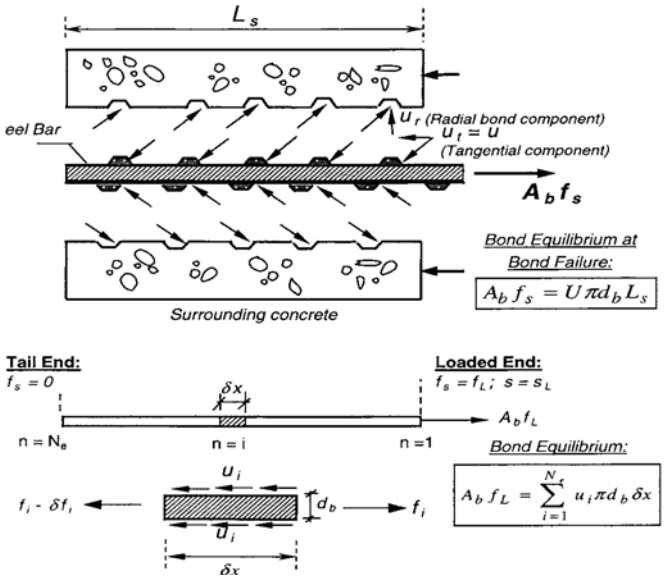

Figure D.9 Bond failure mechanism and steel bar discretization for bond analysis [Harajli, 2007]

[Harajli, 2007] performed a series of experimental and analytical studies for evaluating the bond characteristics of bars in tension under different design and strength variables. The average bond strength at bond failure was evaluated by integrating experimentally based local bond laws into a numerical analysis technique. Using multiregression analysis of the experimental data, the characteristic parameters of the local bond stress–slip relationship were derived for different concrete compressive strengths and confinement parameters (Figure D.8).

It should be noted that, according to other authors, since the bond stress is defined from the change in steel stress over a certain measurement length and the relative slip is determined externally or internally, it is practically impossible to establish a local bond stress-slip relation, since the measured bond stress-slip relation generally represents the average relation over the measurement length.

In the analytical model (Figure D.9), the bar is subdivided into a discrete number N_e of small elements of length δx, and the bond stress, steel stress and slip variations along the bar development/splice length are calculated numerically using bond force equilibrium and slip compatibility equations. At any discrete location along the bar length corresponding to element i, the slip s_i and stress f_i of the bar are expressed as:

$$s_i = s_L - \sum_{n=1}^{i} \varepsilon_n \delta x \qquad f_i = f_L - \frac{\sum_{n=1}^{i} u_n \pi d_b \delta x}{A_b} \tag{D.10}$$

in which s_L and f_L are the slip and steel stress at the loaded end, $\varepsilon = G(f)$ and $u = F(s)$ are the stress-strain relationship and the local bond stress-slip law of the reinforcing bar.

In the analysis, the slip at the loaded end is increased in small increments. At any slip level, the steel stress at the loaded end, and the corresponding bond stress, steel stress and slip distribution along the bar length are obtained through an iterative procedure to satisfy the steel stress boundary condition at the far end within some tolerance. The steel stress at the bar end is equal to zero. Splitting cracks initiate at the loaded end when the bond stress at that end reaches the peak local bond strength u_{max}. Total bond failure occurs when the splitting crack has propagated long enough along the splice length so that for any further increase in steel stress or slip at the loaded end the bond force equilibrium equations can no longer be satisfied.

In [Coronelli and Gambarova, 2004], concrete is modelled by means of four-node plane-stress elements, with a thickness equal to the section width. Steel bars are represented by two-node truss elements and a bond-link element exhibiting a relative slip between the two materials couples the concrete elements to the corresponding bar elements. The constitutive models for each component take into account the nonlinear behaviour for monotonic and cyclic loading: incremental stress-strain relation with smeared rotating cracks for concrete (Figure D.10a), elasto-plastic stress strain relation for the steel (Figure D.10b), incremental bond stress-slip relation, (Figure D.10c).

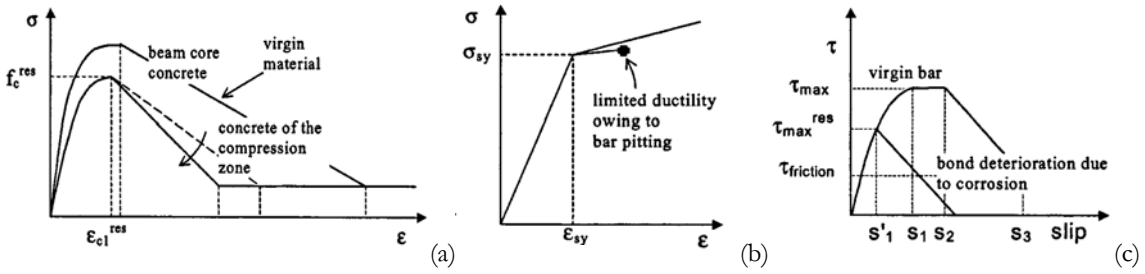

Figure D.10 Constitutive laws: (a) concrete in compression; (b) steel; (c) bond [Coronelli and Gambarova, 2004]

The standard rotating crack model is combined with a scalar damage concept: the stiffness and consequently the stresses in the cracked elements are reduced beyond the cracking strain level, as a

function of a damage parameter. The parameters concerning such properties as material strength, toughness and softening can be specified as well, on the basis of the corrosion level.
Cracking and spalling in the compressed concrete are described by reducing the strength of the concrete elements belonging to the cover and by adopting a brittle postpeak behaviour (Figure D.10a). The reduced concrete strength is calculated as follows:

$$f_c^* = \frac{f_c}{1 + K\varepsilon_1 / \varepsilon_{c0}} \tag{D.11}$$

where K is a coefficient related to bar roughness and diameter (K = 0.1 for medium-diameter ribbed bars), ε_{c0} is the strain at the peak compressive stress f_c, ε_1 is the average (smeared) tensile strain in the cracked concrete at right angles to the direction of the applied compression. The strain ε_1 is evaluated by means of the following equation:

$$\varepsilon_1 = \left(b_f - b_0\right)/ b_0 \tag{D.12}$$

where b_0 is the section width in the virgin state (no corrosion cracks), b_f is the beam width increased by corrosion cracking. An approximation of the increase of the beam width is given by:

$$b_f - b_0 = n_{bars} w_{cr} \tag{D.13}$$

where n_{bars} is the number of the bars in the top layer (compressed bars), w_{cr} is the total crack width for a given corrosion level X, to be evaluated for instance as:

$$w_{cr} = \sum_i u_{i,corr} = 2\pi\left(v_{rs} - 1\right)X \tag{D.14}$$

where v_{rs} is the ratio of volumetric expansion of the oxides with respect to the virgin material, X is the depth of the corrosion attack, $u_{i,corr}$ is the opening of each single corrosion crack. The value v_{rs} is taken equal to 2. Thus, the diameter of each bar increases by 2X.
Eq.(D.14) is based on the hypothesis that all corrosion products accumulate around the corroded bar. Hence, for a single bar the total crack width is equal to the circumference increase, i.e. the right-hand-side term in Eq.(D.14).
The FE code used by the authors easily reproduces the first type of attack, due to carbonation, by reducing the section of each bar element. As for pitting, its effects on bar ductility can be introduced by enforcing lower ultimate strains, compared to the virgin steel. A simplified approach is proposed to describe such a ductility reduction, on the basis of the recent experimental results by [Cairns et al., 1999] and by [Castel et al., 2000]. The percent of reduction of the bar cross section is:

$$\alpha_{pit} = \Delta A_{pit} / A_{bar} \tag{D.15}$$

where ΔA_{pit} is the area reduction due to pitting and A_{bar} is the nominal bar cross section area.
A linear reduction can be introduced to describe the evolution of the ultimate strain of the steel, from $\varepsilon_{su}^{'} = \varepsilon_{su}$ in the virgin material (α_{pit} = 0) to $\varepsilon_{su}^{'} = \varepsilon_{sy}$ ($\alpha_{pit} = \alpha_{pit}^{\max}$, i.e. complete loss of ductility):

$$\varepsilon_{su}^{'} = \varepsilon_{sy} + \left(\varepsilon_{su} - \varepsilon_{sy}\right)\cdot\left(1 - \frac{\alpha_{pit}}{\alpha_{pit}^{\max}}\right) \tag{D.16}$$

This equation is valid for $\alpha_{pit} < \alpha_{pit}^{\max}$. Different values of $\alpha_{pit}^{\max}$ have been measured by various authors and values ranging from 0.5 [Cairns et al., 1999] to 0.1 [Castel et al., 2000] can be found in the literature. The application of Eq.(D.16) is therefore linked to the parameter $\alpha_{pit}^{\max}$, whose evaluation is critical for the description of bar ductility and needs further studies.
In conclusion of their study, the following phenomena were identified by [Coronelli and Gambarova, 2004] as the most important, both at the service and ultimate limit states: the stiffness decay caused by

impaired tension stiffening; the crack pattern evolution accompanied by enhanced shear effects; the strength deterioration in bending and shear; the transition from tension to compression failures in critical sections; bond failure along the span and/or at beam ends.
The finite-element model proposed by [Girard, 2002] is also able to describe the 3D effects through a concrete constitutive law based on a hypoelastic model, considering the loading path and the evolution of mechanical properties according to the stress history. The gradual deterioration of bond is accounted for by the steel and interface constitutive laws. The element used to model the interface explicitly considers the relative slip ξ_r, defined as the difference between the steel ξ_s and concrete ξ_c displacements. The steel strain tensor ε_s, based on the assumption of small displacements, is defined as sum of two components, the concrete elongation ε_c and the relative slip between materials ε_r.
An interesting contribution is given also by [Haskett et al., 2008], proposing an algorithm to obtain the local $\tau - \delta$ relationship from the global load P – slip Δ response. The peak load at which debonding starts is defined by the following equation:

$$P_{\max} = \sqrt{2G_f}\sqrt{L_{per}EA_p} = \sqrt{\tau_{\max}\delta_{\max}}\sqrt{L_{per}EA_p} \tag{D.17}$$

where L_{per} is the contact perimeter of the reinforcement with the surrounding concrete, i.e. the circumference of the bar. The peak load can only be attained when a certain "effective bond length" L_{crit} is provided:

$$L_{crit} = \frac{\pi}{2\sqrt{\frac{\tau_{\max}L_{per}}{\delta_{\max}EA_p}}} \tag{D.18}$$

Increasing the bond length beyond this length, does not increase the ultimate load. As $P_{\max}$ is known from the test results, the product τ_{max} δ_{max} can be derived from Eq.(D.17), as E A_p and L_{per} depend on the geometric and material properties.

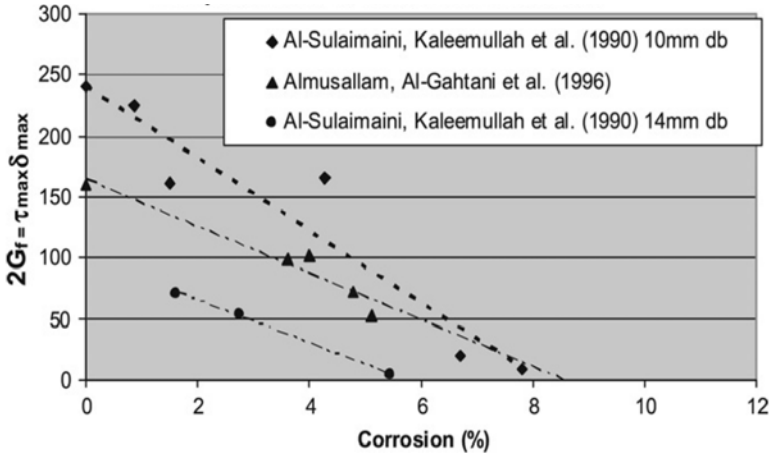

Figure D.11 Influence of corrosion on interfacial fracture energy [Haskett et al., 2008]

The bond law proposed by [Haskett et al., 2008] is based on the $\tau - \delta$ relationship proposed by [CEB-FIP, 1992], in which the frictional component of bond was not considered. The authors considered the influence of corrosion on the interfacial fracture energy G_f of the local bond stress-slip relationship. It was found that the small increases in bond strength under low levels of corrosion were actually compensated by the reduction in the value of δ_{max} in the local $\tau - \delta$ relationship. For all levels of

corrosion, there was an unequivocal reduction in the interfacial fracture energy G_f of the local $\tau - \delta$ relationship, as shown in Figure D.11, where the linear interpolation of experimental results is provided. For example, using the results from [Almusallam et al., 1996b], the influence of corrosion on the interfacial fracture energy G_f is given by:

$$2G_f = 164 - 19(\%c) \tag{D.19}$$

where $\%c$ is the percentage weight loss due to corrosion.

Overview of bond strength-slip relationships

In the following, some of the numerous bond strength-slip relationships available in the literature are summarized in chronological order. One of the most recognized bond laws in the technical literature is the trilinear relationship proposed by [Eligehausen et al., 1983] to describe the local bond stress–slip behaviour of bars embedded in well-confined concrete in which the mode of failure is by pull-out.
It is worth noting that, except for the CEB-FIP model, [CEB-FIP, 1990], of the local bond stress–slip response for unconfined concrete, which is taken similar to that of well-confined concrete but with a reduced envelope curve to account for splitting failure, no general relationship has been proposed in the technical literature until now to generate the full local bond stress–slip behavior for the splitting mode of bond failure with due account to the main parameters that influence the response, [Harajli, 2007].
For the meaning of the notations, please consult the corresponding reference.

Orangun et al., 1975-1977:

$$\frac{U}{f_c'^{1/2}} = 0.1 + 0.25\frac{c}{b_d} + 4.15\frac{b_d}{L_d} + \frac{U_{tr}}{f_c'^{1/2}} \tag{D.20}$$

with:

$$\frac{U_{tr}}{f_c'^{1/2}} = K_{tr} = \frac{A_{tr} f_y}{41.5 s_t n_s d_b} \le 0.25 \tag{D.22a}$$

Eligehausen, 1983:

$$u_{\max} = 1.5 f_{ct}\sqrt{c/d_b} \tag{D.21}$$

CEP-FIP Model Code 90, 1992:

$$u = u_1 (s/s_1)^{\nu} \tag{D.22}$$

Esfahani and Rangan, 1998:

$$u(x) = K \cdot s(x) \tag{D.23}$$

$$u_{\max} = 4.9\frac{c/d_b + 0.5}{c/d_b + 3.6} f_{ct} \quad \text{for NSC } (f_c < 50 \text{ MPa}) \tag{D.25a}$$

$$u_{\max} = 8.6\frac{c/d_b + 0.5}{c/d_b + 5.5} f_{ct} \quad \text{for HSC } (f_c > 50 \text{ MPa}) \tag{D.25b}$$

Zuo and Darwin, 2000:

$$T = \frac{A_b f_s}{f_c^{1/4}} = \frac{T_c + T_s}{f_c^{1/4}} \tag{D.24}$$

with:

$$\frac{T_c}{f_c^{1/4}} = \left[1.44 L_d \left(c + 0.5 d_b\right) + 56.3 A_b\right] \left(0.1 \frac{c_M}{c} + 0.9\right) \tag{D.26a}$$

$$\frac{T_s}{f_c^{1/4}} = 9.0 \cdot t_r t_d \frac{L_d A_{tr}}{s_t n_s} + 743.6 \tag{D.26b}$$

Harajli, 2007:

$$u_{\max} = 0.95 \sqrt{f_c'} \left(c / d_b\right)^{2/3} \text{ for plain HSC } (f_c \leq 50 \text{ MPa}) \tag{D.25}$$

$$u_{\max} = 0.78 \sqrt{f_c'} \left(\frac{c + K_c}{d_b}\right)^{2/3} \text{ for plain NSC or confined concrete} \tag{D.27a}$$

where K_c is the confinement parameter.

APPENDIX D Basics of statistics [Optislang manual, 2008]

Mean, Variance, Coefficient of variation

Basic statistic values of a variable x_i are the mean value μ_{x_i} calculated from the samples $x_i^{(k)}$ as:

$$\mu_{x_i} = \frac{1}{N}\sum_{k=1}^{N} x_i^{(k)} \tag{E.1}$$

and the variance:

$$\sigma_{x_i}^2 = \frac{1}{N-1}\sum_{k=1}^{N}\left(x_i^{(k)} - \mu_{x_i}\right)^2 \tag{E.2}$$

where $\sigma_{x_i}^2$ is the standard deviation.

Provided $\mu \neq 0$, the dimensionless coefficient of variation COV is frequently used to describe the variability:

$$COV_{x_i} = \frac{\sigma_{x_i}}{\mu_{x_i}} \tag{E.3}$$

These values are calculated from the samples of the design values in order to have a statistical control of the used samples of each design variable. The statistical values calculated from the samples of the response variables are used to evaluate their sensitivity. For instance, it is important to investigate response variables whose coefficient of variation is significantly higher than the coefficient of the design parameter.

Linear correlation coefficient, Linear correlation matrix

The evaluation of correlation between the design parameters and the responses may be estimated by means of the non-dimensional linear correlation coefficient ρ_{ij}, calculated from all pair wise combinations of both design variables and response according to:

$$\rho_{ij} = \frac{1}{N-1}\frac{\sum_{k=1}^{N}\left(x_i^{(k)} - \mu_{x_i}\right)\left(x_j^{(k)} - \mu_{x_j}\right)}{\sigma_{x_i}\sigma_{x_j}} \tag{E.4}$$

which measures the strength and the direction of a linear relationship between two variables. The value of ρ_{ij} ranges between −1 and +1. The + and − signs indicate positive and negative linear correlations, respectively. Positive values indicate a relationship between x_i and x_j variables such that as values for x_i increase, values for x_j also increase. Similarly, negative values indicate a relationship between x_i and x_j variables such that as values for x_i increase, values for x_j decrease.

If x_i and x_j have a strong positive (negative) linear correlation, ρ_{ij} is close to +1 (-1), which means perfect positive (negative) fit. If there is no or weak linear correlation, ρ_{ij} is close to 0, that denotes there is a random or nonlinear relationship between the two variables. A correlation greater than 0.7 is generally described as strong, whereas a correlation less than 0.3 is typically described as weak. These values can vary based upon the type of data being examined.

The linear correlation coefficients are assembled in the *linear correlation matrix* C_{xx}. This symmetric matrix is partitioned according to the correlation of the design variables with responses, of the design variables with the design variables and of the responses with the responses.

Quadratic correlation coefficient, Quadratic correlation matrix

The quadratic coefficients of correlation ρ_{ij} are determined by performing a quadratic regression of variable x_j on variable x_i by a least-squares fit on the samples. The values of ρ_{ij} range between 0 and +1. The *quadratic correlation matrix,* differently from the linear one, is not symmetric.

Coefficient of determination

To have an idea of the proportion of the variance (fluctuation) of one variable that is predictable from the other variable, it may be useful to calculate the coefficient of determination *CoD* (or *multiple correlation coefficient*, R^2):

$$R^2 = \frac{\sum_{i=1}^{N} (\hat{y}_i - \bar{y})^2}{\sum_{i=1}^{N} (y_i - \bar{y})^2} \qquad \text{(E.5)}$$

where $\hat{y}_i$ is the predicted response, y_i is the actual response and $\bar{y}_i$ is the mean value of all origin responses. The coefficient of determination is a measure of the dependence of a response value from a set of input parameters x_i in a special regression model context. In other words, the *CoD* represents the percent of the data that is the closest to the regression model best fit and varies between 0 and 1 (i.e. 0% and 100% respectively). In the linear regression case with $i = 1$ only, R^2 is simply the square of the correlation coefficient ρ_{12}. Furthermore, if the coefficient of determination with respect to a linear regression model is $R^2 = 0.850$, this means that 85% of the total variation in x_2 can be explained by the linear relationship between x_1 and x_2. The other 15% of the total variation in x_2 is explained by quadratic relationship or remains unexplained.

Principal component vector

The Principal Component Analysis identifies the dominating components in the responses and their relation to the design values, by solving the eigenvalue problem relative to the correlation matrix:

$$\phi_k^T C_{xx} \phi_k = \lambda_k \phi_k \qquad \text{k = 1, …, N} \qquad \text{(E.6)}$$

The eigenvectors (or *principal component vector*) ϕ_k have the size N of all design variables and responses and they are sorted with the decreasing size of the correspondent eigenvalue (or *weighted PC value*) λ_k. The relative size of the eigenvalues denotes the dominating randomness.

Anthill plot, Cloud plot

The Anthill plot is a two-dimensional scatter-plot of two sample vectors of any design variables and responses, i.e. a 2D-projection of the input-output parameter room of all active designs.

It is advisable to investigate the Anthill plots in addition to the correlation matrix, since the latter can detect only linear dependencies between variables, while in the Anthill plot both linear and nonlinear dependencies (e.g. a bifurcation) may be revealed.

The Cloud plot is a 3D-Anthill (scatter) plot showing a 3D-projection of the input-output variable space.

APPENDIX E Target displacement determination [EC8, 2005]

The target displacement is determined from the elastic response spectrum $S_e(t)$. The capacity curve derives from the pushover analysis for values of the control displacement ranging between zero and the value corresponding to 150% of the target displacement.
The following relation between normalized lateral forces F_i and normalized displacements Φ_i is assumed:

$$F_i = m_i \Phi_i \tag{F.1}$$

where m_i is the mass in the i-th storey.
Displacements are normalized in such a way that $\Phi_n = 1$, where n is the control node usually denoting the roof level. Consequently, $F_n = m_n$.

F.1 Transformation from the MDOF system to an equivalent SDOF system

The mass of the equivalent SDOF system m^* is determined as:

$$m^* = \sum m_i \Phi_i = \sum F_i \tag{F.2}$$

and the transformation factor is given by:

$$\Gamma = \frac{m^*}{\sum m_i \Phi_i^2} = \frac{\sum F_i}{\sum \frac{F_i^2}{m_i}} \tag{F.3}$$

The force F^* and displacement d^* of the equivalent SDOF system are computed as:

$$F^* = \frac{F_b}{\Gamma} \tag{F.4}$$

$$d^* = \frac{d_n}{\Gamma} \tag{F.5}$$

where F_b and d_n are, respectively, the base shear force and the control node displacement of the MDOF system.

F.2 Determination of the idealized elasto-perfectly plastic force – displacement relationship

The yield force F_y^*, representing also the ultimate strength of the idealized system, is equal to the base shear force at the formation of the plastic mechanism. The initial stiffness of the idealized system is determined in such a way that the areas under the actual and the idealized force – deformation curves are equal (see Figure F.12).
Based on this assumption, the yield displacement of the idealised SDOF system d_y^* is given by:

$$d_y^* = 2\left(d_m^* - \frac{E_m^*}{F_y^*}\right) \tag{F.6}$$

where E_m^* is the actual deformation energy up to the formation of the plastic mechanism.

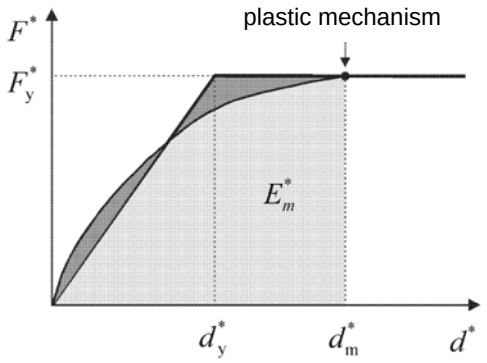

Figure F.12 Determination of the idealized elasto-perfectly plastic force vs. displacement relationship

F.3 Determination of the period of the idealized equivalent SDOF system

The period T^* of the idealized equivalent SDOF system is determined as:

$$T^* = 2\pi\sqrt{\frac{m^* d_y^*}{F_y^*}} \tag{F.7}$$

F.4 Determination of the target displacement for the equivalent SDOF system

The target displacement of the structure with period T^* and unlimited elastic behaviour is given by:

$$d_{et}^* = S_e\left(T^*\right)\left[\frac{T^*}{2\pi}\right]^2 \tag{F.8}$$

where $S_e(T^*)$ is the elastic acceleration response spectrum at the period T^*.

For the determination of the target displacement d_t^* for structures in the short-period range and for structures in the medium and long-period ranges different expressions should be used, as indicated

Figure F.13a: $T^* < T_C$ (short range period)

If $F_y^* / m^* \geq S_e\left(T^*\right)$, the response is elastic and

$$d_t^* = d_{et}^* \tag{F.9}$$

If $F_y^* / m^* < S_e\left(T^*\right)$, the response is nonlinear and

$$d_t^* = \frac{d_{et}^*}{q_u}\left(1 + \left(q_u - 1\right)\frac{T_C}{T^*}\right) \geq d_{et}^* \tag{F.10}$$

where q_u is the ratio between the acceleration in the structure with unlimited elastic behaviour $S_e(T^*)$ and in the structure with limited strength F_y^* / m^*:

$$q_u = \frac{S_e\left(T^*\right) m^*}{F_y^*} \tag{F.11}$$

Figure F.13b: $T^* \geq T_C$ (medium and long range period)

$$d_t^* = d_{et}^* \tag{F.12}$$

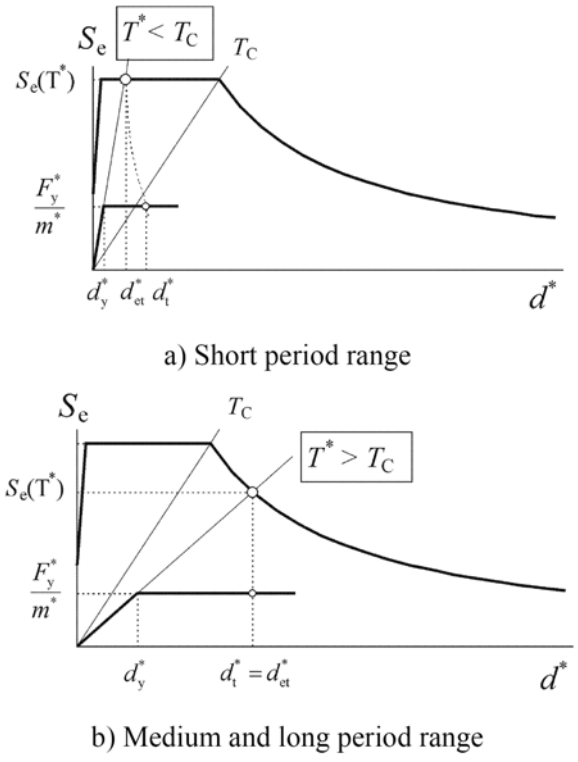

Figure F.13 Determination of the target displacement for the equivalent SDOF system

Figure F.13a-b is plotted in acceleration - displacement format. Period T^* is represented by the radial line from the origin of the coordinate system to the point at the elastic response spectrum defined by coordinates $d^* = S_e(T^*) \cdot (T^*/2\pi)^2$ and $S_e(T^*)$.

F.5 Determination of the target displacement for the MDOF system

The target displacement of the MDOF system, corresponding to the control node, is given by:

$$d_t = \Gamma d_t^* \tag{F.13}$$

APPENDIX F Safety verification criteria [EC8, 2005]

<table>
<tr><th colspan="2" rowspan="2"></th><th colspan="2">Linear Model (LM)</th><th colspan="2">Nonlinear Model</th><th colspan="2">q-factor approach</th></tr>
<tr><th>Demand</th><th>Capacity</th><th>Demand</th><th>Capacity</th><th>Demand</th><th>Capacity</th></tr>
<tr><td rowspan="3">Type of element or mechanism (e/m)</td><td rowspan="2">Ductile</td><td colspan="2">Acceptability of Linear Model (for checking of ρ_i = D_i/C_i values):</td><td rowspan="3">From analysis. Use mean values of properties in model.</td><td rowspan="2">In terms of strength. Use mean values of properties <u>divided</u> by CF and by partial factor.</td><td rowspan="2">From analysis.</td><td rowspan="3">In terms of strength. Use mean values of properties <u>divided</u> by CF and by partial factor.</td></tr>
<tr><td>From analysis. Use mean values of properties in model.</td><td>In terms of strength. Use mean values of properties.</td></tr>
<tr><td>Brittle</td><td colspan="2">Verifications (if LM accepted):
If $\rho_i \leq 1$: from analysis.
If $\rho_i > 1$: from equilibrium with strength of ductile e/m. Use mean values of properties <u>multiplied</u> by CF.</td><td>In terms of strength. Use mean values of properties <u>divided</u> by CF and by partial factor.</td><td>In terms of strength. Use mean values of properties <u>divided</u> by CF and by partial factor</td><td>In accordance with the relevant Section of EN1998-1: 2004.</td></tr>
<tr><td colspan="2">Verifications (if LM accepted):</td><td>From analysis.</td><td>In terms of deformation. Use mean values of properties <u>divided</u> by CF.</td><td colspan="3"></td></tr>
</table>